

Newcastle University

Determining the impact of mitochondrial dysfunction on stem cell dynamics and proliferation within the colon

Volume I of II

Craig Stamp

BSc (Hons) MRes

*This thesis is submitted in partial fulfilment of the
requirements for the degree of*

Doctor of Philosophy

Wellcome Trust Centre for Mitochondrial Research

Institute of Neuroscience

Newcastle University

September 2015

Author's Declaration

This thesis is submitted for the degree of Doctor of Philosophy at Newcastle University. The research was conducted in the Wellcome Trust Centre for Mitochondrial Research, Institute of Neuroscience, and is my own work unless stated otherwise. The research was completed under the supervision of Dr L.C. Greaves and Professor D.M. Turnbull from September 2012 to September 2015.

I certify that none of the material offered in this thesis, with the exception of my MRes results as cited in chapter 3, has been previously submitted by me for a degree or any other qualification at any other university.

Abstract

Clonally expanded mitochondrial DNA (mtDNA) point mutations have been shown to cause mitochondrial dysfunction in the form of cytochrome *c* oxidase deficiency (COX deficiency) within ageing human colonic epithelium. Currently, there are a lack of robust stem cell markers within human colonic epithelium, however the detection of mitochondrial dysfunction has been shown to be a useful stem cell lineage marker, enabling the investigation of stem cell dynamics within colonic crypts.

Using the most robust data set of COX deficiency frequency and mtDNA mutation number, a computational model that simulates stem cell dynamics within human colonic crypts was constructed. *In silico* stem cell modelling suggests: there are approximately 5 stem cells within human colonic crypts, stem cell divisions occur asymmetrically the majority of the time, and that infrequent symmetric stem cell division permits niche succession of individual stem cell clones. However, the *in silico* data was unable to match the biological data when a model simulating neutral drift stem cell dynamics was used, suggesting a change in stem cell biology when mitochondrial dysfunction was present.

In order to assess the impact of mitochondrial dysfunction within colonic stem cells *in vivo*, a mouse model of mitochondrial dysfunction was crossed with a mouse model enabling the visualisation of cells expressing Lgr5 (a well-accepted stem cell marker). Double thymidine analogue labelling was used to identify cells traversing through the cell cycle, together with a marker of proliferation. This data suggests that stem cells with mitochondrial dysfunction have a small but significant increase in cell cycle progression rate compared to normal stem cells. When these data were included in the model, a better fit to the biological data was achieved.

These findings suggest that mitochondrial dysfunction does significantly impact on stem cell homeostasis. As stem cells with mitochondrial dysfunction are more likely to out-compete normal stem cells over time, this may have potential implications for an increased risk of cancer propagation within the colon.

Acknowledgements

There are so many people that I would like to thank that have allowed me to progress through my PhD. Firstly, I would like to thank my supervisors, Dr Laura Greaves and Professor Doug Turnbull, for the conception of the project and providing invaluable support and guidance throughout.

Thank you to Dr Anze Zupanic for introducing me to the MATLAB scripting language and for his patience when explaining how we can use MATLAB to design a model of stem cell dynamics. I thank Dr Elizabeth Stoll for suggesting and enabling me to implement a double thymidine analogue labelling methodology for mouse colonic epithelium. Furthermore, I would again like to thank Dr Laura Greaves for providing data regarding the number of mtDNA mutations present within human colonic epithelium cells that was vital for the modelling work. I would also like to thank Dr Holly Baines for providing me with COX deficiency frequency data within mitochondrial mutator mice that was necessary to optimise a model of clonal expansion within a population of stem cells. I thank Karen Vousden at the Beatson Institute for Cancer Research for kindly donating the *Lgr5-EGFP-Ires-CreERT2* mice that were essential for identifying functional stem cells within mouse colonic epithelium. I am also very grateful to Chris, Brigid and Emma in the animal house for maintaining the mouse colonies. Additional thanks go to Anna Smith for her help with the microtome tissue cutting towards the end of my project. Finally, I would also like to thank the whole of the Wellcome Trust Centre for Mitochondrial Research as I'm sure each member has helped me at some point along the way.

As well as the people who were involved in shaping the project I present to you within this thesis, I can't go without thanking all the other people who have supported me along the way. Firstly, I have to thank my beautiful fiancée, Holly, who I can't wait to marry next year. She has supported me emotionally, financially, and in every other way possible, allowing me to achieve what you see here before you. I thank my future mother and father in-law, Jan and Nigel Packer, whose help, especially with our house moves, has been hugely appreciated over the past four years since I moved to Newcastle. Finally, I would like to thank my Mum and Dad, who have been there for me since I can remember, and who have supported every decision I have made that has led me to this point. I am especially fond of the chats my Dad and I have had about my future career ever since I was in school, which I believe was the reason I worked so hard, allowing me to progress to the point where I am now.

Table of Contents

<i>Chapter 1 Introduction</i>	2
1.1 Mitochondria.....	2
1.2 Mitochondrial structure	2
1.3 Mitochondrial dynamics.....	4
1.3.1 Mitochondrial fusion	4
1.3.2 Mitochondrial fission	5
1.3.3 Mitochondrial biogenesis.....	5
1.4 Mitochondrial functions.....	6
1.4.1 ATP synthesis	6
1.4.1.1 Complex I.....	7
1.4.1.2 Complex II.....	7
1.4.1.3 Complex III.....	8
1.4.1.4 Complex IV.....	8
1.4.1.5 Complex V.....	9
1.4.2 Iron-sulphur cluster biogenesis.....	12
1.4.3 Apoptosis.....	12
1.4.4 ROS production.....	12
1.4.5 Calcium homeostasis	13
1.5 Mitochondrial genome.....	13
1.5.1 MtDNA transcription.....	16
1.5.2 MtDNA translation.....	17
1.5.3 MtDNA replication.....	18
1.5.3.1 MtDNA replication machinery	18
1.5.3.2 MtDNA replication models	19
1.6 Mitochondrial genetics.....	20
1.6.1 Heteroplasmy.....	20
1.6.2 Clonal expansion	20
1.6.2.1 Threshold effect	21
1.6.3 Mitotic segregation.....	22
1.6.4 Maternal inheritance	23
1.7 Ageing.....	24

1.7.1	Evolutionary theories of ageing.....	24
1.7.2	Molecular theories of ageing.....	25
1.7.2.1	The mitochondrial free radical theory of ageing	26
1.7.3	Mitochondrial dysfunction and ageing.....	27
1.7.4	Mouse models of mitochondrial dysfunction.....	28
1.7.4.1	TFAM knockout mice	28
1.7.4.2	MtDNA mutator mouse.....	29
1.8	The Colon	30
1.8.1	Structure of the colon.....	30
1.8.2	Stem cell markers within crypts.....	31
1.8.3	The stem cell niche within crypts.....	33
1.8.4	Functions of the colon	35
1.8.5	Mitochondrial dysfunction within the colon	36
1.8.6	Modelling stem cell dynamics within crypts	37
1.9	Aims and objectives	41
<i>Chapter 2</i>	<i>Materials and methods.....</i>	44
2.1	Materials.....	44
2.1.1	Equipment and computer software	44
2.1.2	Consumables.....	44
2.1.2.1	General consumables.....	44
2.1.2.2	Antibodies.....	45
2.1.3	Solutions.....	46
2.2	Methods.....	47
2.2.1	Subjects and colorectal mucosal samples.....	47
2.2.2	Mouse models.....	47
2.2.2.1	PolyA ^(-/-) mitochondrial mutator mice.....	47
2.2.2.2	Lgr5-EGFP-Ires-CreERT2 mice and PolyA ^(-/-) mitochondrial mutator mice	48
2.2.3	Double thymidine analogue labelling	49
2.2.4	Mouse tissue harvesting	50
2.2.5	Immunofluorescence for mitochondrial dysfunction.....	50
2.2.6	Immunofluorescence for cell cycle kinetics.....	51
2.2.7	Fluorescence microscopy and image analysis	52
2.2.8	COX/SDH histochemistry.....	53

2.2.9	COX/SDH histochemical analysis.....	54
2.2.10	Computational modelling of respiratory deficient stem cells	54
2.2.10.1	Mouse stem cell population model.....	54
2.2.10.2	Human stem cell niche model	55
2.2.10.3	COX deficient stem cell distribution model.....	57
Chapter 3	<i>Mitochondrial dysfunction within human colon.....</i>	62
3.1	Introduction.....	62
3.1.1	Mitochondrial dysfunction and ageing	62
3.1.2	Mitochondrial dysfunction within human colon.....	62
3.1.3	Monoclonal conversion of crypts.....	63
3.2	Aims of study.....	65
3.3	Methodology.....	66
3.3.1	COX deficiency quantification within human colonic mucosa	66
3.3.2	Relating COX deficiency observed to fraction of stem cells.....	66
3.4	Results.....	67
3.4.1	Characteristics of human colon epithelium after COX/SDH histochemistry.....	67
3.4.2	Partially COX deficient crypts and stem cell number within human colon.....	69
3.4.3	COX deficiency within human colon samples.....	71
3.4.4	Crypt fission occurrence within human colon	73
3.4.5	COX deficient crypt colonies within human colon	77
3.4.6	Removal of crypt colonies from biological data.....	80
3.4.7	Relating COX deficiency percentage to number of COX deficient stem cells.....	82
3.4.8	Biological data converted to stem cell number.....	85
3.5	Discussion.....	87
3.6	Conclusion.....	88
Chapter 4	<i>Modelling stem cell dynamics within colonic epithelium</i>	91
4.1	Introduction.....	91
4.2	Aims of study.....	93
4.3	Methodology.....	94
4.3.1	Computational model of human colonic stem cell dynamics.....	94
4.4	Results.....	97

4.4.1	Human niche succession model.....	97
4.4.2	Human niche succession model testing.....	100
4.4.2.1	Asymmetric division probability.....	100
4.4.2.2	De novo mtDNA mutation rate.....	102
4.4.2.3	Crypt fission	105
4.4.2.4	COX deficient stem cell advantage.....	107
4.4.2.5	mtDNA copy number and asymmetric division probability – part 1.....	109
4.4.2.6	mtDNA copy number and asymmetric division probability – part 2.....	111
4.4.3	Multiple mtDNA mutations	115
4.4.3.1	Multiple mtDNA mutations detected within aged human colon.....	115
4.4.3.2	Tracking multiple mtDNA mutations within human niche succession model.....	116
4.4.3.3	Parameter effects on multiple mutations.....	119
4.4.4	Impact of altered mtDNA segregation upon division	121
4.4.4.1	Mutation distribution spectra with random mtDNA segregation upon division..	121
4.4.4.2	Biasing mutated mtDNA segregation upon division.....	123
4.4.4.3	Mutation distribution spectra with biased mtDNA segregation upon division....	125
4.4.4.4	Effects of biasing mtDNA segregation upon division.....	127
4.4.5	Model optimisation	129
4.4.5.1	COX deficiency frequency from human colon	130
4.4.5.2	Best fit COX deficiency frequency and number of mutations	131
4.4.5.3	Best fit data tables.....	133
4.4.5.4	Stem cell number validation from human niche succession model.....	134
4.5	Discussion.....	136
4.6	Conclusion.....	141
Chapter 5	<i>Development and validation of a mouse model to investigate stem cell dynamics....</i>	143
5.1	Introduction.....	143
5.2	Aims of study.....	145
5.3	Methodology.....	146
5.3.1	Modelling focal respiratory chain deficiency within mouse colon	146
5.3.2	Quantifying mitochondrial dysfunction within mouse colon	146
5.4	Results.....	147
5.4.1	Mitochondrial mutator mouse phenotype	147

5.4.2	COX deficiency frequency within mitochondrial mutator mice	147
5.4.2.1	MtDNA mutation clonal expansion model.....	150
5.4.2.2	Mutation rate and mtDNA copy number within stem cells.....	151
5.4.2.3	Population model best fits with mitochondrial mutator mouse models	154
5.4.3	Observed mitochondrial dysfunction within mouse colon	155
5.4.4	Comparison of mitochondrial dysfunction between mouse genotypes.....	160
5.4.5	Multiple respiratory deficiency within mouse colon.....	162
5.5	Discussion.....	164
5.6	Conclusion.....	166
Chapter 6	<i>Cell cycle kinetics of cells with mitochondrial dysfunction within mouse colon</i>	168
6.1	Introduction.....	168
6.1.1	Stem cell ageing	168
6.1.2	Mitochondria and stem cell ageing.....	168
6.1.2.1	Impact of mitochondrial dysfunction on stem cell ageing.....	168
6.1.2.2	MtDNA mutations and colorectal cancer.....	169
6.1.3	Mouse models.....	170
6.2	Aims of study.....	171
6.3	Methodology.....	172
6.3.1	Double thymidine analogue labelling	172
6.3.2	Detection of mitochondrial dysfunction and cell cyde kinetic markers.....	172
6.4	Results.....	173
6.4.1	Determining cell cycle kinetics within mouse colon.....	173
6.4.2	Number of cells within crypts.....	180
6.4.3	Frequency of proliferating cells within mouse colon	182
6.4.4	Frequency of cells that incorporated a thymidine analogue.....	184
6.4.5	Frequency of newly divided cells	186
6.4.6	Frequency of cells re-entering the cell cyde	188
6.4.7	Frequency of cells re-entering the cell cyde within <i>PolyA</i> heterozygote mice	190
6.4.8	Cell cycle kinetics by individual complex deficiency.....	192
6.5	Discussion.....	196
6.6	Conclusion.....	199
Chapter 7	<i>Final discussion and future work</i>	201

7.1	Accumulation of mitochondrial dysfunction.....	201
7.2	Impact of mitochondrial dysfunction.....	203
7.3	Modelling combined effects.....	204
7.4	Future work.....	206
7.5	Final conclusion	207
<i>Chapter 8</i>	<i>Bibliography.....</i>	<i>209</i>

Table of Figures

Figure 1-1 Mitochondrial structure	3
Figure 1-2 Oxidative phosphorylation	10
Figure 1-3 The human mitochondrial genome.....	15
Figure 1-4 MtDNA replication machinery	19
Figure 1-5 MtDNA heteroplasmy and the threshold effect	22
Figure 1-6 Mutated mtDNA clonal expansion via mitotic segregation	23
Figure 1-7 Structure of a colonic crypt	31
Figure 2-1 Mitochondrial mutator mouse breeding scheme	48
Figure 2-2 Lgr5 and mitochondrial mutator mouse breeding scheme	49
Figure 3-1 Characteristics of Human colon after COX/SDH histochemistry.....	68
Figure 3-2 Pooled partially COX deficient crypts	70
Figure 3-3 Human colon COX deficiency	72
Figure 3-4 Crypt fission frequency between normal and COX deficient crypts	75
Figure 3-5 COX deficient crypt colonies within human colon.....	78
Figure 3-6 Crypt colony correction for human colon COX deficiency data.	81
Figure 3-7 Model relating percentage COX deficiency observed to likely number of COX deficient stem cells	83
Figure 3-8 Distributional binning for COX deficient stem cell number.....	86
Figure 4-1 Schematic diagram of niche succession model	98
Figure 4-2 Asymmetric division probability.....	101
Figure 4-3 Constant <i>de novo</i> mutation rate	103
Figure 4-4 Increasing <i>de novo</i> mutation rate	104
Figure 4-5 Crypt fission	106
Figure 4-6 Increasing COX deficient stem cell advantage	108
Figure 4-7 Clonal expansion probability and niche succession success	110

Figure 4-8 Interplay between symmetric division and mtDNA clonal expansion success	113
Figure 4-9 Number of mtDNA mutations detected within aged human colonic cells	115
Figure 4-10 mtDNA species tracking of whole crypts	117
Figure 4-11 Influencing number of mutations within individual cells	120
Figure 4-12 Random segregation and number of mutations detected	122
Figure 4-13 Biasing mutated mtDNA segregation upon asymmetric stem cell division	124
Figure 4-14 Biased segregation and number of mutations detected	126
Figure 4-15 Biased segregation impact on mutated mtDNA clonal expansion	128
Figure 4-16 COX deficiency frequency within human colon epithelium.....	130
Figure 4-17 Best fit data.....	131
Figure 4-18 Best fit data with COX deficient stem cell advantage	132
Figure 4-19 Stem cell number validation via partially COX deficient crypts.	134
Figure 5-1 COX deficiency within mitochondrial mutator mice with age	149
Figure 5-2 Mutated mtDNA clonal expansion within individual stem cells	150
Figure 5-3 Mutation rate within clonal expansion model	152
Figure 5-4 MtDNA copy number within the clonal expansion model	153
Figure 5-5 Optimised clonal expansion model	154
Figure 5-6 Mitochondrial dysfunction within <i>Lgr5^(+/-)PolyA^(+/+)</i> mouse colon.....	157
Figure 5-7 Mitochondrial dysfunction within <i>Lgr5^(+/-)PolyA^(+/-)</i> mouse colon	158
Figure 5-8 Mitochondrial dysfunction within <i>Lgr5^(+/-)PolyA^(-/-)</i> mouse colon.....	159
Figure 5-9 Comparison of mitochondrial dysfunction within mouse colon	161
Figure 5-10 Comparison of multiple respiratory chain complex loss within mouse colon ...	163
Figure 6-1 Mitochondrial dysfunction and cell cycle kinetic labelling method	172
Figure 6-2 Cell cycle kinetics and mitochondrial dysfunction within <i>Lgr5^(+/-)PolyA^(+/+)</i> mice	175
Figure 6-3 Cell cycle kinetics and mitochondrial dysfunction within <i>Lgr5^(+/-)PolyA^(+/-)</i> mice	176

Figure 6-4 Cell cycle kinetics and mitochondrial dysfunction within <i>Lgr5^(+/-)PolyA^(-/-)</i> mice	177
Figure 6-5 Mitochondrial OXPHOS status sampling fractions	178
Figure 6-6 Number of cells in crypts	181
Figure 6-7 Ki67 proliferating cell marker.....	183
Figure 6-8 Thymidine analogue cell division marker	185
Figure 6-9 Cells undergoing division within ~15 hours of animals death.....	187
Figure 6-10 Cell cycle re-entry before animals death.....	189
Figure 6-11 Cell cycle re-entry within <i>PolyA^(+/-)</i> crypts.....	191
Figure 6-12 Cell cycle kinetics and multiple complex deficiency.....	194
Figure 7-1 Modelling combined effects within niche succession model.....	205

List of Tables

Table 4-1 Table of parameters and functionality	94
Table 4-2 Evolution of model parameters	96
Table 4-3 Parameters tested with corresponding section reference	100
Table 4-4 Parameter values for best fit data	133
Table 4-5 Parameter values for best fit data with COX deficient stem cell advantage	133
Table 4-6 Least squares value for model fits with varying stem cell number	135
Table 5-1 List of mice used within mitochondrial dysfunction study	148
Table 6-1 Number of stem cells and crypts quantified per mouse	179

Abbreviations

ADP	Adenosine diphosphate
ATP	Adenosine triphosphate
Ca ²⁺	Calcium ion
CldU	5-Chloro-2-deoxyuridine
CM	Cristae membrane
CoA	Coenzyme A
COX	Cytochrome <i>c</i> oxidase
D-loop	Displacement loop
DNA	Deoxyribonucleic acid
EGFP	Enhanced green fluorescent protein
EM	Electron microscopy
EYFP	Enhanced yellow fluorescent protein
FACS	Fluorescence-activated cell sorting
FADH ₂	Flavin adenine dinucleotide
Fe-S	Iron-sulphur cluster
GTP	Guanosine triphosphate
HCl	Hydrochloric acid
HSP	Heavy strand promoter
IBM	Inner boundary membrane
IdU	5-Iodo-2-deoxyuridine
IMM	Inner mitochondrial membrane
IP	Intra-peritoneal
LSP	Light strand promoter
MFRTA	Mitochondrial free radical theory of ageing

Mg^{2+}	Magnesium ion
mRNA	Messenger ribonucleic acid
MtDNA	Mitochondrial DNA
mTERF	Mitochondrial termination factors
mtSSB	Mitochondrial single stranded DNA binding protein
NADH	Nicotinamide adenine dinucleotide
NaOH	Sodium hydroxide
NDS	Normal donkey serum
NGS	Normal goat serum
NOD/SCID	Nonobese diabetic/severe combined immunodeficiency
O _H	Origin of heavy strand replication
O _L	Origin of light strand replication
OMM	Outer mitochondrial membrane
OXPHOS	Oxidative phosphorylation
PBS	Phosphate buffered saline
PGC1- α	Peroxisome proliferator-activated receptor gamma, coactivator 1 alpha
P _i	Inorganic phosphate
POLMRT	Mitochondrial ribonucleic acid polymerase
PolyA	Catalytic subunit of polymerase gamma
PolyB	Accessory subunit of polymerase gamma
Q	Ubiquinone
Q ⁻	Semiubiquinone
QH ₂	Ubiquinol
RITOLS	Ribonucleotide incorporation throughout the lagging strand
RNA	Ribonucleic acid

ROS	Reactive Oxygen species
rRNA	Ribosomal ribonucleic acid
SD	Standard deviation
SDH	Succinate dehydrogenase
SEM	Standard error of the mean
TBS	Tris buffered saline
TBST	Tris buffered saline with Tween
TCA	Tricarboxylic acid cycle
TFAM	Mitochondrial transcription factor A
TFB1M	Mitochondrial transcription factor B1
TFB2M	Mitochondrial transcription factor B2
tRNA	Transfer ribonucleic acid
VDAC	Voltage dependent anion channel

Chapter 1

Introduction

Chapter 1 Introduction

1.1 MITOCHONDRIA

Mitochondria are dynamic organelles within all nucleated mammalian cells. They have a number of functions including: adenosine triphosphate (ATP) synthesis, calcium handling (Pozzan *et al.*, 2000), iron-sulphur (Fe-S) cluster formation (Rouault and Tong, 2005) and apoptosis (Newmeyer and Ferguson-Miller, 2003). Mitochondria are the only extra nuclear source of DNA, with mitochondrial DNA encoding integral proteins for ATP synthesis. Though mitochondria contain their own DNA, many more proteins are encoded by the nuclear DNA that are essential for the mitochondria to carry out their function (Anderson *et al.*, 1981). Mitochondria are believed to have evolved from free-living Eubacteria, whereby Eubacteria were engulfed by the Archaeabacterium, leading to the creation of primitive eukaryotic cells (Margulis, 1971). This process is termed endosymbiosis and was thought to have manifested due to the increasing atmospheric O₂ concentrations present at the time. Another explanation for endosymbiosis suggests that the mitochondrion and nucleus were formed simultaneously upon the fusion of hydrogen dependent archaeabacterium and hydrogen producing eubacterium (Martin and Muller, 1998).

1.2 MITOCHONDRIAL STRUCTURE

Mitochondria are typically thought of as elongated rod-shaped structures with a double plasma membrane. Electron microscopy (EM) studies show that mitochondria measure ~2.5μm in length and ~0.5μm in diameter and have a highly folded inner membrane, termed cristae, all enveloped by an outer membrane (Palade, 1952). This is depicted within Figure 1.1.

The outer mitochondrial membrane (OMM) contains high levels of the mitochondrial voltage dependent anion channel (VDAC) which allows molecules of up to 10kDa in size through to the intermembrane space (Alberts, 2002). The inner mitochondrial membrane (IMM) separates the intermembrane space from the mitochondrial matrix. Due to the presence of cardiolipin, it is effectively an impermeable barrier, with entry to and exit from the matrix

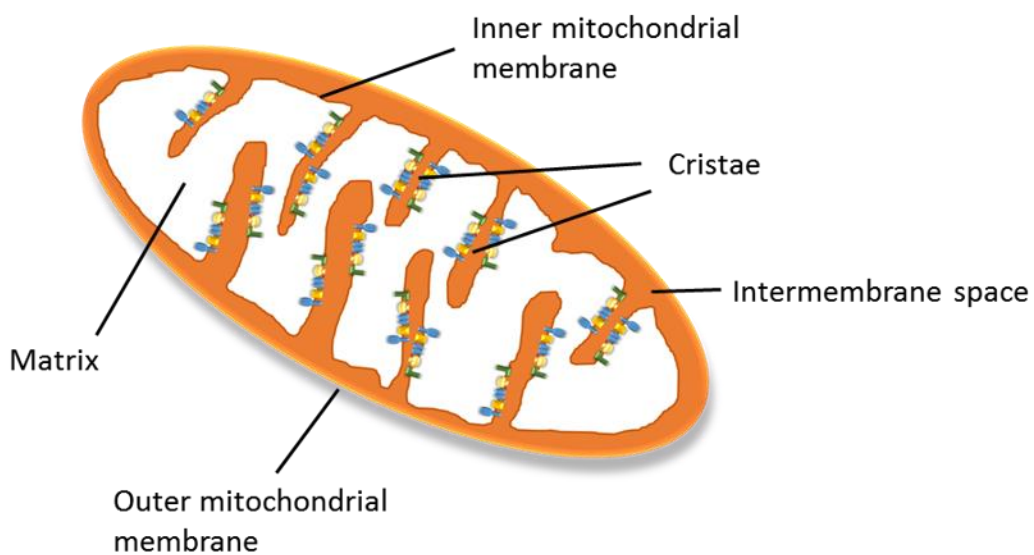


Figure 1-1 Mitochondrial structure

Electron micrograph of the mitochondrion organelle (upper panel). Schematic of a mitochondrion organelle with labelled structure and compartments. Scale bar represents 500nm. *EM image courtesy of Dr Amy Reeve (Newcastle University) and Dr Eve Simcox (Newcastle University).*

dependent on transport proteins, with the exception of O₂, CO₂, H₂O and NH₃ which can pass freely. The IMM is comprised of the inner boundary membrane (IBM) and the cristae membrane (CM) (Frey and Mannella, 2000). The IMM contains a high concentration of protein with the CM acting as a scaffold for the respiratory complexes to carry out oxidative phosphorylation (OXPHOS), along with providing an environment where a proton

electrochemical gradient can be generated for the synthesis of ATP (Mitchell, 1961; Ardail *et al.*, 1990). As the CM is highly folded, this effectively creates a large surface area for maximum respiratory complex protein integration for the production of ATP via OXPHOS.

The mitochondrial matrix contains multiple copies of the mitochondrial genome, along with the mtDNA transcription and translation machinery necessary for the expression of respiratory chain protein subunits. Furthermore, it is the site of the TCA cycle and fatty acid β -oxidation, which are integral intermediary steps necessary for oxidative metabolism. Fe-S cluster biogenesis is also carried out within the mitochondrial matrix that is necessary for electron shuttling within the respiratory chain complexes. In order to maintain the electrochemical gradient for OXPHOS, access to the mitochondrial matrix is highly regulated (Alberts, 2002). As the majority of mitochondrial proteins are nuclear encoded, peptides are required to traverse the inner and outer mitochondrial membranes before they can perform their function. TOM (translocase of the outer membrane) allows peptide transport across the outer membrane and TIM (translocase of the inner membrane) allows peptide transport across the inner membrane. TOM and TIM recognise targeting sequences that are attached to the N-terminal of mitochondrial peptides, which are then cleaved and processed further once they have entered the mitochondrial matrix (Hawlitschek *et al.*, 1988; Pfanner *et al.*, 1988).

Adenine nucleotide translocator (ANT) is an extremely abundant transporter within the IMM and is responsible for ATP and ADP transport between the matrix and intermembrane space (Pfaff and Klingenberg, 1968).

1.3 MITOCHONDRIAL DYNAMICS

Live cell imaging has shown that mitochondria are not the simple rod-shaped organelles as was classically thought to be the case, but in fact exist as complex dynamic networks that are constantly undergoing remodelling via fission and fusion (Bereiter-Hahn, 1978; Nunnari *et al.*, 1997). Fission and fusion are thought to be essential for mitochondrial interaction, mitochondrial turnover, and efficient ATP generation throughout the cell (Skulachev, 2001).

1.3.1 Mitochondrial fusion

The aptly named Mitofusin proteins, Mfn1 and Mfn2 are responsible for the process of mitochondrial fusion. They are mammalian outer membrane proteins and are part of the Dynamin protein family. They interact via their exposed cytosolic surface between hydrophobic heptad repeat regions (HR2), with subsequent GTPase activity inducing

conformational changes that result in mitochondrial fusion (Koshiba *et al.*, 2004). Within humans, Opa1, in partnership with Mfn1, is responsible for the fusion of the inner mitochondrial membrane (Cipolat *et al.*, 2004).

1.3.2 Mitochondrial fission

The proteins responsible for mitochondrial fission were identified within yeast cells via genetic screens (Bleazard *et al.*, 1999). Unlike fusion of mitochondria, fission requires only one Dynamin protein, known as Dmn1 in yeast. The homolog of Dmn1 within mammalian cells was found to be Drp1 (Shin *et al.*, 1997). Homologs of Dmn1 are also GTPases and are hypothesised to separate mitochondria by forming a ring-like structure, constricting the mitochondria to achieve separation (Hoppins *et al.*, 2007). Within yeast, a small outer membrane bound protein known as Fis1 is responsible for recruiting Dmn1 (Mozdy *et al.*, 2000), however, within mammalian cells, mitochondrial fission may not require a Fis1 homolog as depletion does not significantly alter mitochondrial fission (Otera *et al.*, 2010).

1.3.3 Mitochondrial biogenesis

As the energy requirements of the cell fluctuate, mitochondria must rapidly respond to the cellular demand to maintain an adequate supply of ATP within the cell at all times. One way of increasing ATP concentrations is by increasing mitochondrial mass via mitochondrial biogenesis. Peroxisome proliferator activated receptor γ coactivator 1 α (PGC-1 α) is the main regulator of mitochondrial biogenesis. It initiates the transcription of nuclear encoded mitochondrial proteins such as nuclear respiratory factors 1 and 2 (NRF1 and NRF2), oestrogen related receptor α (ERR α), forkhead box class-O (FoxO1), and peroxisome proliferator activated receptors (PPARs) (Puigserver and Spiegelman, 2003). Expression of these proteins leads to the eventual increase in mitochondrial mass.

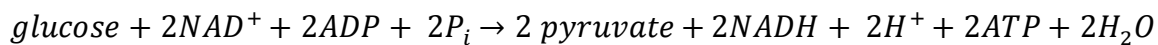
Increased PGC-1 α expression has been shown to occur within skeletal muscle in response to exercise. Exercise within skeletal muscle increases Ca^{2+} signalling, resulting in Ca^{2+} /calmodulin dependent kinase IV (CaMKIV) or calcineurin phosphorylating CREB (cAMP response element binding protein) binding to the CRE (CREB response element), thereby increasing PGC-1 α expression (Herzig *et al.*, 2001). Mitochondrial biogenesis is also triggered by cold temperatures in brown adipose tissues upon β 3 adrenergic receptor activation via the sympathetic nervous system as measure of non-shivering thermogenesis, which involves proton uncoupling protein UCP-1 (Puigserver *et al.*, 1998). On the other

hand, if ATP concentrations within the cell are higher than required, histone acetyltransferase (GCN5) has been shown to trigger the down-regulation of PGC-1 α (Lerin *et al.*, 2006). Furthermore, PGC-1 α is insulin sensitive, with insulin triggering the phosphorylation of FoxO1 by Akt (protein kinase B), with the subsequent inhibition of PGC1- α .

1.4 MITOCHONDRIAL FUNCTIONS

1.4.1 ATP synthesis

ATP is generated via oxidative phosphorylation (OXPHOS). Respiratory complexes within the inner mitochondrial membrane act as electron carriers, transporting electrons from intermediary molecules generated from the tricarboxylic acid (TCA) cycle and fatty acid oxidation (Hatefi, 1985). Glycolysis generates the initial substrates for aerobic respiration. This takes place within the cytoplasm, converting glucose into pyruvate, with the generation of 2 ATP molecules (Berg *et al.*, 2011). Glycolysis is shown in its simplest form in Equation 1-1.



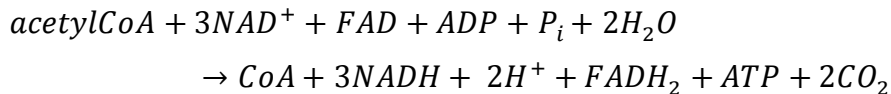
Equation 1-1 Glycolysis

The resulting pyruvate enters the mitochondrial matrix where pyruvate dehydrogenase converts it into acetyl CoA. This is shown in its simplest form in Equation 1-2 (Berg *et al.*, 2011).



Equation 1-2 Pyruvate decarboxylation

Acetyl CoA is the main substrate that feeds into the TCA cycle. The TCA cycle is a series of enzyme-catalysed reactions within the mitochondrial matrix that produces the electron carriers NADH and FADH₂, which are essential for OXPHOS. ATP and CO₂ are also generated from the TCA cycle. The TCA cycle is shown in its simplest form in Equation 1-3 (Berg *et al.*, 2011).

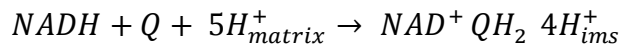


Equation 1-3 TCA cycle overview

NADH and FADH₂ generated from the TCA cycle donate electrons to respiratory chain Complexes I and II which are shuttled to Complexes III and IV with the eventual formation of molecular oxygen. Shuttling electrons across the respiratory complexes allows the transport of protons from the mitochondrial matrix to the intermembrane space, setting up the H⁺ electrochemical potential gradient, allowing Complex V (ATP synthase) to convert ADP and P_i into ATP (Berg *et al.*, 2011). This is depicted in Figure 1-2.

1.4.1.1 Complex I

Complex I, aka NADH: ubiquinone oxidoreductase, comprises ~39 subunits, 7 of which are encoded by the mitochondrial genome (Hirst *et al.*, 2003). Three modules exist within Complex I (N, Q and P), each having a different function. Module N is where NADH is oxidised, resulting in the release of 2 electrons which are then donated to the flavin mononucleotide (FMN) (Walker, 1992). The Q module comprises a chain of Fe-S clusters, allowing the electrons to pass through leading to the eventual reduction of ubiquinone (Q) to ubiquinol (QH₂), adding to the QH₂ pool (Sazanov, 2007). It is thought that Module P undergoes a conformational change in response to electron shuttling, allowing 4H⁺ ions to flow from the matrix into the intermembrane space (Efremov *et al.*, 2010; Baradaran *et al.*, 2013). The simple function of Complex I is shown in Equation 1-4.

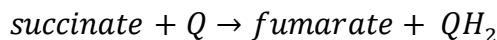


Equation 1-4 Complex I reaction

1.4.1.2 Complex II

Complex II, aka Succinate ubiquinone oxidoreductase, comprises 4 subunits, all encoded by the nuclear genome. SDHA and SDHB are located within the matrix, containing the catalytic

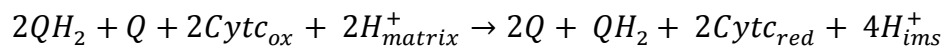
domain, with SDHC and SDHD attaching the whole complex to the inner mitochondrial membrane (Hagerhall, 1997). Complex II is part of the TCA cycle as it converts succinate into fumarate, with FADH₂ generated as a result. FADH₂ is oxidised to FAD⁺ with the donated electrons being shuttled via Fe-S clusters leading to the reduction of Q to QH₂ (Hagerhall, 1997). The simple function of Complex II is shown in Equation 1-5.



Equation 1-5 Complex II reaction

1.4.1.3 Complex III

Complex III, aka Ubiquinol: cytochrome *c* oxidoreductase, comprises 11 subunits, 1 of which is encoded by the mitochondrial genome. Complex III receives electrons from QH₂ via haem containing cytochromes and the Rieske Fe-S cluster (Xia *et al.*, 1997). The transfer of electrons from QH₂ is coupled with the translocation of 2H⁺ from the matrix to the intermembrane space (Mitchell, 1976). When QH₂ is bound to the Q₀ site, two electrons and two protons are released. One electron binds the Rieske Fe-S cluster with subsequent shuttling to cytochrome *c*₁ and then to cytochrome *c* which is released upon reduction. The remaining electron is shuttled to cytochrome *b* and then the haem groups before Q is reduced to semiubiquinone (Q[·]) at the Q₁ site. Subsequently, the Q₀ site binds another QH₂, releasing two electrons and two protons. Again, one electron is eventually transferred to cytochrome *c*, however the second electron is used to further reduce Q[·] to Q (Berg *et al.*, 2011). The Q cycle is integral for the shuttling of electrons between respiratory chain complexes. The simple function of Complex III is shown in Equation 1-6.

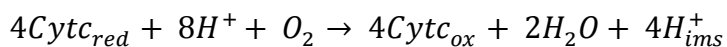


Equation 1-6 Complex III Q cycle

1.4.1.4 Complex IV

Complex IV, aka Cytochrome *c* oxidase, comprises 13 subunits, 3 of which are encoded by the mitochondrial genome. Complex IV is responsible for the reduction of molecular oxygen (O₂) into water (H₂O). Cytochrome *c* donates electrons to Cu_A and then to haem that are then

shuttled to haem_{a3} and CuB (Tsukihara *et al.*, 1996; Faxen *et al.*, 2005). There are two stages of electron transfer for the formation of H₂O and, each stage requires 2 electrons from 2 cytochrome *c* molecules. The first stage sees one electron reducing haem_{a3} and the other reducing CuB. With O₂, a peroxide bridge is established between haem_{a3} and CuB (Faxen *et al.*, 2005). The second stage is similar to the first, however the metal groups are bound by 2H⁺ ions, therefore electron transfer releases the peroxide bridge and two H₂O molecules are formed. 4 shuttled electrons results in the translocation of 4H⁺ and the production of H₂O (Faxen *et al.*, 2005). The simple function of Complex IV is shown in Equation 1-7.



Equation 1-7 Complex IV reaction

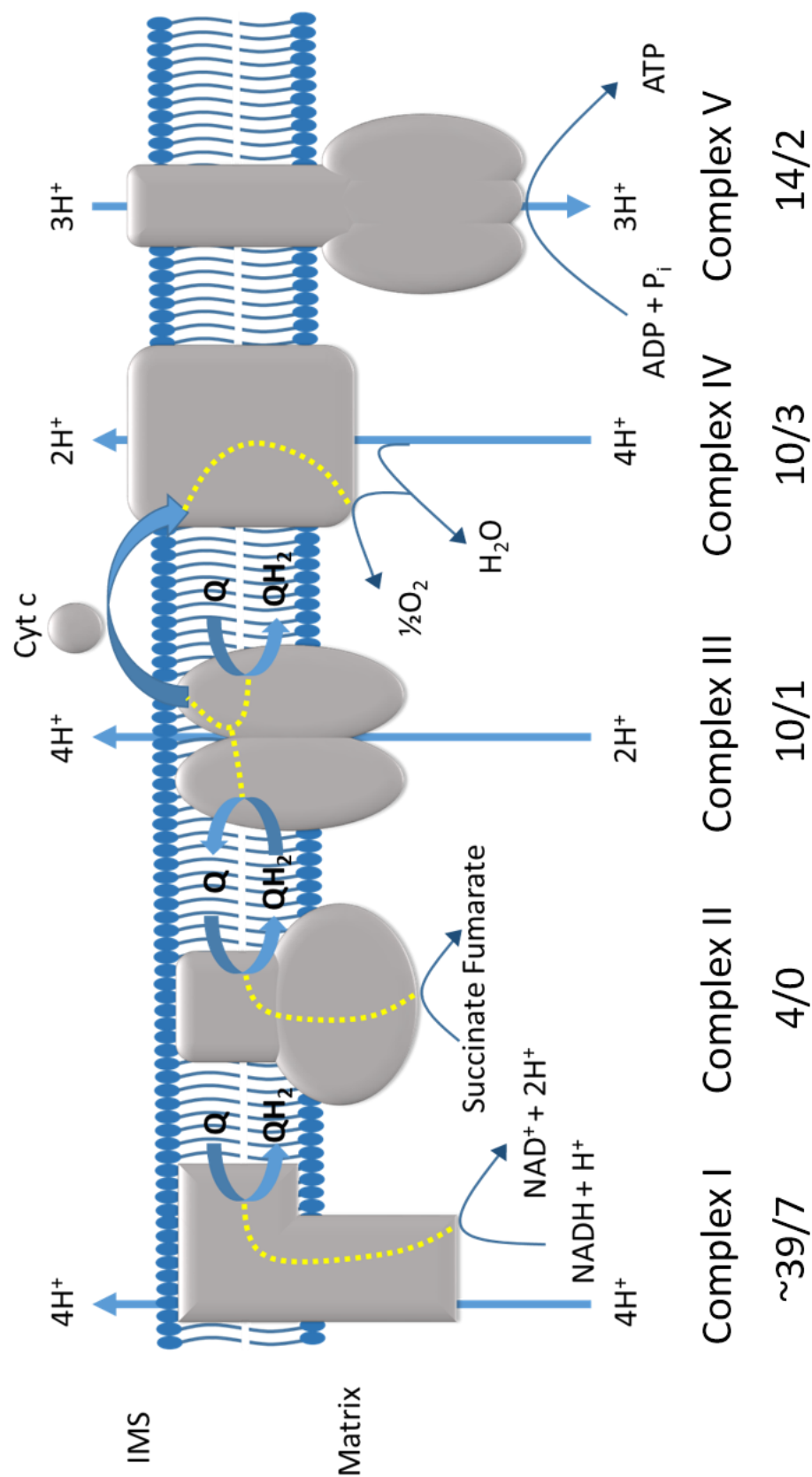
1.4.1.5 Complex V

Complex V, aka F_oF₁ ATP synthase is comprised of 16 subunits, 2 of which are encoded by the mitochondrial genome. Its main function is to synthesise ATP using the H⁺ electrochemical potential energy set up by the translocation of H⁺ ions across the IMM from the matrix to the intermembrane space by Complexes I, III and IV. Complex V is comprised of two domains, the F_o domain, which is fixed within the membrane, and the F₁ domain, which is anchored within the matrix (Yoshida *et al.*, 2001). The F_o domain is made up of 8 hydrophobic c subunits, which form a c ring, allowing protons to pass from the intermembrane space back into the matrix. The F₁ domain is made up of five subunits in total (α , β , γ , δ and ϵ), with 3 α and 3 β subunits making up the stationary ring, and the γ , δ and ϵ subunits constituting the rotary stalk (Wittig and Schagger, 2008; Wittig *et al.*, 2008).

The flow of H⁺ ions through the F_o domain provides the molecular torque necessary for the c ring to rotate about the central stalk. Protonation and deprotonation of glutamate residues within c ring subunits result in the conformational changes required to drive the rotation of α and β subunits of the F₁ domain, allowing the formation of ATP from ADP and P_i (Noji *et al.*, 1997). One full rotation of the c ring allows 8H⁺ ions to pass through, with the formation of 3 ATP molecules (Watt *et al.*, 2010; Berg *et al.*, 2011).

Figure 1-2 Oxidative phosphorylation

Respiratory chain complexes that perform oxidative phosphorylation are located within the inner mitochondrial membrane (IMM). The dotted yellow line shows the path that donated electrons take after they've entered the respiratory chain complexes via Complexes I and II. Electron transport provides the energy for protons to be shuttled across the IMM from the matrix to the inner mitochondrial membrane in order to maintain the electrochemical gradient. Complex V, also known as ATP synthase, uses the electrochemical gradient with the flow of protons from a region of high concentration to a region of low concentration, providing the energy for a conformational change, resulting in ATP synthesis. The number of nuclear encoded mtDNA encoded subunits for each complex has been highlighted underneath each complex. Figure based on (Nijtmans, 2004).



1.4.2 Iron-sulphur cluster biogenesis

Fe-S cluster biogenesis and haem synthesis are carried out within the mitochondrial matrix as the majority of intracellular iron contributes towards the electron transport chain, in particular, within the assembly of Complexes I and III (Schultz and Chan, 2001; Wang and Pantopoulos, 2011). Mitoferins transport reduced iron (Fe^{2+}) into the mitochondrial matrix (Paradkar *et al.*, 2009). Mitochondrial proteins such as Isu1/2, Grx5 and Abcb7 are essential for the formation of Fe-S clusters (Wang and Pantopoulos, 2011). Cysteine desulphurase is the enzyme that releases sulphide ions from cysteine residues for their integration into Fe-S clusters (Tong and Rouault, 2000). There are 12 unique Fe-S clusters which are able to carry electrons, contributing to the function of the electron transport chain with their ability to switch between Fe^{2+} and Fe^{3+} redox states (Schultz and Chan, 2001).

1.4.3 Apoptosis

Apoptosis, also known as programmed cell death, can be triggered by either cell surface receptors or cell damage mediated pathways. Once apoptosis is triggered, this leads to the eventual release of cytochrome *c* from mitochondria. Once cytochrome *c* has been released, it binds with APAF1 to form an apoptosome, activating caspase-9, resulting in the death of the cell (Wang and Youle, 2009). Pro-apoptotic Bcl2 and anti-apoptotic BH3 families of proteins are integral for the prevention and regulation of programmed cell death (Willis *et al.*, 2007). Bax and Bak are members of the Bcl2 family, and when activated, they locate to the outer mitochondrial membrane causing cytochrome *c* release (Wei *et al.*, 2001). Under normal conditions, proteins of the BH3 family inhibit Bcl2 proteins from triggering apoptosis via cytochrome *c* release (Willis *et al.*, 2007).

1.4.4 ROS production

Mitochondria are known to be a major source of reactive oxygen species (ROS) within cells, primarily at the sites of Complex I and III within the electron transport chain (Turrens and Boveris, 1980; Sugioka *et al.*, 1988). Superoxide radicals (O_2^-) are produced at these sites when stray electrons reduce O_2 (Starkov, 2008). Loschen and colleagues showed that hydrogen peroxide (H_2O_2) accumulation, which is produced through the reduction of O_2^- by superoxide dismutase II within the mitochondrial matrix (Brand, 2010), was linked to the rate of OXPHOS respiration within isolated pigeon heart mitochondria (Loschen *et al.*, 1972). ROS cause oxidative stress within cells by damaging macromolecular complexes such as

DNA, proteins and lipids. However, ROS have also been shown to be involved in cellular signalling pathways, impacting on highly regulated cell functions such as differentiation, proliferation, autophagy, senescence and apoptosis (Valko *et al.*, 2007).

1.4.5 Calcium homeostasis

Mitochondria act as the intracellular Ca^{2+} buffers, being able to absorb 1000nmol Ca^{2+}/mg mitochondrial mass (Kirichok *et al.*, 2004). Ca^{2+} concentrations need to be highly regulated as Ca^{2+} can cause perturbations to a variety of cellular functions, including inter-cell communication, apoptosis and ATP generation (Duchen, 2000). Ca^{2+} plays an important role at presynaptic terminals; therefore mitochondrial Ca^{2+} buffering is crucial for the correct transmission of nerve impulses (Jacobson and Duchen, 2004; Abramov and Duchen, 2010). Exercise has been shown to increase Ca^{2+} signalling within skeletal muscle cells which impacts on the rate of mitochondrial biogenesis as previously described (section 1.3.3) (Herzig *et al.*, 2001). It also increases the rate at which intermediary metabolic substrates are generated from the TCA cycle and the rate at which ATP is produced through OXPHOS (McCormack *et al.*, 1990; Jouaville *et al.*, 1999).

1.5 MITOCHONDRIAL GENOME

Mitochondria contain multiple copies of a ~16,569bp circular genome located within the mitochondrial matrix. The mitochondrial genome encodes a total of 37 genes, 13 of which contribute protein subunits towards the OXPHOS complexes. It also encodes 22 tRNAs and 2 rRNAs to enable OXPHOS subunit expression (Anderson *et al.*, 1981). The remaining ~77 proteins required for OXPHOS are encoded by the nuclear genome and are translated within the cytosol and imported into the mitochondria; therefore mitochondria have to rely on both their own genome and the nuclear genome to carry out their function (Anderson *et al.*, 1981). Unlike the nuclear genome, the mitochondrial genome does not contain introns (Anderson *et al.*, 1981). Figure 1-3 is a schematic of the mitochondrial genome, indicating the location of each gene.

The number of mtDNA copies that exist within a cell is dependent on the cell type. Female germline oocytes contain ~100,000 copies of mtDNA, with approximately 1-2 mtDNA molecules present within each mitochondrial organelle (Shoubridge and Wai, 2007). A typical somatic cell has been suggested to contain >1000 copies of mtDNA (Lightowers *et*

al., 1997). However, adult stem cells are postulated to contain ~250 mtDNA molecules due to their small size and high nuclear: cytoplasmic ratio (Coller *et al.*, 2001).

MtDNA content within a cell is linked to energy consumption requirements, therefore cells with a high energy demand, such as muscle and nerve cells, will require the most mtDNA (Shoubridge and Wai, 2007). Super resolution EM has provided evidence to suggest mtDNA cluster as a nucleoprotein complex, which includes proteins necessary for mtDNA replication, transcription and translation, for instance, single stranded DNA binding protein, twinkle helicase and mitochondrial transcription factor A (Garrido *et al.*, 2003; Wang and Bogenhagen, 2006; Brown *et al.*, 2011).

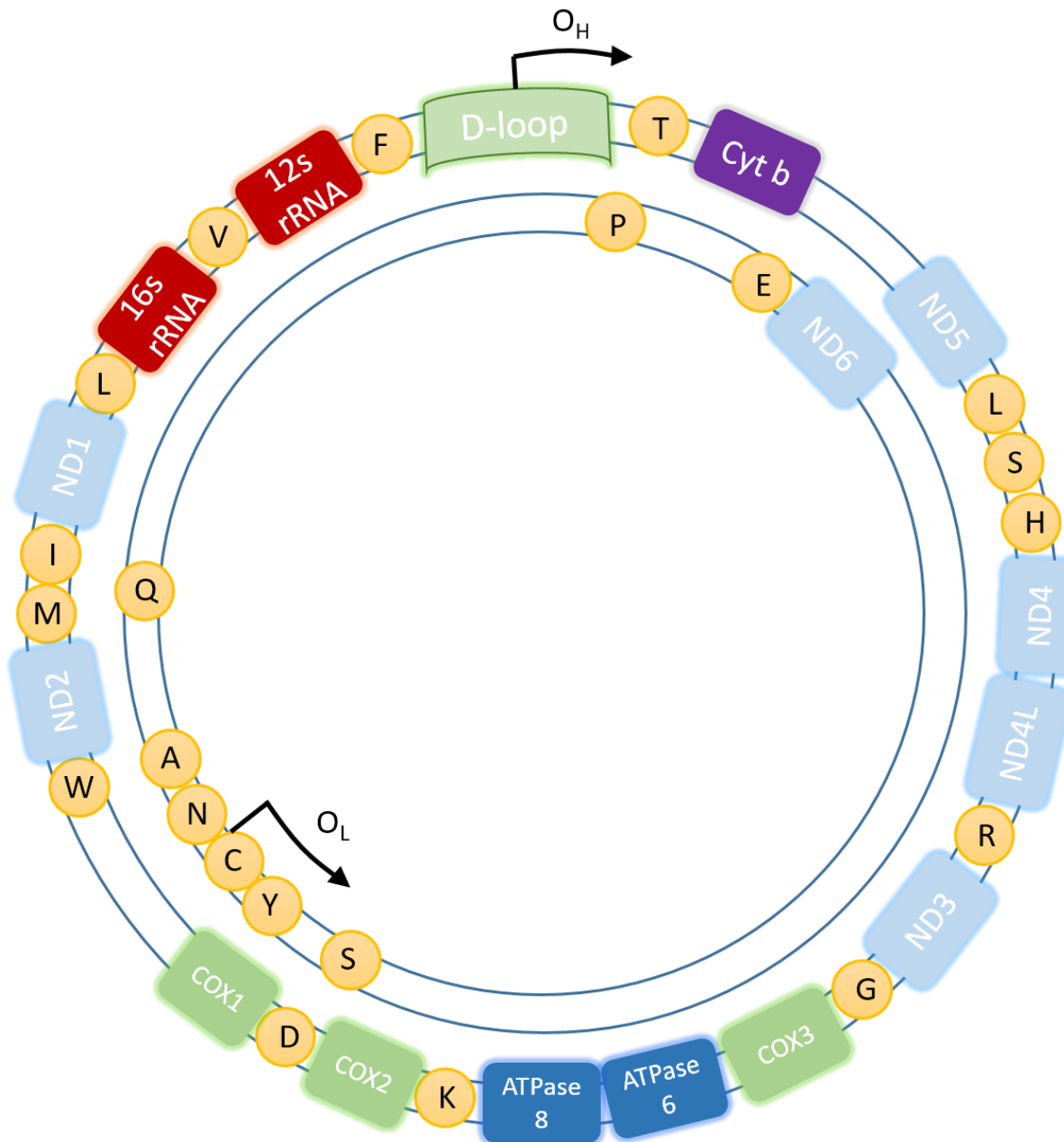


Figure 1-3 The human mitochondrial genome

Human mtDNA is a ~16.6kb circular molecule with both heavy (outer) and light strands (inner) encoding genes. MtDNA encodes 37 genes, 13 protein encoding genes, 2 rRNAs and 22 tRNAs. Protein encoding genes include 5 subunits of Complex I (ND1-5), 1 subunit of Complex III (CytB), 3 subunits of Complex IV (COX1-3), and 2 subunits of Complex V (ATPases 6 and 8). Orange circles with letters in represent the 22 encoded tRNAs. The only non-coding region is the D-loop, where the origin of heavy strand replication (O_H) is located. The origin of light strand replication (O_L) is also shown. Image has been adapted from (Taanman, 1999).

1.5.1 MtDNA transcription

The mitochondrial genome contains three promoter regions that initiate transcription, two heavy strand promoter (HSP) regions (H1 and H2) initiate the transcription of the heavy strand and one light strand promoter (LSP) initiates the transcription of the light strand. The result is a bi-directional transcription of the heavy and light mtDNA strands. The H1 promoter site transcribes the genes encoding both rRNAs and tRNA^{Phe} and tRNA^{Val}. The H2 promoter site transcribes almost the remainder of the heavy strand, thereby producing 2 polycistronic transcripts, one short and one long (Montoya *et al.*, 1982; Chang and Clayton, 1984; Zollo *et al.*, 2012). The polycistronic transcripts are then processed via RNA processing enzymes which target tRNA cloverleaf folds, this is known as the tRNA punctuation model (Ojala *et al.*, 1981). Once the RNase processing enzymes have cleaved the polycistronic transcript, secondary RNase enzymes cleave the 5' and 3' ends of the tRNAs (Dubrovsky *et al.*, 2004; Holzmann *et al.*, 2008).

The mitochondrial transcription machinery is made up of mitochondrial RNA polymerase (POLMRT), mitochondrial transcription factor A (TFAM), and mitochondrial transcription factor B2 (TFB2M), all of which allow mtDNA transcription to be carried out (Falkenberg *et al.*, 2002; Litonin *et al.*, 2010). TFAM is thought to unwind mtDNA promoter regions, allowing POLMRT to initiate transcription (Fisher *et al.*, 1992), however there is some debate as to how essential TFAM is, with the absence of the yeast homolog of TFAM not being required for transcription initiation (Xu and Clayton, 1992). ChIP-seq experiments in fact show that TFAM may be much more important in mtDNA packaging for the formation of the nucleoprotein complex as it appears to bind the whole of the mitochondrial genome (Wang *et al.*, 2013). POLMRT forms a heterodimer with TFB2M in order for transcription to occur; with TFB2M stabilising single stranded DNA (ssDNA) formed during unwinding before transcription can progress (Falkenberg *et al.*, 2007). Once the mitochondrial transcription machinery has transcribed the polycistronic mRNA, mitochondrial termination factors are required. There are four proteins that are believed to have roles in the termination of mitochondrial transcription (mTERF1-4) (Falkenberg *et al.*, 2007). mTERF1 is believed to bend, unwind and melt the DNA duplex followed by base flipping for termination to be carried out (Yakubovskaya *et al.*, 2010). mTERF2-4 are not as well understood, however mTERF2 is hypothesised to be a positive regulator of transcription, with the binding of mTERF3 at the D-loop acting as a transcriptional repressor (Rebelo *et al.*, 2011).

1.5.2 MtDNA translation

Mitochondria are responsible for the translation of their own mitochondrial DNA encoded proteins. They have a unique set of 22 tRNAs which have distinct codon:anti-codon pairings from those founds within the nucleus, and they also have their own rRNAs (12S and 16S) that contribute to the ribosomal translation machinery (Anderson *et al.*, 1981; Bibb *et al.*, 1981). It is assumed that mtDNA translation is similar to bacterial translation with the three main stages being initiation, elongation and termination (Smits *et al.*, 2010). Mammalian mitochondrial tRNAs are similar to cytosolic tRNAs as they form the characteristic cloverleaf structure with 4 stems and 3 loops (i.e. an acceptor stem, a dihydrouridine stem/loop, a TΨ stem/loop and an anticodon stem/loop). The mammalian mitochondrial translation machinery (the mitoribosome) consists of a small 28S subunit, a large 39S subunit and two mitochondrial rRNAs (12S and 16S) and is located within the mitochondrial matrix (Smits *et al.*, 2010). Mammalian mitoribosomes differ to cytosolic ribosomes in that they have a decreased rRNA: protein ratio (Smits *et al.*, 2010). As with most functions of the mitochondria, translation still requires nuclear encoded initiation factors such as aminoacyl-tRNA synthetases and methionyl tRNA transformylase, in addition to elongation and termination factors (Smits *et al.*, 2010).

Translation initiation within mitochondrial genes occurs at AUA and AUU codons within the mRNA, which is in contrast to nuclear encoded genes where translation initiation occurs at the AUG codon instead, highlighting the differences between cytosolic and mitochondrial translation systems (Anderson *et al.*, 1981). Translation termination within mitochondrial genes occurs at UAA and UAG codons within the mRNA which is recognised by the mitochondrial termination factor 1a (mtRF1a), triggering the release of the peptide chain and the mRNA from the ribosome (Barrell *et al.*, 1980; Anderson *et al.*, 1981). It has previously been reported that mtRF1a is sufficient for the termination of all 13 ORFs within mammalian mitochondria (Temperley *et al.*, 2010). Evidence suggests that ribosome stalling at AGA or AGG triplets, due to the absence of tRNAs that recognise these codons, leads to a -1 frameshift that promotes non-canonical translation termination, allowing the synthesis of all 13 polypeptides for integration into the OXPHOS complexes (Temperley *et al.*, 2010).

1.5.3 MtDNA replication

1.5.3.1 *MtDNA replication machinery*

Mitochondrial DNA replication requires the expression of the replication machinery from the nuclear genome. The replication machinery is made up of mtDNA polymerase γ (Poly γ), single stranded DNA binding protein (mtSSB), and the mitochondrial TWINKLE DNA helicase (Falkenberg *et al.*, 2007). Replication is orchestrated from the D-loop located at the origin of heavy strand replication (O_H). Poly γ is the mitochondrial DNA polymerase and comprises the 140kDa catalytic PolyA domain and the 55kDa accessory subunit PolyB domain, forming a heterodimer (PolyAB₂) that performs the replication of mtDNA as shown in Figure 1-4 (Gray and Wong, 1992; Yakubovskaya *et al.*, 2006). The catalytic domain (PolyA) also has 3'-5' exonuclease activity, thereby providing a replication proofreading function (Pinz and Bogenhagen, 1998; Kaguni, 2004). The accessory subunit domain (PolyB) binds double stranded mtDNA, enhancing the catalytic activity of PolyA (Kaguni, 2004). RNA primers are provided by POLRMT in order for replication to be initiated at the origin of replication sites for both the heavy (O_H) and the light (O_L) strands (Shadel and Clayton, 1997).

TWINKLE is responsible for the ATP dependent unwinding of mtDNA ahead of Poly in the 5' to 3' direction as can be seen in Figure 1-4 (Korhonen *et al.*, 2003). Once unwound, a ~14kDa single stranded DNA binding protein (mtSSB) stabilises the single stranded DNA for uninterrupted replication, increasing the processivity of Poly (Kaguni, 2004). Even though Poly γ , TWINKLE and mtSSB form the essential apparatus for mtDNA replication, other proteins are involved, for instance, Ribonuclease H1, which removes primers from the origin of replication sites (Cerritelli *et al.*, 2003), and also mitochondrial topoisomerase (TOP1mt)

which reduces the torsional force that is created during replication (Zhang *et al.*, 2001).

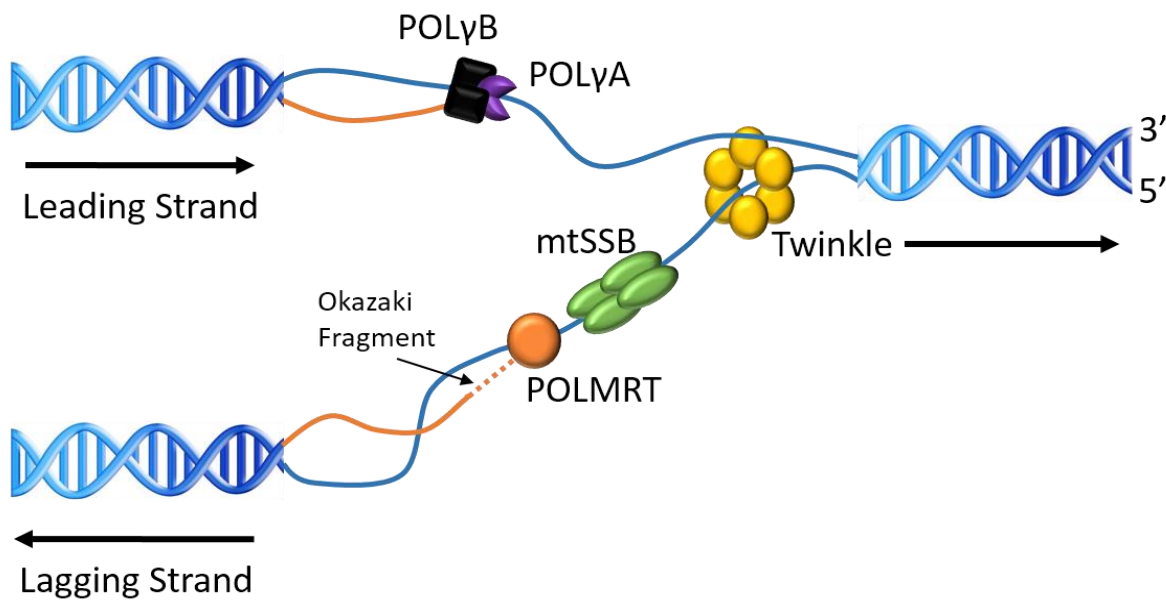


Figure 1-4 MtDNA replication machinery

TWINKLE unwinds double stranded mtDNA, creating a replication fork travelling in the 3' to 5' direction. Single stranded DNA binding proteins (mtSSB) stabilise the single stranded DNA, allowing Poly (PolyAB₂) to carry out mtDNA replication.

1.5.3.2 *MtDNA replication models*

There are two models of mtDNA replication that have been proposed, with experimental evidence supporting both. One is termed the asynchronous strand displacement model (Clayton, 1982) and the other is termed the synchronous model (Holt *et al.*, 2000).

The asynchronous strand displacement model suggests that leading heavy strand replication starts at the O_H site, due to the presence of RNA primers from transcription, and proceeds two-thirds around the genome until it reaches the O_L site, which becomes exposed as single stranded DNA. The presence of single stranded DNA at the O_L site allows the replication machinery to bind to the light strand, allowing replication to commence for the lagging strand. MtDNA replication then proceeds to completion for both the leading (heavy strand) and the lagging (light strand) (Clayton, 1982). Once replication is complete, mtDNA is circularised via ligation and supercoils are introduced via mitochondrial topoisomerases (Clayton, 1982). Evidence suggests that mammalian mtDNA replicates itself in ~90 minutes (Clayton, 1982).

The synchronous model suggests that replication of the leading (heavy strand) and the lagging (light strand) occur simultaneously, as evidence shows the existence of replication intermediates that are resistant to single stranded nuclease digestion (Holt *et al.*, 2000). Therefore, the lagging strand would have to generate multiple Okazaki fragments which would have to be processed before a newly synthesised mtDNA molecule was completed (Holt *et al.*, 2000). Within vertebrates, a method known as RITOLS (ribonucleotide incorporation throughout the lagging strand) has been suggested as the method that allows synchronous strand replication (Yasukawa *et al.*, 2006). RNA fragments of various length bind to the lagging strand, which are eventually processed into DNA before mtDNA completion (Yasukawa *et al.*, 2006).

1.6 MITOCHONDRIAL GENETICS

1.6.1 Heteroplasmy

As there are multiple copies of mtDNA molecules within cells, different species of mtDNA can exist within the same cell. Different species can be classed as polymorphic or pathogenic variants. A cell with a mixture of mtDNA variants is termed heteroplasmic. Percentage heteroplasmy is determined by the fraction of mutated mtDNA within a cell. Changes in heteroplasmy can lead to a cell that comprises purely mutated mtDNA, this is termed homoplasmy (Taylor and Turnbull, 2005).

A good example of how heteroplasmy can change significantly between generations is provided by experiments conducted on Holstein cows, which have been shown to harbour two mitochondrial genotypes (one with a polymorphic variant) (Hauswirth and Laipis, 1982). It was shown that a cow with 35% heteroplasmy gave rise to offspring that had lost the mutant mitochondrial genotype, or had heteroplasmy levels ranging between 20-80% (Ashley *et al.*, 1989).

1.6.2 Clonal expansion

Clonal expansion is the term that describes the gradual increase in one mutant mtDNA species within an individual cell over time. Several hypotheses have been proposed to explain clonal expansion. MtDNA molecules with a deletion mutation were postulated to have an advantage over wild type mtDNA molecules as they are shorter and so take less time to replicate, enabling their clonal expansion (Wallace, 1992). However, this would not explain the clonal expansion of mtDNA point mutations, for instance the m.3243A>G mtDNA

mutation within cybrid cell lines that was also shown to clonally expand (Yoneda *et al.*, 1992). In an effort to explain the clonal expansion of mtDNA point mutations, the “sick mitochondria” theory was postulated. This theory states that mitochondria with a high mtDNA mutation load proliferate quicker to negate the effects of their deficiency, enabling the clonal expansion of both deletion and point mutations within cells (Yoneda *et al.*, 1992).

The assumption that an advantage was required to allow mutated mtDNA molecules to clonally expand with cells was tested (Elson *et al.*, 2001). Random genetic drift was simulated, which describes a pool of mtDNA molecules, containing both normal and mutated mtDNA, having an equal chance of replicating over time. This was simulated for post-mitotic cells with parameters including: number of mtDNA molecules per cell (1000), number of cells simulated (600) and mtDNA half-life (10 days). For every degraded mtDNA, a randomly chosen mtDNA molecule was replicated with a copy error probability associated with it (5×10^{-5} mutated mtDNA per mtDNA replication). With these parameters, mutated mtDNA were able to clonally expand. It was also shown that those mutations occurring earlier were able to clonally expand to higher heteroplasmy levels (Elson *et al.*, 2001). This indicates that clonal expansion of mutated mitochondrial genomes may be simply subject to random genetic drift and that mutations occurring during development and early adulthood may have greater significance in later life.

1.6.2.1 *Threshold effect*

As there are many mtDNA molecules within cells, there exists a high level of functional redundancy whereby wild-type mtDNA is able to compensate for the presence of mutated mtDNA (Sciacco *et al.*, 1994). Before a cell displays a functional deficit, a threshold level of mutation must be surpassed. This is exemplified within Figure 1-5. The threshold level is dependent on the type of mutation present, for instance 60% for mtDNA deletions, ~85% for mtDNA point mutations and ~90% for tRNA mutations (Boulet *et al.*, 1992; Chomyn *et al.*, 1992; Sciacco *et al.*, 1994). However, the threshold level will always be dependent on the specific type of mutation present, for instance some tRNA mutations require only a 7% mutant fraction before a cell displays a deficient phenotype (Alston *et al.*, 2010).

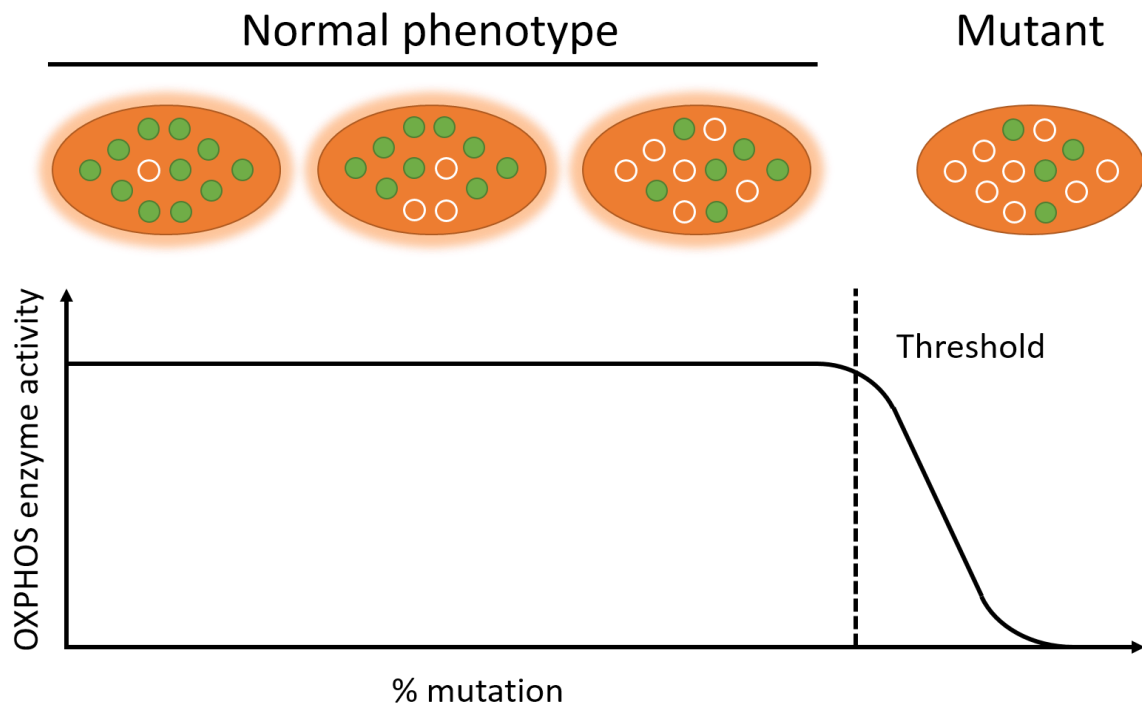


Figure 1-5 MtDNA heteroplasmy and the threshold effect

The fraction of mutated mtDNA molecules determines the heteroplasmy level within individual cells. Wild type mtDNA (green circles) compensate for the mutated mtDNA (white circles) to maintain normal OXPHOS activity. This is true up until a threshold level is reached, at which point OXPHOS activity is compromised and the cell will have a mutant phenotype. The threshold level will be determined by the type of mutation that is present within the cell.

1.6.3 Mitotic segregation

Mitotic segregation is another mechanism that can permit the clonal expansion of mutated mtDNA within a population of dividing cells. With the example of stem cell divisions, in order for daughter cells to maintain the same number of mtDNA as the stem cell, the mtDNA population is required to double. If there are mutations within the stem cell pool before division, replication of the mtDNA pool is likely to increase the number of mutated mtDNA molecules. Upon stem cell division, one daughter cell may get more, less, or the same number of mutated mtDNA as the original stem cell, thereby allowing clonal expansion to occur. This mechanism is exemplified within Figure 1-6. Clonal expansion via mitotic segregation was modelled computationally and was successfully fitted to experimental data from normal buccal epithelial cells and tumour cells (Coller *et al.*, 2001). It is likely that a

combination of random genetic drift and mitotic segregation contribute towards the clonal expansion of mutated mtDNA (Coller *et al.*, 2001; Elson *et al.*, 2001).

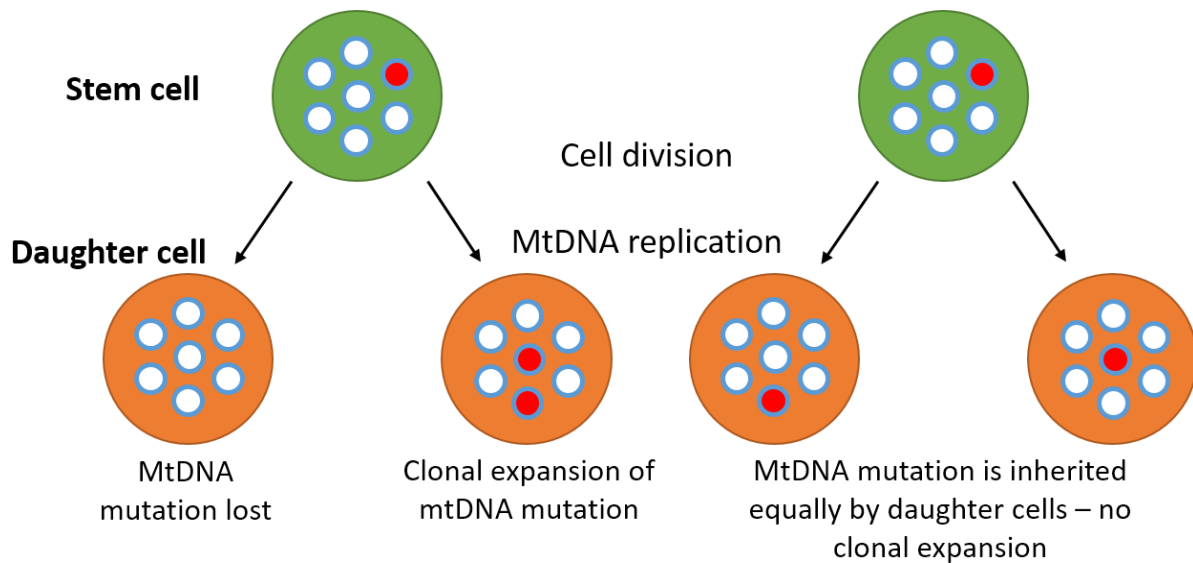


Figure 1-6 Mutated mtDNA clonal expansion via mitotic segregation

Mitotic tissues permit clonal expansion of mutated mtDNA via random segregation upon division. As stem cells are the only cells that persist within the tissue for substantial periods of time, it is likely that mutated mtDNA clonally expand purely within the stem cell pool, with increasing and decreasing heteroplasmy levels subject to the retention and disappearance of mutated mtDNA from the stem cell pool upon division.

1.6.4 Maternal inheritance

Mammalian mtDNA is inherited strictly through the maternal lineage within mammals and is therefore not subject to Mendelian inheritance unlike nuclear DNA. The number of oocyte mitochondria vastly outweighs the number of sperm mitochondria, with sperm mitochondria being degraded by proteolysis and autophagy after fertilisation (Cummins *et al.*, 1997; Moreno *et al.*, 2000; Al Rawi *et al.*, 2011). Therefore, only pathogenic mtDNA mutations can be transmitted through the maternal germline (Giles *et al.*, 1980). The transmission of pathogenic mutations through the germline can be rather complex as there exists a restriction amplification step during oocyte maturation, termed the genetic “bottleneck”. This involves mtDNA within primordial germ cells being selectively segregated into each primary oocyte, with subsequent amplification of mtDNA during oocyte development (Taylor and Turnbull, 2005). If pathogenic mtDNA mutations are present within the germline, this leads to substantial heteroplasmy variability in the offspring. It is likely that the genetic bottleneck

evolved in an effort to reduce the likelihood of pathogenic mtDNA mutations being transmitted through the germline (Fan *et al.*, 2008; Stewart *et al.*, 2008).

1.7 AGEING

Ageing has been described as the accumulation of molecular and cellular damage that leads to diminished fecundity with an increased likelihood of death (Kirkwood, 2008). As the human population is transitioning to a more elderly demographic, the social and economic challenges society faces have never been so demanding. Ageing research not only aims to understand the causes of ageing and why it makes us more susceptible to disease, it also aims to provide the means for people to live healthier lives for longer, benefiting both the individual and their impact on society. There are a number of theories proposed to explain why we age, these can be classed into two categories: evolutionary and molecular. However, it is unlikely that one theory can explain ageing as a whole as it may be that ageing is in fact an emergent multi-factorial process.

1.7.1 Evolutionary theories of ageing

As different species have different lifespans, with the subtle differences between species being determined by their genomes, this suggested that ageing was also under the control of the genome and that it was in fact programmed (Finch and Tanzi, 1997). The influence of the genome on ageing has laid the foundation for evolutionary theories postulated over the years. It was first suggested by August Weismann in 1889 that there was an ‘ageing gene’ that existed in order to maintain the population size of a species. It was later suggested by Medawar in 1952 that ageing was driven by the accumulation of deleterious mutations throughout life, leading to a progressive ageing phenotype (Medawar, 1952). Whether ageing is programmed or not, it is still likely that genes influence the ageing process. The Antagonistic Pleiotropy theory is a recurrent concept within the ageing field, stating that the selection of genes that favour increased reproductive advantage drives the evolution of a species, even if that gene is detrimental later on in life (Williams, 1957). The Disposable Soma theory states that ageing is brought about due to metabolic trade-offs made between reproduction, cell growth and repair within somatic cells (Kirkwood, 1977). Furthermore, it states that energy resources are allocated in favour of reproduction, leading to a lack of energy resources for cell maintenance and repair, hence driving the ageing process (Kirkwood, 1977). It makes sense that genes are more likely to be retained within a species if they increase the chance of reproduction. However, the selection of genes that are deleterious

to an organism's survival is a major source of contention for evolutionary theories of ageing (Kirkwood, 1995).

1.7.2 Molecular theories of ageing

Molecular theories of ageing state that ageing is due to the accumulation of cellular damage that takes place during normal metabolic processes within cells. Damage to DNA, telomeres, proteins, lipids, and macromolecular complexes within cells, is thought to be the cause of ageing phenotypes observed within a variety of organisms observed.

The accumulation of DNA mutations throughout life is thought to be a leading cause of cellular dysfunction which contributes to the ageing process (Szilard, 1959). This is compounded by the fact that with increasing age there is a reduced base-excision DNA repair capacity, which has been linked to the longevity of a species (Hart and Setlow, 1974). Age associated telomere damage is also thought to contribute towards the ageing process (Harley *et al.*, 1992). Telomeres are the repeat regions that exist at the end of chromosomes. Due to the end replication problem, there is a natural shortening of telomeres with each cell division event. Within embryonic stem cells and some adult stem cells, telomerase is expressed which maintains the length of the telomere, however most somatic cells do not express it. Once a telomere limit has been reached, the cell undergoes replicative senescence (Harley *et al.*, 1992). Telomere DNA damage can therefore increase the rate at which cells enter replicative senescence, leading to a functional decline within tissues, contributing to the ageing process (Harley *et al.*, 1992). Abnormal protein turnover and homeostasis can also contribute towards the ageing process (Cuervo and Dice, 2000). Abnormal peptide cross-linking during post-translational modification can cause damage to the DNA replication machinery, contributing to DNA damage (Bjorksten and Tenhu, 1990). In 1956, Harman proposed the free radical theory of ageing that suggested oxidative damage was at the centre of age related decline in function of an organism (Harman, 1956). Since then, oxidative damage has been shown to accumulate within a variety of ageing tissues (Balaban *et al.*, 2005). It is now known that ROS can cause oxidative damage to DNA, proteins, lipids and macromolecules, with OXPHOS being a major source of ROS. Therefore, what was once the free radical theory of ageing became the mitochondrial free radical theory of ageing (MFRTA) (Harman, 1972).

1.7.2.1 *The mitochondrial free radical theory of ageing*

It is now known that mitochondria are the main source of ROS production, with ~90% of total cellular ROS generated via OXPHOS (Balaban *et al.*, 2005). This leads to the accumulation of oxidative damage that has been hypothesised to contribute towards ageing (Harman, 1956; Harman, 1972). The main ROS that are generated from OXPHOS are superoxide radicals (O_2^-) and hydroxyl radicals (OH^{\cdot}). Mitochondria have adapted to the presence of O_2^- via superoxide dismutase expression within the mitochondrial matrix, attenuating the burden of ROS induced oxidative damage (McCord and Fridovich, 1969). However, OH have such a short half-life that no enzyme exists for it to be metabolised and therefore can be very damaging to the cell (Cadenas and Davies, 2000). As the mtDNA molecules are in such close proximity to the site of ROS generation, mtDNA is vulnerable to high levels of oxidative damage (Harman, 1972). It is thought that mtDNA has a high mutation rate due to the increased oxidative damage burden which results in attenuated OXPHOS function in later life (Miquel *et al.*, 1980). It is likely that attenuated OXPHOS function leads to increased electron “leakage” from the electron transport chain, increasing ROS concentrations in the cell. This is the foundation of the “vicious cycle” theory where increased ROS leads to increased mtDNA mutations leading to increased ROS (Harman, 1972). This increasing level of ROS generation and oxidative damage as a result is thought to lead to the cells eventual death (Harman, 1972).

There are a number of studies that have demonstrated a link between ROS induced oxidative damage and longevity. One study showed that there was reduced superoxide radical concentrations within the heart, liver and kidneys of species with increased lifespans (Sohal *et al.*, 1989). Another study showed that there was decreased protein oxidation within longer lived species (Agarwal and Sohal, 1996). Furthermore, it was shown that Pigeon mitochondria release 30% less hydrogen peroxide compared with mitochondria from rats, which have a ~7 year shorter lifespan. These studies provide compelling evidence to suggest mitochondria, and the ROS they produce, play a major role within the ageing process.

Due to mitochondria having such an integral role within the cell, it is likely that perturbations bestowed to the mitochondria’s function will have a significant effect on the cell as a whole and have the potential to contribute towards the ageing process.

1.7.3 Mitochondrial dysfunction and ageing

A variety of aged human tissues have been shown to display mitochondrial dysfunction in the form of focal respiratory chain deficiency for cytochrome *c* oxidase enzymatic activity (COX deficiency). This has been shown in skeletal muscle (Muller-Hocker, 1990), brain (Cottrell *et al.*, 2001), colon (Taylor *et al.*, 2003), liver (Fellous *et al.*, 2009), and stomach (McDonald *et al.*, 2008). It would seem that there is a progressive accumulation of COX deficiency with age within these tissues, as is the case within human colon (Taylor *et al.*, 2003). It has been shown that aged human cells presenting with COX deficiency harbour single clonally expanded mtDNA mutations (Brierley *et al.*, 1998). This casts doubt over the “vicious cycle” hypothesis of ROS induced mtDNA mutation accumulation as this mechanism would lead to multiple mtDNA mutations being present within aged cells. Therefore, it is more likely that the mtDNA mutations that are acquired in early life through mtDNA replication errors and oxidative damage go onto clonally expand to become the dominant species within aged cells (Elson *et al.*, 2001; Greaves *et al.*, 2014).

Interestingly, the types of mtDNA mutations that cause mitochondrial dysfunction in aged tissue are different between mitotic and post-mitotic tissues. Previous studies have shown that aged skeletal muscle fibres predominantly harbour clonally expanded mtDNA deletions (Kopsidas *et al.*, 1998). Furthermore, aged post-mitotic tissues can harbour a mosaic pattern of mtDNA deletions, with different mtDNA deletions present in different cells of the same tissue (Brierley *et al.*, 1998; Bender *et al.*, 2006; Kraytsberg *et al.*, 2006). This is in contrast to mitotic tissues, for instance aged colon, which predominantly harbour clonally expanded point mutations (Taylor *et al.*, 2003; Greaves *et al.*, 2006; Greaves *et al.*, 2010). There are a number of reasons as to why this may be the case. For instance, it may reflect alternate mechanisms of clonal expansion between mitotic and post-mitotic tissues, even though computational modelling suggests random genetic drift is sufficient to explain clonal expansion within mitotic and post mitotic tissues (Coller *et al.*, 2001; Elson *et al.*, 2001). It could be that the post-mitotic cellular environment is more conducive for the acquisition of mtDNA deletions. On the other hand, it may be that mitotic cells (such as stem cells) have enhanced DNA repair mechanisms.

It is clear that mtDNA mutations do accumulate within post-mitotic and mitotic tissues and that these mutations go onto cause mitochondrial dysfunction as seen via focal respiratory chain enzyme deficiency. Mitochondrial dysfunction has the potential to severely affect a

cells ability to function, which can lead to cellular senescence, apoptosis and eventual tissue failure (Taylor and Turnbull, 2005). Therefore, it is vital we understand the acquisition and subsequent clonal expansion of mtDNA mutations within all cell and tissue types, as this will make it easier to identify potential methods of halting the accumulation of mitochondrial dysfunction within ageing tissues.

1.7.4 Mouse models of mitochondrial dysfunction

Mouse models are an important tool which are used to try and understand the link between mitochondrial dysfunction and ageing. Mitochondrial abnormalities that are of relevance to ageing human tissues can be investigated in their entirety. Two such mouse models are the TFAM knockout mice (Silva and Larsson, 2002; Wredenberg *et al.*, 2006; Ekstrand *et al.*, 2007; Vernochet *et al.*, 2012) and the *PolyA* “mitochondrial mutator” mice (Trifunovic *et al.*, 2004; Kujoth *et al.*, 2005), which allow the effects of mtDNA reduction and mutagenesis to be observed.

1.7.4.1 *TFAM knockout mice*

TFAM knockout mice are one such mouse model that can be used to investigate this link. TFAM is a transcriptional activator within mitochondria and is also important for mitochondrial DNA replication (Reyes *et al.*, 2002). As such, heterozygous TFAM knockout mice (*Tfam*^(+/-)) have reduced mtDNA copy number with associated respiratory chain complex deficiency, however, homozygous TFAM knockout mice (*Tfam*^(-/-)) were embryonic lethal at embryonic day (E) 8.5 and (E) 10.5. Therefore, tissue specific TFAM knockouts were created using *cre-loxP*-mediated recombination. This was done within pancreatic β-cell specific TFAM knockout mice, where β-cells exhibited disrupted mitochondrial membrane potential along with altered calcium buffering upon Cre-recombinase induction (Silva and Larsson, 2002). Mitochondrial dysfunction within TFAM knockout mice was directly linked to reduced β-cell insulin secretion along with an increased loss of β-cells with age, resembling the acquisition of diabetes in human ageing (Silva and Larsson, 2002). A dopaminergic (DA) neuron specific knockout of TFAM was also engineered, which resulted in respiratory chain deficiency. Mice with this alteration displayed tremors, slow progressive movement, and age associated Parkinson’s disease (Ekstrand *et al.*, 2007). These studies indicate that mitochondrial dysfunction can bring about the characteristics within cells that lead to age related diseases. However, it has been shown that mitochondrial dysfunction affects different tissue types in different ways. For instance, tissue specific TFAM knockouts

in skeletal muscle (Wredenberg *et al.*, 2006) and adipose tissue (Vernochet *et al.*, 2012) do not result in age related disease. This indicates that the potential for mitochondrial dysfunction to cause age-related phenotypes is dependent on the tissue type in which it resides, adding to the complexity of how mitochondrial dysfunction contributes towards ageing within humans.

1.7.4.2 *MtDNA mutator mouse*

MtDNA mutator mice are another mouse model that can be used to investigate the link between mitochondrial dysfunction and ageing. They are associated with a progressive accumulation of mtDNA mutations along with the development of age related phenotypes. Homozygote mitochondrial mutator mice (*PolyA*^(-/-)) were generated with a knock-in missense mutation (D257A) that changes the amino acid from aspartic acid to alanine within the second proofreading domain of the PolyA catalytic subunit of the mtDNA polymerase gamma (Trifunovic *et al.*, 2004; Kujoth *et al.*, 2005). The mitochondrial mutator mouse created by Trifunovic et al has a C57Bl/6N background which includes the Flp-recombinase system, meaning the POLG gene is flanked by two loxP sites (Trifunovic *et al.*, 2004). However, the mitochondrial mutator mouse created by Kujoth et al has a C57Bl/6J background which includes a Cre-recombinase system with only one loxP site present (Kujoth *et al.*, 2005). Both mitochondrial mutator mice have an increased rate of mutation accumulation and a substantially increased rate of respiratory chain deficiency with age. Homozygote mice display an ageing phenotype from 25 weeks old which includes; weight loss, anaemia, osteoporosis, kyphosis, reduced subcutaneous fat, reduced fertility and a reduced lifespan <12 months, mirroring the phenotypes associated with human ageing (Trifunovic *et al.*, 2004; Kujoth *et al.*, 2005). The overwhelming majority of mutations that are acquired within *PolyA*^(-/-) mice are point mutations, where for every 1000 mtDNA point mutations, there is 1 mtDNA deletion (Kraytsberg *et al.*, 2009). Even though there is an increased rate of mtDNA point mutation accumulation within *PolyA*^(-/-) mice, this was originally thought not to be associated with an increasing rate of ROS production and macromolecule oxidation with age, which provided evidence against the ‘vicious cycle’ hypothesis (Trifunovic *et al.*, 2004; Kujoth *et al.*, 2005). More recent studies have started to dispute these findings with one study showing that there exists increased oxidative damage within muscle from aged *PolyA*^(-/-) mice (Kolesar *et al.*, 2014). Another study has also showed that there exists an elevated level of hydrogen peroxide within aged *PolyA*^(-/-) mice which has been hypothesised to have pro-apoptotic and pro-inflammatory effects (Logan *et al.*, 2014).

1.8 THE COLON

It is clear that mitochondrial dysfunction occurs within ageing tissues as has been previously described. However, the consequences of mitochondrial dysfunction within ageing tissues requires further investigation. As part of this thesis, the colon was used as a model tissue within both human and mouse to understand the impact of mitochondrial dysfunction on adult stem cells. The structure of the colon is unique and ideal for investigating stem cell dynamics and so is examined in greater detail below.

1.8.1 Structure of the colon

The colon is made up of four sections: the ascending, transverse, descending and sigmoid colon. Each section has four associated layers: the mucosa (epithelium containing crypts), the muscularis mucosae (thin muscle layer), the submucosa (connective tissue layer), and the muscularis externa (circular and longitudinal muscle responsible for peristalsis). The colonic epithelium is an array of millions of tubular shaped structures known as crypts. The structure of the crypt is shown in Figure 1-7.

The epithelium of the colon regenerates at an extraordinarily fast rate, this has been shown to be approximately every day within mouse and every week within humans (Potten and Loeffler, 1990). The drivers of such fast regeneration are the multipotent stem cells that are contained at the base of crypts, which are able to generate all cell lineages required for crypts to perform their function (Schmidt *et al.*, 1988; Potten, 1998). The cell lineages derived from stem cells includes: columnar enterocytes (colonocytes), goblet cells, and enteroendocrine cells (McKay, 2005). As all the cells of the crypt are derived from the stem cells at the base, any genetic mutations that exist within the stem cells will be transmitted to the progeny cells. The number of stem cells contained within colonic crypts still requires clarification due to the lack of robust stem cell markers. However, the consensus is that there is a low number of stem cells within human colonic crypts, possibly between 4 and 6 (Taylor *et al.*, 2003; Baker *et al.*, 2014). This is in good agreement with mouse studies that have shown there are ~7 stem cells within mouse colonic crypts (Kozar *et al.*, 2013).

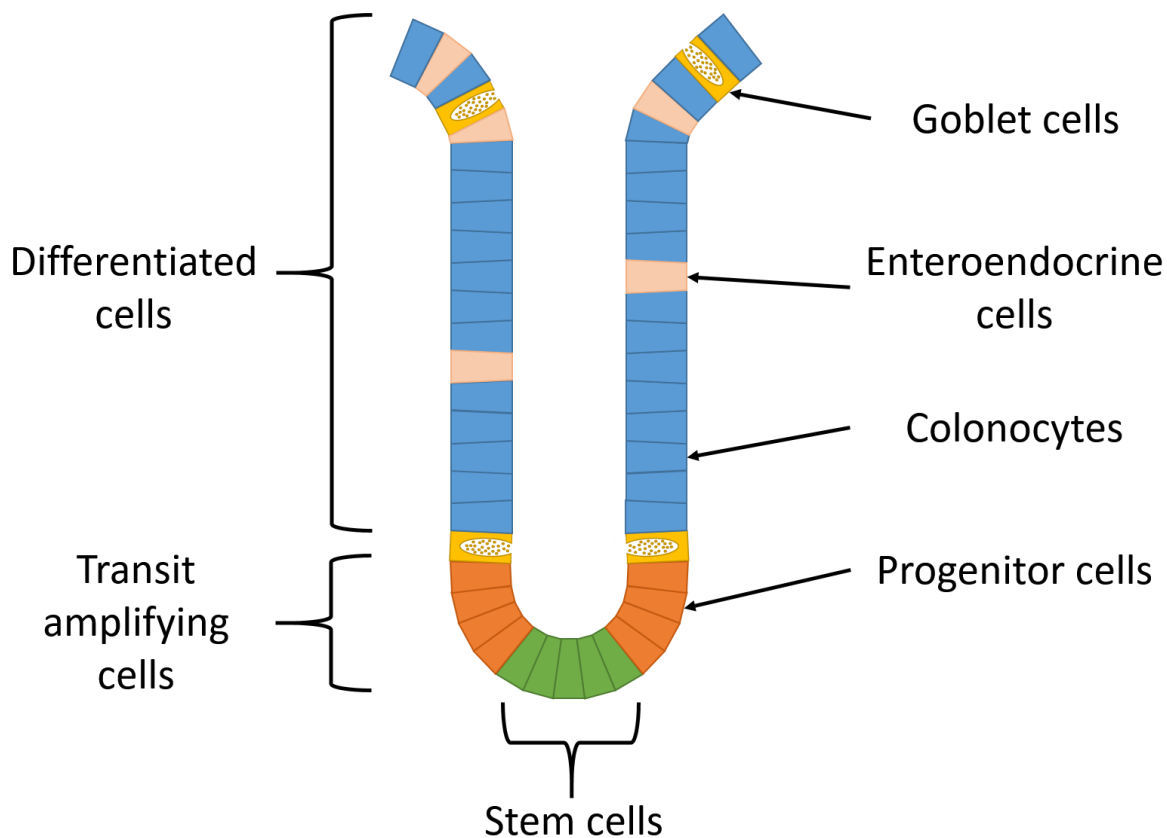


Figure 1-7 Structure of a colonic crypt

Colonic crypts are located within the mucosal layer of the colon. They contain stem cells at the base which proliferate to generate stem cell progeny transit amplifying cells that go onto generate all the cell types present within the crypt. As cells divide, they migrate up the crypt axis until they are fully differentiated (goblet cells, colonocytes or enteroendocrine cells). They continue to migrate until they are eventually sloughed off into the gut lumen.

1.8.2 Stem cell markers within crypts

Identifying the stem cells contained within crypts has been a constantly evolving area of research over the last two decades. Potten and Loeffler first described the stem cell niche within crypts as highly dynamic, with individual cells possessing definitive levels of clonogenicity, with clonogenicity highly correlated with cell position within the crypt (Potten and Loeffler, 1990). Therefore, the ability to identify stem cells within crypts was based solely on the functional characteristics of the cells in question. It is now well established that the likely origin of tumour formation within colorectal and intestinal cancers are the stem cells themselves that have undergone malignant transformation, giving birth to the term ‘cancer stem cells’ (Reya *et al.*, 2001; Li and Neaves, 2006; Vermeulen *et al.*, 2008; Barker *et al.*, 2009). Therefore, the identification of stem cell markers is not only important for

understanding stem cell biology, but could also be useful in understand the biology of cancer as well. Identifying stem cell markers within crypts requires the enrichment of highly clonogenic cells from the small intestinal and colonic epithelium, with subsequent gene expression profiling to determine what sets these cells apart. Many highly expressed genes within cells that display stem cell characteristics have been brought to light via this method.

Within mouse colon, *Lgr5*, which encodes a leucine rich repeat containing G-protein coupled receptor (*Lgr5*), was investigated due to its involvement within the Wnt pathway (contributing to a cells ability to proliferate) and its abundance within cells at the base of crypts (Barker *et al.*, 2007). The *Lgr5-EGFP-Ires-CreERT2* mouse model was engineered which allowed a lineage tracing methodology to be used to determine the characteristics of cells with highly expressed *Lgr5* (Barker *et al.*, 2007). These cells had the ability to give rise to all differentiated cells lineages over time, suggesting that cells with highly expressed *Lgr5* were the functional stem cells within colonic epithelium. This was also shown to be the case within mouse small intestinal crypts as well (Snippert *et al.*, 2010). Interestingly, another marker showed similar characteristics within small intestinal epithelium. *Bmil*, which is a member of the Polycomb group gene family and has essential roles in chromatin silencing, was found to be highly expressed within cells that were, on average, 4 cell positions above the base of the crypt, unlike cells that had highly expressed *Lgr5* which were located interspersed between Paneth cells. Using the *Bmil-EGFP-Ires-CreERT2* mouse model, these cells were also shown to give rise to all differentiated cell lineages over time (Sangiorgi and Capecchi, 2008). Furthermore, loss of *Bmil*-expressing cells lead to crypt loss, indicating them to be another subset of stem cells within the small intestinal epithelium (Sangiorgi and Capecchi, 2008). More recently, *Lgr5* and *Bmil* highly expressing cells have been identified as functionally distinct stem cell populations, postulated to provide contrasting functions to ensure homeostatic tissue maintenance (Yan *et al.*, 2012). *Lgr5* stem cells are mitotically active, ensuring normal tissue regeneration, whereas *Bmil* stem cells are mostly quiescent/slow cycling with minimal input to tissue maintenance under homeostatic conditions (Yan *et al.*, 2012). *Bmil* cells are in the same +4 position as DNA label retaining cells that have previously been located (Potten *et al.*, 1974; Potten *et al.*, 2002), indicating that label retaining cells and quiescent/slow cycling *Bmil* stem cells are one and the same. Evidence suggests that *Bmil* stem cells function as a reserve intestinal stem cell pool upon tissue injury and *Lgr5* stem cell ablation (Tian *et al.*, 2011; Yan *et al.*, 2012).

Lgr5 and Bmil stem cell populations also enrich distinct genes that can be further used for their characterisation. For instance Lgr5 stem cells enrich a Wnt target gene known as *Ascl2* (Achaete scute-like-2) which has been shown to control the Lgr5 stem cell fate, with its deletion resulting in the disappearance of Lgr5 stem cells (van der Flier *et al.*, 2009). They also enrich *Olfm4* which encodes a protein that acts as a BMP antagonist (Inomata *et al.*, 2008; Schuijers *et al.*, 2014). However, deletion of *Olfm4* does not result in any observable phenotype, questioning its potential role within Lgr5 stem cells (Schuijers *et al.*, 2014). On the other hand, Bmil stem cells enrich *Hopx* which is an atypical homeodomain containing protein (Takeda *et al.*, 2011). It was shown that Hopx expressing cells give rise to Lgr5 stem cells, but also Lgr5 stem cells give rise to Hopx/Bmil expressing label retaining cells, indicating an interconversion between the two stem cell populations (Takeda *et al.*, 2011).

At present, there is a paucity of literature about Bmil stem cells within colonic epithelium, unlike within small intestinal epithelium. However, the expression of Bmil within colorectal adenocarcinomas has been investigated in-depth with regards to the cancer stem cell hypothesis, with the inhibition of Bmil impairing the ability of colorectal cancer initiating cells from self-renewing (Kreso *et al.*, 2014). CD133+ (Prominin-1 and AC133) cells have been described as having stem cell like qualities within the colonic epithelium, able to sustain long-term tumorigenesis within NOD/SCID mice (Shmelkov *et al.*, 2008). However, it may be that this marker is not exclusive to stem cell populations and that its identification may only be possible under tumour growth conditions (O'Brien *et al.*, 2007; Shmelkov *et al.*, 2008). The mammalian Musashi-1 homolog has been shown to be localised at the base of normal colonic crypts, which may indicate its potential use as a stem cell marker (Nishimura *et al.*, 2003). Musashi is an RNA-binding protein thought to be involved in asymmetric divisions during *Drosophila* neural development (Nakamura *et al.*, 1994). It is postulated that Musashi-1 is key for asymmetric stem cell divisions within the colonic epithelium, potentially allowing the identification of stem cells within the colon (Nishimura *et al.*, 2003).

1.8.3 The stem cell niche within crypts

Multiple cellular markers have been identified within crypts which identify cells that can function as multipotent stem cells, as has been exemplified within the previous section (section 1.8.2). However, simply possessing cellular markers of stemness may not be sufficient for those cells to function as stem cells, adding to the complexity for investigating true functioning stem cells within crypts (Walther and Graham, 2014). A well accepted

school of thought now suggests that the stem cell niche is a dynamic interplay between the stem cell niche environment and the cells that occupy its space, with the goal of regenerating the crypt to maintain epithelium homeostasis (Walther and Graham, 2014).

Experiments conducted by Ritsma and colleagues suggest that for a stem cell to remain and function as a stem cell, position within the stem cell niche is key (Ritsma *et al.*, 2014). They used a novel intravital multiphoton imaging approach to track the migration of dividing Lgr5+ cells *in situ*. They classified each cell according to its initial position within the niche and saw that, upon division, cells that were closest to the base of the crypt, i.e. closest to the stem cell niche, were more likely to remain within the stem cell niche over time. As there is a competition for privileged stem cell niche space within crypts, the preferential retention of cells located in a particular position suggests extrinsic factors are contributing to stem cell homeostasis (Ritsma *et al.*, 2014). It may be that there are many cells within the crypt that have the potential to function as a stem cell but are not exposed to the correct extracellular cues that are found within the stem cell niche to enable them to do this (Ritsma *et al.*, 2014).

Experiments conducted by Hua Tain and colleagues support this idea where Lgr5+ stem cells within mice were successfully ablated using the Cre recombinase induction of human diphtheria toxin (Tian *et al.*, 2011). This would cause the temporary ablation of all Lgr5 expressing cells within the stem cell niche. The subsequent regeneration of the stem cell niche by Bmi1 expressing cells would give rise to Lgr5 expressing cells, maintaining crypt homeostasis. This suggests that the stem cell niche was providing signalling cues to the occupying cells to function as stem cells. This could be explained by the environment within the stem cell niche itself influencing the gene expression profiles of the cells present within the stem cell niche.

The stem cell niche within small intestinal crypts contains specialised cells known as Paneth cells which are interspersed between the crypt base columnar (CBC) cells that express Lgr5, i.e. the functional stem cells. These cells secrete factors EGF, TGF-alpha, Wnt3 and Notch ligand Dll4 (Sato *et al.*, 2009). These factors are known to maintain the CBC cells as intestinal stem cells, with the ablation of Paneth cells subsequently ablating the CBC cells, providing evidence to suggest that Paneth cells contribute to the small intestinal stem cell niche (Sato *et al.*, 2011).

Crypt stem cell homeostasis is mainly controlled by the Wnt and BMP signalling pathways, constituents that allow intestinal crypt organoids to be grown in culture (Sato and Clevers,

2013). A concentration gradient of Wnt isoforms exists along the crypt axis, with the highest concentrations existing within the stem cell niche (Pinto *et al.*, 2003). Once extracellular Wnt binds to the frizzled cell surface receptor, this triggers a signalling cascade which results in β -catenin locating to the nucleus and triggering the gene expression that allows for stem cell self-renewal and proliferation. Abnormal activation of β -catenin results in adenomatous polyposis coli due to aberrant stem cell proliferation.

However, Wnt signalling is not sufficient for self-renewal and proliferation of stem cells within the stem cell niche. BMP signalling inhibits stem cell renewal and proliferation by regulating PTEN activity, resulting in the inhibition of β -catenin activity within the nucleus (Scoville *et al.*, 2008). BMP isoforms are expressed within the mesenchyme, allowing the self-renewal and proliferation of stem cells to be kept in check. In order to override the BMP signalling to allow stem cell self-renewal and proliferation to take place, the BMP antagonist “noggin” is required (He *et al.*, 2004). Noggin is expressed in the submucosal region, next to the crypt base, thereby only allowing the cells in close proximity to the Noggin concentration gradient to self-renew and proliferate, making this location the true stem cell niche (He *et al.*, 2004; Scoville *et al.*, 2008). Abnormal activation of BMP represses de novo crypt formation during development (Haramis *et al.*, 2004).

From this it would appear that the stem cell niche is just as important as the stem cells themselves, with a complex inter-relationship existing via signalling molecules, cell-cell interactions, and extracellular matrix components maintaining the controlled regenerative capacity that the stem cells provide. It seems logical that not only changes in stem cell characteristics cause perturbations that can result in tissue pathology and bowel disease in later life, but also perturbations to the stem cell niche has the potential to do this as well.

1.8.4 Functions of the colon

The main responsibility of the colon is to store and compact faecal matter before it is expunged via the anus in defecation. Before this happens, water and electrolytes (Ca^{2+} , Mg^{2+}) are absorbed. End stage digestion of dietary nutrients also takes place, producing short chain fatty acids, carbon dioxide and methane (Cummings, 1975). Urea is also broken down in the colon, producing ammonia which is absorbed, and carbonic acid (Cummings, 1975). The microflora (bacteria) that exist within the colon have an important role in end stage digestion as they break down dietary fibre allowing the synthesis of vitamin K, which is important for blood coagulation (Baron, 1996). In addition to the role of nutrient absorption, the microflora

act as an important immune barrier, protecting the mucosa from harmful pathogen colonisation (Berg, 1996). This barrier function is enhanced with the secretion of mucins from goblet cells, helping the microflora to maintain a protective barrier (Johansson *et al.*, 2008). Furthermore, colonocytes and goblet cells secrete anti-microbial proteins in response to microflora colonisation, enhancing the protective barrier (Peterson and Artis, 2014). With this it is clear that the colon is highly specialised for the end stages of digestion with roles in immune defence, as well as the processing and excretion of faeces.

1.8.5 Mitochondrial dysfunction within the colon

Human colonic epithelium has been shown to accumulate mitochondrial dysfunction, in the form of COX deficiency, exponentially with age (Taylor *et al.*, 2003). Clonally expanded mtDNA point mutations have been shown to be the cause of the observed COX deficiency within human colon (Taylor *et al.*, 2003; Greaves *et al.*, 2009). Partially and fully COX deficient crypts can be observed within aged human colonic epithelium, suggesting COX deficiency as a potential stem cell lineage marker (Taylor *et al.*, 2003). In a subsequent study, the mitochondrial genome was sequenced from COX deficient crypt cells undergoing fission and also neighbouring COX deficient crypts (Greaves *et al.*, 2006). The same clonally expanded mtDNA mutation was present in the two arms of a bifurcating crypt and also in two adjacent crypts, suggesting that adjacent COX deficient crypts are clonally derived from the same founder stem cell clone and that their occurrence is via crypt fission (Greaves *et al.*, 2006). The minimal odds ratio of two adjacent crypts harbouring the same clonally expanded mtDNA point mutation by chance was calculated to be $>2.48 \times 10^9:1$ ([16,600:1 (genome size) \times 3 (possible transition mutations)]²) (Greaves *et al.*, 2006).

The effects of mitochondrial dysfunction were investigated within aged human colon biopsies (Nooteboom *et al.*, 2010). Crypt length, number of cells undergoing apoptosis, and number of proliferating cells were compared between normal and COX deficient crypts (Nooteboom *et al.*, 2010). Respiratory deficient crypts showed an ~20% reduction in the number of stem cell progeny cells actively proliferating, indicating that COX deficiency was causing small but significant changes to cellular functions which could lead to imbalanced tissue homeostasis, potentially contributing towards the ageing process (Nooteboom *et al.*, 2010).

1.8.6 Modelling stem cell dynamics within crypts

Modelling stem cell dynamics within crypts is an active area of research that aims to understand all aspects behind the niche succession phenomenon under normal and perturbed conditions. Niche succession is the ability of a stem cell clone to become dominant within its niche. This has been carried out using a variety of mathematical and stochastic computational modelling methodologies along with experimental methods for acquiring the necessary biological data.

Lopez-Garcia et al used an inducible labelling system that allowed the proliferative population within intestinal crypts to be targeted via Cre-mediated recombination within *Ahcre^{ERT}* mice. It was assumed that labelled cell clones producing partially and fully labelled crypts are derived from single proliferative cells (Lopez-Garcia *et al.*, 2010). Their aim was to determine whether the small intestinal long-lived stem cells were organised hierarchically or as an equipotent pool. A hierarchical organisation is described as having one master stem cell that gives rise to an additional pool of stem cells with a reduced proliferative potential that perform the role of regenerating the cells of the crypt (Griffiths *et al.*, 1988; Winton and Ponder, 1990). An equipotent pool of stem cells means all stem cells are equal and have the same potential to generate stem cells and stem cell progeny alike (Potten and Loeffler, 1990). Intuitively, the equipotent organisation would mean loss of one stem cell would be corrected by the duplication of another to maintain homeostasis. A scaling form mathematical equation was used that allowed the hierarchical and equipotent stem cell organisations to be distinguished (Lopez-Garcia *et al.*, 2010). There data exhibiting features of monoclonal conversion fitted the ‘scaling form’ mathematical equation, agreeing with an equipotent stem cell organisation where stem cells are being replaced laterally according to neutral drift dynamics.

A similar study was conducted by Snippert et al who used an inducible labelling system that was able to express multiple fluorescent markers within Lgr5+ stem cells of the crypt also via Cre-mediated recombination (Snippert *et al.*, 2010). They also used a version of the ‘scaling form’ mathematical equation to give some insight into their clone size distributions data over time. They found that Lgr5+ stem cells showed a convergence onto scaling behaviour over time, meaning Lgr5+ stem cells were following a pattern of neutral drift stem cell dynamics with stem cell clone loss compensated by stem cell clone gain. This study partially ruled out the existence of a hierarchical stem cell organisation over short time periods. This indicates

that the likely organisation of stem cells within crypts is of an equipotent stem cell population undergoing loss and replacement via a mechanism of neutral drift dynamics via symmetric stem cell division.

In recent years, there has been much debate over the gene expression profile that defines the definitive stem cell population within crypts. This is due to the heterogeneity in gene expression profiles found within clonogenic cells at the crypt base. *Lgr5* and *Bmi1* are two of the most highly expressed genes within crypt base columnar (CBC) cells, with cells expressing high levels of these genes having the capacity to regenerate crypts (Sangiorgi and Capecchi, 2008; Munoz *et al.*, 2012). The stem cell niche of crypts may well contain stem cells with varying degrees of clonogenicity and functional redundancy that cannot be compartmentalised. However, *Lgr5* expression seems to be the most favoured stem cell marker within small intestine due to their ability to regenerate all cell types of the crypt, and that fact that they fully contribute to tissue maintenance under normal conditions (Barker *et al.*, 2007; Sato *et al.*, 2009). The *Lgr5*+ cell lineage has even been identified within mouse intestinal adenomas, indicating that not only can they regenerate crypts, but also are the driving cells involved in tumour growth (Sato *et al.*, 2009; Schepers *et al.*, 2012). Stem cell markers have been described in detail within section 1.8.2.

Due to the uncertainty in stem cell markers within mouse small intestinal crypt, a study was recently carried out that used a stem cell independent method of continuous clonal labelling (Kozar *et al.*, 2013). This was carried out using a mouse model with an out of frame *SYNbg1A* reporter gene within the constitutively expressed Rosa26 housekeeping locus within mice. The reporter gene included a dinucleotide repeat tract ([CA]₃₀) that was susceptible to frameshift mutation. Once a frameshift mutation occurred, this would bring the reporter gene into frame, allowing the expression of the detectable marker protein (EYFP). As stem cells are the only cells that are long lived within crypts over the lifetime of the mouse, the majority of partially and fully labelled crypts detected within the intestinal epithelium must be derived from the stem cells. A mathematical model was constructed which modelled the appearance of partially and fully labelled clones, taking into account a constant mutation rate that was determined for frameshift mutation to occur, allowing the expression of the marker. A model of neutral drift was developed. They were able to fit their data to a model where between 5-7 stem cells are present with a stem cell replacement rate between 0.2-0.3 stem cells per day.

It is more difficult to understand stem cell dynamics within human crypts as reporter gene insertion is not an option. Therefore, one must rely on naturally occurring characteristics within cells to define stem cell lineage. Methylation pattern analysis has previously been used to determine clonal populations within human colonic crypts (Yatabe *et al.*, 2001). They showed that methylation within crypt cells increased with age. However, they saw that there were considerable differences in methylation patterns between crypts, and was dependent on inter-crypt distances. Even so, a crypt model was developed to explain their data. An immortal stem cell neutral drift model was developed. Methylation pattern data fitted a model of neutral stem cell drift within a defined stem cell niche that incorporated elements of both symmetric and asymmetric stem cell division.

Somatic mtDNA mutations resulting in COX deficient cells are also acquired with age and is another naturally occurring process which can be used for identifying stem cell lineage within crypts (see section 1.8.4) (Taylor *et al.*, 2003). Neighbouring crypts that share the same somatic mtDNA point mutation have been shown to have extremely divergent methylation patterns (Graham *et al.*, 2011). Neighbouring crypts sharing the same somatic mtDNA point mutation by chance has been shown to be extremely unlikely, with an odds ratio of $>=2.48 \times 10^9 : 1$ (see section 1.8.4). (Greaves *et al.*, 2006). This indicates that the mtDNA mutation was acquired and was able to expand via crypt fission, whilst in that same time frame, methylation patterns had diverged considerably. This demonstrates that COX deficiency may be a better method of stem cell lineage tracing compared with methylation patterns to determine stem cell dynamics within human crypts.

Using somatic mtDNA mutations that result in COX deficiency as a stem cell lineage marker has recently been investigated using a limited number of patient samples (Baker *et al.*, 2014). They rationalise that the crypt is a cellular conveyor belt where cells are shuttled from the stem cells to the orifice where they are shed into the gut lumen (Wright and Alison, 1984). From their patient samples they identify partially COX deficient crypts which are then serially sectioned and reconstructed as a three-dimensional crypt image. Mapping longitudinal crypts shows increasing and decreasing clone width from the bottom to the top of the crypt. They hypothesised that an increase in clone width meant there was symmetric stem cell division of a COX deficient stem cell resulting in the replacement of a neighbouring COX normal stem cell. A decrease in clone width was taken to mean a COX normal cell has replaced a COX deficient stem cell. They tested this theory using a computational model of crypt cellular dynamics which was constructed by van Leeuwen *et al* (van Leeuwen *et al.*,

2009). The model showed that their hypothesis was indeed correct for their specified parameters. The changes in clone width within normal crypts were shown to be balanced, indicating a neutral drift type process. Their data also indicated that there were between 4 and 6 stem cells within normal crypts. They also looked at adenomatous crypts which indicated there was an increased number of stem cells present with an increased stem cell replacement rate compared to normal crypts (Baker *et al.*, 2014).

Mathematical and computational modelling are extremely powerful tools, allowing hypotheses to be tested against an array of biological data. Unlike biological data, which has often been captured at a single time-point for each sample acquired, modelling allows the full lifetime of the process to be simulated, providing invaluable insight into the process as a whole. The model constructed by van Leeuwen et al (van Leeuwen *et al.*, 2009) and used to validate a hypothesis by Baker et al (Baker *et al.*, 2014) is a good example of the interplay between experimental and computational modelling approaches.

The model by van Leeuwen et al was based on a previous model by Meineke et al (Meineke *et al.*, 2001). The original model treated a 3-dimensional crypt as an unfolded 2 dimensional rectangular surface with the introduction of cell boundaries. Each cell was modelled deterministically which responded to intra, inter and extra cellular cues. The Meineke model included cell division, differentiation, and apoptosis parameters, along with mechanical force determination on each cell boundary. Each cell boundary used Delaunay triangulation and Voroni tessellation to determine each cell's centre, shape and size. The addition of the van Leeuwen model incorporated specific Wnt features (van Leeuwen *et al.*, 2009). This included an extra-cellular Wnt concentration gradient. A cell-cell adhesion module which would be dependent on Wnt concentration due to β -catenin's involvement with both the Wnt pathway (APC destruction complex) and cell-cell adhesion (binding to the cytosolic tail of the cell-cell interacting protein E-cadherin). A cell cycle module was also incorporated as Wnt has an effect on downstream gene transcription and translation, in particular, those genes involved in cell cycle control. Therefore, making a more robust model of crypts as a whole. The project was part of an international endeavour for integrative biology which led to the modelling of other tissue types, for instance the heart (Gavaghan *et al.*, 2005; van Leeuwen *et al.*, 2007). This led to a fully engineered computational tool for biomedical applications and is now known as CHASTE (Cancer, Heart and Soft Tissue Environment) (Pitt-Francis *et al.*, 2008).

The van Leeuwen model simulated the propagation of COX deficiency within crypts and found that they could only achieve monoclonal conversion of a crypt when stem cell positions were not fixed. Indicating that symmetric division is taking place the majority of the time in order for monoclonal conversion to be achieved within their model (Meineke *et al.*, 2001; van Leeuwen *et al.*, 2009).

1.9 AIMS AND OBJECTIVES

This thesis sets out to understand the mechanism by which mitochondrial dysfunction is able to accumulate within ageing colonic epithelium in conjunction with the potential impact of mitochondrial dysfunction on the stem cells themselves.

- Determine the mechanism by which mitochondrial dysfunction is able to accumulate within: individual stem cells, individual crypts, and within colonic epithelium as a whole using computational modelling techniques by:
 - Acquiring experimental data sets of COX deficiency within human colonic epithelium to use as reference data.
 - Developing a model that incorporates known elements of mtDNA clonal expansion and stem cell niche succession.
 - Investigating whether COX deficiency is indeed a good marker of stem cell lineage tracing within colonic epithelium.
 - Determining optimum parameter sets that shed light on the mechanism by which COX deficient stem cells are able to accumulate within colonic epithelium.
- Determine what the impact is of mitochondrial dysfunction on stem cell function by:
 - Validating a mouse model that allows the visualisation of stem cells in conjunction with accumulating feasible levels of mitochondrial dysfunction to investigate.

- Implement a method that can compare the cell cycle kinetics between normal and respiratory deficient stem cells and crypts as a whole.

Chapter 2

Materials and Methods

Chapter 2 Materials and methods

2.1 MATERIALS

2.1.1 Equipment and computer software

Antigen Retrieval Unit	2100 Retriever
Axioimager	Zeiss
BX51 Stereology Microscope	Olympus
MATLAB R2015a	MathWorks
Microtome	Microm
Rotatest shaker R100	Luckham
Stereoinvestigator	MBF Bioscience
Zen 2011	Carl Zeiss Microscopy

2.1.2 Consumables

2.1.2.1 General consumables

5-Chloro-2-deoxyuridine thymidine (CldU)	Sigma-Aldrich
5-Iodo-2-deoxyuridine (IdU)	Sigma-Aldrich
Avidin/biotin blocking kit	Vector Laboratories
Colourcoat+ adhesion microscope slides	CellPath
Disodium hydrogen phosphate	AnalaR
Ethanol	Fisher Scientific
Ethylenediaminetetraacetic acid, (EDTA) disodium salt, dehydrate	Affymetrix
Formalin solution, neutral buffered, 10%	Sigma-Aldrich
Histoclear	National Diagnostics
Hoechst 33342, trihydrochloride, trihydrate	Life Technologies
Hydrochloric acid 37%	VWR

Normal donkey serum	Abcam
Normal goat serum	Sigma-Aldrich
Paraformaldehyde solution 4% in PBS	Santa-Cruz Biotechnology
PBS tablets	OXOID
Potassium chloride	Sigma-Aldrich
Potassium dihydrogen phosphate	AnalaR
Prolong gold mounting medium	Life Technologies
Sodium chloride	Sigma-Aldrich
Tissue cassettes	CellPath
Tri-sodium citrate dihydrate	VWR
Trizma base	Sigma-Aldrich
Tween®-20	Sigma-Aldrich

2.1.2.2 Antibodies

Donkey anti-Mouse IgG H+L - AffiniPure TRITC	Jackson ImmunoResearch
Donkey anti-Rabbit IgG H+L - Alexa Fluor® 750	Abcam
Donkey anti-Rat IgG H+L - AffiniPure Cy5	Jackson ImmunoResearch
Goat anti-GFP (biotin) antibody	Abcam
Goat anti-Mouse IgG1 (biotin)	Life Technologies
Goat anti-Mouse IgG2a - Alexa Fluor® 546	Life Technologies
Goat anti-Mouse IgG2b - Alexa Fluor® 488	Life Technologies
Mouse anti-IdU antibody	BD Bioscience
Mouse anti-MTCO1 IgG2a antibody	Abcam
Mouse anti-NDUFB8 IgG1 antibody	Abcam
Mouse anti-VDAC1 IgG2b antibody	Abcam

Rabbit anti-Ki67

Abcam

Rat anti-CldU antibody

Novus Biologicals

Streptavidin, Alexa Fluor® 488

Life Technologies

Streptavidin, Alexa Fluor® 647

Life Technologies

2.1.3 Solutions

TBST pH 7.4

5 mM Trizma base

100 mM Sodium chloride

0.1% (v/v) Tween®-20

PBS pH 7.4

137 mM sodium chloride

2.7 mM potassium chloride

10 mM disodium hydrogen phosphate

1.8 mM potassium dihydrogen phosphate

EDTA antigen retrieval buffer pH 8.0

1 mM EDTA

Sodium citrate antigen retrieval buffer pH 6.0

10 mM tri-sodium citrate

2.2 METHODS

2.2.1 Subjects and colorectal mucosal samples

Human colorectal mucosal samples were collected from the same anatomical site (10 cm from the anal verge) from patients (n=148, age range 17-78 years) undergoing colonoscopy for disturbed bowel function in whom no evidence of bowel disease was identified (BORICC 1 Study). Ethical approval was obtained from the Northumbria NHS Trust Local Research Ethics Committee.

2.2.2 Mouse models

2.2.2.1 *PolyA^(-/-) mitochondrial mutator mice*

Mitochondrial mutator mice (*PolyA^(-/-)*) were generated with a knock-in missense mutation (D257A) that changes the amino acid from aspartic acid to alanine within the second proofreading domain of the PolyA catalytic subunit of the mtDNA polymerase gamma (Trifunovic *et al.*, 2004). *PolyA^(-/-)* male mice (n=4) were originally obtained from a well-established colony kindly donated by Tomas Prolla, Department of Genetics and Medical Genetics, University of Wisconsin, Madison, USA. *PolyA^(-/-)* male mice were mated with female C57Bl/6J wild-type mice (Charles River Laboratories). The resulting *PolyA^(+/-)* female and *PolyA^(+/-)* male mice were mated to propagate our own colony of *PolyA^(-/-)* mice (Figure 2-1). All mice were maintained within the comparative biology centre at Newcastle University where they were kept in individually ventilated cages with RM3 expanded chow provided by special diet services. Mice were kept in a room with a constant temperature of 25°C with a 12 hour light/dark cycle.

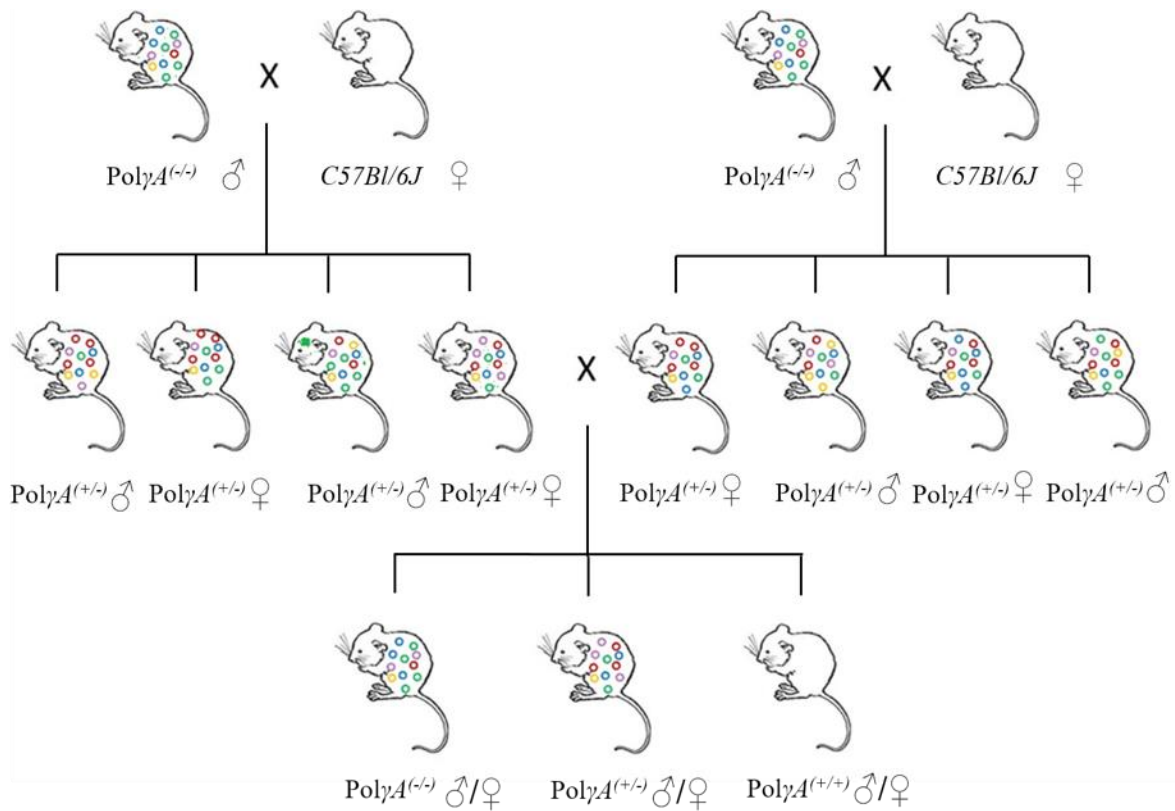


Figure 2-1 Mitochondrial mutator mouse breeding scheme

PolyA^(-/-) male mice were mated with *wild type C57Bl/6J* female mice. The resulting *PolyA^(+/-)* female and *PolyA^(+/-)* male mice were mated to propagate the colony of *PolyA^(-/-)*, *PolyA^(+/-)* and *PolyA^(+/+)* mice.

2.2.2.2 *Lgr5-EGFP-Ires-CreERT2* mice and *PolyA^(-/-)* mitochondrial mutator mice

Lgr5-EGFP-Ires-CreERT2 (*Lgr5^(+/-)*) mice were generated by homologous recombination in embryonic stem cells targeting an *EGFP-Ires-CreERT2* cassette to the ATG of *Lgr5*. This resulted in the constitutive expression of the EGFP fluorescent reporter protein within cells that normally express *Lgr5*, with the abolishment of *Lgr5* gene expression (Barker *et al.*, 2007). *Lgr5^(-/-)* mice were embryonic lethal, indicating the importance of *Lgr5* during development. *Lgr5^(+/-)* were backcrossed with C57Bl/6J mice for at least 4 generations before being donated to Jackson Laboratories, where they were mated with C57Bl/6J inbred mice. *Lgr5-EGFP-Ires-CreERT2* were kindly donated by Karen Vousden, Beatson Institute for Cancer Research, Glasgow, UK. *PolyA^(+/-)* male mice were mated with female *Lgr5^(+/-)* mice. The resulting *PolyA^(+/-)Lgr5^(+/-)* female and *PolyA^(+/-)Lgr5^(+/+)* male mice were mated to propagate our own colony of mice (Figure 2-2). All mice were maintained within the comparative biology centre at Newcastle University where they were kept in individually

ventilated cages with RM3 expanded chow provided by special diet services. Mice were kept in a room with a constant temperature of 25°C with a 12 hour light/dark cycle.

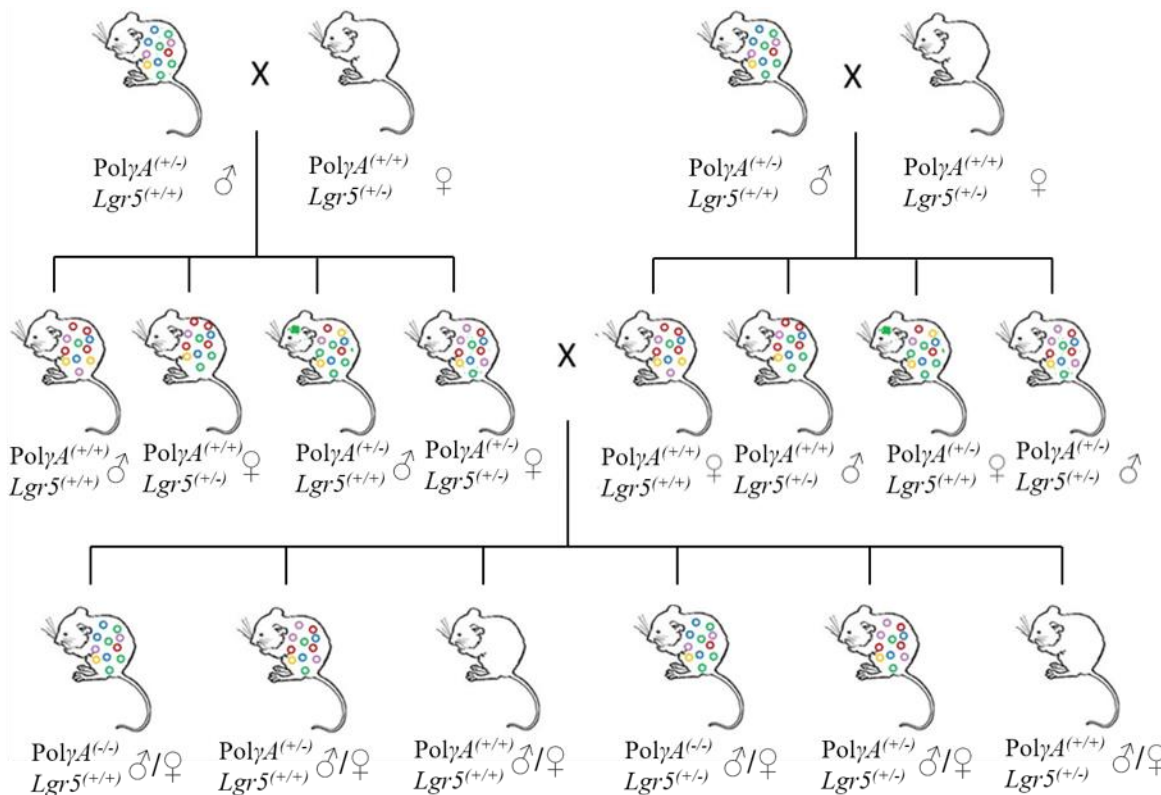


Figure 2-2 Lgr5 and mitochondrial mutator mouse breeding scheme

$PolyA^{(+/+)}$ male mice were mated with $Lgr5^{(+/-)}$ female mice. The resulting $PolyA^{(+/-)}Lgr5^{(+/-)}$ female and $PolyA^{(+/-)}Lgr5^{(+/+)}$ male mice were mated to propagate the colony of $PolyA^{(-/-)}Lgr5^{(+/+)}$, $PolyA^{(+/-)}Lgr5^{(+/+)}$ and $PolyA^{(+/+)}Lgr5^{(+/-)}$ mice.

2.2.3 Double thymidine analogue labelling

Thymidine analogue labelling allows cells undergoing DNA replication to be identified via immunohistochemical and immunofluorescence techniques. With the help of Dr Elizabeth Stoll (Newcastle University), a method was adapted for thymidine analogue labelling of cells within the gut (Stoll *et al.*, 2011). ClDU (Sigma Aldrich) and IdU (Sigma Aldrich) were made up at a concentration of 5mg/ml in PBS and then filter sterilised. The dissolution of IdU required 55°C for 8 hours followed by dropwise addition of 2M NaOH. The IdU solution was then set to pH7.4. The *in vivo* concentration was 50mg/kg, therefore, the injection volume was 10 μ l per gram of animal weight. Thymidine analogues were administered via intraperitoneal injection. The injection schedule was as follows:

Day 1

Injection 1 10am CldU 50 mg/kg

Injection 2 6pm CldU 50 mg/kg

Day 2

Injection 3 10am CldU 50 mg/kg

Injection 4 6pm CldU 50 mg/kg

Day 3

Injection 5 10am CldU 50 mg/kg

Injection 6 6pm CldU 50 mg/kg

Day 4

Injection 7 10am CldU 50 mg/kg

Injection 8 6pm IdU 50 mg/kg

Day 5

Animal sacrificed between 8-10am (~15 hours after IdU injection).

2.2.4 Mouse tissue harvesting

Mice were killed by cervical neck dislocation. All tissues were harvested. Mouse colons were removed and flushed with phosphate buffered saline (PBS), pH7.4 to remove any faeces and pellets. The colon was then cut longitudinally, placed onto a paraffin wax dish and splayed open before pins were inserted around the edge. All tissues were fixed using 10% neutral buffered formalin for 24 hours. After fixing, the colon was rolled up into a coil with a pin inserted to keep the orientation. All tissues were then transferred to 70% ethanol to await tissue processing and paraffin embedding.

2.2.5 Immunofluorescence for mitochondrial dysfunction

Formalin fixed paraffin embedded mouse colon blocks were cut at a thickness of 3 µm using the microtome. Tissue sections were floated out at 40°C and lifted onto glass slides. They

were dried in the 37°C incubator overnight before immunofluorescence was carried out.

Sections were deparaffinised and rehydrated via a 20 minute incubation at 60°C followed by 2 x 10 minute submersion in HistoClear (National Diagnostics), 2 x 5 minute submersion in 100% Ethanol, 1 x 5 minute submersion in 95% Ethanol, 1 x 5 minute submersion in 70% Ethanol, 1 x 5 minute submersion in distilled water. Antigen retrieval was carried out via submerging the sections in 1mM EDTA for 40 minutes within the antigen retrieval unit (2100 Retriever). Sections were then washed 3 x 5 minutes in TBST on the shaking incubator, all subsequent wash steps were performed this way. The sections were then incubated with 10% normal goat serum (NGS) (Sigma Aldrich) for 1 hour at room temperature followed by a wash step. An Avidin/Biotin blocking kit (Vector Laboratories) was used due to the types of antibodies that were being used. Avidin was added to the sections for 15 minutes at room temperature followed by a wash step. Biotin was added to the sections for 15 minutes at room temperature followed by a wash step. Primary antibodies were added to the sections and incubated at 4°C overnight followed by a wash step. Primary antibodies included mouse α -NDUFB8 IgG1 (Abcam) at a 1:50 dilution, mouse α -MTCO1 IgG2a (Abcam) at a 1:200 dilution, and mouse α -VDAC1 IgG2b (Abcam) at 1:200 dilution. Secondary antibodies were added to the sections and incubated in the dark at 4°C for 2 hours followed by a wash step. Secondary antibodies included goat α -mouse IgG1 biotin (Life Technologies) at a 1:400 dilution, goat α -mouse IgG2a-TRITC (Life Technologies) at a 1:400 dilution, and goat α -mouse IgG2b-FITC (Life Technologies) at a 1:400 dilution. Streptavidin conjugated Cy5 (Life Technologies) was added to the sections at a dilution of 1:200 and incubated in the dark at 4°C for 2 hours followed by a wash step. Hoechst (Life Technologies) was added to the sections as a nuclear counterstain at a dilution of 1:1200 and incubated in the dark at room temperature for 15 minutes followed by a wash step. The sections were mounted in Prolong gold (Life Technologies) using a coverslip and placed in the -20° freezer until ready to be viewed by fluorescence microscopy.

2.2.6 Immunofluorescence for cell cycle kinetics

Formalin fixed paraffin embedded mouse colon blocks were cut at a thickness of 3 μm using the microtome. Tissue sections were floated out at 40°C and lifted onto glass slides. They

were dried in the 37°C incubator overnight before immunofluorescence was carried out.

Sections were deparaffinised and rehydrated via a 20 minute incubation at 60°C followed by 2 x 10 minute submersion in HistoClear (National Diagnostics), 2 x 5 minute submersion in 100% Ethanol, 1 x 5 minute submersion in 95% Ethanol, 1 x 5 minute submersion in 70% Ethanol, 1 x 5 minute submersion in distilled water. Antigen retrieval was carried out via submerging the sections in sodium citrate antigen retrieval buffer for 40 minutes within the antigen retrieval unit (2100 Retriever). Further antigen retrieval was carried out by submerging the sections in 1.5M HCl at room temperature for 40 minutes. Sections were then washed 3 x 5 minutes in TBST on the shaking incubator, all subsequent wash steps were performed this way. The sections were then incubated with 10% normal donkey serum (NDS) (Abcam) for 1 hour at room temperature followed by a wash step. An Avidin/Biotin blocking kit (Vector Laboratories) was used due to the types of antibodies that were being used. Avidin was added to the sections for 15 minutes at room temperature followed by a wash step. Biotin was added to the sections for 15 minutes at room temperature followed by a wash step. Primary antibodies were added to the sections and incubated at 4°C overnight followed by a wash step. Primary antibodies included rabbit α-Ki67 IgG (Abcam) at a 1:50 dilution, rat α-Clu IgG (Novus Biologicals) at a 1:200 dilution, mouse α-Idu IgG (BD Biosciences) at a 1:100 dilution, and goat α-GFP IgG biotin (Abcam) at a 1:100 dilution. Secondary antibodies were added to the sections and incubated in the dark at 4°C for 2 hours followed by a wash step. Secondary antibodies included streptavidin conjugated FITC (Life Technologies) at a 1:400 dilution, donkey α-mouse IgG (H+L) TRITC (Jackson ImmunoResearch) at a 1:200 dilution, donkey α-rat IgG (H+L) Cy5 (Jackson ImmunoResearch) at a 1:100 dilution, and donkey α-rabbit IgG (H+L) Cy7 (Abcam) at a 1:50 dilution. Hoechst (Life Technologies) was added to the sections as a nuclear counterstain at a dilution of 1:1200 and incubated in the dark at room temperature for 15 minutes followed by a wash step. The sections were mounted in Prolong gold (Life Technologies) using a coverslip and placed in the -20° freezer until ready to be viewed by fluorescence microscopy.

2.2.7 Fluorescence microscopy and image analysis

An Axioimager (Zeiss) microscope was used to image the tissue sections that had undergone immunofluorescence (described in section 2.2.5 and 2.2.6). Axiovision software was used in

conjunction with the Axioimager microscope to take fluorescence images. Using the monochrome camera, no primary control sections were used to optimise exposure times to eliminate autofluorescence and secondary antibody non-specific binding. With those exposure times, a large tiled fluorescence image of the whole tissue section was constructed from individual 10x images for those sections that had primary antibodies applied. Large tiled images were used to count crypts that had COX-1 (Complex IV) and NDUFB8 (Complex I) loss of expression. Large tiled images were also used to identify crypts that contained cells that were EGFP+, indicating their Lgr5+ status. Individual crypts that were EGFP+ had 40x images taken from serial sections that had undergone immunofluorescence for mitochondrial dysfunction and cell cycle kinetics. Therefore, the OXPHOS status, cell cycle kinetics, and Lgr5+ stem cells were identified for each crypt and for each cell within that crypt. Analysis of OXPHOS status, cell cycle markers, and Lgr5+ stem cells was conducted using the ZEN 2011 software with its graphical user interface console.

2.2.8 COX/SDH histochemistry

COX/SDH histochemistry was carried out on patient biopsy sections by Dr Laura Greaves in 2006 using the following protocol:

Normal human colonic mucosal biopsies were attained from patients ranging between 17 – 78 years of age. Colon samples were mounted for sectioning and frozen in isopentane, previously cooled to -160°C in liquid nitrogen. A dual histochemical assay was used to determine the cytochrome c oxidase activity (proxy for respiratory deficiency) of the crypts. Cryostat sections (12 µm) were first incubated in cytochrome c oxidase medium (100 µM cytochrome c, 4 mM diaminobenzidine tetrahydrochloride, and 20 µg / ml catalase in 0.2 M phosphate buffer, pH 7.0) at 37°C for 50 minutes. Sections were then washed in PBS (3 x 5 minutes) and incubated in succinate dehydrogenase (SDH) medium (130 mM sodium succinate, 200 µM phenazine methosulphate, 1 mM sodium azide, 1.5 mM nitroblue tetrazolium in 0.2M phosphate buffer, pH7.0) at 37°C for 40 minutes. Sections were washed in PBS, pH 7.4 (3 x 5 minutes) dehydrated in graded ethanol series (70%, 95%, 2 x 100%), cleared in HistoClear (National Diagnostics, Atlanta, Georgia, USA), and mounted in DPX (BDH Laboratory Supplies, Poole, United Kingdom). The same protocol was used in (Taylor *et al.*, 2003).

2.2.9 COX/SDH histochemical analysis

The Olympus BX51 microscope was used in conjunction with the Stereoinvestigator software (MBF Biosciences) to view the tissue sections that had previously undergone COX/SDH histochemistry. The slides were placed on the microscope stage and the 10x magnification lens was selected. Using the software programme, an auto-white balance was performed and a point of origin was selected for each tissue sample. The proportion of COX deficiency within every crypt exhibiting COX deficiency was calculated using the software's contour option, which allowed the area to be calculated, allowing a percentage COX deficiency to be determined. For each patient biopsy, the number of partially and fully COX deficient crypts was recorded (Craig Stamp MRes 2012). Crypts which appeared to be undergoing fission were also counted and were also recorded as being normal or COX deficient. Furthermore, the number of COX deficient crypt colonies was recorded along with the number of COX deficient crypts within those colonies. The total number of crypts within the tissue section was counted in order for the data to be normalised.

2.2.10 Computational modelling of respiratory deficient stem cells

2.2.10.1 *Mouse stem cell population model*

A stem cell model that simulated mtDNA relaxed replication and mtDNA random segregation within a population of rapidly dividing stem cells was developed within MATLAB (MathWorks). MtDNA mutation rate upon replication was modelled using a probability of acquiring a new mutated mtDNA molecule during replication of a normal mtDNA molecule. In the case of a mutation event, the number of mutated mtDNA molecules would be increased by one. The number of mtDNA molecules per cell was set at 200 based on previous simulations of mitotic cells (Coller *et al.*, 2001). A parameter scan was conducted to determine the optimum mutation rate that matched experimentally observed COX deficiency data from *wild-type C57Bl/6J*, *PolyA^(+/-)* and *PolyA^(-/-)* mice when a level of >75% mutated mtDNA signified a COX deficient stem cell. Other parameters included the division rate which was once per day, hence 1080 divisions were used to account for a simulation time of 36 months. One-thousand cells were simulated to measure the percentage of cells harbouring COX Deficiency at each time point. Model code is included in the appendices (appendix 1.3.1)

2.2.10.2 Human stem cell niche model

A more biologically relevant model of stem cell dynamics, mtDNA relaxed replication and mtDNA random segregation was developed within MATLAB (MathWorks) in order to test hypothesis of stem cell dynamics using human colon COX deficiency data as a reference. The computational multi-level model that was developed simulates the occurrence of mtDNA mutations within the human colon and their subsequent expansion/disappearance over the average human lifespan of 80 years. In the model, the colon is divided into individual crypts of approximately 2500 cells (Yatabe *et al.*, 2001; Nicolas *et al.*, 2007; Nooteboom *et al.*, 2010), of which all but the stem cells are constantly being lost and replaced by stem cell symmetric and asymmetric division. It's assumed that only mutations occurring/expanding in the stem cells (but also present in the other cells of the crypt) survive for long enough to allow clonal expansion to take place in order for COX deficiency to be observed. Therefore, only the stem cells of the crypt are explicitly modelled. The model can simulate any fixed number of stem cells and any fixed number of mtDNA molecules throughout the simulation time of 80 years. Asynchronous stem cell division takes place approximately once per week (Potten *et al.*, 1992; Kim and Shibata, 2002). For each stem cell upon division, the number of mtDNA doubles via relaxed replication, followed by random segregation of the mtDNA into 2 groups, each representing a daughter cell compartment. The division can either be asymmetric, in which case one of the daughter cells is a stem cell and the other daughter cell is lost, or symmetric, in which case both or none of the daughter cells are stem cells. To keep the number of stem cells in the crypt constant, in case the number of stem cells in the crypt is different from the starting number after division, a randomly chosen stem cell either divides or is deleted.

The stem cells are simulated to undergo 4171 asynchronous divisions during the lifetime of the crypt, based on the division rate being once every 7 days and the crypt being simulated for 80 years ((365/7)*80). Therefore, within an individual crypt simulation, there is a record of the number of mutated mtDNA molecules at each time point for each stem cell simulated. Before each division for each stem cell, the model simulates the acquisition of *de novo* mtDNA mutations according to the mutation rate specified and the use of a random number generator that generates a number between 0 and 1. Random doubling of mtDNA molecules occurs before division to simulate random genetic drift via relaxed replication. This was carried out using the following transition matrices which were designed by Dr Anze Zupanic (Eawag aquatic research) and then implemented into the model code.

A) Transition matrix for mtDNA molecule clonal expansion in a stem cell

In each division cycle there are N_{tot} mtDNA molecules in the cell, out of which any number can carry a mutation. In the doubling step, N mtDNAs are chosen to replicate, however some of them can replicate more than once and some not at all (the choice is a random N -combination with repetitions from a set of size N_{tot}). The transition matrix gives the probability that i mtDNA molecules carrying the mutation will be picked j times, and the non-mutant carrying mtDNA molecules $N-j$ times. Each element of the matrix can be calculated by:

$$T_{1A}(i,j) = \begin{cases} 1 & ; i,j = 0 \text{ or } i,j = N \\ \left(\frac{i}{N_{tot}}\right)^j \left(\frac{N_{tot}-i}{N_{tot}}\right)^{N-j} \binom{N}{j} & ; \text{otherwise} \end{cases}$$

where $i \in [0, N_{tot}]$ is the number of mtDNA molecules carrying a mutation in the stem cells before mtDNA replication and $j \in [0, N_{tot}]$ is the number of mtDNA molecules carrying the mutation gained in the process of replication. If we insert $N = N_{tot} = 200$ into the equation above, we get:

$$T_{1A}(i,j) = \begin{cases} 1 & ; i,j = 0 \text{ or } i,j = 200 \\ \left(\frac{i}{200}\right)^j \left(\frac{200-i}{200}\right)^{200-j} \binom{200}{j} & ; \text{otherwise} \end{cases}$$

For easier construction of the complete transition matrix, we can transform T_{1A} into a 201x401 size matrix T_{1B} by moving each matrix row of T_{1A} i columns to the right (which is equivalent to adding the number of mtDNA molecules carrying the mutation before replication to the new mtDNA molecules – the columns of T_{1B} now represent the probability of getting a certain number of mtDNA molecules with a mutation after replication):

$$T_{1B}(i, jj + i) = T_{1A}(i, j)$$

B) Transition matrix for mtDNA molecule segregation upon division

After replication of mtDNA, the $N_{tot} + N$ mtDNA molecules are divided into two sets of the same size (the choice is a random $(N_{tot} + N)/2$ -combination without repetitions). The transition matrix gives the probabilities that out of the k mtDNA molecules carrying the mutation in the mother stem cell, m will be chosen for one daughter cell. The transition matrix is of size 401x201, and each element can be calculated by:

$$T_2(k, m) = \begin{cases} 0 & ; (m > k) \text{ or } (m < k - (N + N_{tot})/2) \\ 1 & ; k, m = 0 \text{ or } k = 400, m = 200 \\ \frac{(\frac{N_{tot} + N}{2} - 1)!}{(N_{tot} + N)!} \prod_{x=0}^{m-1} (k - x) \prod_{y=0}^{\frac{N_{tot} + N}{2} - 1 - m} (N_{tot} + N - k - y) \binom{(N_{tot} + N)/2}{m} & ; \text{otherwise} \end{cases}$$

where $k \in [0, N_{tot} + N]$ is the number of mtDNA molecules carrying a mutation before division in the mother stem cell and $m \in [0, (N_{tot} + N)/2]$ is the number of mtDNA molecules carrying the mutation in one of the daughter cells after division. If we insert $N = N_{tot} = 200$ into the equation above, we get:

$$T_2(k, m) = \begin{cases} 0 & ; (m > k) \text{ or } (m < k - 200) \\ 1 & ; k, m = 0 \text{ or } k = 400, m = 200 \\ \frac{199!}{400!} \prod_{x=0}^{m-1} (k - x) \prod_{y=0}^{199-m} (400 - k - y) \binom{200}{m} & ; \text{otherwise} \end{cases}$$

Model code and transition matrices generation code are included within appendix 1.3.2 (model code), 1.3.3.5 (relaxed replication transition matrices), and 1.3.3.6 (random segregation transition matrices).

A figure of the model has been added to appendix 1.1.

2.2.10.3 COX deficient stem cell distribution model

The stem cell niche model simulates the emergence of COX deficient stem cells and their expansion and extinction over time. However, the biological data attained from human colonic tissue biopsies is a measure of COX deficiency percentage of individual crypts when viewed in transverse cross sections. Depending on where the tissue was cut will determine at which level the crypt is observed. As the majority of the crypt is made up of stem cell progeny and differentiated cells, it is highly likely that it is these cells that are observed as opposed to the stem cells at the base of the crypt. Therefore, a method for determining how

the number of COX deficient stem cells translates to the COX deficiency percentage higher up the crypt was required in order for the model data to be comparable with the biological data.

‘Functional’ stem cells divide to produce stem cell progeny that rapidly divide and differentiate while they are being shuttled up the crypt due to expansion in cell numbers. This is analogous to a ‘conveyor belt’ of cells that are eventually shed off into the gut lumen. It is reasonable to assume that there is a scaling up of the number of cells that are clonally derived from a single ‘functional’ stem cell due to expansion in cell numbers. As it has been shown previously (Baker *et al.*, 2014), within partially COX deficient human colonic crypts there is a ‘wiggle’ of COX deficiency from the base to the top of the crypt. This was explained by increased and decreased activity of COX deficient stem cell clones dividing symmetrically, creating a ribbon imprint of COX deficiency on the crypt wall. However, as there will also be competition between the stem cell progeny (derived from asynchronous stem cell divisions) that are rapidly dividing, it is likely that this will also contribute to the ‘wiggle’ that is observed within human colonic crypts. With this rationale, for each number of COX deficient stem cells that are present within the stem cell niche, there must be an associated probability distribution for the likely COX deficiency percentage observed.

Therefore, a model was developed that assumes there is a doubling of the number of cells until a certain number of cells is surpassed (to replicate the cell expansion process), starting with the number of ‘functional’ stem cells. For each of the ‘functional’ stem cells that are COX deficient, random replication is simulated until the number of cells at the next level is reached. This process is repeated for each cell expansion level. The number of COX deficient cells at the top level is recorded (observation level). The simulation was run 100,000 times to determine a distribution for the number of COX deficient cells there are at the observation level (appendix 1.3.4.1). The data is then transformed into a probability distribution and used to convert the biological data into the number of likely COX deficient stem cells it likely represents (appendix 1.3.4.2 to 1.3.4.5). This probability distribution can also be reversed to relate COX deficient stem cell number to likely % COX deficiency (appendix 1.3.4.6).

A method of random replication of cells to reach the subsequent level of the crypt was used to simulate the competition between equally fit competing populations within the crypt. The iterative equation used to carry out this random replication of COX deficient cells is described in Equation 2-1.

$$p = \frac{m}{t + r - 1}$$

Equation 2.1 – Crypt Cell Expansion Equation

Iterative equation describes how the probability is calculated to determine how many COX deficient stem cells will occupy the successive level in order to relate number of stem cells to number of potential transit amplifying cells that are COX deficient at the observation level. p = probability of COX deficient stem cell dividing to take up a place in the successive level, m = number of mutated stem cells, t = total number of cells at current level and r = replication event number where $r = 1: t-1$. The probability is recalculated for each dividing cell until the total number of cells at the current level is reached. The process is started again for each subsequent level with m initially set to the value it was at the end of the previous level.

Chapter 3

Mitochondrial Dysfunction

within Human Colon

Chapter 3 Mitochondrial dysfunction within human colon

3.1 INTRODUCTION

3.1.1 Mitochondrial dysfunction and ageing

Ageing is characterised by the decline in an organism's ability to function, manifesting with an increased likelihood of developing diseases and disabilities leading to the organism's eventual death. This is caused by intracellular and extracellular damage accumulation (Kirkwood, 2005).

Ageing was initially thought to be the result of normal cellular metabolism generating free radicals that go onto damage cellular constituents and connective tissues (Harman, 1956). It was later refined to involve mitochondria when it was discovered that they were the main source of reactive oxygen species (ROS) when the rate of oxygen consumption was linked to the accumulation of mitochondrial damage by radical oxygen species (ROS) (Harman, 1972). Therefore the free radical theory of ageing was transformed into the mitochondrial free radical theory of ageing (MFRTA). ROS inflict damage upon mitochondrial respiratory chain complexes and the mtDNA due to their close proximity to the site of ROS generation, leading to mitochondrial dysfunction (Fleming *et al.*, 1982; Linnane *et al.*, 1989). Mitochondrial dysfunction is a commonly observed feature within a variety of ageing tissues, for example prostate (Blackwood *et al.*, 2011), liver (Fellous *et al.*, 2009), stomach (McDonald *et al.*, 2008), and colon (Taylor *et al.*, 2003). Morphological changes of dysfunctional mitochondria include size increase and decreased ultrastructural organisation within the cell (Miquel *et al.*, 1980; Beregi *et al.*, 1988). They also exhibit decreased membrane potential, decreased ATP production and increased ROS generation (Ozawa, 1997; Kushnareva *et al.*, 2002). Somatic mtDNA mutations that cause mitochondrial dysfunction have been linked to a variety of age-related diseases which include macular degeneration (Blasiak *et al.*, 2013), diabetes mellitus (Sivitz and Yorek, 2010) and certain neurodegenerative diseases such as Alzheimer's and Parkinson's disease (Reeve *et al.*, 2008).

3.1.2 Mitochondrial dysfunction within human colon

Human colon is made up of millions of crypt-like structures, each containing approximately 2000-5000 cells (Kim and Shibata, 2002). They contain multiple stem cells at the base which continually proliferate throughout life to renew the stem cell pool and generate stem cell progeny which regenerate the colonic epithelium (Loeffler *et al.*, 1997). Unfortunately, there

are no robust markers for human colonic stem cells at present as current markers like CD44+ and CD133+ which enrich colon cancer initiating cells are too broadly expressed (see section 1.8.2) (Haraguchi *et al.*, 2008).

Clonally expanded point mutations have been shown to cause mitochondrial dysfunction within human colonic crypts with age (Taylor *et al.*, 2003). Through the histochemical reaction for COX activity, mitochondrial dysfunction can be observed within individual crypts and has been shown to increase exponentially with age (Taylor *et al.*, 2003). Full and partially COX deficient crypts have been observed within these tissue sections. 3D reconstruction of a partial crypt shows a ribbon pattern emanating from the base of the crypt, demonstrating that respiratory deficiency is transferred from stem cells at the base of the crypts to their progeny. COX deficiency is essentially an irreversible marker of the respiratory deficient stem cell lineage (Taylor *et al.*, 2003). Due to the stochastic nature of how the stem cell progeny migrate upwards through the crypt axis, it can be seen that there will be a range for the proportion of the crypt that is COX deficient, when viewed as a transverse cross section.

However, even though there is an increase in mitochondrial dysfunction within human colon with age, due to the vast pool of functional redundancy (i.e. a vast array of crypts that have normal mitochondrial function when assessed via COX/SDH histochemistry) the colon is still able to carry out its function, if not to a reduced capacity. It is still debated as to the specific impact mitochondrial dysfunction has on crypts but it has been shown to have a mild effect on the proliferative capacity within the stem cell progeny (Nooteboom *et al.*, 2010).

3.1.3 Monoclonal conversion of crypts

Human colonic crypts have been shown to be clonal in nature, meaning that over time all the cells originate from the same founding stem cell clone. This has been shown in patients with the XO/XY genetic background whereby their crypts either contain wholly XY sex chromosomes, or wholly XO sex chromosomes (Novelli *et al.*, 1996). This phenomenon was explored using the R26R-Confetti/Cre recombinase reporter mouse where random expression of different fluorescent proteins could be induced within mouse small intestinal crypts (Snippert *et al.*, 2010). At first, each crypt contained multiple fluorescent colours; however, after 30 weeks, each crypt contained a single fluorescent colour, highlighting the process of monoclonal conversion over time within individual crypts. Kozar *et al.* investigated stem cell lineage tracing within mouse small intestinal crypts. They constructed a mouse that had a

[CA]₃₀ dinucleotide repeat unit in the promoter region of a reporter gene, which was susceptible to frameshift mutation due to strand slippage during replication. Upon frameshift mutation, the gene would be brought into frame allowing expression of the reporter gene. Mice were killed at different time points and the expression of the reporter was analysed within the small intestine. Partially and fully labelled crypts were observed. Levels of partially labelled crypts remained constant with age, whereas levels of fully labelled crypts increased linearly with age (Kozar *et al.*, 2013). This further highlights the process of monoclonal conversion over time within individual crypts. As fully and partially COX deficient crypts can be observed within human colon, this suggests that, like the examples above, they are in a state of undergoing monoclonal conversion. At present, the number of functional stem cells within human colonic crypts is an active area of research. Estimates within mouse studies suggest there are approximately 16 stem cells within mouse small intestinal crypts (Snippert *et al.*, 2010), whereas estimates range between 4 and 7 stem cells for mouse and human colonic crypts (Kozar *et al.*, 2013; Baker *et al.*, 2014).

3.2 AIMS OF STUDY

This study aimed to quantify the extent of mitochondrial dysfunction (COX deficiency) within human colon tissue biopsies at a depth that has not been achieved previously. This was in order to possess a robust data set that would allow further investigation into the process of monoclonal conversion within human colonic epithelium tissue. The in-depth quantification included:

1. Number of partially / fully COX deficient crypts (Craig Stamp MRes Dissertation 2012).
2. Percentage COX deficiency of each individual crypt (Craig Stamp MRes Dissertation 2012).
3. Number of normal / COX deficient crypts undergoing crypt fission.
 - a. Percentage COX deficiency of each crypt undergoing fission.
4. Number of COX deficient crypt colonies.
5. Number of COX deficient crypts making up each colony.
 - a. Percentage COX deficiency of each crypt within a colony.

This chapter forms the in-depth quantification and analysis of human colon biological data that was necessary to carry out further work into understanding the mechanism of monoclonal conversion that allows mitochondrial dysfunction to accumulate within human colonic epithelium.

3.3 METHODOLOGY

3.3.1 COX deficiency quantification within human colonic mucosa

148 slides containing human colon tissue sections had already undergone COX/SDH histochemistry by Dr Laura Greaves (Newcastle University) in order to visualise focal respiratory chain enzyme deficiency (cytochrome *c* oxidase (COX) deficiency at Complex IV), which was the result of clonally expanded mtDNA point mutations (section 2.2.8). COX deficiency was quantified using the Olympus BX51 microscope (section 2.2.9). The percentage fraction of partially and fully COX deficient crypts for each individual crypt was quantified (Craig Stamp MRes Dissertation). The number of normal and COX deficient crypts undergoing fission was quantified. The number of COX deficient crypt colonies or patches was quantified, together with the number and percentage fraction of COX deficiency of each crypt within each colony. Data was normalised as a percentage of the total number of crypts present within the tissue section.

3.3.2 Relating COX deficiency observed to fraction of stem cells

COX deficiency fractions were quantified for transverse COX deficient crypts. However, the accumulation of COX deficiency would be modelled purely within the stem cell compartment (section 2.2.10.2). Stem cell dynamics have been well characterised within mouse models using the assumption that the fraction of stem cell progeny cells displaying a stem cell lineage marker represents the same fraction of stem cells with that marker (Lopez-Garcia *et al.*, 2010; Snippert *et al.*, 2010; Kozar *et al.*, 2013). Within this study however, a relationship between the fraction of COX deficient stem cells present within the stem cell niche and the fraction of COX deficient stem cell progeny cells was sought. This would allow model and biological data to be comparable. The model that was developed relating the number of stem cells COX deficient and the observed COX deficiency fraction has been described (section 2.2.10.3) with model code contained within appendix 1.3.4.

3.4 RESULTS

3.4.1 Characteristics of human colon epithelium after COX/SDH histochemistry

There are a range of features present within human colonic epithelium after COX/SDH histochemistry has been performed. Features include partially and fully COX deficient crypts, patches of COX deficient crypts and crypts undergoing fission. The identification and quantification of these features forms the majority of this chapter. It was important to be able to identify these features in order to achieve the most reliable data set that shows how COX deficiency within human colon changes with age. Figure 3-1A shows a crypt that is completely brown following COX/SDH histochemistry. Therefore, all the cells/stem cell progeny observed in this crypt's transverse cross section have normal cytochrome *c* oxidase activity and are deemed respiratory normal or COX positive (COX^{+ve}). Figure 3-1B shows a crypt that is partially blue with the rest being brown following COX/SDH histochemistry. Only a fraction of the cells/stem cell progeny observed in this crypt's transverse cross section have deficient cytochrome *c* oxidase activity and are deemed respiratory deficient or COX deficient (COX^{-ve}), making this a partially COX deficient crypt. Figure 3-1C shows a crypt that is completely blue following COX/SDH histochemistry. This means that all the cells/stem cell progeny observed in this crypt's transverse cross section have deficient cytochrome *c* oxidase activity, making this a fully COX deficient crypt. Figure 3-1D shows two respiratory normal crypts in the process of fission. Crypt fission is important for growth and repair of the colon and to keep the tissue in a homeostatic balance between crypt death and crypt renewal and is an important feature that must be taken into account. Figure 3-1E shows two COX deficient crypts undergoing fission, highlighting the fact that crypt fission occurs in both normal and COX deficient crypts. Figure 3-1F shows a colony of four COX deficient crypts and are thought to arise from one COX deficient stem cell clone. The majority of crypts that contribute towards a COX deficient crypt colony are fully COX deficient, however, where this was not the case, the percentage COX deficiency of each individual crypt that contributes towards a COX deficient crypt colony was ascertained.

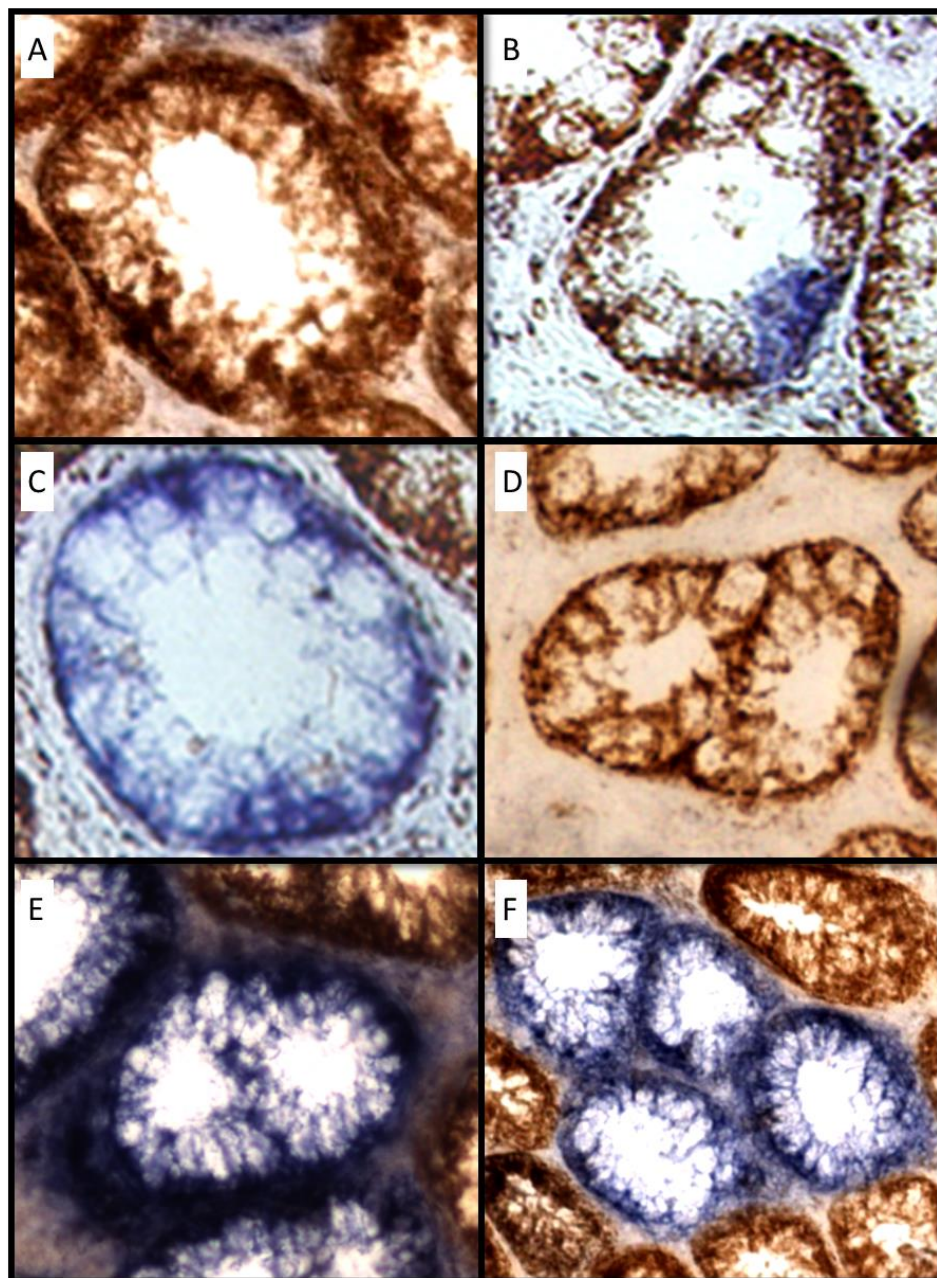


Figure 3-1 Characteristics of Human colon after COX/SDH histochemistry

The percentage COX deficiency of individual crypts was quantified from human colon tissue biopsies that had been sectioned and subjected to COX/SDH histochemistry. 148 human colon biopsies were included within this patient cohort with ages ranging from 17-78 years. A variety of features are present within patient biopsies after COX/SDH histochemistry. (A) Respiratory normal crypts (cytochrome *c* oxidase activity present). (B) Partially COX deficient crypts (cytochrome *c* oxidase activity is only present in a fraction of cells observed). (C) Fully COX deficient crypt (cytochrome *c* oxidase is completely absent from all cells observed). (D) Respiratory normal crypts undergoing fission. (E) Respiratory deficient crypts undergoing fission. (F) COX deficient crypt colony of four fully COX deficient crypts.

3.4.2 Partially COX deficient crypts and stem cell number within human colon

Partially COX deficient crypt percentages were pooled together from all patient samples to see the spread of the data as a whole. Figure 3-2A shows a schematic of partially COX deficient crypts with their associated percentage COX deficiency and is an example of how the pooled crypts were segregated into their nearest groups. Figure 3-2B shows the distribution of partially COX deficient crypts when they are grouped into 5% COX deficiency fractions. There is an increasing number of crypts in each fraction up until the 20% fraction. After this, we see a gradual decrease until we reach the 95% fraction. This suggests that partially COX deficient crypts are more likely to exist with a low COX deficiency fraction compared to those with a high COX deficiency fraction. One explanation is that the frequency for a certain fraction is equivalent to the average amount of time that a partially COX deficient crypt can exist as that fraction. If this is the case, there must be a biological mechanism acting on this system to produce this result. The mechanism responsible for this effect has been investigated and is contained within chapter 4.

As there is a peak in the data at the 0.2 COX deficiency fraction, this may represent the point at which the first COX deficient stem cell is acquired within the stem cell niche. If we say COX deficiency fraction peak is equal to $1/N$ ($N = \text{Number of stem cells present within a human colonic crypt}$). Then this would mean that there are approximately 5 stem cells contained within human colonic crypts. This is an emergent property when looking at pooled COX deficiency percentages within human colonic epithelium. A small number of stem cells within crypts, in line with approximately 5 has been corroborated within recent publications (Kozar *et al.*, 2013; Baker *et al.*, 2014). Therefore, for simplicity, the biological data was segregated into 6 fractions (0.0, 0.2, 0.4, 0.6, 0.8, 1.0) from now on to represent the presence of 5 stem cells within human colonic crypts

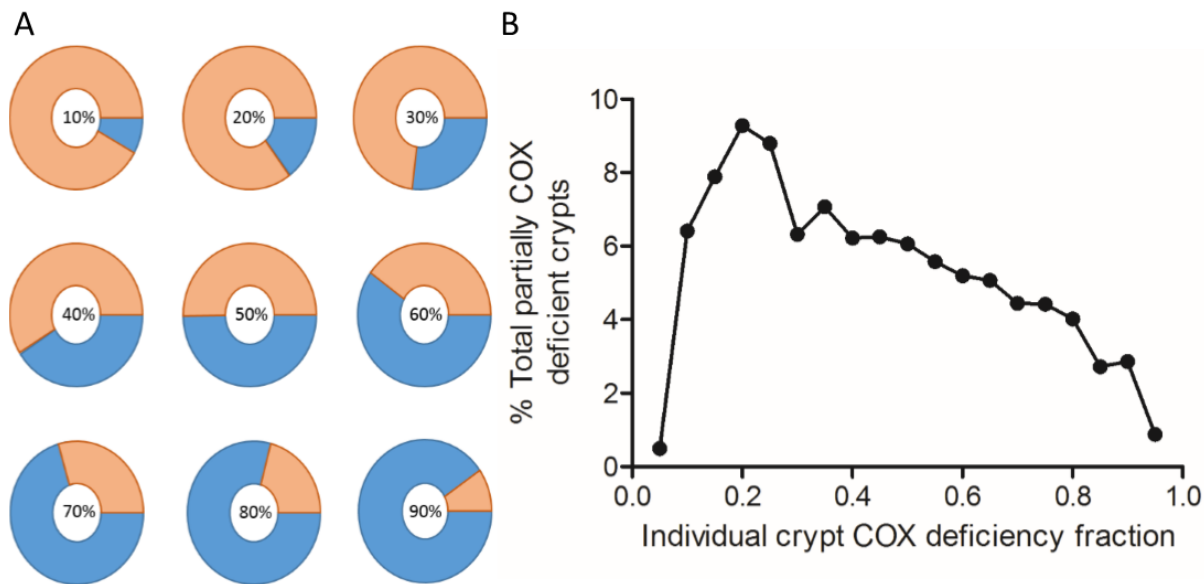


Figure 3-2 Pooled partially COX deficient crypts

The percentage COX deficiency of individual crypts was quantified from human colon tissue biopsies that had been sectioned and subjected to COX/SDH histochemistry. 148 human colon biopsies were included within this patient cohort with ages ranging from 17-78 years. Partially COX deficient crypt percentages were pooled from all patient samples of all ages. (A) Example schematic of transverse cross sections of crypts allocated to a specific percentage of COX deficiency from exact percentage data. (B) Graph showing the distribution of pooled partially COX deficient crypts separated into 5% COX deficiency fractions.

3.4.3 COX deficiency within human colon samples

The percentage COX deficiency of each individual crypt from each individual patient biopsy section was quantified previously (Craig Stamp MRes 2012). The number of partially and fully COX deficient crypts along with the total number of crypts was also counted for each patient sample. Figure 3-3A shows that there is an exponential increase in partially COX deficient crypts with age (non-linear regression exponential doubling time 17.65 years, $R^2 = 0.39$). Figure 3-3B shows that there is an even greater exponential increase in fully COX deficient crypts with age (non-linear regression exponential doubling time 12.5 years, $R^2 = 0.38$). Figure 3-3C shows that there is a statistically significant increase in the ratio between fully and partially COX deficient crypts with age (linear regression $R^2 = 0.19$, $p < 0.001$). This means that with increasing age, fully COX deficient crypts make up an increasing majority of COX deficient crypts present within human colon tissue. This indicates that a fully COX deficient crypt becomes fixed, with regards to a biological end-point, and persists within human colonic epithelium. This is what one would expect with monoclonal conversion of a single crypt. Figure 3-3D shows the data when the COX deficiency fraction of individual crypts is taken into account. Here, the data is grouped within 10 year age brackets and split into 6 COX deficiency fractions. What becomes clear from this graph is that with an increasing COX deficiency fraction, there is a decreasing frequency of COX deficient crypts for all age brackets up to fraction 0.8. This is then followed by a large increase in fully COX deficient crypts within fraction 1.0. It would also appear that the exponential increase we see in partially COX deficient crypts with age (Figure 3-3A) is also mirrored for each partially COX deficient fraction (Figure 3-3D).

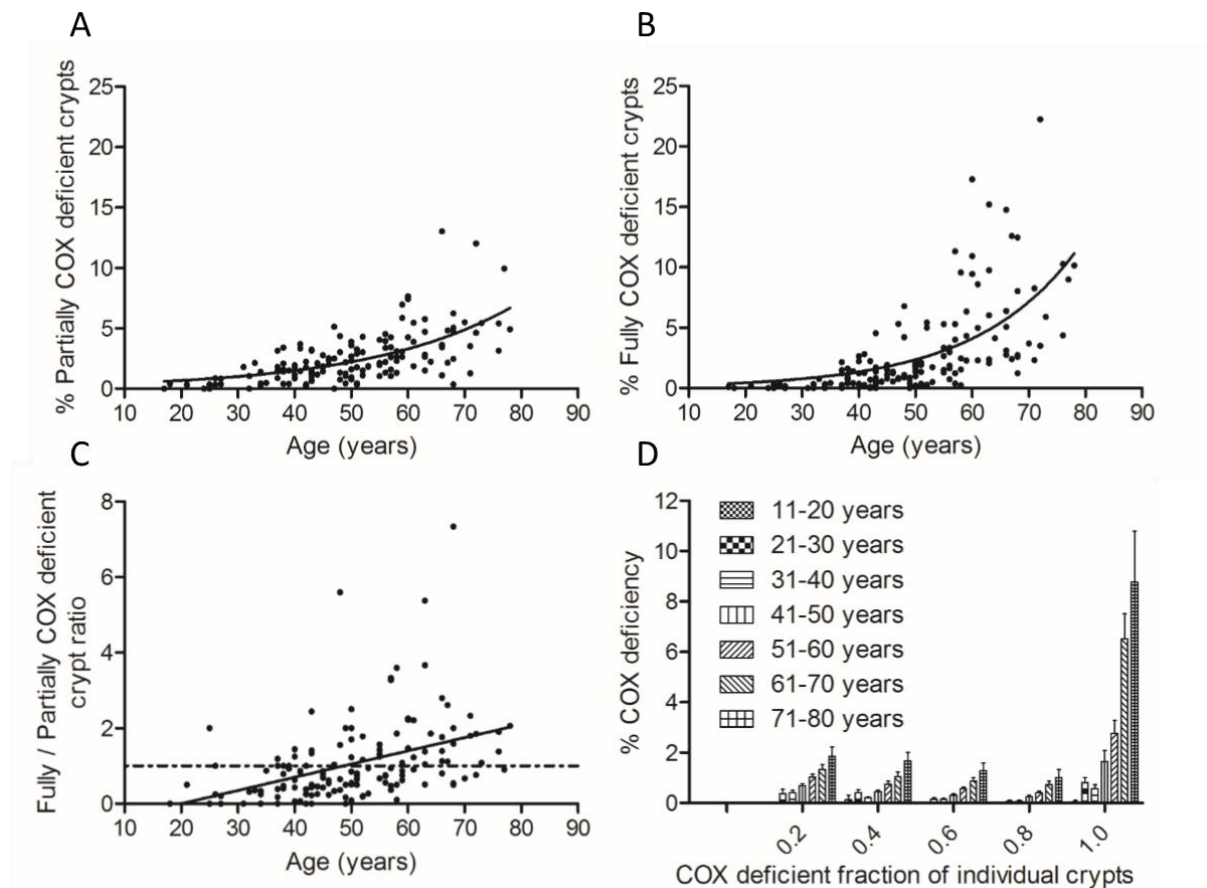


Figure 3-3 Human colon COX deficiency

The percentage COX deficiency of individual crypts was quantified from human colon tissue biopsies that had been sectioned and subjected to COX/SDH histochemistry. 148 human colon biopsies were included within this patient cohort with ages ranging from 17-78 years. (A) Percentage of total crypts that are partially COX deficient correlated with age of sample (exponential curve doubling time = 17.65 yrs, $R^2=0.39$). (B) Percentage of total crypts that are fully COX deficient correlated with age of sample (exponential curve doubling time = 12.50 yrs, $R^2=0.38$). (C) Ratio between fully and partially COX deficient crypts correlated with age of sample (linear regression $R^2 = 0.17$, $P<0.0001$). Line at $y=1$ represents the point at which the number of fully and partially COX deficient crypts are equal. (D) COX deficient crypt percentage segregated based on the nearest COX deficiency fraction and split into 10 year age brackets. Error bars represent SEM.

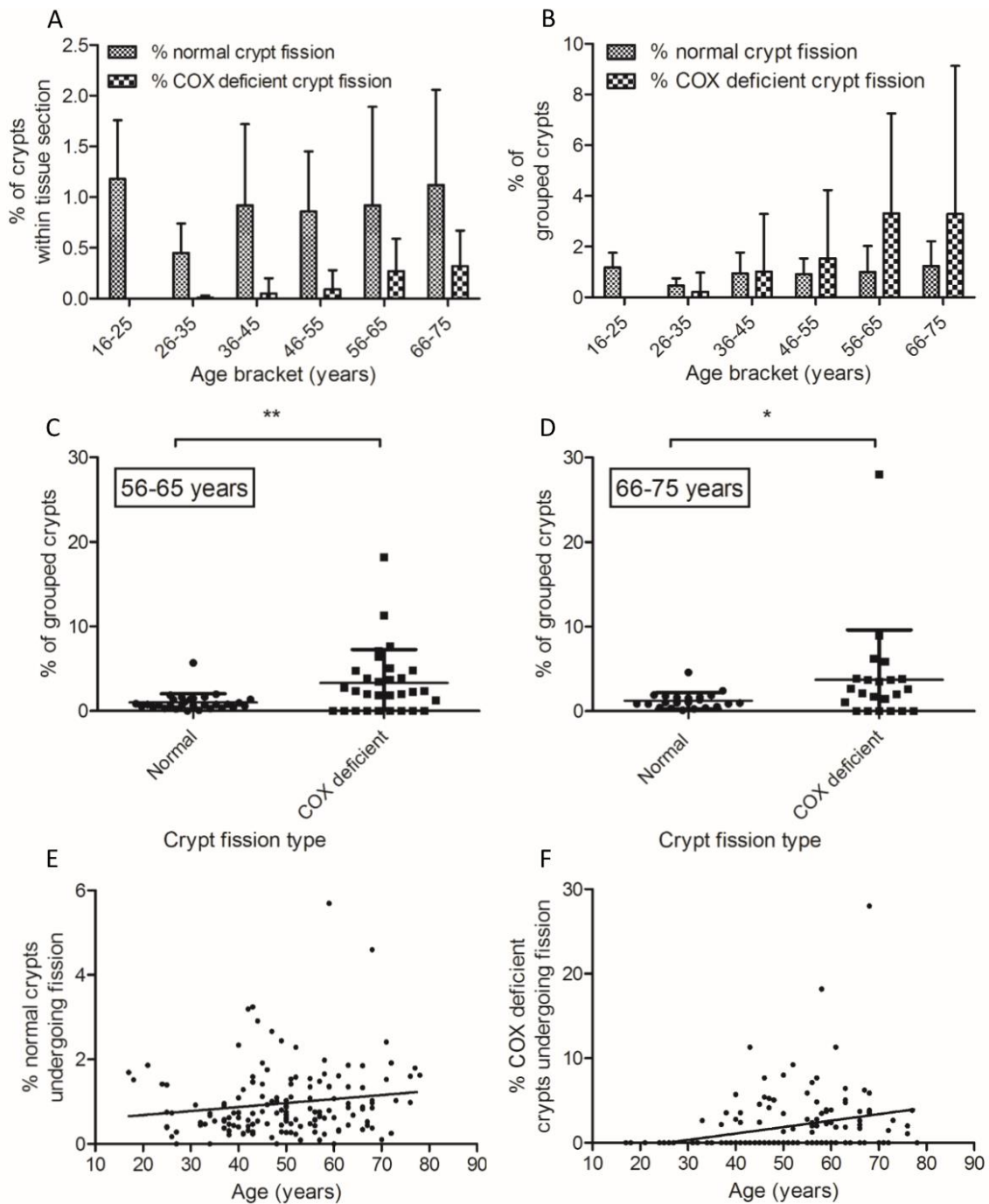
3.4.4 Crypt fission occurrence within human colon

Another feature that was present within human colon tissue samples was crypt fission. As can be seen in Figure 3-1D/E, this occurs within both normal and COX deficient crypts. As crypt fission has the potential to influence the number of COX deficient crypts within human colon, it was prudent to quantify the extent of crypt fission for both normal and COX deficient crypts. Figure 3-4A shows the percentage of total crypts that were undergoing fission, grouped for both normal and COX deficient crypts. The majority of COX deficient crypt fission events were those where both crypts observed within the fission event were fully COX deficient. Where this was not the case, the percentage COX deficiency of each individual crypt contributing towards crypt fission was recorded. For simplicity, all crypts harbouring any fraction of COX deficiency were labelled as COX deficient crypts undergoing fission. There were no instances where one crypt taking part in fission was normal and the other was COX deficient. This highlights the fact that crypt fission is essentially a transfer of the older crypts phenotype to the new crypt. This is most likely via stem cell duplication of existing stem cells, with the subsequent migration into new stem cell niche space, triggering the crypt fission event (Loeffler *et al.*, 1993; Park *et al.*, 1995; Loeffler *et al.*, 1997; Garcia *et al.*, 1999; Greaves *et al.*, 2006). Figure 3-4A shows crypt fission events as a percentage of the total number of crypts within the tissue sections. The data has been grouped into 10 year age brackets and segregated based on whether normal or COX deficient crypt fission is taking place. Due to the large standard deviation, there seems to be a lot of variance within this data set. However, the mean value for each 10 year age bracket appears to be approximately 1% for normal crypt fission events. This is in contrast to COX deficient crypt fission events which have a smaller variance for each 10 year age bracket and an apparent increase with age. However, this may be due to there being more COX deficient crypts present within older human colon samples, meaning more chance of observing a COX deficient crypt fission event in the higher age brackets. Figure 3-4B shows crypt fission events as a percentage of either normal crypts or COX deficient crypts. Therefore, the influence of increasing number of COX deficient crypts with age was negated. Unsurprisingly, we still see normal crypts undergoing crypt fission at approximately 1% because they make up the overwhelming majority of crypts present. However, it does appear that there is an increase in the proportion of COX deficient crypts undergoing fission with increasing age. Furthermore, there seems to be a difference in the means between normal and COX deficient crypts in the higher age groups (56-65 years and 66-75 years) in Figure 3-4B. Therefore, this data was extracted for

the two groups and compared using a Mann Whitney U test for non-parametric data to see if there was a truly statistically significant difference between the two groups for both age brackets (Figures 3-4C/D). This test showed that there was a difference between normal and COX deficient percentage in the higher age groups only, indicating that in the higher age groups, crypts were more likely to undergo crypt fission if they were COX deficient. Linear regression was carried out on the fraction of normal crypts undergoing fission and the fraction of COX deficient crypts undergoing fission (Figure 3-4E/F). Normal crypts didn't show any increase with age (linear regression $R^2 = 0.023$, $p = 0.0613$), whereas COX deficient crypts show a statistically significant increase with age when a linear regression model with a Poisson distribution for non-parametric data was fitted to the data ($p < 0.001$).

Figure 3-4 Crypt fission frequency between normal and COX deficient crypts

Crypt fission occurrence was recorded from human colon tissue biopsies that had been sectioned and subjected to COX/SDH histochemistry. 148 human colon biopsies were included within this patient cohort with ages ranging from 17-78 years. Occurrence was segregated depending on whether the crypt was normal or COX deficient. (A) Crypt fission data was split into 10 year age brackets and graphed separately for normal and COX deficient crypts. Error bars represent standard deviation (B) Crypt fission data was grouped into either normal or COX deficient groups to determine the percentage of crypt fission occurring within the two groups. The data was split into 10 year age brackets and graphed separately for the normal and COX deficient groups. Error bars represent standard deviation. (C) The data from the 56-65 age bracket was extracted so normal vs COX deficient crypt fission could be compared. A Mann Whitney U test was performed for non-parametric data and showed that there was a statistically significant difference between the two groups ($p = 0.0096$). (D) The data from the 66-75 age bracket was extracted so normal vs COX deficient crypt fission could be compared. A Mann Whitney U test was performed for non-parametric data and showed that there was a statistically significant difference between the two groups ($p = 0.0361$). (E) The percentage of crypts undergoing fission in the normal group from each patient sample was graphed in an x-y scatter plot and subjected to linear regression. There was no statistically significant increase with age ($R^2 = 0.023$, $p = 0.0613$). (F) The percentage of crypts undergoing fission in the COX deficient group from each patient sample was graphed in an x-y scatter plot and subjected to a generalised linear regression model with a Poisson distribution for non-parametric data. There was a statistically significant increase with age ($p < 0.001$).



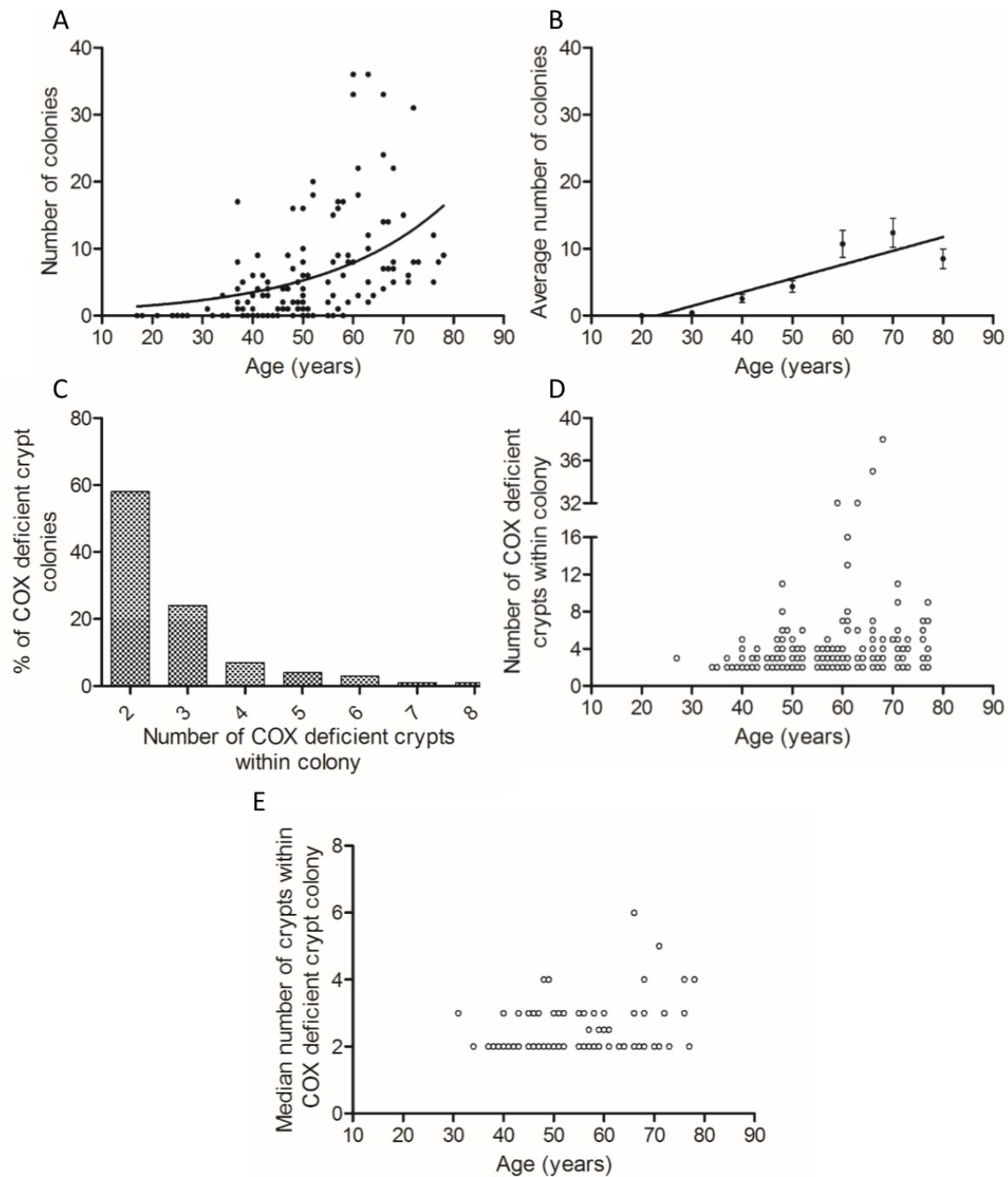
3.4.5 COX deficient crypt colonies within human colon

The last feature examined within human colonic epithelium were COX deficient crypt colonies. These are exemplified in Figure 3-1F. It has previously been shown that patches of fully COX deficient crypts within human colon are clonally related, with those crypts harbouring the same mtDNA mutation (Greaves *et al.*, 2006). The overwhelming majority of COX deficient crypt colonies contained only fully COX deficient crypts. If there were colonies that harboured partially COX deficient crypts, the percentage COX deficiency of those crypts was recorded. For simplicity, the subsequent analysis counted partially COX deficient crypts as COX deficient and no distinction between partially and fully COX deficient was made. Figure 3-5A shows that there is an exponential increase in the number of COX deficient crypt colonies with age (exponential curve doubling time = 17.03 yrs, $R^2=0.21$). When the COX deficient crypt colony data is split into 10 year age brackets and linear regression is conducted, there is a statistically significant increase in the number of COX deficient crypt colonies with age (linear regression $R^2 = 0.79$, $p = 0.0073$) (Figure 3-5B). The next question that was addressed was whether there was an increase in the average number of COX deficient crypts that contribute to a colony. It has been shown that there is an increase in the mean COX deficient patch size with age (Greaves *et al.*, 2006). Figures 3-5C/D address if this data set replicates this finding. It was determined from Figure 3-5C that the data contributing to this plot was not normally distributed as the smallest number of crypts that contribute to a colony is 2, which make up the majority of crypt colonies. Therefore, a method of non-parametric data analysis to determine whether there was an increase in the number of COX deficient crypts that contribute towards a colony was required. In order to do this, the median colony size was plotted for each patient sample (Figure 3-5D) and this data was subject to a generalised linear regression model with a Poisson distribution to test for a statistically significant increase in the median colony size with age. The result showed that there was not a statistically significant increase in the median colony size with age ($R^2 = 0.09$, $p = 0.157$).

Figure 3-5 COX deficient crypt colonies within human colon

The frequency of COX deficient crypt colonies and the number of crypts within each colony was recorded from human colon tissue biopsies that had been sectioned and subjected to COX/SDH histochemistry. 148 human colon biopsies were included within this patient cohort with ages ranging between 17-78 years. The percentage COX deficiency of each crypt contained within a COX deficient crypt colony was recorded. A crypt was included in the analysis of colonies if >20% of the crypt was COX deficient.

(A) The number of COX deficient crypt colonies from each colon biopsy was correlated with age (exponential curve doubling time = 17.03 yrs, $R^2=0.21$). (B) The number of COX deficient crypt colonies were grouped into 10 year age brackets and correlated with age. There was a statistically significant increase with age (linear regression $R^2 = 0.79$, $p = 0.0073$). Error bars represent standard deviation. (C) The distribution of the number of COX deficient crypts that contribute to a COX deficient crypt colony. (D) The number of COX deficient crypts within each colony was recorded and graphed according to age of sample. (E) The median number of crypts within a COX deficient crypt colony was graphed according to age of sample and fitted to a generalised linear regression model with a Poisson distribution for non-parametric data. There was not a statistically significant increase with age ($R^2 = 0.09$, $p = 0.157$).



3.4.6 Removal of crypt colonies from biological data

We have assumed from previous literature that the emergence of COX deficient crypt colonies are the result of COX deficient crypt fission (Greaves *et al.*, 2006). In chapter 4 it was necessary to model the accumulation of COX deficiency within human colonic epithelium with age. In order to have a wide variety of biological data to model, an additional data set that would remove the impact that COX deficient colony formation via crypt fission has on the biological data was required. The additional data set would contain only the *de novo* COX deficient crypts, thereby providing a data set that removed the effect of crypt fission. Figure 3-6A is a depiction of how the human colon COX deficiency data was manipulated. In the case of a crypt colony made up of purely fully COX deficient crypts, this would now only represent one fully COX deficient crypt in order to emphasise the *de novo* COX deficient crypts. However, as previously mentioned, a small minority of crypt colonies contained partially COX deficient crypts. In this case, the most frequent COX deficiency fraction was used to represent the colony. In the case of a colony being made up purely by partially COX deficient crypts, the mean COX deficiency fraction was used to represent the colony. Figure 3-6B shows the biological data before manipulation and Figure 3-6C shows the biological data after manipulation. Both data sets have been split into 10 year age brackets and according to COX deficiency fraction. From comparing the difference between the two data sets, we see that removing COX deficient colonies has impacted fully COX deficient crypts the most, highlighting the fact that the majority of crypts within COX deficient crypt colonies are fully COX deficient.

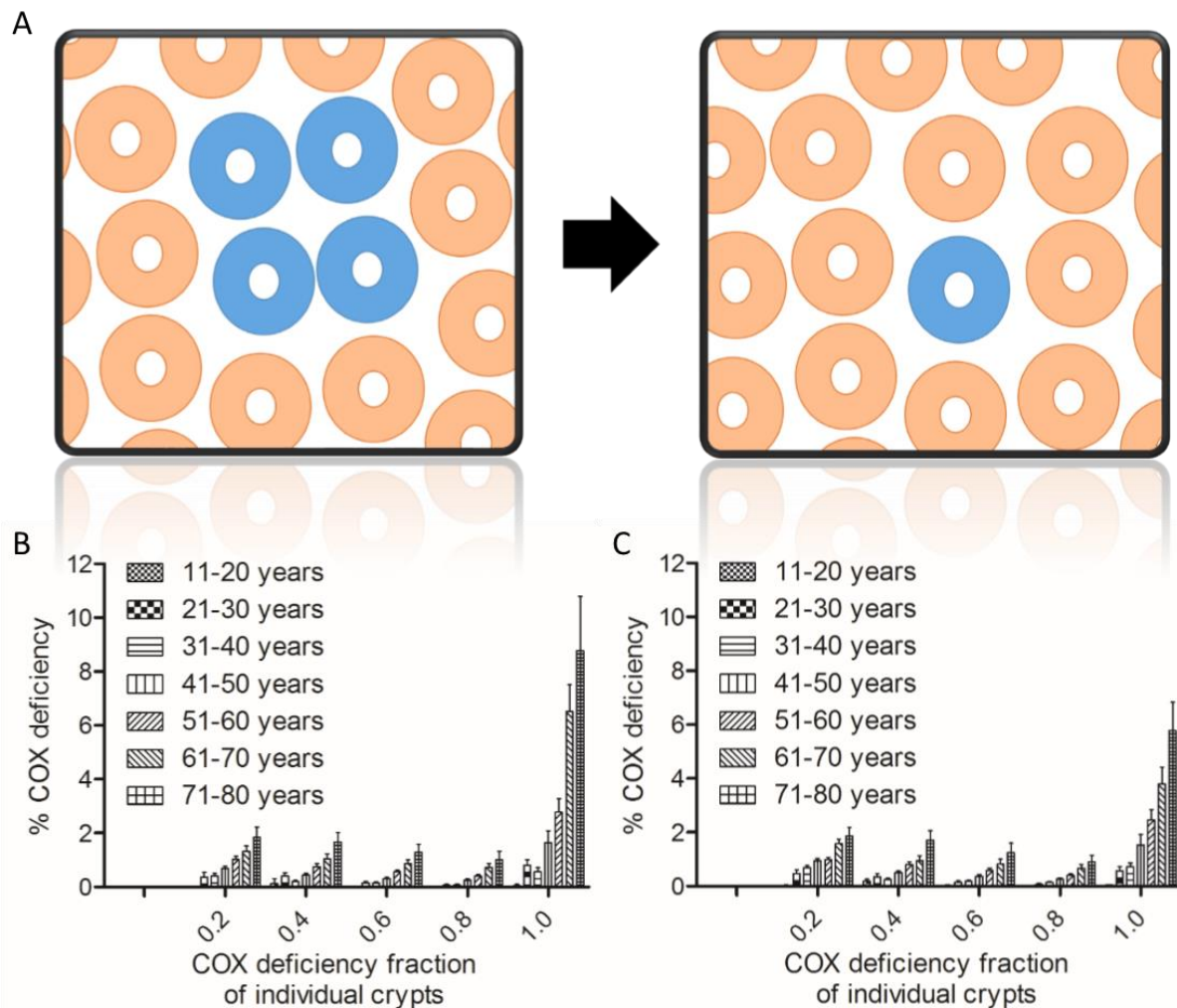


Figure 3-6 Crypt colony correction for human colon COX deficiency data.

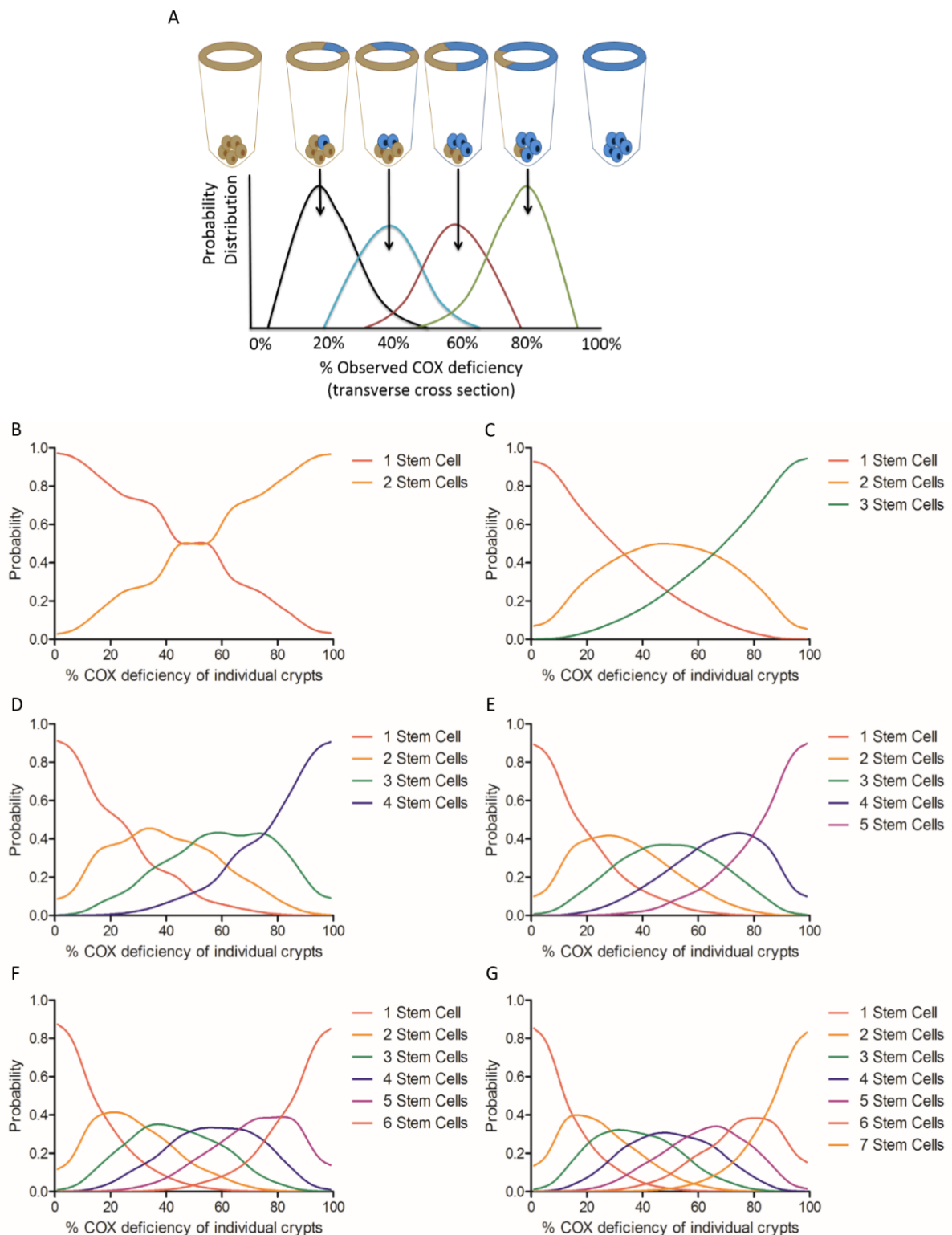
The percentage COX deficiency of individual crypts along with the number of colonies and the number of COX deficient crypts within those colonies was quantified from human colon tissue biopsies that had been sectioned and subjected to COX/SDH histochemistry. 148 human colon biopsies were included within this patient cohort with ages ranging from 17-78 years. (A) Schematic representation of data manipulation that takes into account the presence of COX deficient crypt colonies. A COX deficient crypt colony was reduced to one COX deficient crypt with its percentage COX deficiency equal to that of the mode of the entire colony, in the majority of cases this was equal to 100%. If the colony was made up of partially COX deficient crypts only, the percentage COX deficiency was equal to the mean of the entire colony. (B) COX deficient crypt percentage segregated based on the nearest COX deficiency fraction and split into 10 year age brackets. Error bars represent SEM. (C) COX deficient crypt percentage segregated based on the nearest COX deficiency fraction and split into 10 year age brackets after the COX deficient crypt colony correction was performed. Error bars represent SEM.

3.4.7 Relating COX deficiency percentage to number of COX deficient stem cells

In chapter 4, it was necessary to model the accumulation of COX deficiency within human colonic epithelium with age. This was done by assuming there is a relationship between the percentage COX deficiency that is observed within transverse cross sections of crypts, and the fraction of stem cells that are COX deficient within the stem cell niche of crypts. However, it can be assumed that there will be a distribution for the percentage COX deficiency observed for each fraction of COX deficient stem cells contained within the stem cell niche due to stochastic variation in the migration of COX deficient stem cell progeny. Therefore, a model was developed to simulate this stochastic variation in order to generate probability distributions that can be used for any number of stem cells that are said to be contained within the stem cell niche of human colonic crypts (appendix 1.3.4). Figure 3-7A depicts how the probability distributions can be used to relate number of COX deficient stem cells to percentage COX deficiency observed, and vice versa. Figures 3-7B-G shows the constructed probability distributions for 3 to 8 stem cells present in the stem cell niche, respectively. These generated probability distributions can be used to convert the COX deficiency data attained from human colon epithelium in the form of percentages per crypt into number of stem cells that are COX deficient within individual crypts when the total number of stem cells is assumed. These probability distributions can also be used to relate the number of stem cells COX deficient to a percentage COX deficiency observed at the transverse cross section. It can be seen that the more stem cells that are assumed to be present within the crypt, the narrower the probability distribution becomes for each number of stem cells within a crypt.

Figure 3-7 Model relating percentage COX deficiency observed to likely number of COX deficient stem cells

A model was developed that stochastically simulated the propagation of COX deficient stem cell progeny as they migrate to the level at which the COX deficiency can be observed (appendix 1.3.4.1). Probability distributions were generated that allow the conversion of % COX deficiency observed to the likely number of COX deficient stem cells the percentage represents (appendix 1.3.4). (A) Schematic representation of a probability distribution where a crypt contains 5 stem cells. A probability distribution will be associated to each number of COX deficient stem cells, between 1 and 4 in this case. 0 and 5 stem cells will have a probability of 1 for being associated with 0% and 100% observed, respectively. Probability distributions have been generated for crypts containing (B) 3 stem cells (C) 4 stem cells (D) 5 stem cells (E) 6 stem cells (F) 7 stem cells (G) 8 stem cells.



3.4.8 Biological data converted to stem cell number

In chapter 4, it was necessary to model the accumulation of COX deficiency within human colonic epithelium with age. The probability distributions generated in section 3.4.7 were used to convert COX deficiency percentage observed to number of stem cells COX deficient in order for subsequent modelling work to be comparable. Figures 3-8(A-F) shows the biological data represented as crypts containing a total of 3-8 stem cells, respectively. It can be seen that the probability distribution manipulation does not affect fully COX deficient crypts as they were initially represented as 100% COX deficiency, which will always correspond to the total number of stem cells contained within the stem cell niche being COX deficient. The same is true for 0% COX deficient (normal crypts), as these will always represent 0 stem cells being COX deficient, therefore probability distributions are not required for manipulating 0% and 100% COX deficiency to stem cell number.

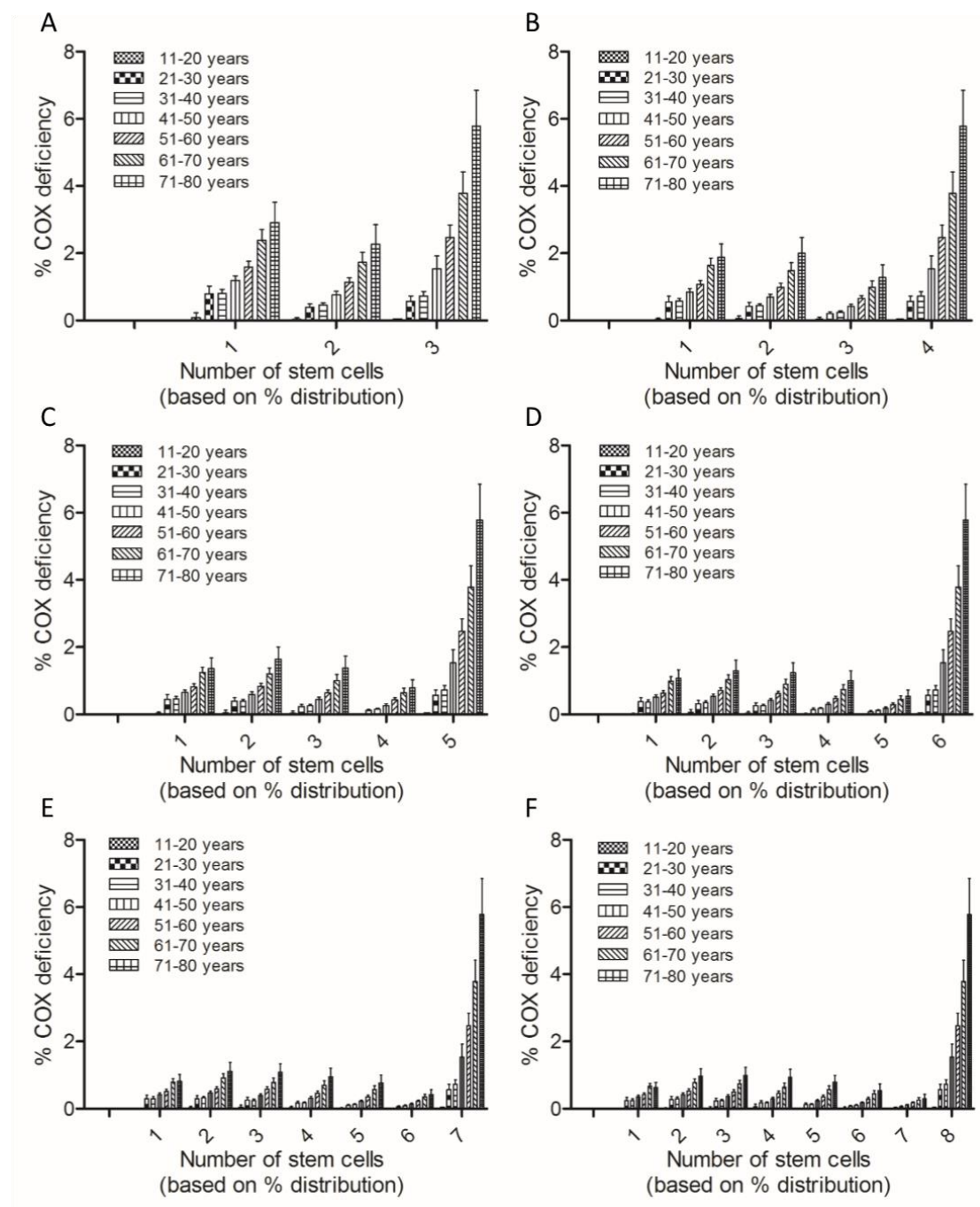


Figure 3-8 Distributional binning for COX deficient stem cell number

Probability distributions were generated in order to relate the percentage COX deficiency observed at the transverse cross section of a crypt to the likely number of COX deficient stem cells that were present at the base of a crypt. Probability distributions can be generated for any number of stem cells specified to be present within the stem cell niche. The COX deficiency data from human colon was converted to number of stem cells using the probability distributions for (A) 3 stem cells, (B) 4 stem cells, (C) 5 stem cells, (D) 6 stem cells, (E) 7 stem cells and (F) 8 stem cells being present within the stem cell niche of human colonic crypts.

3.5 DISCUSSION

The quantification of COX deficiency within human colon tissue biopsies has previously been assessed (Taylor *et al.*, 2003). However, this study classed a COX deficient crypt as those containing >50% COX deficiency. All other crypts were classified as normal for COX activity. Furthermore, the COX deficiency fraction of individual crypts was not taken into account, meaning the data obtained within this study has more depth and can be more useful when assessing the mechanism that allows the accumulation of COX deficiency within human colon. On the other hand, Taylor et al also showed that there was an exponential increase in COX deficient crypts with age, reaching ~16% at >80 years of age (Taylor *et al.*, 2003).

The assessment of partially COX deficient crypts within this study has showed some interesting features. For instance, not only is there an exponential increase in the number of fully COX deficient crypts with age, but there is also an exponential increase in the number of partially COX deficient crypts as well, but to a lesser extent. This has important implications as in order to achieve this exponential in partially COX deficient crypts with age, there must be something driving an increase in the rate of partially COX deficient crypt acquisition. This is in contrast to what is shown in (Kozar *et al.*, 2013) where they see a constant level of partially labelled crypts with age using their system. Granted, we are not comparing like for like between these two systems, for instance, mouse small intestine using a fluorescent reporter marker as a stem cell lineage marker vs human colon using COX deficiency as a stem cell lineage marker.

Another interesting feature is the distribution of partially COX deficient crypts. For instance, the decreasing frequency of crypts with increasing COX deficiency fraction with a substantial frequency peak at the 0.2 COX deficiency fraction. This indicates that there are approximately 5 stem cells present within human colonic crypts and that partially COX deficient crypts spend more time in their small fraction form compared to their large fraction form. Baker et al corroborate that 4-6 functional stem cells reside within human colonic crypts also (Baker *et al.*, 2014). Unfortunately, it was not possible to split the data up into 10 year age brackets to determine whether the peak at the 0.2 COX deficiency fraction was present at all ages. This was because there was a substantial reduction and an unequal skew for the number of COX deficient crypts available within each age bracket. The only option was to pool the data from all 148 patient samples, which represented ~140,000 partially COX

deficient crypts, and determine the distribution for all age groups. If there were an infinite number of partially COX deficient crypts available, one should expect equal peaks at varying frequencies, with each peak being equal to the number of stem cells that are COX deficient at the base of the crypt, hence making it clearer as to the number of stem cells contained within human colonic crypts. The distribution of partially COX deficient stem cells is something that needs to be replicated when modelling accumulation of COX deficiency within human colon.

Crypt fission has also been observed within this study. The data shows that when looking at the proportion of normal and COX deficient crypts undergoing fission, there is a statistically significant increase in the proportion of COX deficient crypts undergoing fission with age (Figure 3-4F). The data also shows a statistically significant difference between the fraction of normal crypts undergoing fission (around 1%) and the fraction of COX deficient crypts undergoing fission (around 3%) within age groups >56 years of age. This indicates that there is a greater chance of COX deficient crypts undergoing fission compared to normal crypts. As crypt fission is likely triggered by the actions of the stem cells contained at the base of crypts (Loeffler *et al.*, 1993; Park *et al.*, 1995; Loeffler *et al.*, 1997; Garcia *et al.*, 1999; Greaves *et al.*, 2006), it is likely that stem cell perturbations caused by COX deficiency result in the increased likelihood of COX deficient crypts to undergo fission. Crypt fission is an important mechanism that has the potential to facilitate the increase in COX deficiency within the colon. This is an important feature that needs to be taken into account when modelling COX deficiency accumulation within the colon.

COX deficient crypt colonies have also been observed within this study. We see there is an exponential increase in the number of COX deficient crypt colonies with age. This correlates well with the exponential increase in COX deficient crypts with age. However, unlike in a previous study (Greaves *et al.*, 2006), this data does not show a statistically significant increase in COX deficient crypt colony size with age. The majority of COX deficient crypt colonies exist as 2 crypts. This adds weight to the hypothesis that crypt fission takes a substantial amount of time to complete and the chance of having many crypt fission events taking place within the same colony within the average human lifespan is small.

3.6 CONCLUSION

Conducting an in-depth investigation of COX deficiency within human colon from such a large cohort of patient samples has provided the framework for further work that sets out to

understand the processes involved in monoclonal conversion, which can account for the accumulation of COX deficiency within normal human colon tissue.

Data sets have been generated which are comparable to data that can be produced from modelling the process of niche succession within individual crypts, with and without the influencing factor of crypt fission. This has been achieved by characterising crypt fission and COX deficient crypt colonies within human colonic epithelium. This has been further elucidated by accounting for the variation in COX deficiency percentage data and its relationship to the potential number of stem cells the COX deficiency percentage represents. This was an essential piece of data that was required before anything else and is why the first results chapter of this thesis is dedicated to the acquisition of the biological data from human colonic epithelium.

Chapter 4

Modelling Stem Cell

Dynamics within Colonic

Epithelium

Chapter 4 Modelling stem cell dynamics within colonic epithelium

4.1 INTRODUCTION

Gut epithelium is one of the most attractive tissue types for studying the complex relationships that exists between many different cell types due to its defined stem cell niche and hierarchical structure. Small intestinal epithelium and colonic epithelium are the most widely looked at when investigating these relationships. The study of other tissue types is possible, however these often have an undefined stem cell niche, making it harder to study the complex interactions taking place between stem cells and their progeny (Morrison and Spradling, 2008).

Intestinal and colonic epithelium harbour an array of millions of crypt-like structures that reside within the mucosal layer and is supported by the muscularis mucosae and muscularis externa muscle layers. Whereas the colonic epithelium is made up only of crypts, the small intestine contains additional protrusions into the lumen, called villi, in order to increase the epithelial surface area for maximum absorption of nutrients. As crypts are the independent units common to both tissue types, they have become the focus of many investigations that try to understand the mechanisms that drive the regeneration of the epithelium. This is not only to understand the mechanism that drives homeostasis within crypts, but also to understand how these mechanisms become perturbed, for instance during tumour formation and cancer progression. Crypt architecture makes these tissues ideally suited for the investigation of stem cell dynamics.

It is widely known that multiple stem cells are present at the base of crypts (Scoville *et al.*, 2008) which function to regenerate the cells of the crypt throughout life, and hence the epithelium. This has been demonstrated by the fact that individual crypts can manifest multiple phenotypes (Griffiths *et al.*, 1988; Winton *et al.*, 1988; Park *et al.*, 1995). There are many studies that have documented the process of monoclonal conversion of crypts from one phenotype, often a native state, to an altered phenotype, either induced or natural. As it has become widely known, the phenotype of the crypt is derived from the phenotype of the stem cells themselves. Monoclonal conversion of a crypt occurs due to the existence of competing phenotypes within the stem cell pool which are passed on to the stem cell progeny, and hence the crypt itself. All stem cells derived from a single founder are termed stem cell clones. With this in mind, it is reasonable to assume that the clone width (i.e. the number of cells observed within a crypt with an altered phenotype), as a percentage of the whole crypt, serves as a

fraction of stems cell clones present within the crypt (Lopez-Garcia *et al.*, 2010; Snippert *et al.*, 2010; Kozar *et al.*, 2013). When all the stem cells within a niche become derived from the one stem cell clone, this is termed niche succession. It is assumed niche succession is the result of the complex stem cell dynamics that take place within the stem cell niche of crypts, which are influenced by both cell intrinsic and cell extrinsic factors. When stem cell dynamics are referred to, this takes into account the type of division event a stem cell undergoes and the resulting effect on the other stem cells within the same stem cell niche. Stem cell division events can be asymmetric (renewed stem cell and stem cell progeny) or symmetric (either two renewed stem cells or two stem cell progeny) in nature. Monoclonal conversion rules out purely asymmetric stem cell division tissue maintenance. Stem cell replacement via symmetric stem cell division allows stem cell clones to expand within their niche and explains the emergence of monophenotypic crypts over time.

Aged human colonic epithelium contains both partially and fully COX deficient crypts (Taylor *et al.*, 2003). Due to the presence of partially COX deficient crypts, this suggests that COX deficiency could be used as a stem cell lineage marker (Taylor *et al.*, 2003). This is akin to studies conducted within mice that investigate stem cell dynamics using either inducible or stochastic markers for cell lineage tracing (Lopez-Garcia *et al.*, 2010; Snippert *et al.*, 2010; Kozar *et al.*, 2013). Recently, COX deficiency was used to investigate stem cell dynamics within aged human colon (Baker *et al.*, 2014). However, the use of COX deficiency as a neutral stem cell lineage marker requires more in-depth investigation as, unlike markers of mouse stem cell lineage, COX deficiency is by definition a pathogenic alteration to the stem cells cellular function.

4.2 AIMS OF STUDY

This study aimed to investigate the mechanism by which COX deficiency accumulates within human colonic epithelium with age. A robust computational model would be developed that sheds light on the intra-crypt accumulation of COX deficiency with age.

In order to be as biologically accurate as possible, the acquisition of COX deficiency within individual stem cells would be stochastically simulated via relaxed replication and random segregation of mutated mtDNA molecules. Using biological data from human patients described in chapter 3, hypotheses would be tested as to the mechanism by which COX deficiency accumulates within colonic epithelium.

Hypothesis were tested as variable parameters which included:

1. Stem cell division dynamics (asymmetric vs symmetric stem cell division)
2. Number of stem cells present within human colonic crypts
3. Mitochondrial DNA mutation rate
4. Crypt fission occurrence
5. COX deficient stem cell advantage/disadvantage

Using the most robust biological data in conjunction with the most biologically accurate model, optimum parameter sets were sought in order to explain how the process of niche succession, monoclonal conversion and hence, COX deficiency accumulation takes place within normal human colonic epithelium.

4.3 METHODOLOGY

4.3.1 Computational model of human colonic stem cell dynamics

A model simulating the accumulation of COX deficiency within a population of crypts was designed and constructed within MATLAB (MathWorks). It can be described as a multi-scale model simulating the acquisition and subsequent clonal expansion of mutated mtDNA molecules within individual stem cells, whilst simultaneously simulating the stem cell dynamics (asymmetric/symmetric stem cell division) within a stem cell niche, potentially leading to niche succession. A detailed description of the model is contained within section 2.2.10.2. The model has been developed over the course of my MRes and PhD. A model development timeline is shown in Table 4-2. Each model has additional parameters that either allow hypothesis testing to be carried out, or make the model more biologically relevant. Models 1 and 2 were constructed during my MRes degree (Craig Stamp MRes Dissertation). Models 3-10 were constructed during my PhD and represent major enhancements. Table 4-1 describes each parameter and enhanced functionality that is incorporated into the model.

Table 4-1 Table of parameters and functionality

Parameter	Description
numRuns	The number of crypts being simulated within simulated colon.
mutThreshold	The fraction of mutated mtDNA (heteroplasmy) within individual stem cells that denotes a COX deficient stem cell.
numDiv	The number of division events per crypt.
mtDNA	The number of mtDNA molecules that are contained within each stem cell.
initS	The number of stem cells that are simulated within each crypt.
P(asymmetric)	The probability that a stem cell will undergo asymmetric stem cell division. The probability for symmetric division ($P^{(symmetric)}$) is therefore $1 - P_{asymmetric}$. $P_1^{(symmetric)}$ is the probability that a stem cell will divide to produce 2 new stem cells. $P_2^{(symmetric)}$ is the probability that a stem cell will divide to produce 2 stem cell progeny cells. For each type of symmetric division ($P_1^{(symmetric)}$ and $P_2^{(symmetric)}$) the probability is $1 - P_{asymmetric}/2$.
P(COXDefSC)	The probability that a dividing stem cell will mutate into a COX deficient stem cell.
Adv(COXDefSC)	The symmetric division advantage conveyed to COX deficient stem cells. Therefore, the probability that a COX deficient stem cell will divide symmetrically to produce 2 new stem cells is $P_1^{(symmetric)} * Adv(COXDefSC)$.

	With this, asymmetric stem cell division is reduced by this increased amount. $P_{\text{new}}^{\text{(asymmetric)}} = P^{\text{(asymmetric)}} - ((P_1^{\text{(symmetric)}} * \text{Adv(COXDefSC)}) - P_1^{\text{(symmetric)}})$.
mutationRate	For each mtDNA replication, a mutation rate as a probability that a mtDNA replication event will lead to the acquisition of a pathogenic mutation effecting COX activity if clonal expansion occurs.
mutationRateFold	The mutation rate fold increase from the first stem cell division to the stem cell division that represents an 80 year lifespan of a human.
cryptNormalPercentage	The probability that crypt fission will be initiated at each stem cell division step.
cryptFissionFactor	The probability increase ($\text{cryptNormalPercentage} * \text{cryptFissionFactor}$) that determines the crypt fission probability for COX deficient crypts at each stem cell division step.
mtDNASpeciesTracking1	The ability to track each newly acquired mtDNA mutation as an individual mtDNA species. Once a mtDNA molecule has acquired a mutation, no more mutations can be added.
mtDNASpeciesTracking2	The ability to track each newly acquired mtDNA mutation as an individual mtDNA species. Multiple mutations can be acquired for each simulated mtDNA molecule.
COXCorrectionFactor	The number of stem cell divisions that occur for normal stem cells before COX deficient stem cells incorporate an additional division.
COXDefCycleRepeats	The number of additional divisions COX deficient stem cells undergo at the time point determined by COXCorrectionFactor.
DivisionSegregationAdvantage	The ability of mutated mtDNA molecules to incorporate a segregation bias upon asymmetric stem cell division.

Table 4-2 Evolution of model parameters

Parameter	Model Permutation									
	Model 1	Model 2	Model 3	Model 4	Model 5	Model 6	Model 7	Model 8	Model 9	Model 10
numRuns	✓	✓	✓	✓	✓	✓	✓	✓	✓	✓
mutThreshold			✓	✓	✓	✓	✓	✓	✓	✓
numDiv	✓	✓	✓	✓	✓	✓	✓	✓	✓	✓
mtDNA				✓	✓	✓	✓	✓	✓	✓
initS	✓	✓	✓	✓	✓	✓	✓	✓	✓	✓
P(asymmetric)	✓	✓	✓	✓	✓	✓	✓	✓	✓	✓
P(COXDefSC)	✓	✓	✓							
Adv(COXDefSC)		✓	✓	✓	✓	✓	✓	✓	✓	✓
mutationRate			✓	✓	✓	✓	✓	✓	✓	✓
mutationRateFold				✓	✓	✓	✓	✓	✓	✓
cryptNormalPercentage	✓	✓	✓	✓	✓	✓	✓	✓	✓	✓
cryptFissionFactor	✓	✓	✓	✓	✓	✓	✓	✓	✓	✓
mtDNA Species Tracking 1				✓	✓	✓	✓	✓	✓	
mtDNA Species Tracking 2					✓	✓	✓	✓	✓	
COXCorrectionFactor						✓	✓	✓	✓	
COXDefCycleRepeats							✓	✓	✓	
Division Segregation Advantage										✓

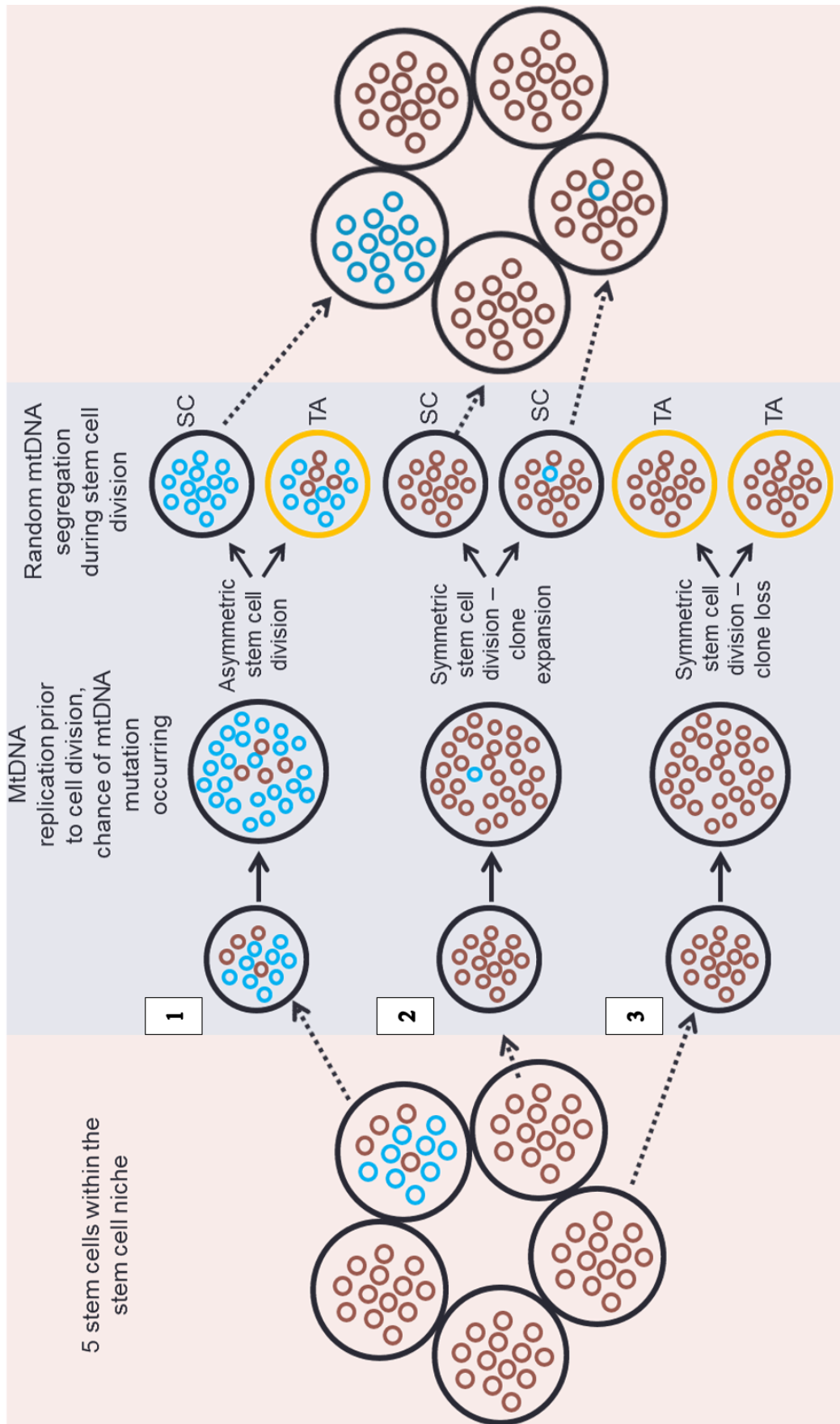
4.4 RESULTS

4.4.1 Human niche succession model

A model of COX deficiency accumulation within human colon epithelium was developed and is described in section 2.2.10.2 with model code contained within appendix 1.3.2. The model simulates a population of crypts (numRuns). Each crypt contains a specified number of stem cells (initS), with each stem cell containing a specified number of mtDNA molecules (mtDNA). Asynchronous stem cell division occurs once per week, making the total number of divisions per stem cell equal to 4171 over 80 years (numDivs). Asymmetric (stem cell divides to replicate itself and produce a stem cell progeny cell) and symmetric (stem cell divides to produce two renewed stem cells or two stem cell progeny cells) stem cell division can take place at division and is determined by the probability of asymmetric division occurring (Pa). If $Pa < 1$, then symmetric stem cell division probability is $1 - Pa$, with each form of symmetric division having a probability of occurring equal to $\frac{1}{2}(1 - Pa)$. The base model simulates relaxed replication and random segregation of mtDNA molecules upon division. More simply, each stem cell division results in the stochastic doubling of the mtDNA pool with their subsequent stochastic segregation into two groups (i.e two daughter cells). Figure 4-1 depicts the fate outcomes for each type of division that can take place within the model. Once the simulation is complete, an algorithm (appendix 1.3.3.4) takes the model data and converts it into COX deficiency frequency using 75% mutated mtDNA to confer a stem cell as COX deficient (mutThreshold). This allows the model data to be comparable to the biological data acquired. The model allows the emergence of partially and fully COX deficient crypts, therefore allowing the niche succession phenomenon to be investigated within human colon epithelium.

Figure 4-1 Schematic diagram of niche succession model

Graphical representation of the niche succession model. Portrayed are the 3 possible outcomes for a stem cell undergoing division within the model. The stem cells on the left (pink shaded) represent the state of the stem cells before division with their defined mtDNA content. Red circles represent normal mtDNA and blue circles represent mutated mtDNA. The stem cells on the right (pink shaded) represent the state of the stem cells after division. The middle (blue shaded) represents the intermediary phase which includes mtDNA population doubling via relaxed replication and mtDNA segregation into daughter cells. Each stem cell can either undergo (1) asymmetric division (1 stem cell and 1 stem cell progeny cell) (2) symmetric division (2 stem cells) (3) symmetric division (2 stem cell progeny cells). The first possible outcome also portrays clonal expansion of mutated mtDNA within a single stem cell. The second possible outcome portrays mtDNA mutation acquisition within a single stem cell.



4.4.2 Human niche succession model testing

Once the model was constructed, the model was tested by varying each parameter and determining the effect this has on the model output. The model output was in the form of COX deficiency frequency within simulated colon, segregated into 10 year age brackets, akin to the biological data. All model testing was performed assuming 5 stem cells were contained within the stem cell niche (section 3.4.2). Table 4.3 gives section references for each parameter tested.

Table 4-3 Parameters tested with corresponding section reference

Parameter	Section
Asymmetric division probability	4.4.2.1, 4.4.2.5 and 4.4.2.6
De novo mutation rate	4.4.2.2
Crypt fission	4.4.2.3
COX deficient stem cell advantage	4.4.2.4
mtDNA copy number	4.4.2.5 and 4.4.2.6

4.4.2.1 Asymmetric division probability

The first parameter that was tested was the effect of changing the asymmetric stem cell division probability. Figure 4-2 exemplifies the effect of changing the asymmetric stem cell division probability. When the probability of asymmetric stem cell division is increased, there is an increased frequency of partially COX deficient crypts and a decreased frequency of fully COX deficient crypts. It would appear that in order to achieve partially COX deficient crypts at a frequency seen within human colonic epithelium, the probability of asymmetric stem cell division needs to be >0.97 . However, when the probability of asymmetric stem cell division is high enough (Figure 4-2F/G), partially COX deficient crypt frequency becomes too high and fully COX deficient crypt frequency becomes too low, effectively reaching an inversion threshold. A model where purely asymmetric stem cell division is simulated (Figure 4-2H) results in the emergence of purely partially COX deficient crypts. If symmetric stem cell division is absent, niche succession and monoclonal conversion cannot occur to result in a fully COX deficient crypt. The acquisition of a fully COX deficient crypt in this scenario would be extremely rare, requiring an extremely high mtDNA mutation rate, resulting in a COX deficiency frequency that does not match the biological data.

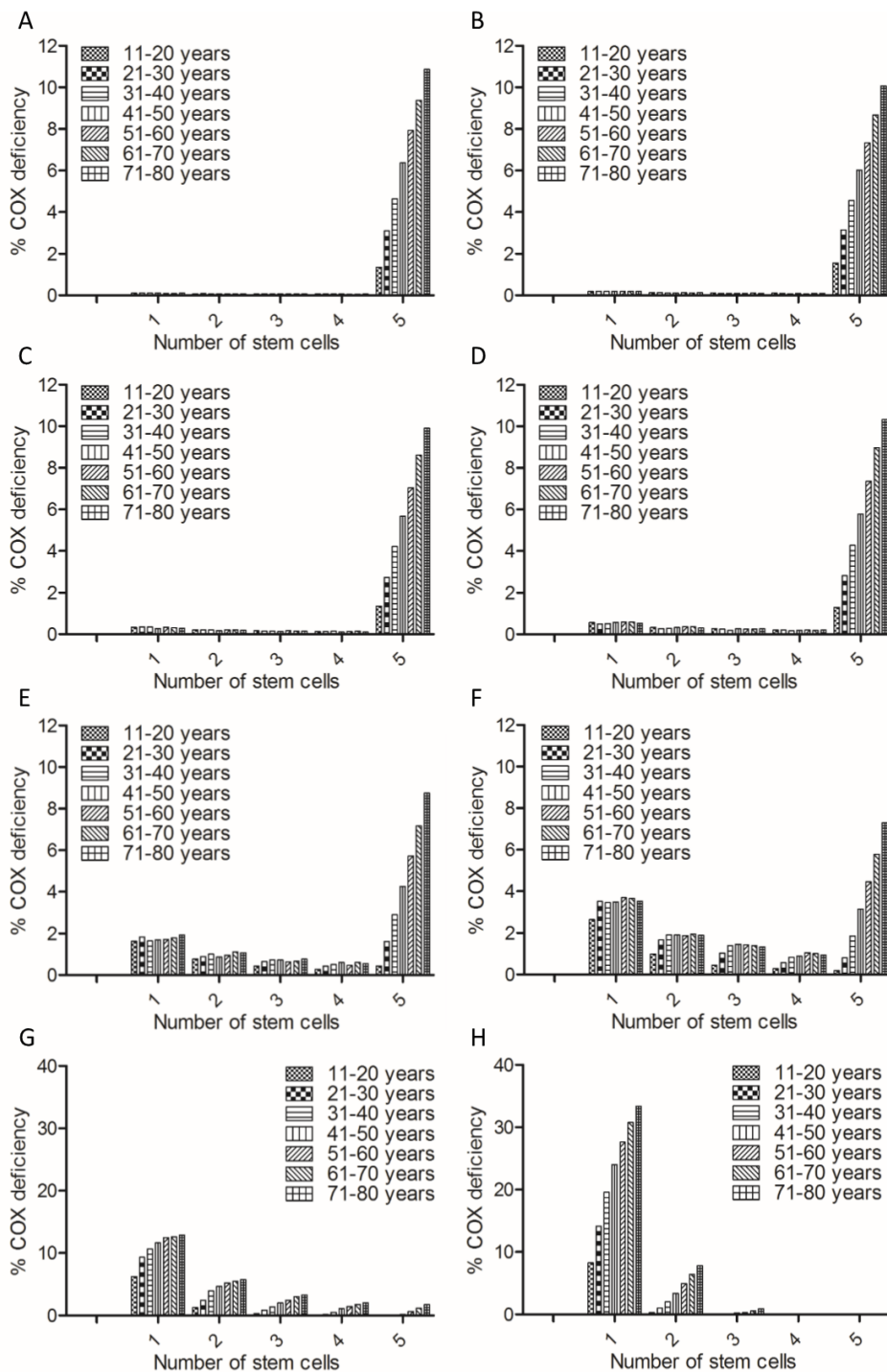


Figure 4-2 Asymmetric division probability

The effect of changing asymmetric division probability within the human niche succession model was ascertained. 5000 crypts were simulated, 75% mutated mtDNA conferred COX deficiency to a stem cell. 5 stem cells were simulated, each with 100 mtDNA molecules present. A constant *de novo* mutation rate was set to 3×10^{-5} mutated mtDNA/mtDNA replication. Simulations were carried out with asymmetric division probabilities (A) 0.75 (B) 0.90 (C) 0.95 (D) 0.97 (E) 0.99 (F) 0.995 (G) 0.999 (H) 1.00.

4.4.2.2 *De novo* mtDNA mutation rate

The effect of altering the *de novo* mtDNA mutation rate was ascertained. Figure 4-3 exemplifies the effect of changing the *de novo* mtDNA mutation rate. When the mutation rate is increased, there is an increased frequency of both partially and fully COX deficient crypts. It would appear that in order to achieve partially and fully COX deficient crypts at a frequency seen within human colonic epithelium, the mutation rate must be between 1×10^{-5} and 5×10^{-5} mutated mtDNA(mtDNA) replication. This would be equivalent to 3.02×10^{-7} and 6.04×10^{-8} mutations per bp per generation, which is similar to the estimated mtDNA mutation rate quoted by Coller et al of between $3 \times 10^{-7} - 3 \times 10^{-8}$ mutations per bp per generation (Coller *et al.*, 2001). Once the mutation rate is high enough, there is a plateauing effect where there is a reduction in the number of partially COX deficient crypts with age along with a decreasing rate of accumulation of COX deficient crypts (Figure 4-3E/F). The acquisition of a *de novo* mutation, which is controlled by the mutation rate, is the start of the clonal expansion process, be it destined for extinction or fixation. Once the mutation rate is high enough, clonal expansion of mutated mtDNA becomes less important due to the shear rate of *de novo* mutation acquisition resulting in a stem cell's COX deficiency. This explains the COX deficiency frequency in the scenario within Figures 4-3E/F.

The effect of increasing *de novo* mtDNA mutation rate with age was also investigated. Figure 4-4 exemplifies the effect of changing the *de novo* mtDNA mutation rate with age. Increasing the *de novo* mutation rate increased the frequency of both partially and fully COX deficient crypts with age. The greater the increase in *de novo* mtDNA mutation rate with age, the greater the increase in COX deficient crypts with age.

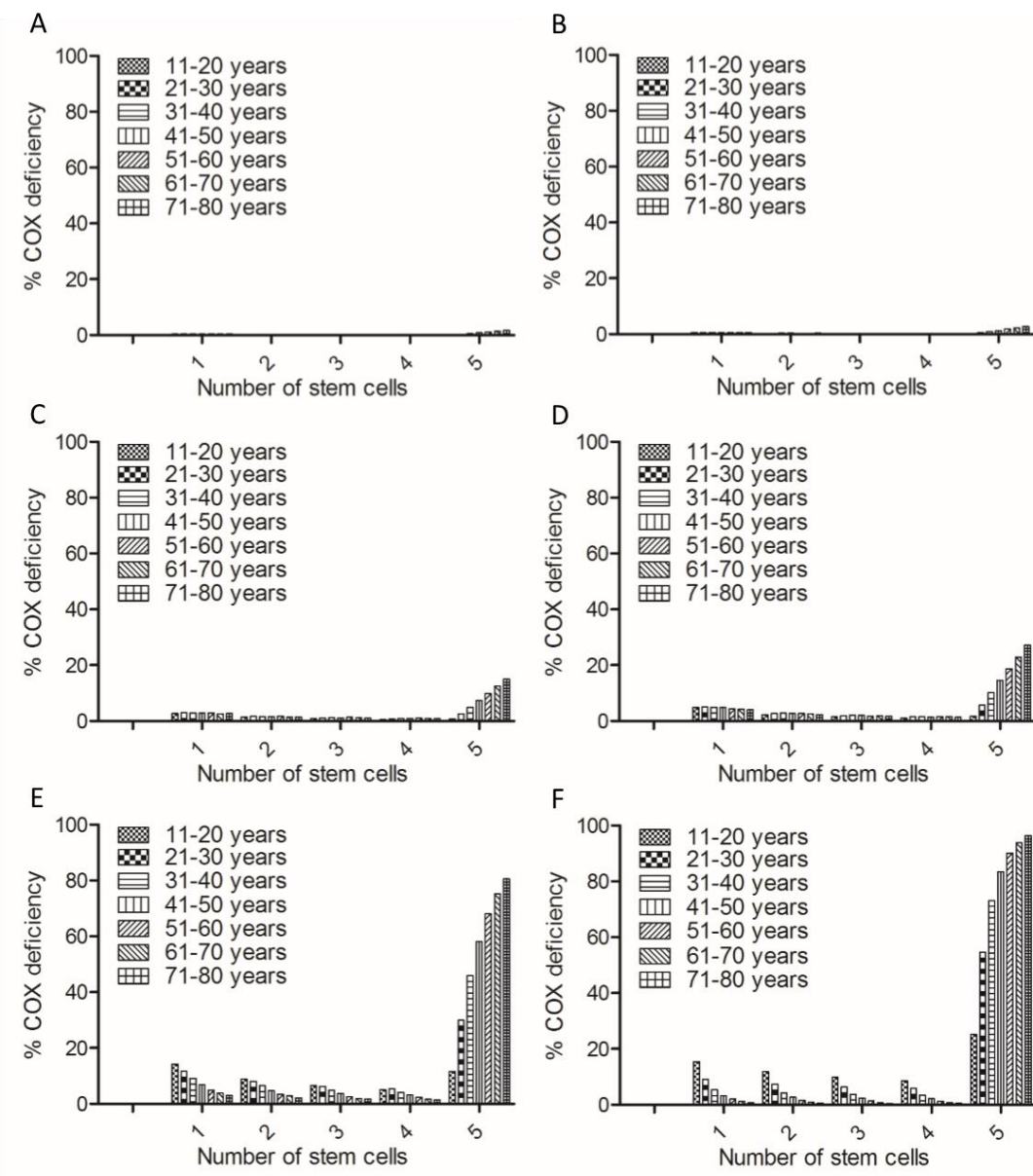


Figure 4-3 Constant *de novo* mutation rate

The effect of changing the *de novo* mutation rate within the human niche succession model was ascertained. 5000 crypts were simulated, 75% mutated mtDNA conferred COX deficiency to a stem cell. 5 stem cells were simulated, each with 100 mtDNA molecules present. Asymmetric division probability was set to 0.99. Simulations were carried out with a constant *de novo* mutation rate of (A) 5×10^{-6} (B) 1×10^{-5} (C) 5×10^{-5} (D) 1×10^{-4} (E) 5×10^{-4} (F) 1×10^{-3} mutated mtDNA/mtDNA replication.

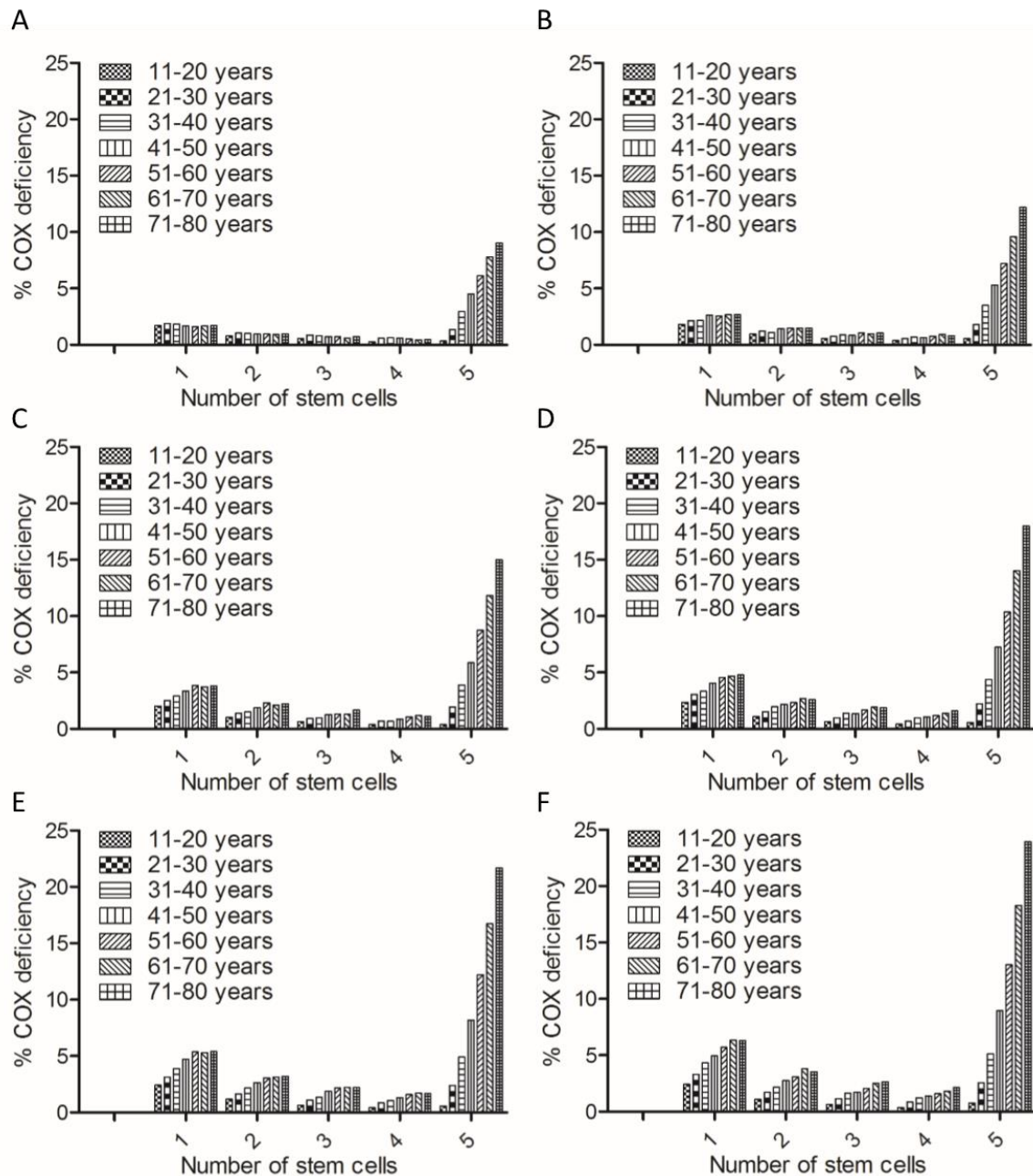


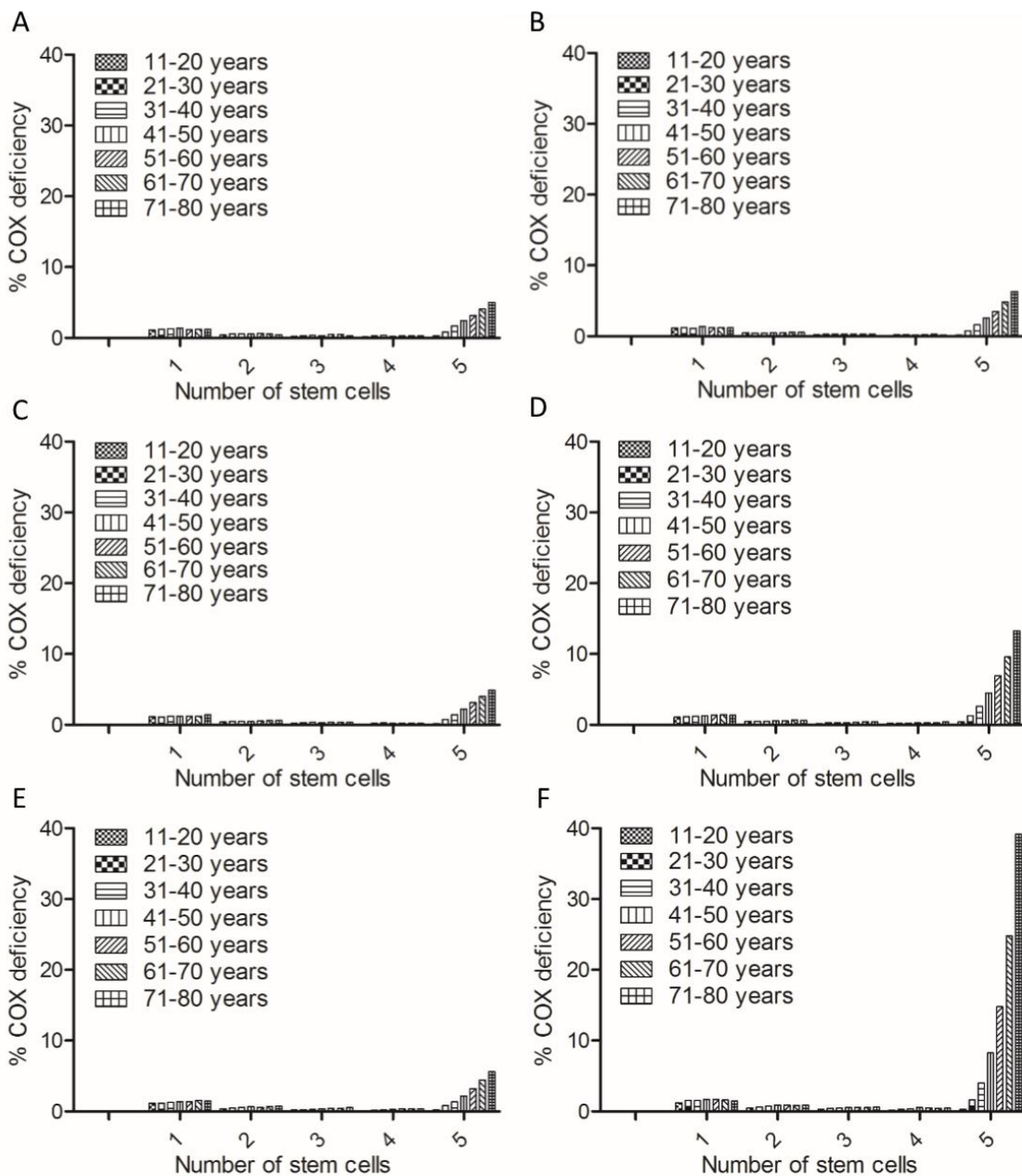
Figure 4-4 Increasing *de novo* mutation rate

The effect of increasing the *de novo* mutation rate with age within the human niche succession model was ascertained. 5000 crypts were simulated, 75% mutated mtDNA conferred COX deficiency to a stem cell. 5 stem cells were simulated, each with 100 mtDNA molecules present. Asymmetric division probability was set to 0.99. Simulations were carried out with a starting *de novo* mutation rate of 3×10^{-5} mutated mtDNA(mtDNA) replication. The *de novo* mutation rate was increased linearly (A) 1x (B) 2x (C) 3x (D) 4x (E) 5x (F) 6x over 80 simulated years.

4.4.2.3 *Crypt fission*

The effect of crypt fission within the model was ascertained. The model had to be adapted for crypt fission integration. The model code is contained within appendix 1.3.2. The probability of a crypt undergoing fission during its lifetime was added as a parameter (`cryptFisProb`). If crypt fission occurred at any point during its lifetime, an additional crypt was simulated from the timepoint at which crypt fission occurred. A COX deficiency advantage was also included (`cryptFisFactor`) which would increase the probability of a crypt undergoing fission if it was harbouring COX deficiency and was included based on findings from chapter 3. Figure 4-5 exemplifies the effects of changing the `cryptFisProb` and `cryptFisFactor` parameters.

Changing the `cryptFisProb` on its own had no effect on COX deficiency frequency. There had to be a substantial advantage endowed upon COX deficient crypts to undergo crypt fission in order for an exponential increase in fully COX deficient crypts with age to be observed. However, this did not result in a similar exponential increase in partially COX deficient crypts with age. Unfortunately, parameters that were much higher than those observed within the biological data were required to produce an effect within the model. For example, from the biological data, there appears to be a 1% chance of crypt fission occurring for normal crypts at the higher age groups, with COX deficient crypts having a 3% chance of fission. This would translate to a `CryptFisProb` of 1% with a `cryptFisFactor` of 3. However, a `cryptFisProb` of 2.5% with a `cryptFis Factor` of 10 (Figure 4-5A/B) does not significantly alter the model output.

**Figure 4-5 Crypt fission**

The effect of crypt fission occurring within the human niche succession model was ascertained. 5000 crypts were simulated, 75% mutated mtDNA conferred COX deficiency to a stem cell. 5 stem cells were simulated, each with 100 mtDNA molecules present. Asymmetric division probability was set to 0.99. A constant *de novo* mutation rate was set at 3×10^{-5} mutated mtDNA/mtDNA replication. Simulations were carried out with an overall crypt fission occurrence probability of 0.025 (A,B), 0.050 (C,D) 0.100 (E,F). The presence of COX deficiency increasing the chance of crypt fission was simulated for x2 (A,C,E) and x10 (B,D,F).

4.4.2.4 COX deficient stem cell advantage

As an unrealistic advantage for COX deficient crypts to undergo fission more often than normal crypts was required in order to increase the frequency of COX deficient crypts within the model output, a COX deficiency advantage at the stem cell level was investigated. As crypt fission is thought to be initiated following an increase in stem cell number (Greaves *et al.*, 2006), which is a result of symmetric stem cell divisions (2 stem cells), perhaps it is an increase in symmetric stem cell divisions that triggers crypt fission. Therefore, an advantage being conveyed to COX deficient stem cells for them to undergo symmetric stem cell division (two renewed stem cells) more often was incorporated into the model. This would allow hypothesised perturbations to stem cell dynamics caused by respiratory deficiency to be simulated. The model had to be adapted to take this into account. The model code is contained within appendix 1.3.2. Figure 4-6 exemplifies the effect of increasing COX deficient stem cell advantage. Increasing the advantage that is conferred to COX deficient stem cells increased both partially and fully COX deficient crypt frequency. Once a stem cell acquires COX deficiency, it is more likely to remain and expand within the stem cell niche. The greater the COX deficiency advantage, the greater the COX deficiency frequency within simulated colonic epithelium. As long as there are sufficient *de novo* mtDNA mutations that are able to clonally expand to the point where the stem cell becomes COX deficient, this remains the case. Figure 4-6F shows that there is a decrease in partially COX deficient crypts after the 31-40 years age bracket. This indicates a plateau has been reached where the *de novo* mtDNA mutation rate can no longer provide enough mutations that go onto clonally expand, to maintain the increase in partially COX deficient crypts with age, with increasing advantage. There is also a corresponding decrease in the rate of fully COX deficient crypts with age in this case.

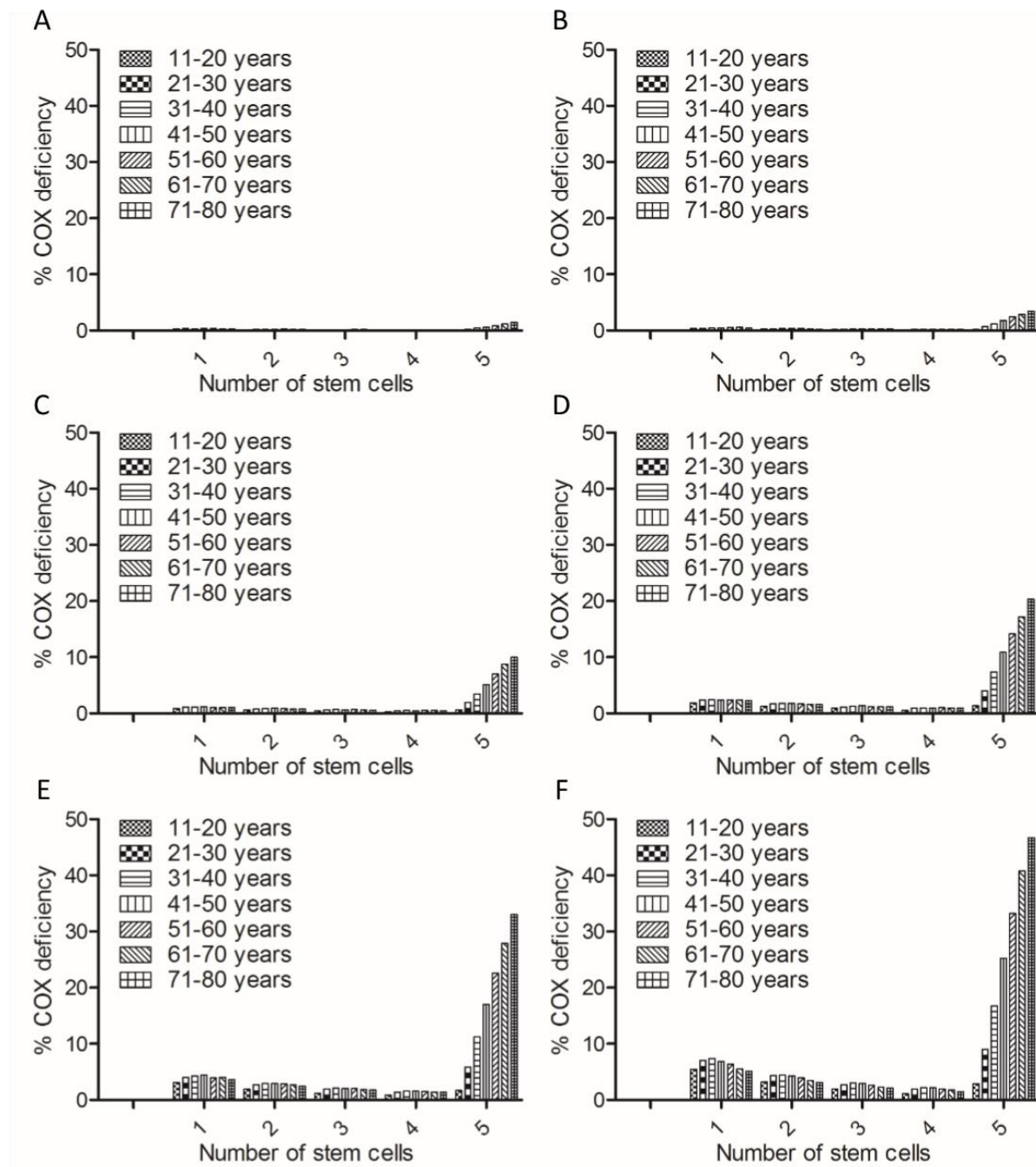


Figure 4-6 Increasing COX deficient stem cell advantage

The effect of COX deficient stem cell advantage within the human niche succession model was ascertained. 5000 crypts were simulated, 75% mutated mtDNA conferred COX deficiency to a stem cell. 5 stem cells were simulated, each with 100 mtDNA molecules present. Asymmetric division probability was set to 0.99. A constant *de novo* mutation rate was set at 5×10^{-6} mutated mtDNA/mtDNA replication. Simulations were carried out with a COX deficient stem cell advantage of (A) 1 (B) 2 (C) 5 (D) 10 (E) 20 (F) 50.

4.4.2.5 mtDNA copy number and asymmetric division probability – part 1

The human niche succession model was constructed so that the probability of a *de novo* mtDNA mutation going onto become fixed within a stem cell and also the time taken for fixation to occur could be recorded. It was also constructed so that the probability of a *de novo* COX deficient stem cell going onto become fixed within the stem cell niche and also the time taken for niche succession to occur could be recorded. This provided the model with metrics that allowed each simulation to be fully quantifiable. Figure 4-7 exemplifies the 4 metrics that can be extremely useful for characterising changes in parameter sets. Figure 4-7A shows how mtDNA copy number impacts on the clonal expansion success probability. It shows that with increasing mtDNA copy number, there is a reduction in the clonal expansion probability and is roughly equal to $1/\text{mtDNA copy number}$, which is indicative of a Moran type process when all stem cell divisions are asymmetric (Moran, 1962). Figure 4-7B shows how mtDNA copy number impacts on the number of stem cell divisions it takes for a mutated mtDNA to reach fixation. It shows that with increasing mtDNA copy number, there is an increase in the time it takes for mutated mtDNA to reach fixation. The number of stem cell divisions for it to reach fixation is roughly equal to $2 \times \text{mtDNA copy number}$ when all stem cell divisions are asymmetric. Figure 4-7C shows how the asymmetric stem cell division probability impacts on the niche succession probability of a *de novo* COX deficient stem cell. It shows that with increased probabilities of asymmetric stem cell division, there is a decrease in the probability of a *de novo* COX deficient stem cell becoming fixed within the stem cell niche, meaning less chance of niche succession occurring. Figure 4-7D shows how asymmetric stem cell division probability impacts on the number of stem cell divisions it takes for a *de novo* COX deficient stem cell to reach fixation within the stem cell niche. It shows that with increasing asymmetric stem cell division probability, there is an increase in the time it takes for a *de novo* COX deficient stem cell to reach fixation, hence niche succession and monoclonal conversion within the crypt.

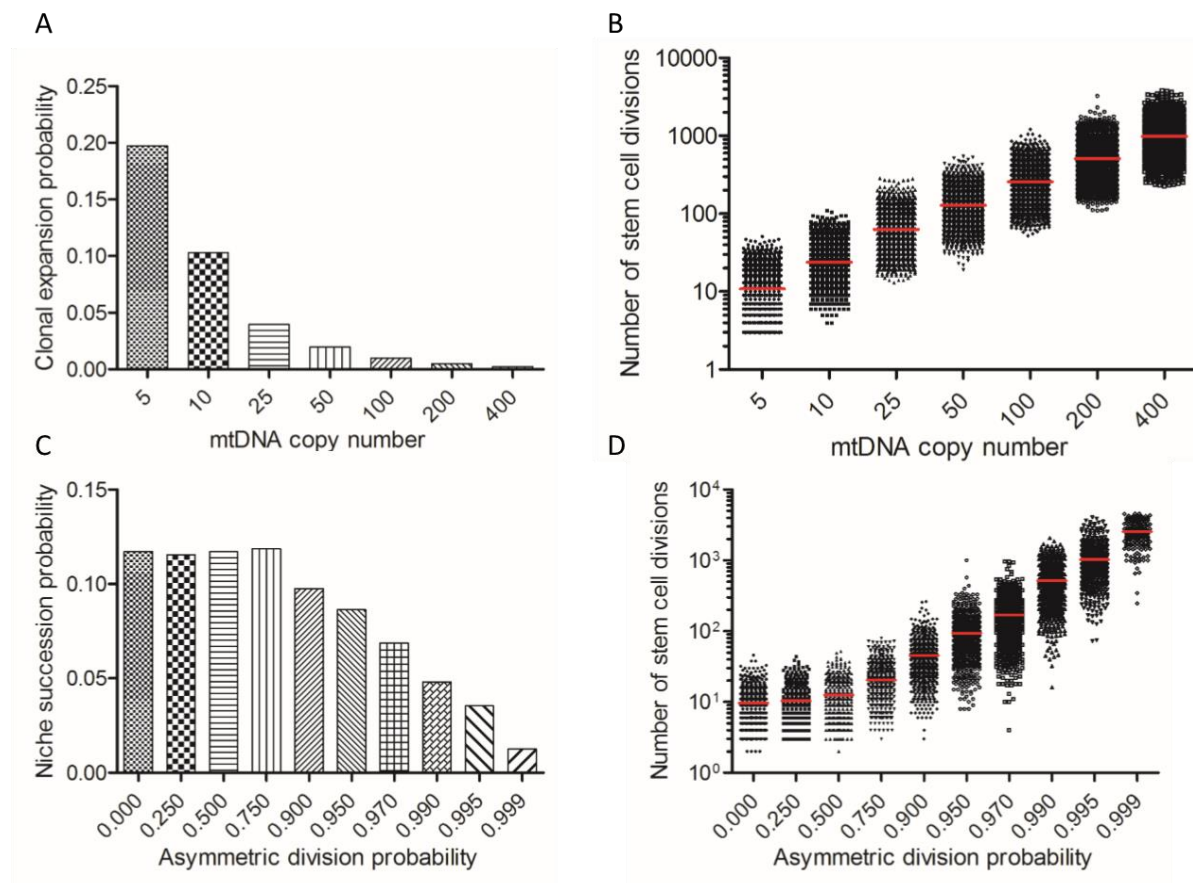


Figure 4-7 Clonal expansion probability and niche succession success

The effect of mtDNA copy number and asymmetric division probability within the human niche succession model was ascertained. The effect of mtDNA copy number was determined when purely asymmetric division was simulated by (A) measuring the probability of a mutated mtDNA fixation event (B) measuring the number of stem cell divisions it takes for mutated mtDNA fixation to occur. The effect of asymmetric division probability was ascertained when 100 mtDNA molecules were simulated per stem cell by (C) measuring the probability of a successful niche succession event by a COX deficient stem cell (D) Measuring the number of stem cell divisions it takes for fixation of a COX deficient stem cell to occur.

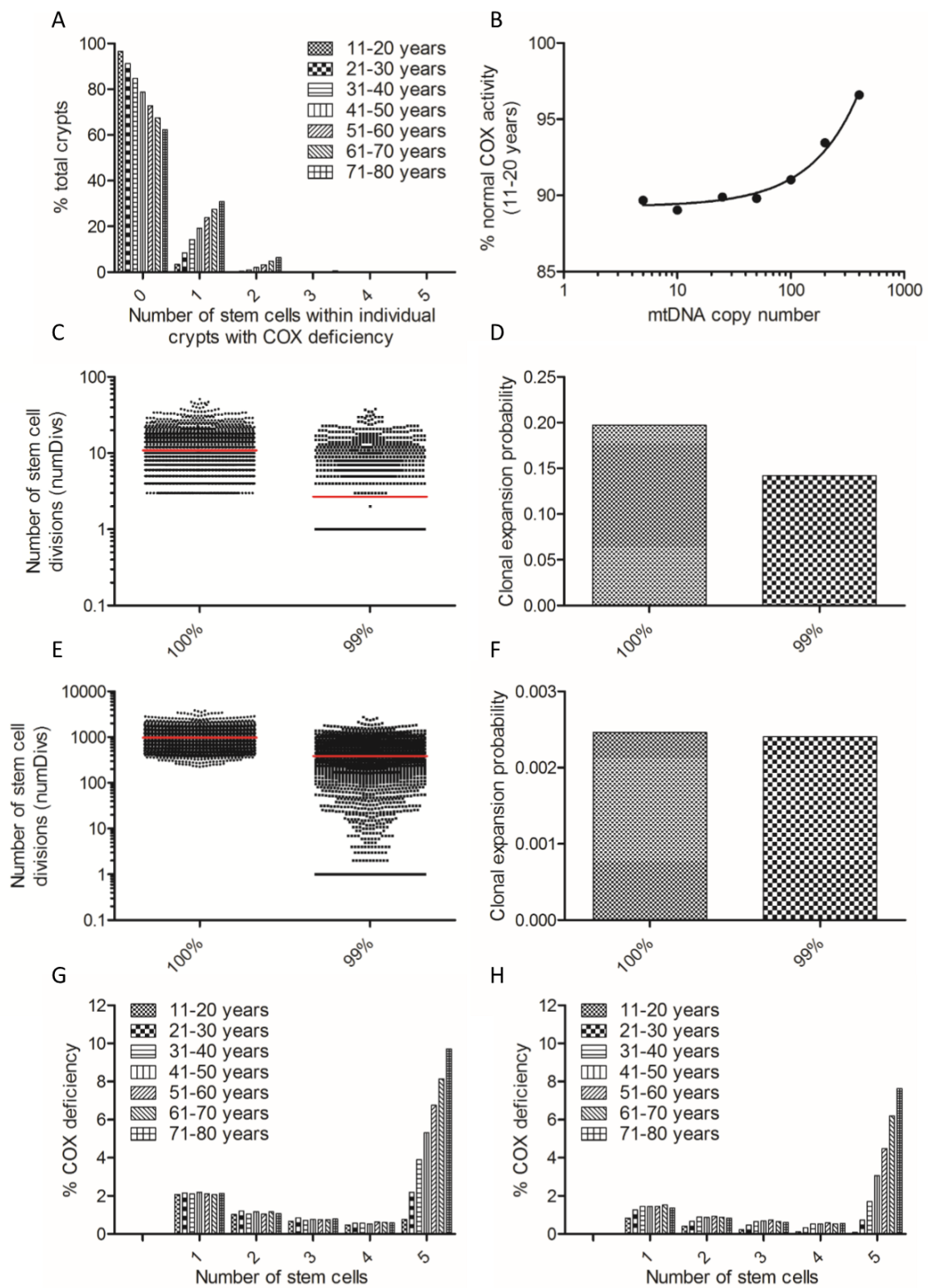
4.4.2.6 mtDNA copy number and asymmetric division probability – part 2

The metrics described in section 4.4.2.5 were used to determine the impact of symmetric stem cell division in conjunction with mtDNA copy number within the human niche succession model. The mutated mtDNA clonal expansion fixation probability and time taken for mutated mtDNA were used to determine its effects on the model as whole. Figure 4-8 shows the effects symmetric stem cell division and mtDNA copy number have on the model. Figure 4-8A shows the COX deficiency frequency within a model where purely asymmetric stem cell division and 400 mtDNA molecules per stem cell are being simulated. We see that the majority of the crypts within simulated colon epithelium are normal, with a decrease in normal crypts with age. Figure 4-8B shows the effect mtDNA copy number has on the percentage of normal crypts at the 11-20 age bracket. With increasing mtDNA copy number there is an increase in normal crypts in this age bracket. It is a small difference, for example, a ~100 fold increase in the mtDNA copy number results in a ~6% increase in normal crypts within this age bracket. Even so, this indicates that with increasing mtDNA copy number, mutated mtDNA fixation time is increased due to the reduction in COX deficient crypts. This concurs with Figure 4-7B. Figures 4-8C/D show the mutated mtDNA fixation time and probability between a purely asymmetric stem cell division model and a model where 1% symmetric division is being simulated, with both models simulating 5 mtDNA molecules per stem cell. Figure 4-8C shows that with the introduction of a 0.01 symmetric stem cell division probability, there is a larger distribution of fixation times, resulting in a reduced median fixation time. The majority of fixation times are the result of a normal stem cell being taken over by a COX deficient stem cell where mutated mtDNA has already become fixed. Figure 4-8D shows that the probability of mutated mtDNA becoming fixed within a stem cell is also reduced within a model where symmetric stem cell division is simulated. This is due to symmetric stem cell division allowing a COX deficient stem cell to be replaced by a normal symmetrically dividing stem cell. This finding is also replicated in models where 400 mtDNA molecules are simulated (Figure 4-8E/F), however, the difference in mutated mtDNA fixation probability in this case is marginal. This indicates that with increasing mtDNA copy number within stem cells, symmetric stem cell division has a decreasing effect on mutated mtDNA fixation probability. Figures 4-8G/H show the difference between a model where 5 mtDNA molecules are simulated per stem cell and one with 400 mtDNA molecules. The model where 400 mtDNA molecules are simulated per stem cell (Figure 4-8H) shows a gradual increase in partially COX deficient crypts until the 31-40 age bracket.

This is compared to the model where 5 mtDNA molecules are simulated per stem cell (Figure 4-8G) where there is no gradual increase in partially COX deficient crypts with age. This reflects the time it takes for mutated mtDNA molecules to reach fixation between 5 and 400 mtDNA molecules (Figures 4-8E and 4-8G). There is also a slight reduction in COX deficiency frequency in the model with 400 mtDNA molecules being simulated when compared to the model with 5 mtDNA molecules being simulated. This reflects the difference in mutated mtDNA fixation probability.

Figure 4-8 Interplay between symmetric division and mtDNA clonal expansion success

The effect of mtDNA copy number in conjunction with asymmetric stem cell division was assessed. 5000 crypts were simulated, 75% mutated mtDNA conferred COX deficiency to a stem cell. 5 stem cells were simulated. A constant *de novo* mutation rate was set to 5×10^{-5} mutated mtDNA(mtDNA) replication. (A) 100% asymmetric stem cell division. (B) Effect of increasing mtDNA copy number on the percentage of normal crypts at 11-20 years of age. (C) Clonal expansion fixation time between a model with purely asymmetric division and one with 99% asymmetric division when 5 mtDNA molecules are simulated. (D) Mutated mtDNA fixation probability between a model with purely asymmetric division and one with 99% asymmetric division when 5 mtDNA molecules are simulated. (E) Clonal expansion fixation time between a model with purely asymmetric division and one with 99% asymmetric division when 400 mtDNA molecules are simulated. (F) Mutated mtDNA fixation probability between a model with purely asymmetric division and one with 99% asymmetric division when 400 mtDNA molecules are simulated. (G) The percentage COX deficiency present within a model where 99% asymmetric stem cell division and 5 mtDNA molecules per stem cell is simulated. (H) The percentage COX deficiency present within a model where 99% asymmetric stem cell division and 400 mtDNA molecules per stem cell is simulated.



4.4.3 Multiple mtDNA mutations

4.4.3.1 Multiple mtDNA mutations detected within aged human colon

It has previously been shown that cells within human colonic epithelium can contain multiple clonally expanded mtDNA point mutations with the majority being the cause of the cells COX deficiency (Taylor *et al.*, 2003; Greaves *et al.*, 2006; Greaves *et al.*, 2010). Data has been provided by Dr Laura Greaves on the numbers of mtDNA mutations that have clonally expanded within aged human colonic epithelium cells and has been plotted in Figure 4-9. Data has been grouped based on whether the cells are normal or COX deficient. The majority of mutations found in normal cells were synonymous non-pathogenic mutations, where this was not the case, low heteroplasmy was detected. The majority of mutations found in COX deficient cells were non-synonymous pathogenic mutations. This data indicates that a model that simulates mutated mtDNA verses normal mtDNA may be too simplistic compared to the biology of the process which may have multiple mutations clonally expanding simultaneously within the same cell. Therefore, a more biologically relevant model was developed.

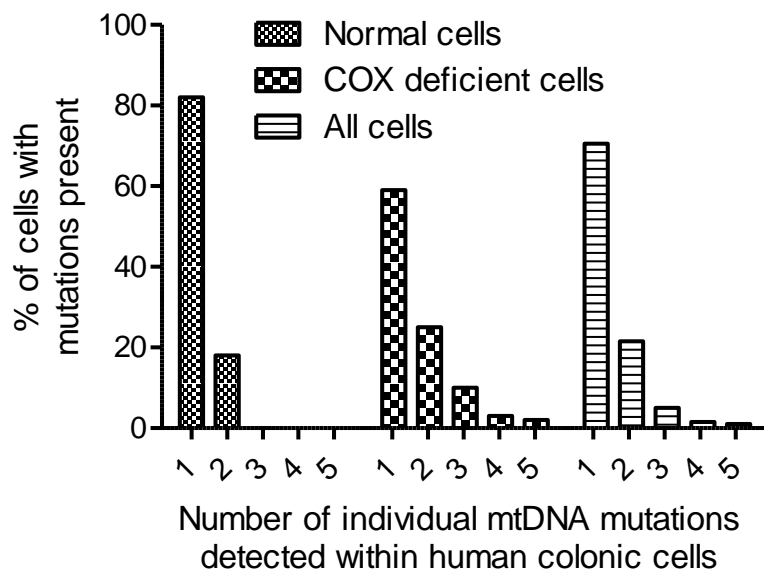


Figure 4-9 Number of mtDNA mutations detected within aged human colonic cells

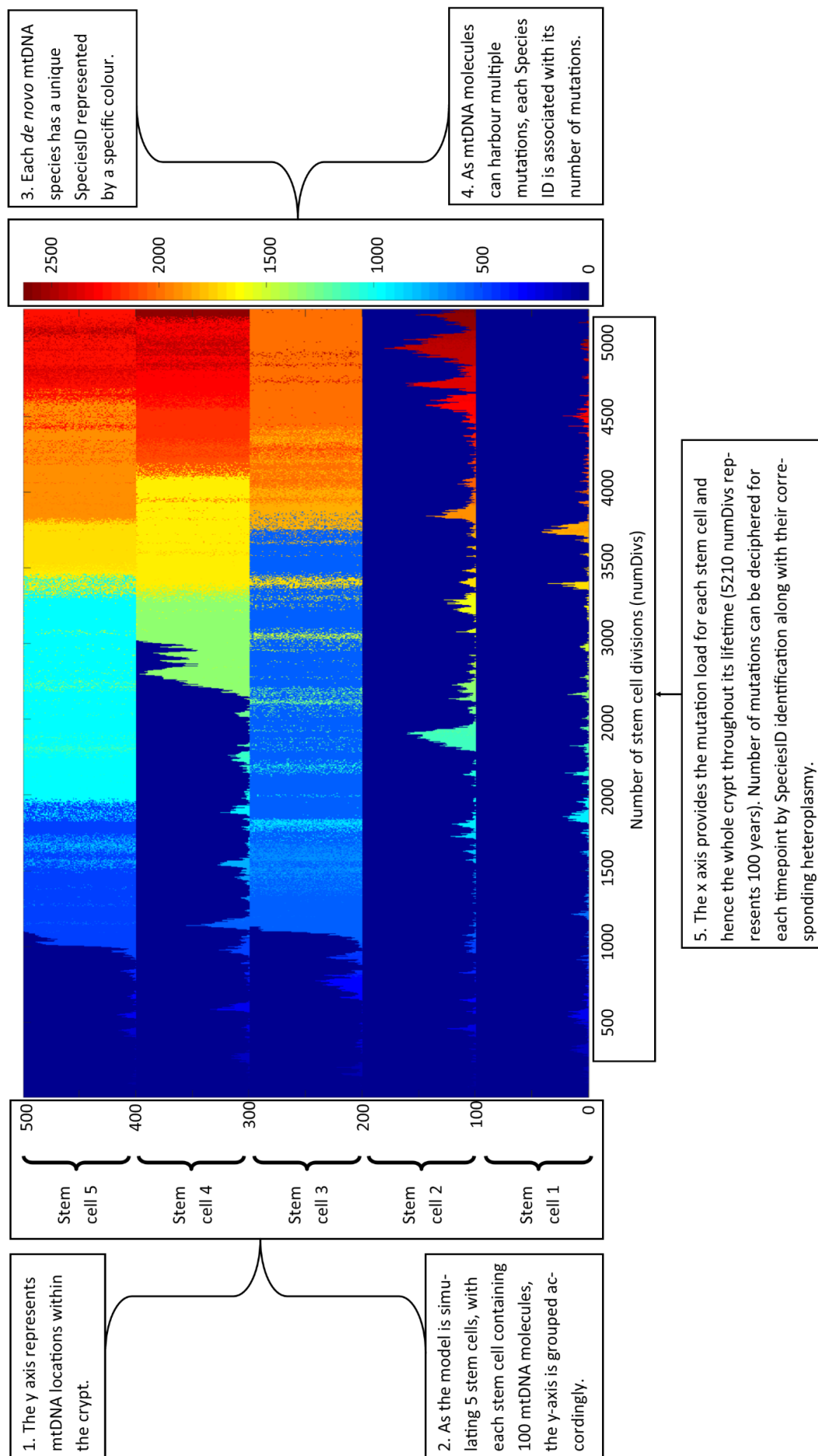
Data kindly provided by Dr Laura Greaves showing the number of mtDNA mutations detected within aged (>70 years) human colonic cells (Taylor *et al.*, 2003; Greaves *et al.*, 2006; Greaves *et al.*, 2010) was attained via laser microdissection of individual cells from whole mount tissue sections that had undergone COX/SDH histochemistry followed by mtDNA sequencing.

4.4.3.2 *Tracking multiple mtDNA mutations within human niche succession model*

The human niche succession model was further developed to allow each *de novo* mtDNA species to be tracked. The model was adjusted so that each mtDNA molecule is able to acquire multiple mutations upon replication to make it more biologically robust. Newly acquired *de novo* mtDNA mutations were given a new species ID, with all clones given the same species ID. Each mtDNA species ID was linked to the number of mutations that were present on those mtDNA clones. Figure 4-10 is a crypt map showing each individual stem cell with each individual mtDNA species ID as a different colour throughout the crypts life. It is possible to see that at certain time points, individual stem cells contain multiple mtDNA species, indicating the presence of >1 mutations present within the stem cell. However, due to each species being able to harbour multiple mutations, the number of mutations within that stem could be much more than the number of mtDNA species present within the crypt map.

Figure 4-10 mtDNA species tracking of whole crypts

The human niche succession model was further developed to track each mtDNA molecule, with each mtDNA molecule being tagged with a species identification number. Once a *de novo* mtDNA mutation is acquired, that mtDNA molecule is given a new (incremented by 1) species identification number. Any mtDNA molecule that is a clone will have the same species identification number as the original mtDNA molecule. The model was further developed to track multiple mutations on the same mtDNA molecule, making it more biologically realistic. Therefore, each species identification number is linked to the number of unique mutations that the mtDNA molecule harbours. Depicted is a graphical representation of each mtDNA species (represented by an individual colour) within each stem cell throughout the life of the crypt. A mitochondrial species number of 0 represents a wild-type copy of mtDNA (dark blue). The example above was taken from an individual crypt where purely asymmetric stem cell division was being simulated, 5 stem cells were contained within the crypt, each stem cell contained 100 mtDNA molecules, with a *de novo* mutation rate of 1×10^{-3} mutated mtDNA/mtDNA replication.



4.4.3.3 Parameter effects on multiple mutations

Key parameters within the model were investigated to see how varying their values would influence the number of mutations that were present within individual stem cells. The key parameters included mtDNA copy number, asymmetric stem cell division probability and mutation rate. Figure 4-11 shows how key parameter alterations influence the mutation distribution. Changes to mtDNA copy number and asymmetric division probability (Figure 4-11A/B) did not have any observable effect on the distribution of number of mutations present within individual stem cells. However, changes to *de novo* mtDNA mutation rate showed a dramatic effect between parameter values 1×10^{-4} and 5×10^{-4} mutated mtDNA/mtDNA replication. Increasing the mutation rate allows for a broader range of mutations within individual stem cells, meaning stem cells are more likely to contain a greater number of individual mutations

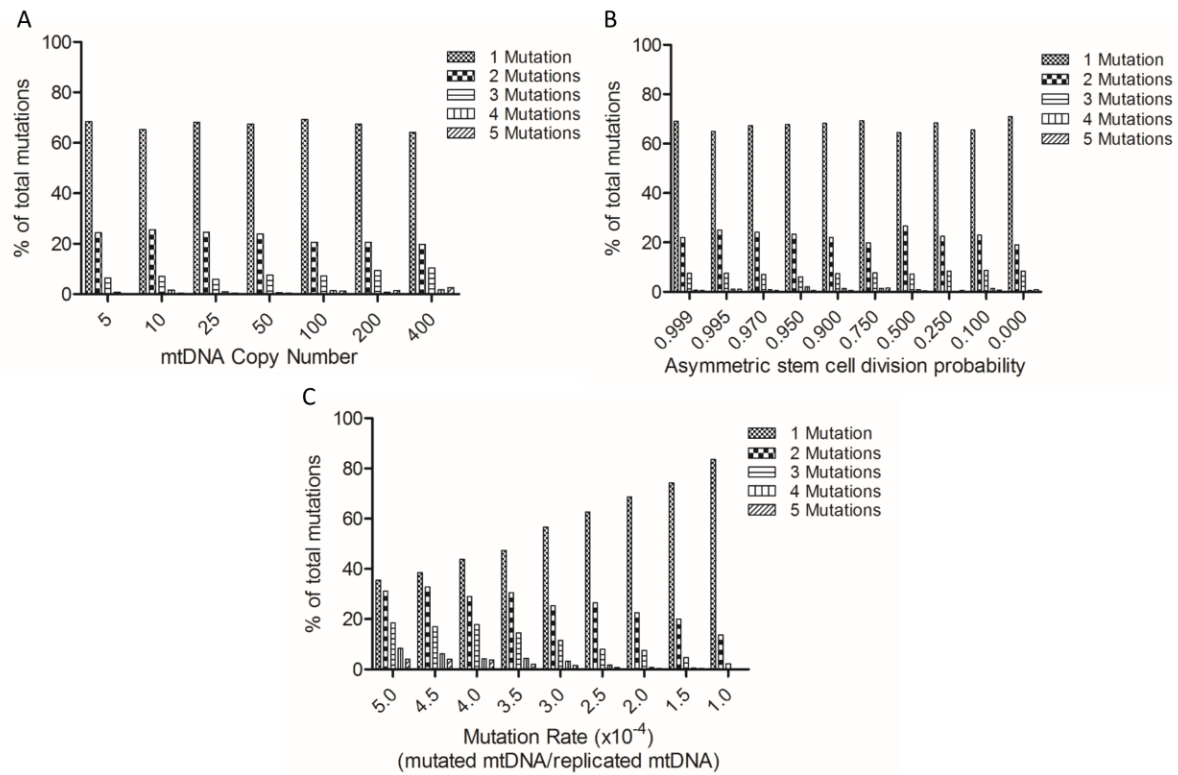


Figure 4-11 Influencing number of mutations within individual cells

A parameter scan was conducted with mtDNA copy number, asymmetric stem cell division probability and mutation rate to determine how the number of mutations within individual cells would be influenced by altered parameters. Unless stated within the graphs, 5000 crypts were simulated, 75% mutated mtDNA conferred COX deficiency to a stem cell. 5 stem cells were simulated, each with 100 mtDNA molecules present.

Asymmetric division probability was set to 0.99. A constant *de novo* mutation rate was set at 2×10^{-4} mutated mtDNA/mtDNA replication. Number of mutations within individual cells was measured with changing (A) mtDNA copy number (B) Asymmetric stem cell division probability (C) Mutation rate.

4.4.4 Impact of altered mtDNA segregation upon division

4.4.4.1 *Mutation distribution spectra with random mtDNA segregation upon division*

Model simulations were carried out to determine how the COX deficiency frequency and the number of mutations within individual stem cells corresponded with each other. Figure 4-12 exemplifies the effect of increasing the *de novo* mtDNA mutation rate 10-fold. Figure 4-12A/B shows the COX deficiency frequency and number of mutations with a mutation rate of 5×10^{-5} mutated mtDNA/mtDNA replication. Fully COX deficient crypts reach ~15% within the simulated colon at the 71-80 year age bracket (Figure 4-12A). However, when we examine the mutation distribution, ~90% contain only one mutation, with <10% harbouring multiple mutations (Figure 4-12B). Figure 4-12C/D shows the COX deficiency frequency and number of mutations with a mutation rate of 5×10^{-4} mutated mtDNA/mtDNA replication. Fully COX deficient crypts reach ~80% within simulated colon at the 71-80 year age bracket (Figure 4-12C). However, when we examine the mutation distribution, ~35% contain only one mutation, with the remainder harbouring multiple mutations with quite a broad distribution (Figure 4-12D). A mutation rate of 5×10^{-4} mutated mtDNA/mtDNA replication gives a COX deficiency frequency that is twice that compared with the biological data (Figure 3-8C) but gives a mutation distribution that does not correspond to the number of mutations detected within cells from human colon epithelium (Figure 4-9). It is clear to see from these results that relaxed replication and random segregation of mutated mtDNA will not allow both the COX deficiency frequency and the number of mutations within individual cells from human colon epithelium to be matched simultaneously.

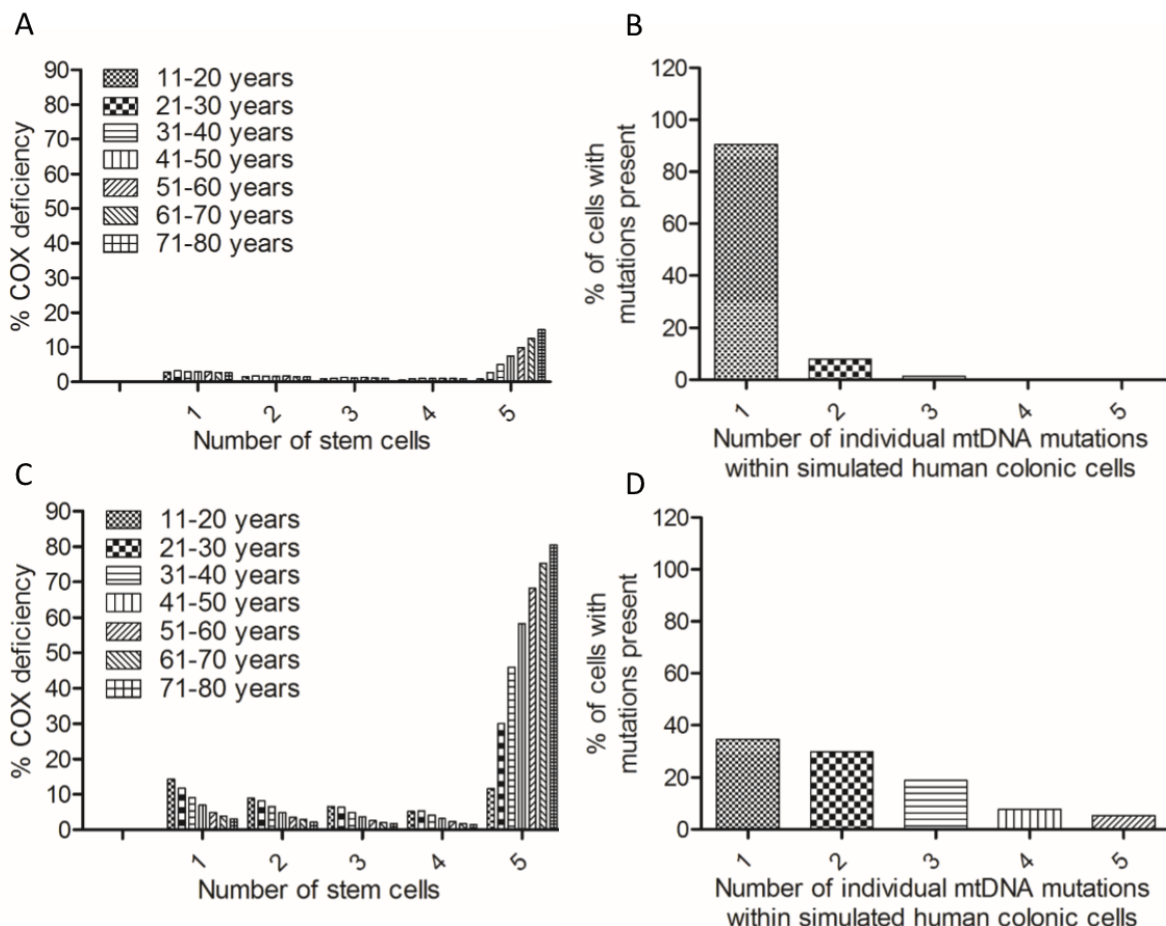


Figure 4-12 Random segregation and number of mutations detected

Mutation rate was assessed when looking at COX deficiency frequency and the number of mutations present within individual cells simultaneously. 5000 crypts were simulated, 75% mutated mtDNA conferred COX deficiency to a stem cell. 5 stem cells were simulated, each with 100 mtDNA molecules present. Asymmetric division probability was set to 0.99. (A) COX deficiency when a model is simulated with a *de novo* mutation rate set to 5×10^{-5} mutated mtDNA/mtDNA replication. (B) Number of mutations within individual cells when a model is simulated with a *de novo* mutation rate set to 5×10^{-5} mutated mtDNA/mtDNA replication. (C) COX deficiency when a model is simulated with a *de novo* mutation rate set to 5×10^{-4} mutated mtDNA/mtDNA replication. (D) Number of mutations within individual cells when a model is simulated with a *de novo* mutation rate set to 5×10^{-4} mutated mtDNA/mtDNA replication.

4.4.4.2 Biasing mutated mtDNA segregation upon division

Relaxed replication and random segregation have been shown to explain the emergence of respiratory deficiency computationally within post-mitotic muscle tissue and mitotic epithelial tissue (Coller *et al.*, 2001; Elson *et al.*, 2001). However, there is still debate over the exact mechanism of clonal expansion and could be subject to the characteristics of the tissues in which the cells inhabit. Katajisto et al have data that suggests asymmetrically dividing mammary stem cells apportion their aged vs young mitochondria asymmetrically (Katajisto *et al.*, 2015). They used a photoactivatable GFP system which incorporated a specific mitochondrial organelle localisation signal. They activated the GFP with a UV laser pulse, aged the cells and imaged the apportioning of aged vs new mitochondria between daughter cells. Upon asymmetric division, 80% of the old mitochondria were segregated into one cell and 20% into the other. This is achieved by old mitochondrial organelles being restricted to the perinuclear region of the mother cell (Katajisto *et al.*, 2015). If there is evidence suggesting that mitochondria are apportioned asymmetrically, this may be true for the apportioning of mtDNA upon asymmetric stem cell division as well. For instance, newly replicated mtDNA (most likely to harbour mtDNA replication errors) may be more likely to be segregated into the stem cell progeny cell in order to reduce mtDNA mutation accumulation within the stem cell pool.

A new algorithm was constructed that would generate new division transition matrices according to there being an increased likelihood of mutated mtDNA being segregated out into the stem cell progeny cell upon asymmetric stem cell division (appendix 1.3.3.7). Division matrices were generated with varying degrees of bias for mutated mtDNA molecules to be segregated out of the stem cell pool upon asymmetric stem cell division. Figure 4-13 shows the impact that a mutated mtDNA segregation bias has upon mutated mtDNA fixation probability. A division segregation factor of 1 means that segregation is random. A division segregation factor of 2 means mutated mtDNA molecules are twice as likely to be segregated out of the stem cell pool upon asymmetric stem cell division. A small increase in bias results in a large decrease in mutated mtDNA fixation probability with all *de novo* mtDNA mutation rates tested.

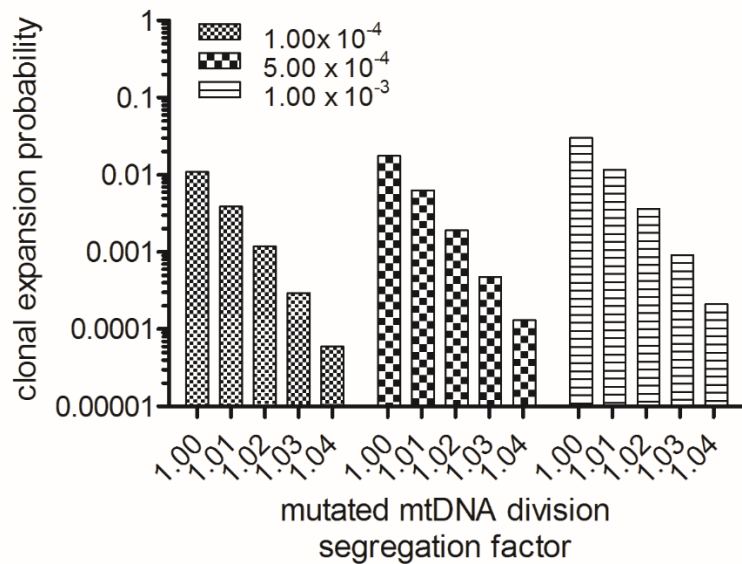


Figure 4-13 Biasing mutated mtDNA segregation upon asymmetric stem cell division

The mutated mtDNA segregation advantage was assessed using the mutated mtDNA fixation probability. 5000 crypts were simulated, 75% mutated mtDNA conferred COX deficiency to a stem cell. 5 stem cells were simulated, each with 100 mtDNA molecules present. Asymmetric division probability was set to 0.99. The *de novo* mutation rate was changed as shown in the figure to determine its effect. A division segregation factor of 2 means a mutated mtDNA molecule is twice as likely to be segregated out of the stem cell pool upon asymmetric stem cell division.

4.4.4.3 Mutation distribution spectra with biased mtDNA segregation upon division.

Model simulations were carried out to determine how COX deficiency frequency corresponded with number of mutations within individual stem cells with a division segregation factor of 1.03. Figure 4-14 exemplifies the effect of increasing *de novo* mtDNA mutation rate 10-fold. Figure 4-14A/B shows the COX deficiency frequency and number of mutations with a mutation rate of 5×10^{-5} mutated mtDNA/mtDNA replication. This time, fully COX deficient crypts fail to reach even 1% within the simulated colon at the 71-80 year age bracket (Figure 4-14A). When we examine the mutation distribution, ~97% contain only one mutation, with <3% harbouring multiple mutations (Figure 4-14B). Figure 4-14C/D shows the COX deficiency frequency and number of mutations with a mutation rate of 5×10^{-4} mutated mtDNA/mtDNA replication. Fully COX deficient crypts reach ~5% within simulated colon at the 71-80 year age bracket (Figure 4-14C). When we examine the mutation distribution, ~60% contain only one mutation, with the remainder harbouring multiple mutations with quite a broad distribution (Figure 4-14D). A mutation rate of 5×10^{-4} gives a COX deficiency frequency that is much more biologically relevant (Figure 3-8C) and gives a mutation distribution that does correspond to the number of mutations detected within cells from human colonic epithelium (Figure 4-9).

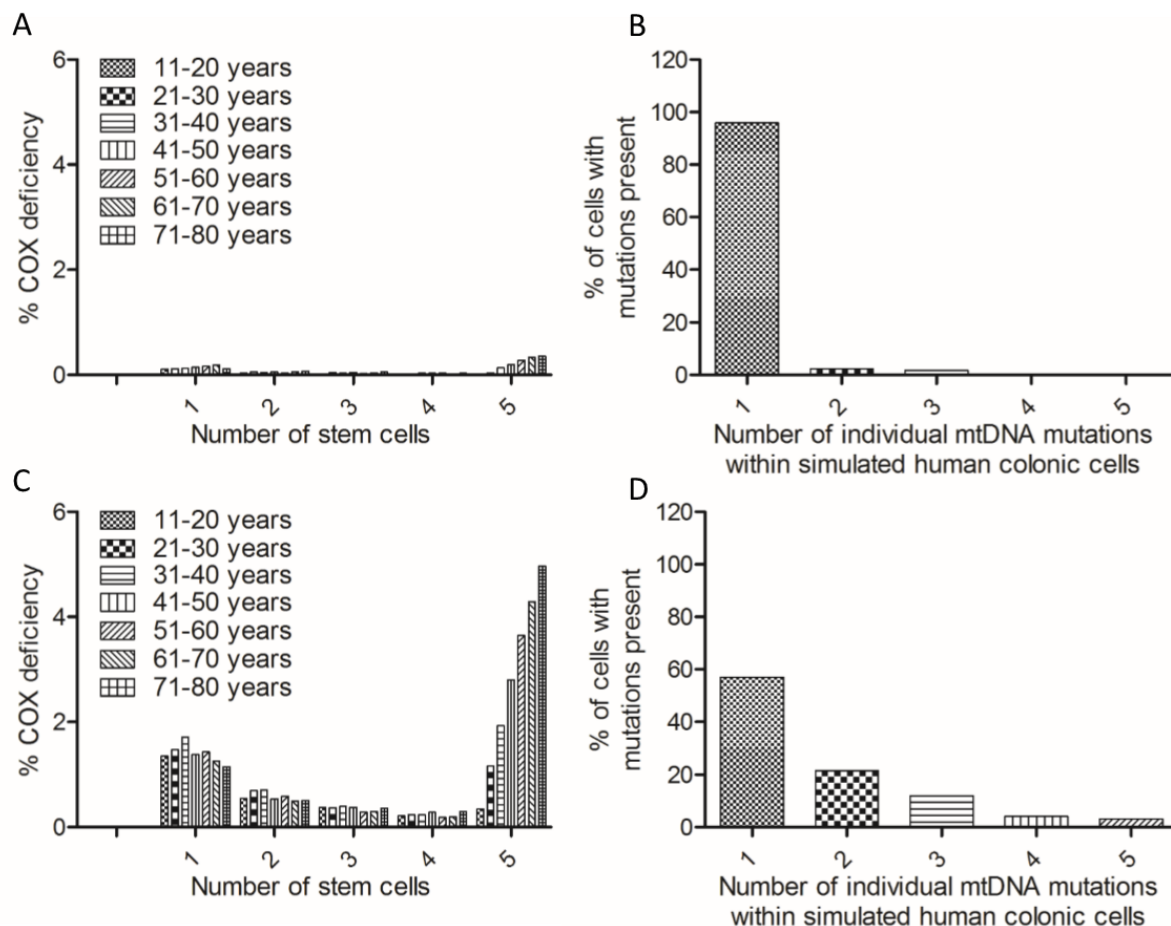


Figure 4-14 Biased segregation and number of mutations detected

Mutation rate was assessed when looking at COX deficiency frequency and the number of mutations present within individual cells simultaneously. A segregation bias was introduced into the model code. The results detailed here are from a model where mutated mtDNA were more likely to be segregated into the stem cell progeny during asymmetric division by a factor of 1.03. 5000 crypts were simulated, 75% mutated mtDNA conferred COX deficiency to a stem cell. 5 stem cells were simulated, each with 100 mtDNA molecules present. Asymmetric division probability was set to 0.99. (A) COX deficiency frequency when a model is simulated with a *de novo* mutation rate set to 5×10^{-5} mutated mtDNA/mtDNA replication. (B) Number of mutations within individual cells when a model is simulated with a *de novo* mutation rate set to 5×10^{-5} mutated mtDNA/mtDNA replication. (C) COX deficiency frequency when a model is simulated with a *de novo* mutation rate set to 5×10^{-4} mutated mtDNA/mtDNA replication. (D) Number of mutations within individual cells when a model is simulated with a *de novo* mutation rate set to 5×10^{-4} mutated mtDNA/mtDNA replication.

4.4.4.4 Effects of biasing mtDNA segregation upon division

The effect of using a segregation bias was further investigated by examining the mutated mtDNA fixation probability and time taken with a bias of 1.03. Figure 4-15 highlights the difference between random and biased segregation with a mutation rate of 5×10^{-5} mutated mtDNA/mtDNA replication (Figure 4-15A/B) and 5×10^{-4} mutated mtDNA/mtDNA replication (Figure 4-15C/D). As has been shown previously, there is a decrease in the mutated mtDNA fixation probability (Figure 4-13). What can also be seen is that there is a reduced number of mutated mtDNA molecules undergoing fixation for both mutation rates tested. From this we can say that the bias acts to reduce the probability of mutated mtDNA becoming fixed within a cell by their removal from the stem cell pool. This can be overcome by increasing the mutation rate which, in so doing, increases the number of different types of mtDNA present within the stem cell.

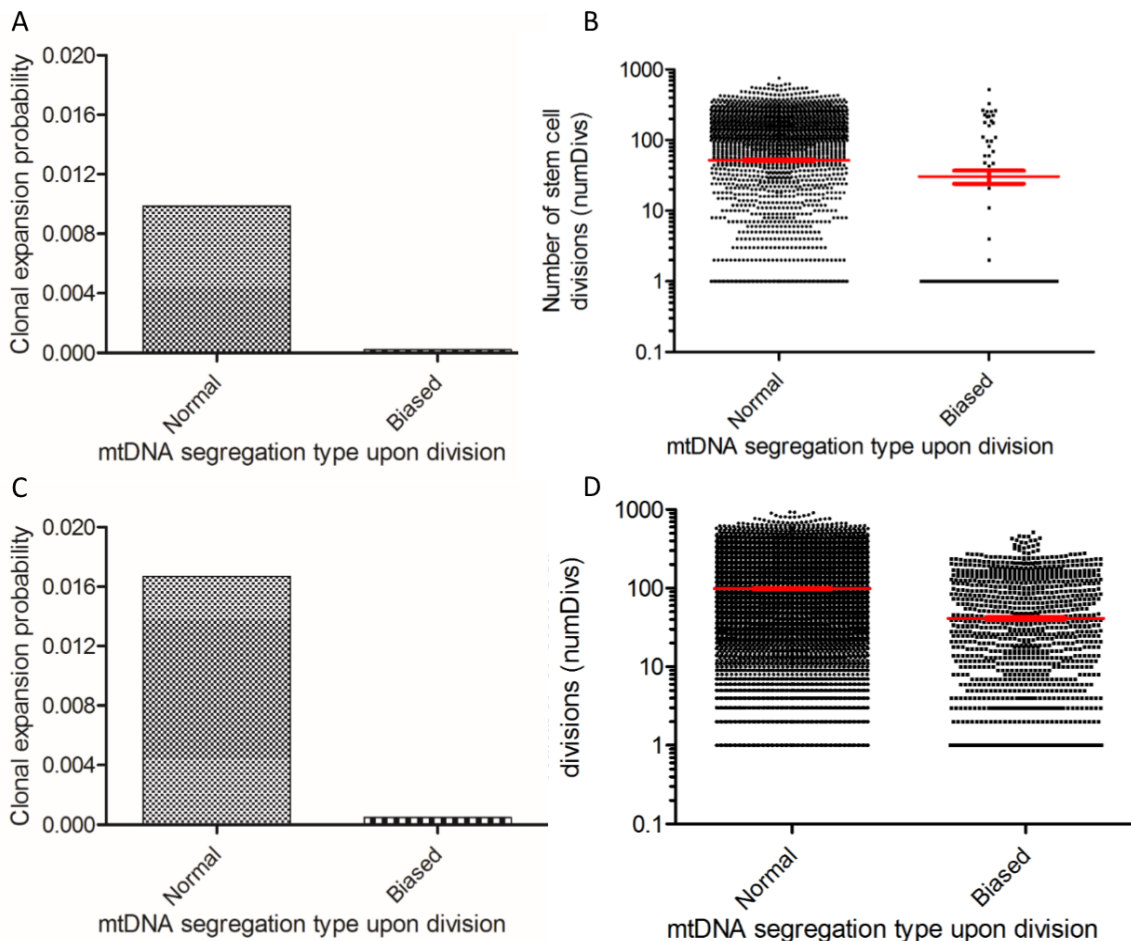


Figure 4-15 Biased segregation impact on mutated mtDNA clonal expansion

A segregation bias was introduced into the model code. The results detailed here compare the difference between a model where random mtDNA segregation take place with one where mutated mtDNA were more likely to be segregated into the stem cell progeny during asymmetric division by a factor of 1.03. 5000 crypts were simulated, 75% mutated mtDNA conferred COX deficiency to a stem cell. 5 stem cells were simulated, each with 100 mtDNA molecules present. Asymmetric division probability was set to 0.99. (A) Compares the mutated mtDNA fixation probability between a model with random segregation and a model with biased segregation when a mutation rate is set to 5×10^{-5} mutated mtDNA/mtDNA replication. (B) Compares the mutated mtDNA fixation time between a model with random segregation and a model with biased segregation when a mutation rate is set to 5×10^{-5} mutated mtDNA/mtDNA (C) Compares the mutated mtDNA fixation probability between a model with random segregation and a model with biased segregation when a mutation rate is set to 5×10^{-4} mutated mtDNA/mtDNA replication. (D) Compares the mutated mtDNA fixation time between a model with random segregation and a model with biased segregation when a mutation rate is set to 5×10^{-4} mutated mtDNA/mtDNA.

4.4.5 Model optimisation

Now that the model was fully characterised and made as biologically robust as possible, a parameter scan was conducted to determine the optimum parameters that would allow the trend in human COX deficiency frequency and the number of mutations detected within human colonic epithelium to be matched. This was done for model simulations with between 3-8 stem cells per crypt. Fixed parameters included COX deficiency threshold and mtDNA copy number. Parameters which were optimised included asymmetric stem cell division probability, advantage to COX deficient stem cells (divide symmetrically more often), division segregation factor and mutation rate.

Figures 4-17 and Figure 4-18 contained best fit COX deficiency frequency graphs for models simulated with 3-8 stem cells with the corresponding number of mutations distribution graphs as an inset. Figure 4-18 contained best fit graphs for models with an advantage endowed to COX deficient stem cells. All best fit parameters are contained within section 4.4.5.3 as Tables 4.4 and 4.5.

4.4.5.1 COX deficiency frequency from human colon

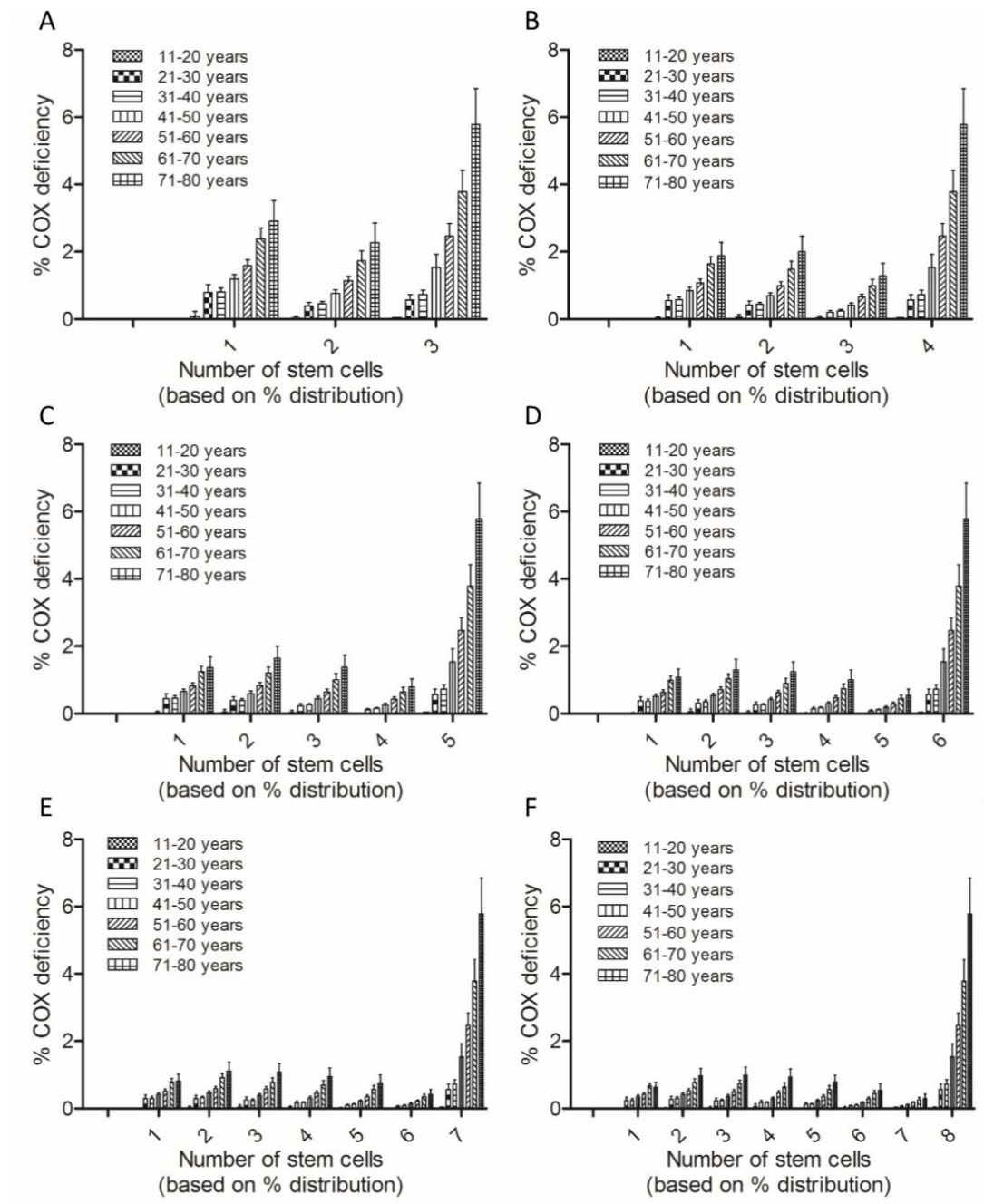


Figure 4-16 COX deficiency frequency within human colon epithelium

Probability distributions were generated in order to relate the percentage COX deficiency observed at the transverse cross section of a crypt to the likely number of COX deficient stem cells that were present at the base of a crypt. Probability distributions can be generated for any number of stem cells specified to be present within the stem cell niche. The COX deficiency data from human colon was converted to number of stem cells using the probability distributions for (A) 3 stem cells, (B) 4 stem cells, (C) 5 stem cells, (D) 6 stem cells, (E) 7 stem cells and (F) 8 stem cells being present within the stem cell niche of human colonic crypts.

4.4.5.2 Best fit COX deficiency frequency and number of mutations

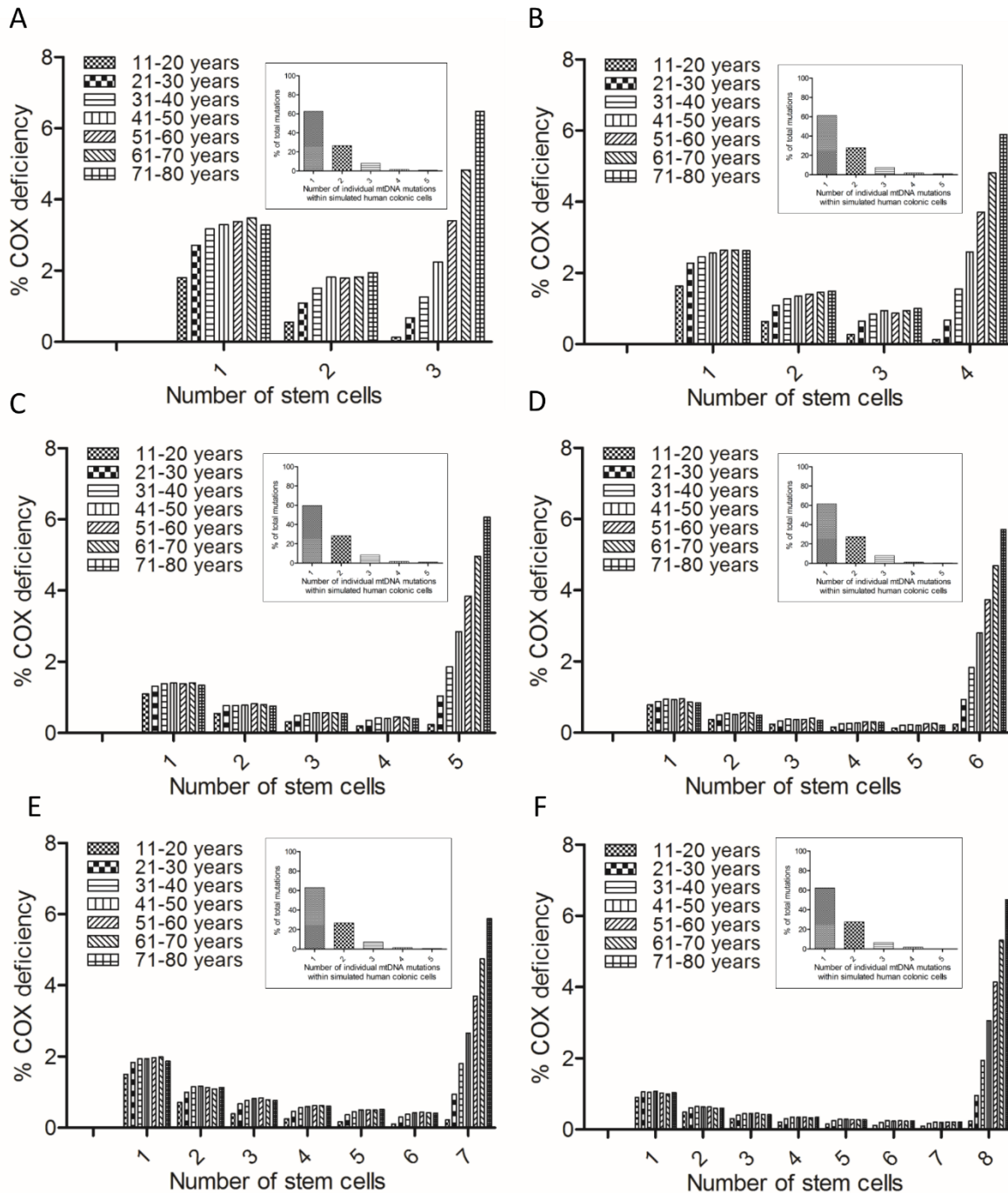


Figure 4-17 Best fit data

A parameter scan was conducted in order to optimise the COX deficiency frequency and the number of mutations within cells that would provide the closest match to the biological data. This was done with models containing (A) 3 (B) 4 (C) 5 (D) 6 (E) 7 (F) 8 stem cells per crypt. Parameters used for each fit are contained in Table 4-4.

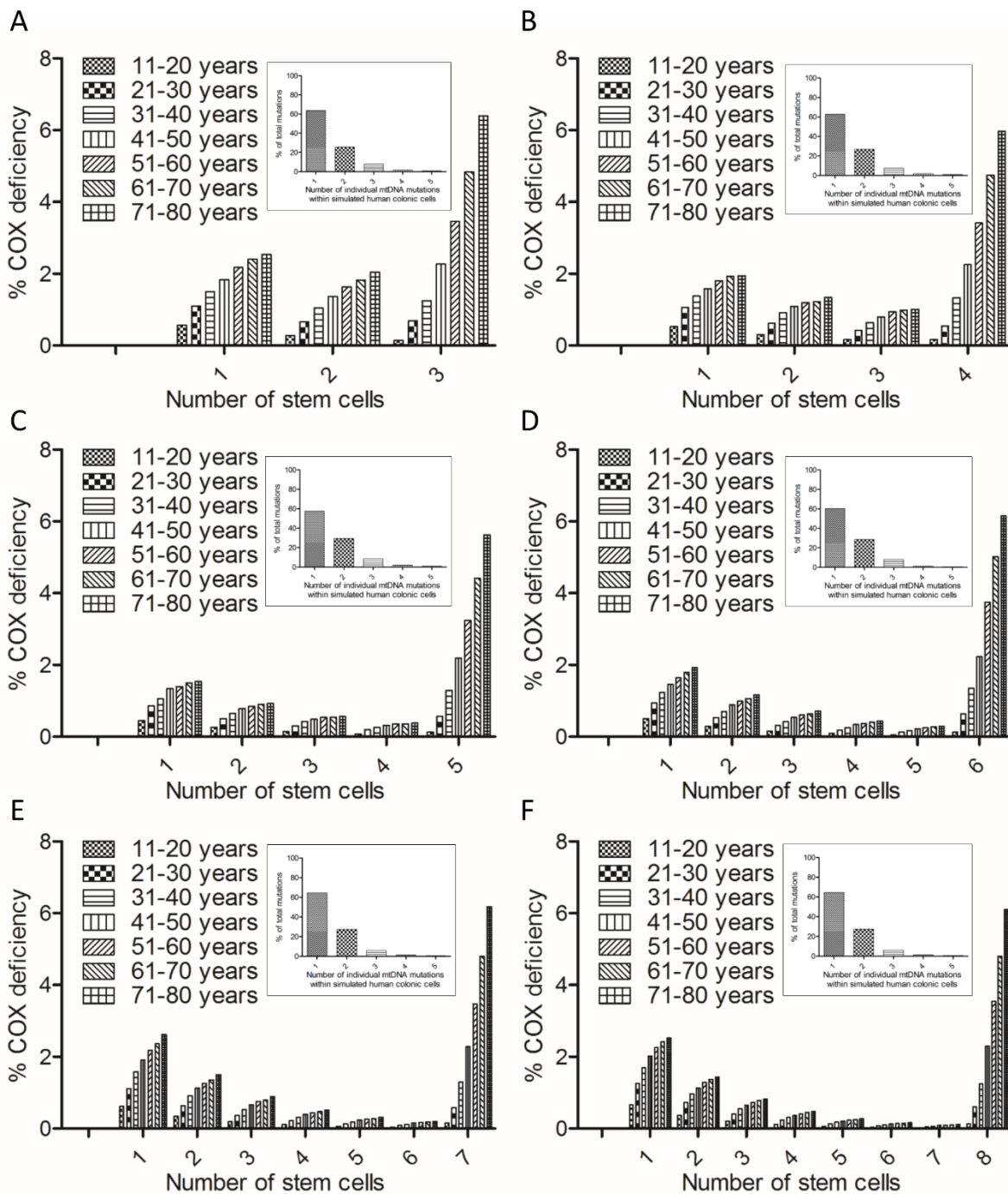


Figure 4-18 Best fit data with COX deficient stem cell advantage

A parameter scan was conducted in order to optimise the COX deficiency frequency and the number of mutations within cells that would provide the closest match to the biological data. An advantage was introduced into the model that would make COX deficient stem cells more likely to undergo symmetric stem cell division. This was done with models containing (A) 3 (B) 4 (C) 5 (D) 6 (E) 7 (F) 8 stem cells per crypt. Parameters used for each fit are contained in Table 4-5.

4.4.5.3 Best fit data tables

Table 4-4 Parameter values for best fit data

Stem Cell Number	Parameters					
	COX deficiency threshold	mtDNA copy number	Pa	COX stem cell advantage	Division Segregation Factor	Mutation Rate
3	75%	100	0.9975	1	1.03	3.0×10^{-4}
4	75%	100	0.996	1	1.03	2.5×10^{-4}
5	75%	100	0.99	1	1.03	2.5×10^{-4}
6	75%	100	0.985	1	1.03	2.0×10^{-4}
7	75%	100	0.99	1	1.03	2.5×10^{-4}
8	75%	100	0.98	1	1.03	2.4×10^{-4}

Table 4-5 Parameter values for best fit data with COX deficient stem cell advantage

Stem Cell Number	Parameters					
	COX deficiency threshold	mtDNA copy number	Pa	COX stem cell advantage	Division Segregation Factor	Mutation Rate
3	75%	100	0.9995	150	1.05	4.5×10^{-4}
4	75%	100	0.997	120	1.05	3.0×10^{-4}
5	75%	100	0.99	30	1.05	2.5×10^{-4}
6	75%	100	0.985	15	1.05	2.5×10^{-4}
7	75%	100	0.95	10	1.05	2.5×10^{-4}
8	75%	100	0.75	7	1.05	2.5×10^{-4}

4.4.5.4 Stem cell number validation from human niche succession model

The optimum number of stem cells contained within human colonic crypts was determined using the best-fit data from models simulated with parameters from Table 4-5. In chapter 3, partially COX deficient crypts were used to determine how many stem cells were contained within human colonic crypts. The same was done from a modelling perspective. Each model with different numbers of stem cells had their partially COX deficient crypts pooled. The data was transformed using the distribution model described in chapter 3 using the algorithm contained within appendix 1.3.4. This allowed the biological and model data to be in the same format for a probability density curve to be plotted for each. Figure 4-19 shows that with increasing number of stem cells simulated, there is an increasing ratio between crypts that have low partial COX deficiency fraction compared to those that have a high partial COX deficiency fraction. This ratio best fitted with a model that had 5-6 stem cells present. Least squares analysis of the probability density curves show that a model with 5 stem cells fits the biological data the best (Table 4-6).

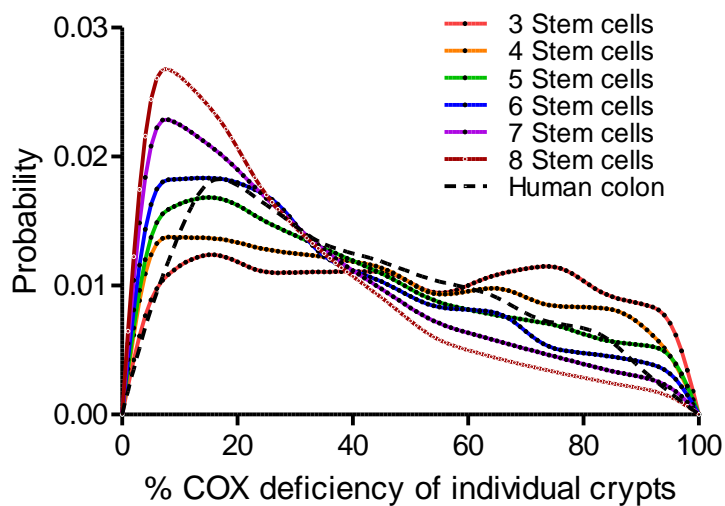


Figure 4-19 Stem cell number validation via partially COX deficient crypts.

The distribution of partially COX deficient crypts from human colon was compared with the distribution of partially COX deficient crypts generated from the optimised models with varying number of stem cells simulated (Table 4-5). The distribution model described in section 3.4.7 (model code and conversion algorithm contained in appendix 1.3.4) were used to transform number of COX deficient stem cells into observed COX deficiency percentage. Each distribution was plotted as a probability density curve for comparison. Each model was compared with the biological data via method of least squares. Least squares goodness of fit values are contained within Table 4-6. A value of 0 represents a perfect match to the biological data.

Table 4-6 Least squares value for model fits with varying stem cell number

Stem Cell Number	Least Squares Value
3	0.29
4	0.19
5	0.14
6	0.17
7	0.28
8	0.40

4.5 DISCUSSION

The human niche succession model developed during my PhD is an advancement to the one that was developed during my MRes (development timeline section 4.3.1). The major step forward was being able to explicitly simulate individual mtDNA molecules within stem cells, with a mutation rate acting upon each mtDNA replication. More adaptations have been introduced into the human niche succession model during my PhD, all in order to make the model as biologically accurate as possible. These include introducing; a variable slope mutation rate with age (constant or linear), the process of crypt fission, individual mtDNA species tracking, and the incorporation of a mutated mtDNA segregation advantage upon stem cell division.

There are a considerable number of parameters that influence the human niche succession model output. The effects of each parameter on the model have been depicted and described within the results section. Briefly, increasing the constant *de novo* mtDNA mutation rate within the human niche succession model (Figure 4-3) increases the COX deficiency frequency observed. An increasing *de novo* mtDNA mutation rate (Figure 4-4) results in an increasing frequency of partially COX deficient crypts with age along with an increasing rate of fully COX deficient crypt accumulation. Increasing the constant *de novo* mtDNA mutation rate also increases the number of individual mutations present within aged stem cells (Figure 4-11, Figure 4-12, and Figure 4-14). A previous study using the Random Mutation Capture (RMC) assay to assess low level mutation frequency which excludes clonally expanded mutations (proxy for mutation rate) provides evidence that there is not a statistically significant difference in low level mtDNA mutation frequency with age within human colonic mucosa ($p = 0.343$, one way ANOVA) (Greaves *et al.*, 2014). However, although the RMC assay is the closest measurement of mtDNA mutation rate currently available, it cannot measure mtDNA mutation rate as a dynamic process, and the assay is intrinsically noisy, therefore a minor increase in mtDNA mutation rate with age cannot be definitively ruled out. An increasing mtDNA mutation rate would fit in with the reactive oxygen species ‘vicious cycle’ hypothesis (Harman 1972).

Within the human niche succession model, increasing mtDNA copy number decreases the probability and increases the amount of time it takes for a mutated mtDNA molecule to become fixed (Figure 4-7). However, with a 100-fold difference in mtDNA copy number, the resulting COX deficiency frequency difference is marginal (Figure 4-8).

Asymmetric stem cell division probability is a parameter that has a considerable effect on the COX deficiency frequency. This parameter has the effect of deciding the ratio between partially and fully COX deficient crypt frequencies with the most dramatic effect observed at a probability >0.95 (Figure 4-2). This is because with increasing asymmetric stem cell division probability, there is a decreasing probability of *de novo* COX deficient crypt niche succession, with an associated increase in the time it takes niche succession to occur (Figure 4-7).

Crypt fission was also introduced into the human niche succession model as this was observed within human colonic crypt biopsy sections and has been hypothesised to aid the expansion of COX deficient crypts within human colonic epithelium (Greaves *et al.*, 2006). However, when crypt fission is simulated with different probabilities of occurrence, there was no significant difference (Figure 4-5). A difference was observed when an advantage for COX deficient crypts to undergo crypt fission was introduced into the model. Within human colon epithelium, there is a 1% occurrence of normal crypts undergoing fission in all age brackets (Figure 3-4). However, in aged samples, there is a 3% occurrence of COX deficient crypts undergoing fission. This would suggest that there is an advantage for COX deficient crypts to undergo crypt fission more often, if only just in aged samples. Unfortunately, the human niche succession model required a considerable crypt fission probability in conjunction with a much larger advantage conveyed to COX deficient crypts to undergo crypt fission than was biologically conceivable. Therefore, as COX deficient crypt colonies are thought to be the result of crypt fission (Greaves *et al.*, 2006), the biological data set had the effect of crypt fission removed (section 3.4.6). This new data set would serve as the biological reference data allowing crypt fission to be ignored within the model.

Perturbed stem cell dynamics was also incorporated into the human niche succession model as a mechanism for crypt fission induction. This was in the form of an advantage conveyed to COX deficient stem cells to undergo symmetric stem cell division (2 renewed stem cells) more often than normal stem cells. It has been suggested that respiratory deficiency would alter the stem cells metabolism considerably via ROS mediated alteration, shifting its cell fate decision (Ryu *et al.*, 2015). Increasing the COX deficient stem cell advantage within the human niche succession model increases both partially and fully COX deficient crypt frequency at all ages (Figure 4-6). This was dependent on there being a large enough *de novo* mtDNA mutation rate present for large advantages conveyed to COX deficient stem cells.

Finally, a bias was introduced into the human niche succession model that would allow mutated mtDNA to be preferentially segregated into the stem cell progeny cell upon asymmetric stem cell division. This was due to the observation that new mitochondria, hence newly replicated mtDNA, are segregated asymmetrically within dividing mammary epithelial stem cells (Katajisto *et al.*, 2015). Relaxed replication and random segregation would not allow COX deficiency frequency and number of mutations to match the trend in the biological data simultaneously (Figure 4-12). Increasing the division segregation factor was shown to reduce the probability of mutated mtDNA molecules becoming fixed due to their segregation out of the stem cell pool (Figure 4-13). This was true for all mutation rates (Figure 4-15). This allowed the number of mtDNA mutations within simulated aged stem cells to be matched to the number of mtDNA mutations found within human colonic mucosa.

The optimised simulations show there exists an advantage for mutated mtDNA to be segregated out of the stem cell pool. This is true for all models with varying stem cell number being simulated within crypts (Figure 4-17). In order to observe an increase in partially COX deficient crypts with age, as is shown within the biological data, there needs to be an advantage conferred to COX deficient stem cells for them to undergo symmetric stem cell division more often (Figure 4-18). With this scenario, there also needs to be a greater division segregation bias conferred to mutated mtDNA. Optimised models have also reinforced the notion that there are an average of 5 functional stem cells contained within human colonic crypts (Figure 4-19 and Table 4-6).

Mouse studies have shown that the emergence of partially and fully labelled crypts follow a pattern of neutral drift dynamics (Lopez-Garcia *et al.*, 2010; Snippert *et al.*, 2010; Kozar *et al.*, 2013). This is exemplified by there being a constant frequency of partially labelled crypts with a linearly increasing frequency of fully labelled crypts throughout the mouse's lifetime. Human colon COX deficiency data shows that there is an increasing rate of accumulation for both partially and fully COX deficient crypts with age. This suggests that human COX deficient stem cells do not follow a pattern of neutral drift. This is reinforced by the human niche succession model which shows that biologically relevant partially COX deficient crypts can only be achieved with an advantage conferred to COX deficient stem cells. This is further reinforced by the fact that a mutated mtDNA segregation bias is required in order to match both COX deficiency frequency and number of mutations present within aged stem cells. Therefore, mutated mtDNA upon stem cell division are not following random segregation

and COX deficient stem cells are not following a pattern of neutral drift, though the perturbation from neutrality is relatively mild.

The human niche succession model explicitly simulates stem cells within their niche, overcoming many obstacles involved in simulating the entire crypt. Simulating the entire crypt involves understanding the cell dynamics of all cell types within the crypt, for example, cell division times, migration, differentiation, apoptosis, and also the assumption of geometric architecture of the crypt. Most models of crypt cell dynamics have to map 3 dimensional crypts as 2 dimensional surfaces (Meineke *et al.*, 2001; van Leeuwen *et al.*, 2009; Fletcher *et al.*, 2012). Extra assumptions and parameter estimations to build such a model adds to its complexity, with its complexity hindering its ability to produce novel findings.

The van Leeuwen model was used to validate an assumption within a study conducted by Baker et al (van Leeuwen *et al.*, 2009; Baker *et al.*, 2014). The assumption was that the expansion and contraction of COX deficient stem cell clones within the stem cell niche produces a chronological COX deficiency imprint on the cell wall. An expansion of a COX deficient stem cell clone via symmetric stem cell division would result in a larger COX deficiency imprint on the cell wall. The fact that a larger fraction of COX deficient stem cells within the niche results in an increased COX deficiency imprint on the crypt wall is in agreement with the COX deficiency distribution model described (section 3.4.7). However, I propose that changes in COX deficiency clone width may have additional factors than those stated in Baker et al. For example, as there are a particular number of ‘functional’ stem cells within the stem cell niche of crypts, there has to be an expansion of stem cell progeny to the numbers that are observed in transverse cross-sections of crypts, especially if there are 5 ‘functional’ stem cells, which our data shows (section 3.4.2 and section 4.4.5.4) and the 5-7 ‘functional’ stem cells stated in Baker et al. This must be achieved via stem cell progeny rapidly proliferating and differentiating further up the crypt as they migrate, which highly likely results in lateral displacement of the COX deficient cells, thereby increasing and decreasing the COX deficiency imprint on the cell wall. It is also highly likely that the ‘functional’ stem cells within crypts divide asynchronously. Asymmetric asynchronous stem cell divisions along with expansion in stem cell progeny must greatly influence the dispersion of the COX deficiency imprint on the cell wall. Furthermore, COX deficiency may not result from a cell having a completely fixed mtDNA mutation within the cell. A heteroplasmy threshold level may exist, depending on the type of mutation present. The expansion and

contraction of the COX deficiency imprint on the crypt wall may be the result of the cells heteroplasmy level falling below the level at which COX deficiency is observed via COX/SDH histochemistry. Therefore, the expansion and contraction of the COX deficiency imprint on the crypt wall can be explained with additional factors and may not be solely influenced by stem cell dynamics. Another important consideration is the regeneration time of human colonic crypts compared with the stem cell division time. It has been shown that human colonic epithelium is regenerated weekly (Potten *et al.*, 1992) with colonic stem cells dividing every 3-5 days (Potten *et al.*, 1992). If this is the case, then a 3-dimensional crypt observed at a single time-point only represents the stem cells that have divided within the previous week. Each stem cell would have only undergone a limited number of stem cell divisions in that time, which limits the insights that can be made about the stem cell dynamics taking place within crypts from this data set. Baker et al used 9 patients' colon biopsies with 11 *en face* serial sections to construct 3 dimensional crypts to gain insight into the 'wiggle' COX deficiency pattern on the crypt wall. With such a limited number of partially COX deficient crypts analysed, it is highly likely that the other factors described influence the size of the COX deficiency imprint on the crypt wall, potentially biasing interpretations of this data type.

The study conducted in this thesis examined 148 human colon biopsy samples from patients ranging between 17 and 78 years of age. This study quantified the COX deficiency present within ~140,000 transverse partially COX deficient crypts from single sections. As so many partially COX deficient crypts were quantified from each age bracket, together with the COX deficiency distribution model constructed, the effects of other factors having an effect on the size of the COX deficiency imprint on the crypt wall were accounted for. This allowed a simpler model of human colon stem cell dynamics to be constructed as opposed to the van Leeuwen model. Number of COX deficient stem cells within the model could be assigned to the COX deficiency fraction observed within transverse crypts using the COX deficiency distribution model.

Even though the human niche succession model is a simpler model than having to simulate an entire crypt, it is still made complex by the incorporation of additional parameters. With each additional parameter added to make the model more biologically realistic, it becomes substantially harder to optimise to biological reference data. With the addition of an extra parameter being optimised, many more simulation had to be run. The most up to date human niche succession model simulated with biologically relevant parameters required ~6 seconds

per crypt simulation to complete, meaning a population of 5000 crypts would take ~8 hours to simulate. Therefore an automatic parameter optimisation algorithm was not possible.

Parameter scanning was conducted by trial and error and is how the optimised models were established (Figure 4-17 and Figure 4-18). Optimisation was based on similar trends in data when comparing model results and biological reference data.

At present the model can incorporate a variable *de novo* mutation rate with age. All other parameters had to be fixed throughout the lifetime of a crypt due to the way the model was constructed in MATLAB. For instance, replication and segregation matrices had to be constructed for each number of mtDNA molecules being simulated within stem cells.

Matrices could not be constructed for mtDNA copy number >400 due to insufficient computer random access memory (RAM) that would be required to construct them. However, given the size of stem cells and the low nuclear:cytoplasmic volume, >400 mtDNA copies is unlikely. The ability to vary each parameter with age would be beneficial because ageing, which is associated with a decline in cellular function, may result in variable parameter values as well.

4.6 CONCLUSION

It is true that no biological model can truly replicate the processes that occur within biological systems as they are a simplification of the processes being investigated. However, the human niche succession model, in conjunction with the human colon COX deficiency data, shows that COX deficiency has the potential to confer altered stem cell dynamics to a stem cell, allowing COX deficiency to accumulate via a non-neutral drift manner within the colon. Investigating the way in which COX deficiency confers an advantage to stem cells should be investigated *in vivo*.

Chapter 5

Development and Validation

of a Mouse Model to

Investigate Stem Cell

Dynamics

Chapter 5 Development and validation of a mouse model to investigate stem cell dynamics

5.1 INTRODUCTION

Mitochondrial dysfunction within ageing human colon has been well studied over the past decade (Taylor *et al.*, 2003; Greaves *et al.*, 2006; Greaves *et al.*, 2010). Furthermore, the similarities and differences between mouse and human mitochondrial dysfunction has been investigated in depth in order to discover a good mouse model of mitochondrial ageing within the colon (Greaves *et al.*, 2011; Baines *et al.*, 2014). It has been shown that aged *wild type* C57Bl/*Icrfa*¹ mice don't accumulate mitochondrial dysfunction in the form of COX deficiency to the same extent as in aged humans (Greaves *et al.*, 2011). For instance, humans at 85 years accumulate ~15% COX deficiency within their colonic epithelium, whereas mice at 36 months, which was deemed equivalent to 85 year old humans, only accumulate ~1%. Contrastingly, the ciliary epithelium within mouse intraocular tissue accumulates ~30% COX deficiency at 36 months, whereas humans only accumulate ~12%. This exemplifies the differences in the rate of COX deficiency accumulation within the same tissues between mice and humans. Furthermore, this demonstrates the reason why ageing *wild type* mice can't be used as a model of human intestinal ageing with regards to mitochondrial dysfunction. COX deficiency determined by COX/SDH histochemistry is a good marker of Complex IV deficiency caused by mtDNA mutations. This has been shown within a variety of human tissues, which include; prostate (Blackwood *et al.*, 2011), liver (Fellous *et al.*, 2009), stomach (McDonald *et al.*, 2008) and colon (Taylor *et al.*, 2003). However, as mtDNA contains genes that encode protein subunits for 3 other respiratory chain complexes, it may be the case that other complexes may be deficient whilst normal COX activity for Complex IV is present. This is brought to light by the observation showing multiple respiratory complexes becoming deficient during normal human ageing within the colon (Greaves *et al.*, 2010).

Mouse models are an important tool in order to understand the link between mitochondrial dysfunction and age related phenotypes. TFAM knockout mice are one such mouse model that can be used to investigate this link. TFAM is a transcriptional activator within mitochondria and is also important for mitochondrial DNA replication (Reyes *et al.*, 2002). As such, TFAM knockout mice (*Tfam*^(+/-)) have reduced mtDNA copy number with associated respiratory chain complex deficiency. TFAM knockout mice have been discussed in detail in section 1.7.4.1.

MtDNA mutator mice are another mouse model that can be used to investigate the link between mitochondrial dysfunction and ageing. They are associated with a progressive accumulation of mtDNA mutations along with the development of age-related phenotypes. Mitochondrial mutator mice are discussed in detail in section 1.7.4.2.

COX deficiency within the colons of mitochondrial mutator *PolyA^(+/-)* mice show a similar level of COX deficiency within their colons (~15%) when compared to humans at an equivalent age, with a similar pattern for the types of mtDNA mutations present as well (Baines *et al.*, 2014). It was also determined that mutations within genes other than MT-CO genes can result in COX deficiency, adding weight to the respiratory supercomplex hypothesis (Schagger and Pfeiffer, 2000). This corroborates the finding that patients with mutations in Complex I genes show multiple respiratory chain deficiency (Hinttala *et al.*, 2006).

Multiple respiratory complex deficiency has been shown within colonic epithelium within normal human ageing (Greaves *et al.*, 2010). For instance, of the total number of crypts that were tested for Complex I, III and IV deficiency, 11.2% harboured some form of complex deficiency (Greaves *et al.*, 2010). Of the 11.2%, 29.9% of crypts had a deficiency in one complex, 19.1% had a deficiency in two complexes, and 51% had a deficiency within all three complexes (Greaves *et al.*, 2010). Furthermore, the majority of deficient crypts (>95%) harboured either Complex I or Complex IV deficiency, with ~70% of those crypts harbouring both Complex I and Complex IV deficiency together (Greaves *et al.*, 2010).

As the cause of the respiratory deficiency of any particular complex can be due to mutations in the genes of another complex, it is important to assess multiple respiratory complexes when determining the respiratory status of a cell or tissue. As mitochondrial mutator *PolyA^(+/-)* mice have been shown to be a good mouse model of ageing (Baines *et al.*, 2014), it would be interesting to assess whether multiple complexes are deficient within these mice as well.

5.2 AIMS OF STUDY

The aim of this study was to validate the use of the *PolyA* mice with the *Lgr5* mice in order to investigate stem cell dynamic perturbations caused by respiratory deficiency. This would be done by examining multiple respiratory chain loss of expression within 11-12 month old mice with varying degrees of mitochondrial polymerase proofreading deficiency. The majority of mtDNA base pairs within protein encoding genes contribute towards subunits of Complex I and Complex IV (82%), therefore these respiratory chain complexes were chosen. The frequency of both Complex I (NDUFB8 subunit) and Complex IV (MTCO1 subunit) expression loss within *Lgr5^(+/-)PolyA⁽⁺⁺⁾*, *Lgr5^(+/-)PolyA⁽⁺⁻⁾* and *Lgr5^(+/-)PolyA⁽⁻⁻⁾* mice at similar ages would be investigated. Therefore, the effect of increasing level of mitochondrial polymerase proofreading deficiency upon replication would be ascertained.

5.3 METHODOLOGY

5.3.1 Modelling focal respiratory chain deficiency within mouse colon

Wild-type C57Bl/6J, PolyA^(+/-) and PolyA^(-/-) mitochondrial mutator mice were bred within the comparative biology centre (Newcastle University) (section 2.2.2.1). Mouse colon COX deficiency frequency data from both mitochondrial mutator mouse species at discrete age steps was provided by Dr Holly Baines (Newcastle University) (Baines *et al.*, 2014). *Wild-type C57Bl/6J* mouse colon COX deficiency frequency data was provided by Dr Laura Greaves (Newcastle University) (Greaves *et al.*, 2010). A model that simulated the clonal expansion of mutated mtDNA molecules within a population of stem cells was constructed (section 2.2.10.1) in order to determine whether mtDNA mutation rate could explain the difference in COX deficiency accumulation between the three mouse genotypes. The main assumption was that a stem cell was likened to a fully COX deficient crypt.

5.3.2 Quantifying mitochondrial dysfunction within mouse colon

Lgr5-EGFP-Ires-CreERT2 (*Lgr5+*) mice were crossed with heterozygote mitochondrial mutator *PolyA^(+/-)* mice within the comparative biology centre (Newcastle University) (section 2.2.2.2). *Lgr5^(+/-)PolyA^(+/-)* (n=4), *Lgr5^(+/-)PolyA^(+/-)* (n=5) and *Lgr5^(+/-)PolyA^(-/-)* (n=4) were aged to 11-12 months and then killed (section 2.2.4). Mouse colons were removed for tissue processing at 11-12 months (section 2.2.4). Immunofluorescence was carried out to determine the expression levels of cytochrome *c* oxidase subunit 1 (MTCO1) of Complex IV and the NDUFB8 subunit of Complex I within mouse colon (section 2.2.5). Fluorescence microscopy and image analysis was conducted on mouse colon sections that had undergone immunofluorescence for mitochondrial OXPHOS subunit expression (section 2.2.7). This allowed the viability of the cross between *Lgr5+* and mitochondrial mutator mice to be determined. It would also allow the pattern of mitochondrial dysfunction within their colon tissue to be quantified before further work could be carried out.

5.4 RESULTS

5.4.1 Mitochondrial mutator mouse phenotype

The observable phenotype for each mouse included within this study was recorded as can be seen in Table 5.1. All *Lgr5^(+/-)PolyA^(+/+)* mice showed a normal phenotype for 12 month old *C57Bl/6J* mice. *PolyA^(+/-)* mice show no observable phenotype associated with ageing due to mitochondrial dysfunction (Trifunovic *et al.*, 2004). Within this study, the majority of *Lgr5^(+/-)PolyA^(+/-)* mice appeared normal when compared to *Lgr5^(+/-)PolyA^(+/+)* mice, however, there were a couple of mice that showed some characteristics associated with its genotype, this included a marginally grey coat. *PolyA^(-/-)* mice show an ageing phenotype from 6 months which includes; weight loss, anaemia, osteoporosis, kyphosis, and reduced subcutaneous fat (Trifunovic *et al.*, 2004). Within this study, an ageing phenotype was also observed with *Lgr5^(+/-)PolyA^(-/-)* mice. The most obvious phenotype was greying of the fur and low weight. However, unlike the *PolyA^(-/-)* used within the study by Trifunovic *et al.*, the kyphosis phenotype was not as severe. The difference in phenotype severity is likely due to the nuclear background as the mitochondrial mutator mice within this study have a *C57Bl/6J* background (Kujoth *et al.*, 2005), as opposed to *C57Bl/6N* (Trifunovic *et al.*, 2004) within the study by Trifunovic *et al.* This may suggest that there is slower clonal expansion of mutated mtDNA within *C57Bl/6J* mice. Therefore, it would appear that the nuclear background significantly impacts on the severity of observable phenotypes within mitochondrial mutator mice.

5.4.2 COX deficiency frequency within mitochondrial mutator mice

A model was developed that was able to replicate the accumulation of COX deficiency within mouse colonic epithelium. In particular, the accumulation of COX deficiency within mouse models of mitochondrial dysfunction, also known as *PolyA* mice. These mice have a proofreading deficiency within the mitochondrial DNA polymerase (D257A substitution) which means they are more likely to incorporate the wrong nucleotide upon replication, leading to mtDNA point mutation accumulation. COX/SDH histochemistry allows the visualisation of respiratory deficient crypts caused by clonal expansion of pathogenic *de novo* mtDNA mutations. Figure 5-1 shows the accumulation of COX deficiency within colonic epithelium of both *PolyA^{+/-}* (heterozygote) and *PolyA^{-/-}* (homozygote) mice and has kindly been provided by Dr Holly Baines (Baines *et al.*, 2014). *PolyA* homozygote mice develop an ageing phenotype between 6 and 9 months (Trifunovic *et al.*, 2004) and have a reduced lifespan compared to wild-type mice which is why there are no data points after 12 months of

age. *PolyA* homozygote mice accumulate COX deficiency within the colon at a faster rate compared to *PolyA* heterozygote. *Wild-type* mice also accumulate COX deficiency with age, but this only reaches ~1.5% by 36 months of age (Greaves *et al.*, 2011). A model was developed in order to determine whether mutation rate alone could explain the difference in COX deficiency frequency between *wild-type*, *PolyA* heterozygote and *PolyA* homozygote mice, in order to validate their use.

Table 5-1 List of mice used within mitochondrial dysfunction study

Mouse	Sex (m/f)	Age (weeks)	Description
<i>wild-type</i>			
<i>LPA446</i>	f	54.0	Normal
<i>LPA457</i>	f	54.0	Normal
<i>LPA497</i>	f	52.3	Normal
<i>LPA499</i>	f	52.3	Normal
<i>PolgA het</i>			
<i>LPA187</i>	f	51.9	Greying coat
<i>LPA245</i>	f	51.7	Normal
<i>LPA281</i>	m	51.7	Normal
<i>LPA247</i>	f	52.0	Normal
<i>LPA280</i>	f	51.7	Normal
<i>PolgA hom</i>			
<i>LPA278</i>	f	48.0	Slight kyphosis, greying coat, low weight
<i>LPA242</i>	f	47.1	Slight kyphosis, greying coat, thinning fur, low weight
<i>LPA213</i>	m	49.3	Slight kyphosis, greying coat, thinning fur
<i>LPA219</i>	m	48.1	Slight kyphosis, fully grey coat, thinning fur

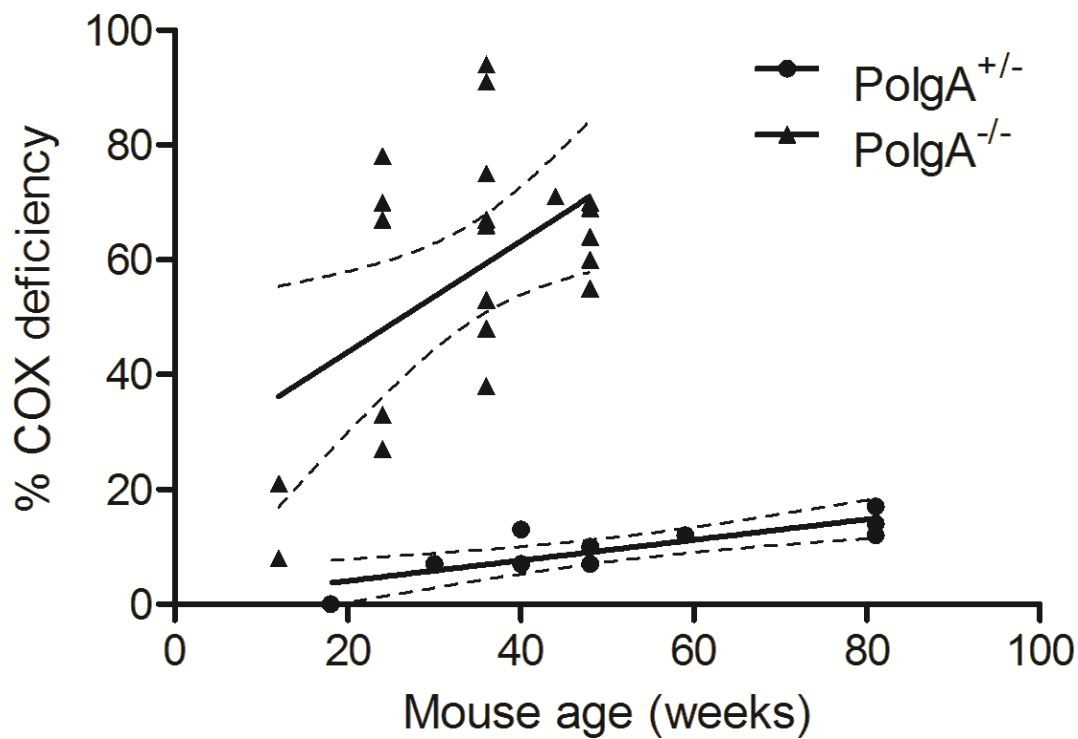


Figure 5-1 COX deficiency within mitochondrial mutator mice with age

Data kindly provided by Dr Holly Baines showing the trend in respiratory deficiency (COX deficiency) within colonic epithelium of mice that have a proofreading deficiency within their mitochondrial polymerase gamma subunit (PolyA). The proofreading deficiency makes replicated mtDNA prone to acquiring point mutations. Both heterozygote and homozygote data is shown (Baines *et al.*, 2014).

5.4.2.1 MtDNA mutation clonal expansion model

A model of COX deficiency accumulation within mouse colon was developed and is described in section 2.2.10.1 with model code contained within appendix 1.3.1. A population of 1000 crypts within the colon was likened to a population of 1000 stem cells within the model, each with a specified mtDNA copy number. Each stem cell undergoes 1080 asymmetric divisions and are simulated independently. Figure 5-2 depicts the clonal expansion of mutated mtDNA molecules within 5 individual stem cells.

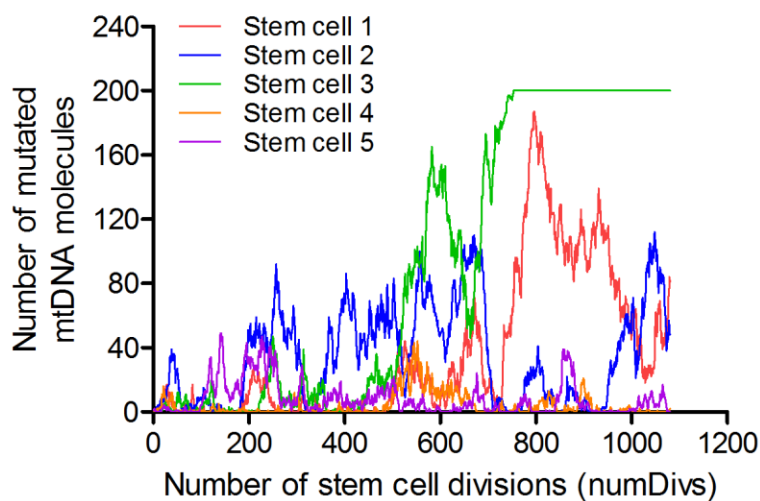


Figure 5-2 Mutated mtDNA clonal expansion within individual stem cells

The clonal expansion model simulates the clonal expansion of mutated mtDNA molecules over time via relaxed replication and random segregation within a population of purely asymmetrically dividing stem cells. 1000 stem cells are simulated with each stem cell containing, in this case, 200 mtDNA molecules. A mutation rate (mutated mtDNA/replicated mtDNA) can be set which introduces *de novo* mtDNA point mutations into the system. Number of mutated mtDNA molecules versus number of stem cell divisions is shown for 5/1000 stem cells simulated to exemplify the stochastic clonal expansion of mutated mtDNA within individual stem cells. Only stem cell 3 reaches fixation. A more detailed explanation of the model is given in section 2.2.10.1 and the model code is contained within appendix 1.3.1.

5.4.2.2 *Mutation rate and mtDNA copy number within stem cells*

The effects of mtDNA copy number and *de novo* mutation rate were assessed within the clonal expansion model. Figure 5-3 shows that with different numbers of mtDNA copy number, increasing the constant *de novo* mutation rate does increase the rate at which COX deficiency accumulates within a population of stem cells, likened to the colon epithelium.

Figure 5-4 shows how mtDNA copy number changes the accumulation of COX deficiency within a population of stem cells. With a smaller mtDNA copy number, there is a slightly faster rate at which COX deficiency accumulates within a population of asymmetrically dividing stem cells. This difference is more pronounced with a low mutation rate, however, with an increased mutation rate, there is only a smaller difference in the rate of COX deficiency accumulation.

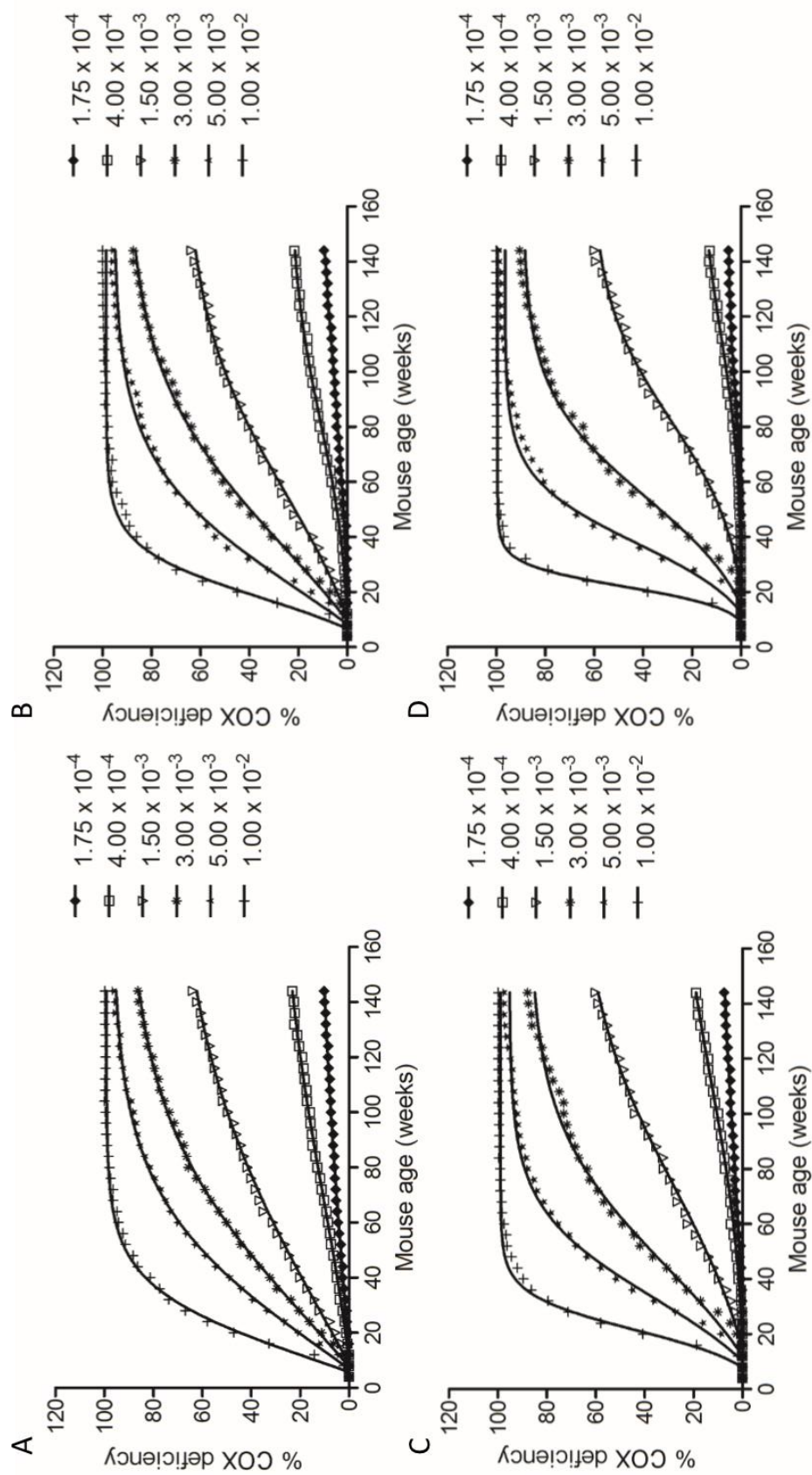


Figure 5-3 Mutation rate within clonal expansion model

The effects of increasing *de novo* mutation rate were ascertained within the mouse clonal expansion model. 75% mutated mtDNA within individual stem cells conferred COX deficiency and was used when determining the percentage COX deficiency within the population. Simulations were carried out with varying mtDNA copy number per stem cell. Simulations were run with (A) 100 mtDNA molecules, (B) 200 mtDNA molecules, (C) 400 mtDNA molecules, and (D) 800 mtDNA molecules present within each stem cell.

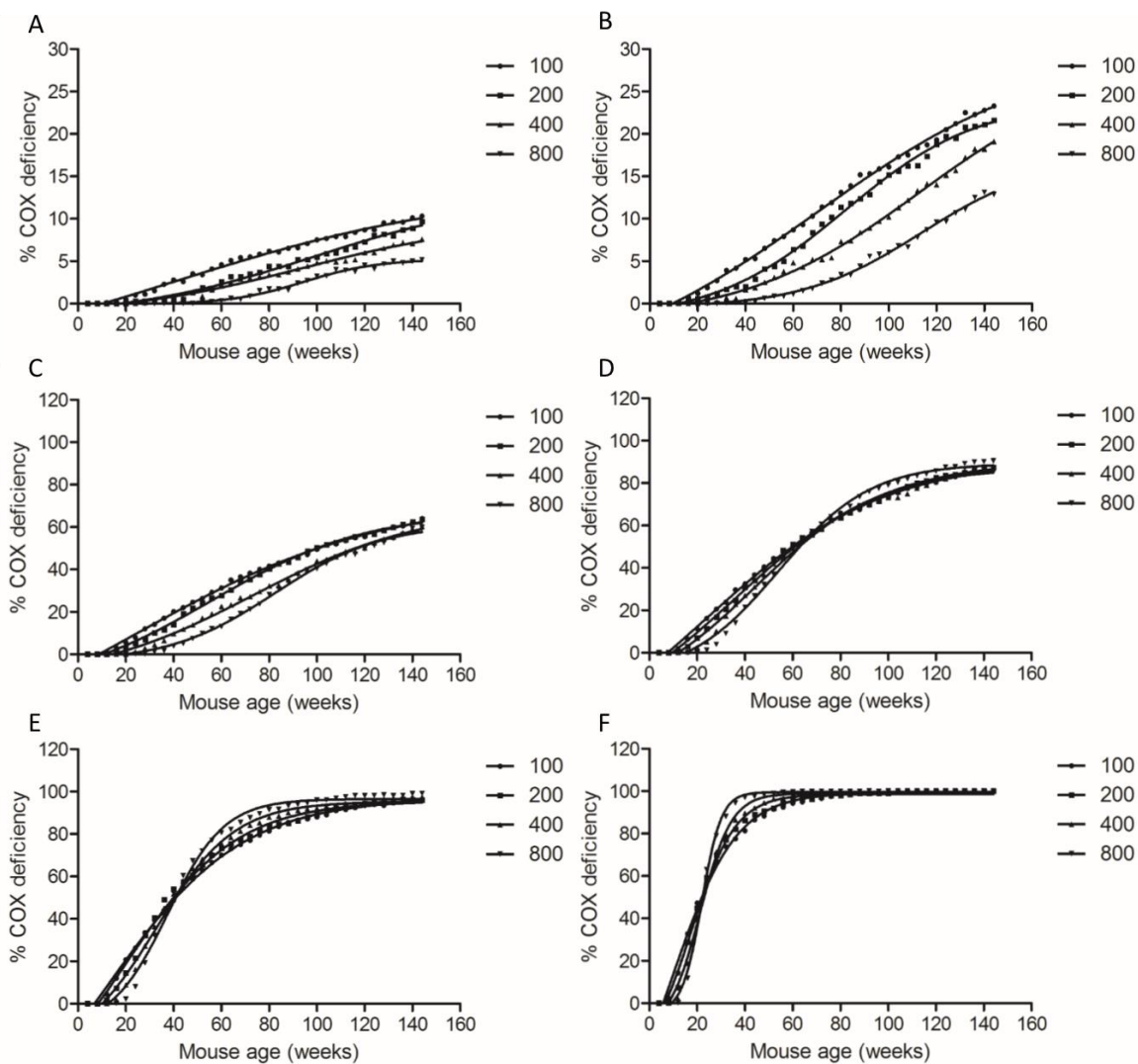


Figure 5-4 MtDNA copy number within the clonal expansion model

The effects of increasing mtDNA copy number were ascertained within the clonal expansion model. 75% mutated mtDNA within individual stem cells conferred COX deficiency and was used when determining the percentage COX deficiency within the population. Simulations were also carried out with varying mutation rate. Simulations were run with mutations rates (A) 1.75×10^{-4} , (B) 4.00×10^{-4} , (C) 1.50×10^{-3} , (D) 3.00×10^{-3} , (E) 5.00×10^{-3} , and (F) 1.00×10^{-2} mutated mtDNA/mtDNA replication

5.4.2.3 Population model best fits with mitochondrial mutator mouse models

As mtDNA copy number did not impact significantly on the rate of COX deficiency accumulation, a copy number of 200 was chosen for the best fit optimisation (Coller *et al.*, 2001). The mutation rate was optimised for *wild-type*, *PolyA* heterozygote and *PolyA* homozygote mice by using COX deficiency reference points from each animal (Figure 5-5). The reference point for *wild type* animals was 1.5% COX deficiency at 36 months. This was matched with a mutation rate of 7×10^{-6} mutated mtDNA/mtDNA replication. The reference point for *PolyA* heterozygote animals was 15% COX deficiency at 20 months. This was matched with a mutation rate of 7×10^{-4} mutated mtDNA/mtDNA replication. The reference point for *PolyA* homozygote animals was 60% at 9 months. This was matched with a mutation rate of 1×10^{-2} mutated mtDNA/mtDNA replication. This indicates there is a 100x and 1428x increase in the chance of a mutation occurring within *PolyA* heterozygote and homozygote animals compared with *wild type* animals, respectively. Also, *PolyA* homozygote animals acquire mutations 14x faster than *PolyA* heterozygote animals. This indicates that mtDNA mutation rate can be the main difference between mouse species that varies the rate of accumulation of focal respiratory deficiency.

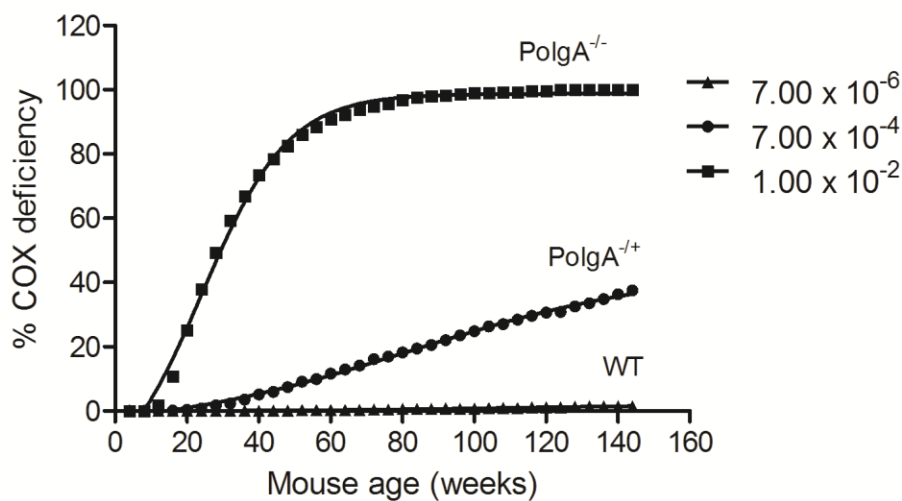


Figure 5-5 Optimised clonal expansion model

Mutation rates were optimised in order to match COX deficiency frequency within *wild-type*, *PolyA*^(+/-) and *PolyA*^(-/-) mice. 7×10^{-6} mutated mtDNA/replicated mtDNA best matched *wild-type* mice. 7×10^{-4} mutated mtDNA/replicated mtDNA best matched *PolyA*^(+/-) mice. 1×10^{-2} mutated mtDNA/replicated mtDNA best matched *PolyA*^(-/-) mice. 200 mtDNA molecules were simulated per stem cell.

5.4.3 Observed mitochondrial dysfunction within mouse colon

Quadruple immunofluorescence and fluorescence microscopy was conducted on *Lgr5^(+/-)PolyA⁽⁺⁺⁾*, *Lgr5^(+/-)PolyA⁽⁺⁻⁾* and *Lgr5^(+/-)PolyA⁽⁻⁻⁾* mouse colons in order to determine the frequency of crypts with MTCO1 (Complex I) and NDUFB8 (Complex IV) loss at 48-54 weeks of age (Table 5.1). Figures 5-6, 5-7 and 5-8 show images for Complex I, Complex IV, VDAC1 (Porin) (mitochondrial mass marker) and DAPI (nuclear counterstain), along with a merged image. There was a clear distinction between expression and loss of expression for each respiratory complex subunit, with no partial down-regulation observed within mouse colon. Therefore, crypts were grouped according to them being normal for Complex I and Complex IV expression, Complex I loss of expression, Complex IV loss of expression, and both Complex I and Complex IV loss of expression. Complex I expression appears red, Complex IV expression appears green, Porin expression appears orange and the cell nucleus appears blue. A merged image provides a clear picture of the mitochondrial OXPHOS status for Complex I and IV. Yellow crypts exemplify the expression of both Complex I and Complex IV. Red crypts exemplify the expression of Complex I only. Green crypts exemplify the expression of Complex IV only. Crypts that do not have a colour exemplify the loss of both Complex I and Complex IV. Figure 5-6 shows an example of what is observed within *Lgr5^(+/-)PolyA⁽⁺⁺⁾* mice. As can be seen within the merged image, all the crypts are yellow, indicating the presence of Complex I and Complex IV. As can be seen in the graph in Figure 5-6F. There is very little Complex I and Complex IV loss across all *Lgr5^(+/-)PolyA⁽⁺⁺⁾* mice observed. There is a slightly higher level of Complex I loss (~1%) compared to Complex IV (~0.1%) within *Lgr5^(+/-)PolyA⁽⁺⁺⁾* mice. Figure 5-7 shows an example of what is observed within *Lgr5^(+/-)PolyA⁽⁺⁻⁾* mice. As can be seen within the merged image, there is a mosaic pattern of yellow, green and red crypts. This indicates that crypts can either be normal for mitochondrial OXPHOS complex expression, Complex I deficient, Complex IV deficient, or harbour multiple complex deficiency (not shown in image). There is much more Complex I (~40%) and Complex IV (~20%) loss within *Lgr5^(+/-)PolyA⁽⁺⁻⁾* compared to *Lgr5^(+/-)PolyA⁽⁺⁺⁾* animals. Figure 5-8 shows an example of what is observed within *Lgr5^(+/-)PolyA⁽⁻⁻⁾* mice. As can be seen within the merged image, there is substantial mitochondrial OXPHOS complex loss for both Complex I and Complex IV. Most of the Complex I (~95%) expression within the colon epithelium is absent with a significant fraction of Complex IV (~60%) expression absent as well. Porin was included within the immunofluorescence assays to determine whether there was an associated decrease in

mitochondrial mass with loss of respiratory chain complex expression. As can be seen within the images for respiratory deficient crypts (Figures 5-7 and 5-8), there was no observable decrease in Porin intensity, indicating that crypts with respiratory chain complex deficiency within mitochondrial mutator mice are not associated with a reduction in mitochondrial mass.

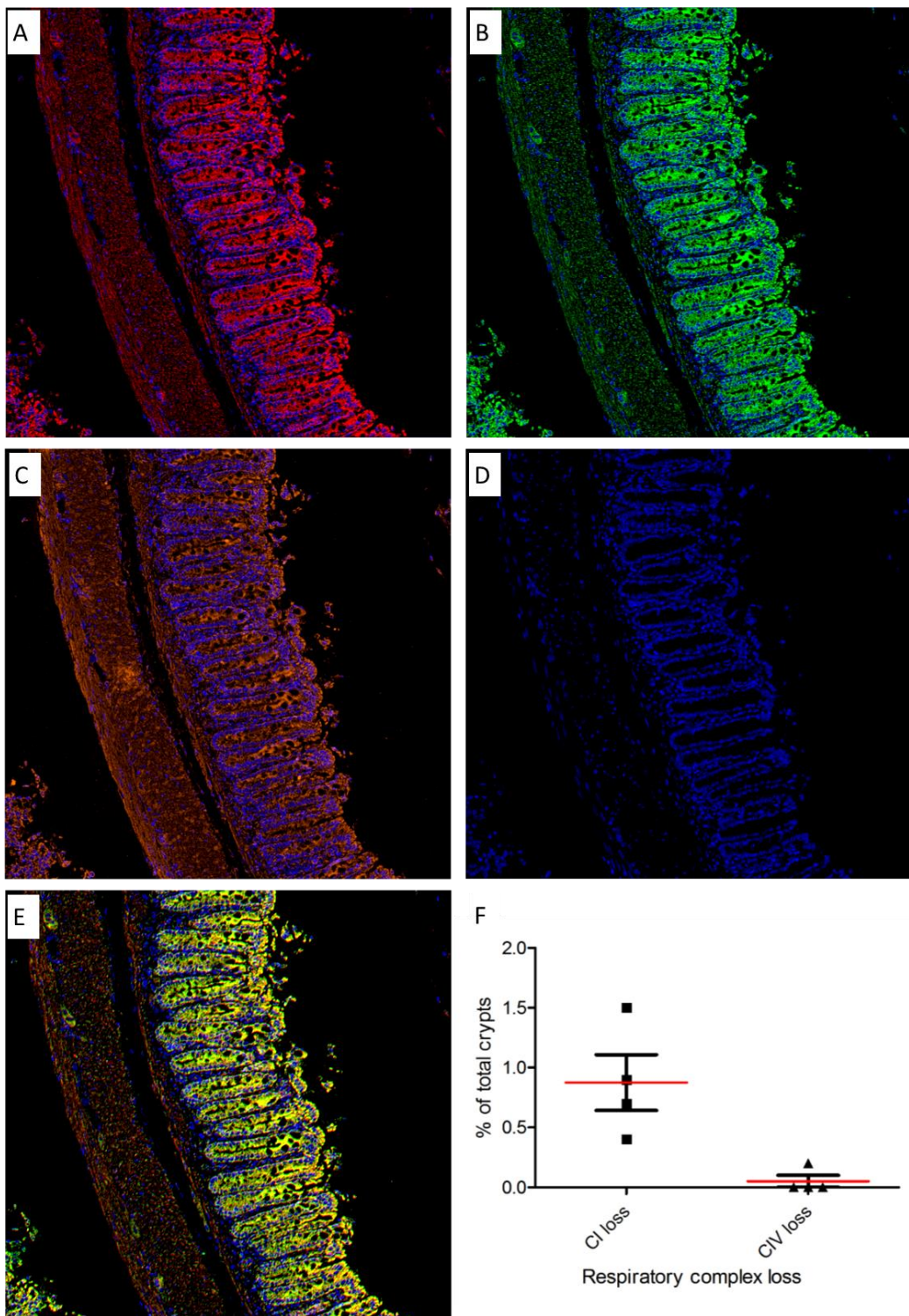


Figure 5-6 Mitochondrial dysfunction within *Lgr5*(^{+/−})*PolyA*(⁺⁺) mouse colon

Immunofluorescence for mitochondrial OXPHOS subunits NDUFB8 (Complex I) and MTCO1 (Complex IV) was performed on *Lgr5*(^{+/−})*PolyA*(⁺⁺) mice ($n=4$) according to the protocol in section 2.2.5. (A) NDUFB8 (Complex I) image (B) MTCO1 (Complex IV) image (C) VDAC1 (Porin) image (D) DAPI image (E) NDUFB8 and MTCO1 merged image (F) Comparison of Complex I and Complex IV loss within *Lgr5*(^{+/−})*PolyA*(⁺⁺) mouse colon.

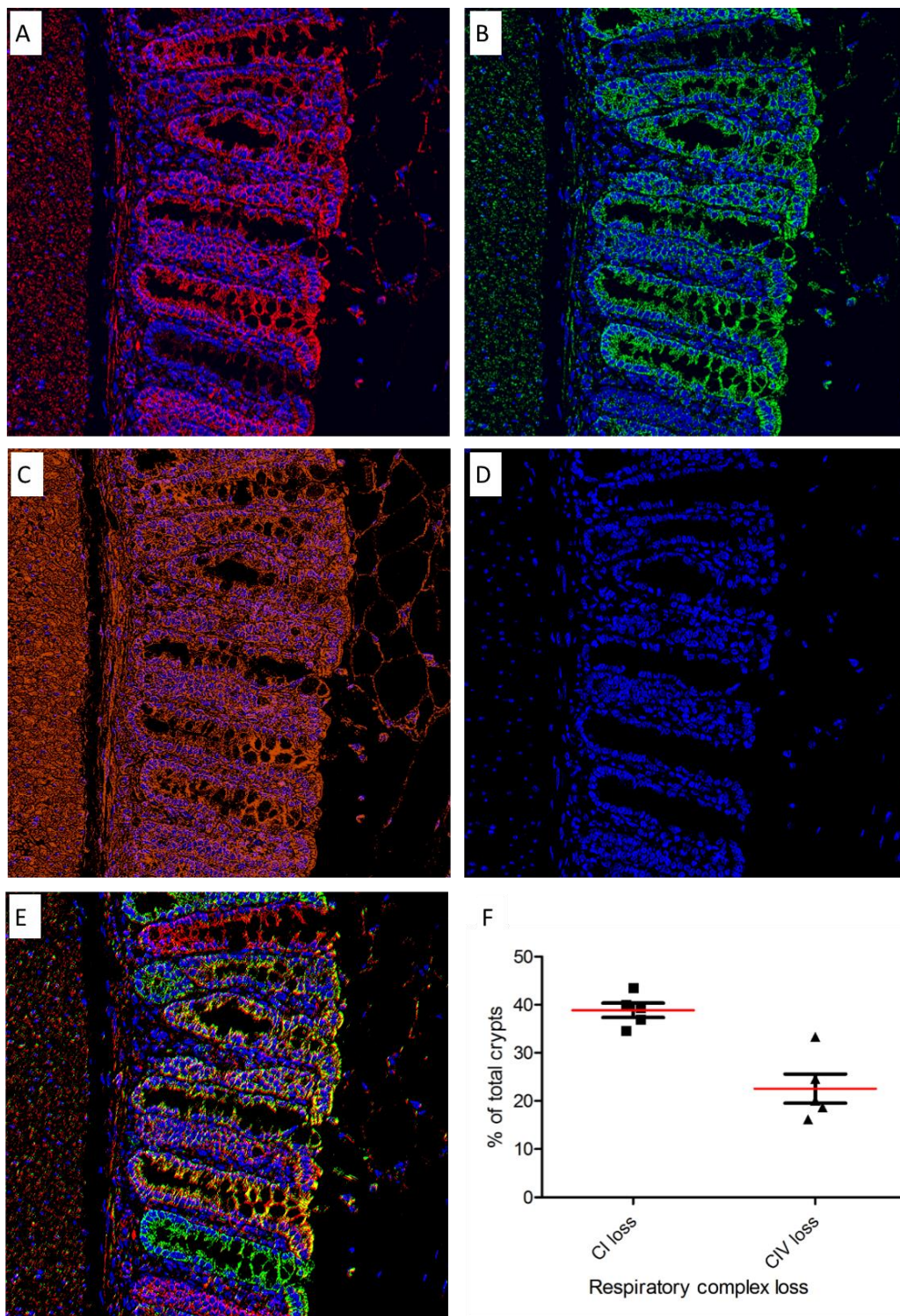


Figure 5-7 Mitochondrial dysfunction within *Lgr5*(^{+/−})*PolyA*(^{+/−}) mouse colon

Immunofluorescence for mitochondrial OXPHOS subunits NDUFB8 (Complex I) and MTCO1 (Complex IV) was performed on *Lgr5*(^{+/−})*PolyA*(^{+/−}) mice ($n=5$) according to the protocol in section 2.2.5. (A) NDUFB8 (Complex I) image (B) MTCO1 (Complex IV) image (C) VDAC1 (Porin) image (D) DAPI image (E) NDUFB8 and MTCO1 merged image (F) Comparison of Complex I and Complex IV loss within *Lgr5*(^{+/−})*PolyA*(^{+/−}) mouse colon.

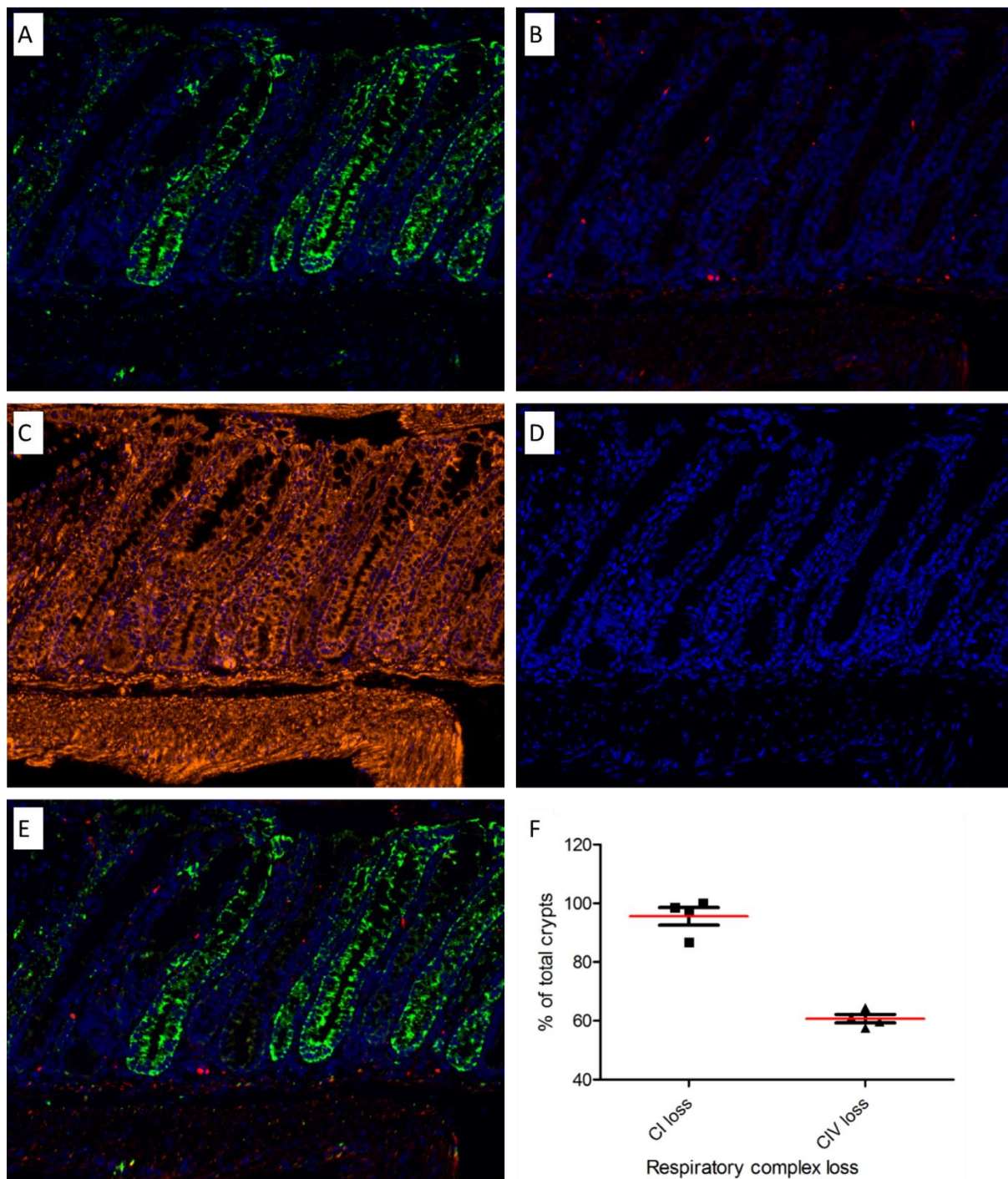


Figure 5-8 Mitochondrial dysfunction within *Lgr5*(^{+/−})*PolyA*(^{−/−}) mouse colon

Immunofluorescence for mitochondrial OXPHOS subunits NDUFB8 (Complex I) and MTCO1 (Complex IV) was performed on *Lgr5*(^{+/−})*PolyA*(^{−/−}) mice ($n=4$) according to the protocol in section 2.2.5. (A) NDUFB8 (Complex I) image (B) MTCO1 (Complex IV) image (C) VDAC1 (Porin) image (D) DAPI image (E) NDUFB8 and MTCO1 merged image (F) Comparison of Complex I and Complex IV loss within *Lgr5*(^{+/−})*PolyA*(^{−/−}) mouse colon.

5.4.4 Comparison of mitochondrial dysfunction between mouse genotypes

The expression levels of both NDUFB8 (Complex I) and MTCO1 (Complex IV) were assessed and compared within *Lgr5^(+/-)PolyA⁽⁺⁺⁾*, *Lgr5^(+/-)PolyA^(+/-)* and *Lgr5^(+/-)PolyA^(-/-)* mice. Figure 5-9 shows the comparisons for all types of crypts in relation to their mitochondrial respiratory complex status. Figure 5-9A shows the frequency of normal crypts for all mice being investigated. Around 99% of crypts are normal within *Lgr5^(+/-)PolyA⁽⁺⁺⁾* mice, ~50% are normal within *Lgr5^(+/-)PolyA^(+/-)* mice, and <1% are normal within *Lgr5^(+/-)PolyA^(-/-)*. Figure 5-9B shows the frequency of crypts with Complex IV loss for all mice being investigated. Less than 1% of crypts have Complex IV loss within *Lgr5^(+/-)PolyA⁽⁺⁺⁾* mice, ~20% of crypts have Complex IV loss within *Lgr5^(+/-)PolyA^(+/-)* mice, and ~60% of crypts have Complex IV loss within *Lgr5^(+/-)PolyA^(-/-)* mice. Figure 5-9C shows the frequency of crypts with Complex I loss for all mice being investigated. Less than 2% of crypts have Complex I loss within *Lgr5^(+/-)PolyA⁽⁺⁺⁾* mice, ~40% of crypts have Complex I loss within *Lgr5^(+/-)PolyA^(+/-)* mice, and ~95% of crypts have Complex I loss within *Lgr5^(+/-)PolyA^(-/-)* mice. Figure 5-9D shows the frequency of crypts with Complex I and Complex IV loss grouped according to mouse genotype. For all mouse genotypes investigated, Complex I loss is significantly higher than Complex IV loss. It would appear, especially for *Lgr5^(+/-)PolyA^(+/-)* and *Lgr5^(+/-)PolyA^(-/-)* mice, that the frequency of crypts with Complex IV loss is approximately two-thirds that of crypts with Complex I loss. It can also be seen that the frequency of both crypts with Complex IV loss and crypts with Complex I loss for *Lgr5^(+/-)PolyA^(-/-)* mice totals >100%, indicating the presence of crypts with multiple respiratory complex loss within the colonic epithelium of *Lgr5^(+/-)PolyA^(-/-)* mice.

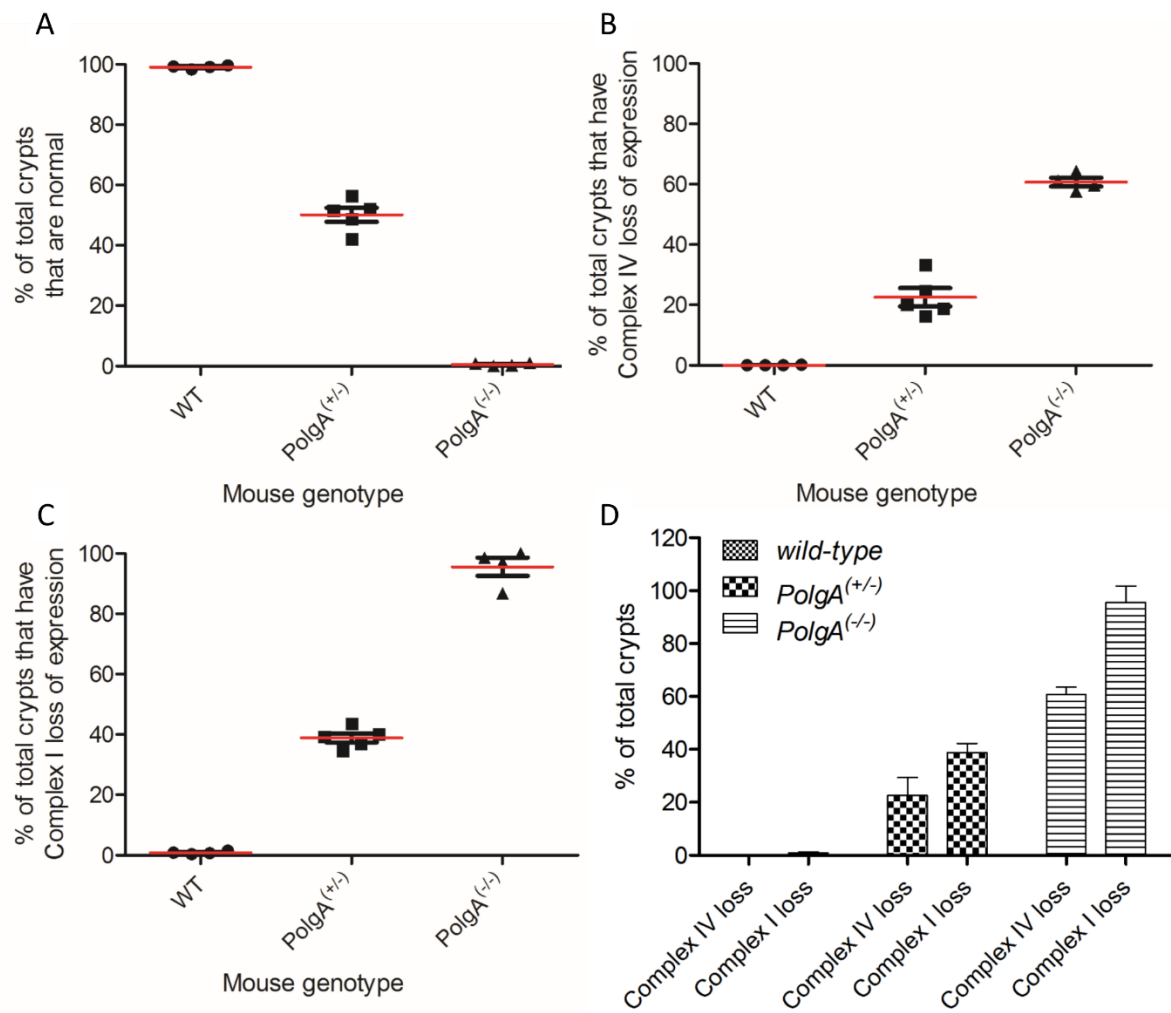


Figure 5-9 Comparison of mitochondrial dysfunction within mouse colon

Immunofluorescence for mitochondrial OXPHOS subunits NDUFB8 (Complex I) and MTCO1 (Complex IV) was performed on *Lgr5*^(+/-)*PolyA*^(+/+) (n=4), *Lgr5*^(+/-)*PolyA*^(+/-) (n=5) and *Lgr5*^(+/-)*PolyA*^(-/-) (n=4) mice according to the protocol in section 2.2.5. (A) Normal crypt comparison between *Lgr5*^(+/-)*PolyA*^(+/+), *Lgr5*^(+/-)*PolyA*^(+/-) and *Lgr5*^(+/-)*PolyA*^(-/-) mice (B) Complex IV comparison between *Lgr5*^(+/-)*PolyA*^(+/+), *Lgr5*^(+/-)*PolyA*^(+/-) and *Lgr5*^(+/-)*PolyA*^(-/-) mice (C) Complex I comparison between *Lgr5*^(+/-)*PolyA*^(+/+), *Lgr5*^(+/-)*PolyA*^(+/-) and *Lgr5*^(+/-)*PolyA*^(-/-) mice (D) Comparison of both Complex I and Complex IV between *Lgr5*^(+/-)*PolyA*^(+/+), *Lgr5*^(+/-)*PolyA*^(+/-) and *Lgr5*^(+/-)*PolyA*^(-/-) mice.

5.4.5 Multiple respiratory deficiency within mouse colon

The mitochondrial OXPHOS status of all crypts was recorded and compared between each mouse and each genotype investigated. Figure 5-10 shows graphs of this data. Within the same data set, crypts were separated according to them being normal, Complex I deficient, Complex IV deficient, or both Complex I and Complex IV deficient. Figure 5-10A shows all crypt types for all *Lgr5^(+/-)PolyA^(+/+)* mice. The overwhelming majority of crypts from all mice were normal (99.5%). Where there was respiratory complex loss of expression, this was most often loss of Complex I (0.4%). Figure 5-10B shows all crypt types for all *Lgr5^(+/-)PolyA^(+/-)* mice. There was a variety of different types of crypts from all 5 *Lgr5^(+/-)PolyA^(+/-)* mice investigated. The majority of crypts were normal within each mouse (50.1%). Complex I loss was significant (27.3%), followed by crypts with Complex IV loss (11.0%) to a lesser extent. There was also a fraction of crypts that had loss of both respiratory complexes (11.6%). Figure 5-10C shows all crypt types for all *Lgr5^(+/-)PolyA^(-/-)* mice. This time, the majority of crypts had loss of expression of both respiratory complexes (57.1%) followed by crypts with loss of Complex I expression only (38.8%). There were crypts that had Complex IV loss of expression (3.8%) and there were a few crypts that were completely normal for Complex I and Complex IV expression (0.5%). Therefore, if a crypt had loss of Complex IV, it was almost certain to have Complex I loss as well. However, if a crypt had Complex I loss, there was a higher chance that Complex IV expression remained intact.

Figure 5-10D shows a comparison of three genotypes investigated. With decreasing mitochondrial polymerase proofreading ability, there is a decreasing shift in the fraction of normal crypts that are observed within mice aged between 11-12 months. It appears that the rate of Complex I loss takes place at an increased rate compared with Complex IV loss within colon epithelium. The higher the effective mutation rate, the less time required for the majority of crypts within the colon epithelium to harbour both Complex I and Complex IV loss.

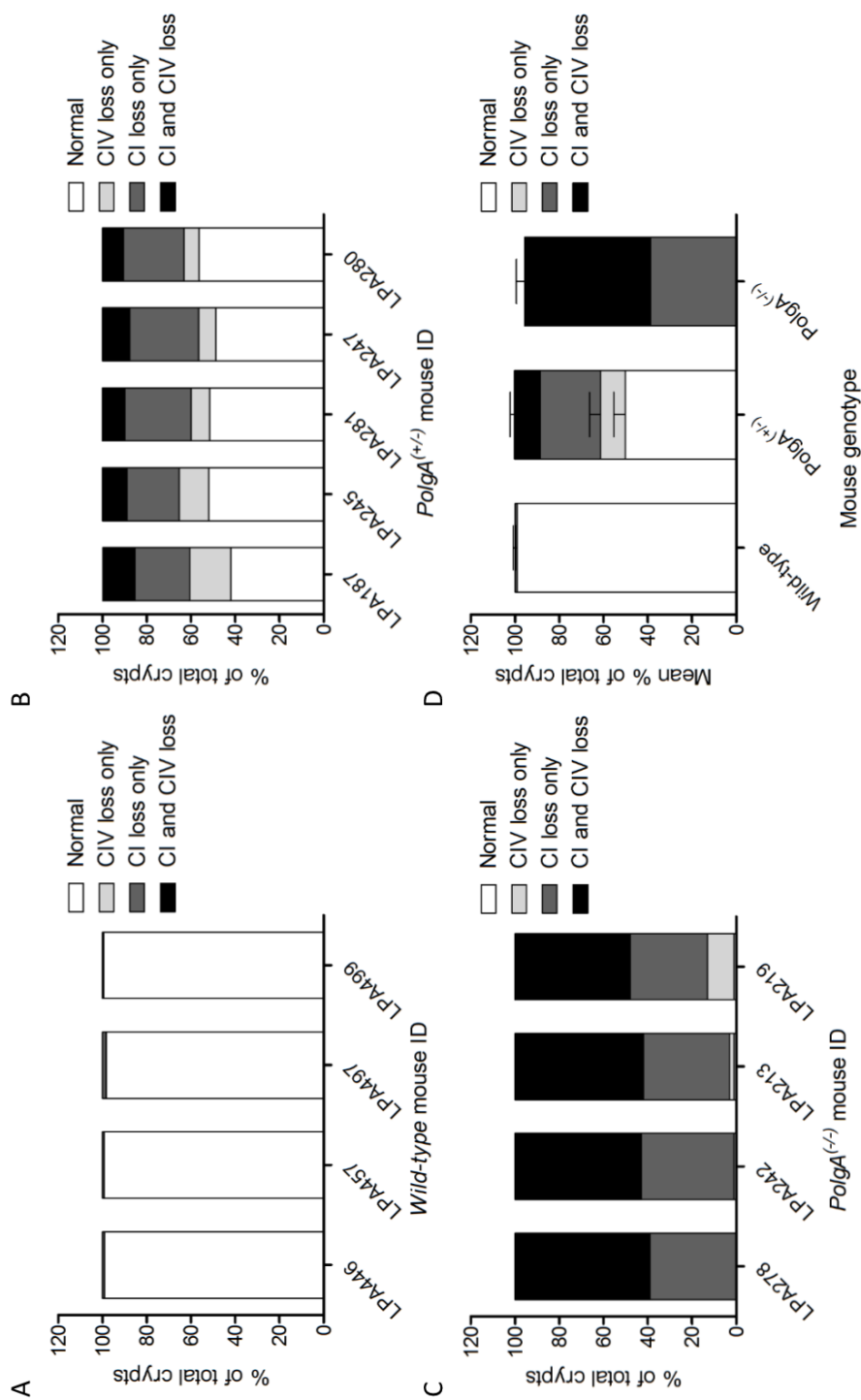


Figure 5-10 Comparison of multiple respiratory chain complex loss within mouse colon

Immuno-fluorescence for mitochondrial OXPHOS subunits NDUFB8 (Complex I) and MTCO1 (Complex IV) was performed on *Lgr5^(+/-)/PolyA^(+/-)* ($n=4$), *Lgr5^(+/-)/PolyA^(+/-)* ($n=5$) and *Lgr5^(+/-)/PolyA^(-/-)* ($n=4$) mice according to the protocol in section 2.2.5. The frequency of crypts that are normal, have Complex IV loss, have Complex I loss and those that have both Complex I and Complex IV loss from the colon of each mouse was recorded. (A) Multiple respiratory chain complex loss for *Lgr5^(+/-)/PolyA^(+/-)* mice. (B) Multiple respiratory chain complex loss for *Lgr5^(+/-)/PolyA^(+/-)* mice. (C) Multiple respiratory chain complex loss for *Lgr5^(+/-)/PolyA^(-/-)* mice. (D) Comparison of multiple respiratory chain complex loss within all mice.

5.5 DISCUSSION

It is clear that there are differences between *Lgr5^(+/-)PolyA⁽⁺⁺⁾*, *Lgr5^(+/-)PolyA^(+/-)* and *Lgr5^(+/-)PolyA^(-/-)* mice in terms of the frequency of respiratory chain complex loss within colonic epithelium. Due to the genotypes of the mice being investigated, this difference can be solely attributed to a decreasing proofreading ability of the mitochondrial polymerase γ , effectively increasing the constant rate of *de novo* point mutation acquisition during mtDNA replication (Figure 5-5). The frequency of crypts harbouring Complex I loss was significantly higher than those harbouring Complex IV loss (Figure 5-6, Figure 5-7 and Figure 5-8). This was true for all mice being investigated and not just a phenomenon attributed to the mitochondrial mutator mice. This indicates that the rate of Complex I loss is much faster than that of Complex IV loss within mouse colonic epithelium. This could be attributable to a variety of causes. Firstly, the mitochondrial genome encodes 7 subunits for Complex I compared to 3 subunits for Complex IV. The number of base pairs that contribute to the 7 genes for Complex I equals 6349 with 19047 possible base substitutions. The number of base pairs that contribute to the 3 genes for Complex IV equals 3007 with 9021 possible base substitutions. The fact that twice as many base pairs contribute towards mitochondrial genome encoded genes for Complex I results in double the chance of Complex I genes acquiring a *de novo* mutation compared to Complex IV genes. Furthermore, the fact that four more mitochondrially encoded genes encode subunits that contribute to Complex I compared to Complex IV increases the chance of there being Complex I dysfunction as *de novo* mutations not only alter the function of the respiratory complex, they also hinder the assembly of the complex as well. Complex I is a highly complex and dynamic structure as shown from 3D electron microscopy from *Y.lipolytica* (Radermacher *et al.*, 2006). ~38 subunits have been described for human Complex I, 7 of which are encoded by the mitochondrial genome (Hirst *et al.*, 2003). Complex I is made of 3 modules (N, Q and P), each performing a different role. NADH oxidation is conducted within the N module, (Walker, 1992) electron transfer and ubiquinone reduction is conducted within the Q module (Sazanov, 2007) and proton transfer across the membrane is conducted within module P, which relies on specific conformational change (Efremov *et al.*, 2010; Baradaran *et al.*, 2013). The Q module consists of all the subunits encoded by the mitochondrial genome, therefore not only will those subunits be important for assembly of Complex I as a whole, lack of mtDNA encoded subunits will result in a reduced capacity to set up the proton gradient, impacting on the cells ability to synthesise ATP.

It is surprising that such a highly proliferative tissue such as the colon is able to tolerate such high levels of Complex I and Complex IV deficiency via NDUFB8 and MTCO1 loss of expression. This could be due to a variety of factors. For instance, a heteroplasmy threshold will exist for every pathogenic mutation present where wild type mtDNA molecules are able to compensate for mutated mtDNA molecules up to a point (Sciacco *et al.*, 1994). There will also be a tissue specific threshold present whereby a certain level of OXPHOS deficiency can be tolerated before a biochemical phenotype is observed (Rossignol *et al.*, 1999). Both these factors may explain why such high levels of respiratory deficiency can be tolerated within the mouse colon.

Having more subunits encoded by the mitochondrial genome increases the chance of a *de novo* mutation disrupting the assembly of the Complex as a whole, resulting in Complex I loss. It is likely that the main contributory factor for the difference in rate of Complex I and IV loss is due to the number of genes and the individual gene sizes within the mitochondrial genome. *De novo* mutations within other regions of the mitochondrial genome, for instance tRNA and rRNA genes, will affect the translation of all mRNA gene products equally once a certain threshold for the fraction of mutated mtDNA has been reached within the cell.

This study shows the presence of crypts with Complex I or Complex IV loss within mouse colonic epithelium. Both types of crypts would be classed as respiratory deficient, resulting in a reduced capacity for mitochondria to synthesise ATP for cellular energy. However, studies that assess whether a cell is respiratory deficient by just looking for Complex IV (COX activity) are more likely missing the cells true OXPHOS status due to Complex I loss being more likely. Therefore, it is important to test for the presence of multiple respiratory complexes in order to classify a cells true mitochondrial OXPHOS status.

Within mitochondrial mutator mice, we see that there exists a significant fraction of crypts that harbour both Complex I and Complex IV loss. This observation has also been shown within ageing human colon (Greaves *et al.*, 2010). Furthermore, some mitochondrial disease patients with only mitochondrial genome encoded Complex I gene mutations show multiple respiratory chain loss (Hinttala *et al.*, 2006). This is reinforced in a recent mouse colon study showing that mutations in mitochondrial genome encoded Complex I genes can result in COX deficiency (Baines *et al.*, 2014). It is thought that respiratory chain Complexes I, III and IV can exist as a supercomplex structure known as a ‘respirasome’ (Schagger and Pfeiffer, 2000). As Complex I is thought to be an integral part of the respirasome structure (Moreno-

Lastres *et al.*, 2012; Winge, 2012), with its assembly dependent on each contributing subunit (Acin-Perez *et al.*, 2008), COX deficiency may result from an individual point mutation within a Complex I gene, hindering the assembly and function of the supercomplex structure, leading to a breakdown and loss of all respiratory complexes involved. Therefore, the fact that a crypt has Complex I loss may make it more likely for Complex IV to be lost as well with the supercomplex rationale, which may also increase the rate of Complex IV loss once Complex I has already been lost.

5.6 CONCLUSION

There are obvious differences between $Lgr5^{(+/-)}PolyA^{(+/+)}$, $Lgr5^{(+/-)}PolyA^{(+/-)}$ and $Lgr5^{(+/-)}PolyA^{(-/-)}$ mice in terms of their phenotype and mitochondrial dysfunction within their colonic epithelium. The frequency of mitochondrial dysfunction within mitochondrial mutator mouse colons allows respiratory deficient crypts and the cells within these crypts to be investigated within the *PolyA* mice crossed with *Lgr5* mice. *C57Bl/6J* mice would not cater for this due to the lack of crypts harbouring mitochondrial dysfunction. There was a similar level of Complex IV deficiency via MTCO1 loss of expression within 12 month old $Lgr5^{(+/-)}PolgA^{(+/-)}$ mouse colon (~20%) compared to COX deficiency within age human colon (~15%), indicating their potential use for making comparisons between mouse and human colonic epithelium. It is also important to assess multiple respiratory complex deficiency in order to understand a crypts true mitochondrial OXPHOS status due to crypts exhibiting deficiency within individual respiratory complexes.

Chapter 6

Cell Cycle Kinetics of Cells with Mitochondrial Dysfunction within Mouse Colon

Chapter 6 Cell cycle kinetics of cells with mitochondrial dysfunction within mouse colon

6.1 INTRODUCTION

6.1.1 Stem cell ageing

The inability of adult stem cell populations to maintain the same level of function throughout life is largely responsible for age-related frailty and disease (Sharpless and DePinho, 2007). A decline in adult stem cell function results in ageing phenotypes such as hair loss, hair greying, decreased wound repair and substantial immune system deficiency (Sharpless and DePinho, 2007). As stem cells are long-lived within the majority of tissues due to their ability to self-renew, they are susceptible to age-related damage via chronological and replicative ageing (Liu and Rando, 2011). Molecular damage such as DNA mutagenesis is one form of age-related damage that accumulates within long-lived stem cell populations, with the rate of accumulation dependent on the rate of tissue regeneration. Therefore, rapidly replicating tissues, such as the gut, are subject to greater replicative ageing via DNA damage (Liu and Rando, 2011). The accumulation of age-related damage has been hypothesised to perturb normal stem cell homeostasis (Liu and Rando, 2011). This has been hypothesised to result in a reduction of stem cell numbers (Maslov *et al.*, 2004), increased probability of tumour formation and cancer progression (Liu and Rando, 2011), and biased differentiation of stem cell progeny cells (Rossi *et al.*, 2005). Understanding the impact age-related damage has on stem cells is of paramount importance so that we can develop novel treatments that maintain stem cell homeostasis for longer, thereby postponing age-related frailty and disease, and increasing quality of life in people of advanced age.

6.1.2 Mitochondria and stem cell ageing

6.1.2.1 Impact of mitochondrial dysfunction on stem cell ageing

A variety of replicative tissues, derived from self-renewing stem cells, have been shown to accumulate mtDNA point mutations with age that result in focal respiratory chain deficiency (Taylor *et al.*, 2003; McDonald *et al.*, 2008; Fellous *et al.*, 2009). As stem cells are the only cell types that persist within rapidly dividing tissues, somatic mtDNA mutations must be acquired and clonally expand within the stem cells (Kirkwood, 2008). As focal respiratory chain deficiency has been shown to increase exponentially with age within human colon (Taylor *et al.*, 2003), mtDNA point mutations may have a contributory role in stem cell

ageing. As has been previously described, colon epithelium is an ideal tissue to study stem cell populations (section 4.1). One such functional study investigated the proliferative capacity of stem cell progeny cells within aged human colonic epithelium between normal and respiratory deficient crypts (Nooteboom *et al.*, 2010). Even though the stem cells were not explicitly investigated within this study, stem cell progeny cells showed an ~20% reduction in the frequency of actively dividing cells between normal crypts and crypts with a cytochrome *c* oxidase subunit I (MTCO1) loss, which is indicative of Complex IV deficiency. Therefore, it would appear that the accumulation of mtDNA mutation within the stem cell pool of crypts is altering the proliferative capacity of the stem cell progeny cells. Though, further investigation is required in order to determine whether these effects translate as perturbed stem cell function as well.

6.1.2.2 *MtDNA mutations and colorectal cancer*

Colorectal cancer is one of the most common types of cancer in the western world, with age being the main risk factor associated with its incidence (Ferlay *et al.*, 2010). The majority of cancer cells are associated with decreased OXPHOS with a corresponding increase in glycolysis, known as the Warburg effect (Warburg, 1956). Therefore, mitochondrial OXPHOS dysfunction has long been hypothesised to be a driving factor behind tumour formation and cancer progression. The role for mitochondrial dysfunction in cancer development is well supported by a variety of evidence. Firstly, mitochondria are heavily involved in apoptosis, a process cancer cells are able to escape (Cavalli and Liang, 1998). Furthermore, cancer cells often display focal respiratory chain deficiency (Carew and Huang, 2002), altered mitochondrial membrane potential (Chen, 1988), and increased ROS generation and oxidative damage (Toyokuni *et al.*, 1995).

Many cancers have been shown to harbour mtDNA point mutations, for instance colorectal, gastric, liver, lung and breast malignancies (Ivanova *et al.*, 1998; Jeronimo *et al.*, 2001; Nomoto *et al.*, 2002; Tan *et al.*, 2002; Lee *et al.*, 2005). Colorectal cancers have been shown to contain homoplasmic and heteroplasmic mtDNA point mutations in a variety of locations within the mitochondrial genome (Polyak *et al.*, 1998; Coller *et al.*, 2001; Lee *et al.*, 2005; Lievre *et al.*, 2005; Nishikawa *et al.*, 2005; Sui *et al.*, 2006). It has been suggested that mtDNA mutations selectively predispose cells to undergo carcinogenesis due to the changes in oxidative environment, ROS signalling and apoptosis (Park *et al.*, 2009). With this, it has

been suggested that mtDNA point mutations could serve as a prognostic tool to determine the rate of colorectal cancer progression and patient survival (Lievre *et al.*, 2005).

However, the presence of mtDNA point mutations within cancer cells does not prove that they are the contributory factor to malignant transformation. However, it is plausible that the accumulation of mtDNA mutations within stem cells with age causes biochemical changes that makes them more susceptible to malignant transformation and early tumorigenesis (Liu and Rando, 2011). Understanding the functional effects of mtDNA point mutations on ageing stem cells needs to be resolved in order to understand normal tissue ageing and age-related diseases, such as cancer.

6.1.3 Mouse models

All cells within the colon epithelium are clonally derived from the stem cells located at the base of crypts. A mouse model known as *Lgr5-EGFP-Ires-CreERT2* was engineered by Barker *et al* that enabled Lgr5+ stem cells to express high levels of EGFP, hence allowing their detection (Barker *et al.*, 2007). A Cre-recombinase system was also incorporated, allowing Lgr5+ cell specific excision of any gene flanked by *loxP* sites upon tamoxifen induction. Lgr5+ stem cells have been shown to be the long-lived functional stem cells with the capacity of regenerating all the cells of the crypt throughout life (Barker *et al.*, 2007). Single Lgr5+ stem cells from mouse small intestinal epithelium have been shown to build crypt villus organoids in culture (Sato *et al.*, 2009), reinforcing the ability of these cells to regenerate entire crypts. Lgr5+ stem cell dynamics have also been intensely investigated within mouse colon in order to understand the stem cell niche succession phenomenon, providing insight into stem cell replacement under normal tissue homeostasis (Snippert *et al.*, 2010). They have also been shown to be the primary cells that drive tumour growth within APC knock-out mice, caused by constitutive Wnt-pathway activation (Barker *et al.*, 2009). The evidence discussed suggests that cells with high levels of Lgr5 receptor expression are the true stem cells within intestinal and colonic epithelium and all studies investigating these stem cells should do so by identifying Lgr5 expression.

As has been detailed in section 5.4.2, *PolyA* mitochondrial mutator mice have an increased rate of somatic mtDNA point mutation accumulation, resulting in an increased frequency of respiratory chain deficient cells with age. The crossing of mitochondrial mutator mice with Lgr5+ mice would allow the functional consequences of respiratory chain deficiency to be investigated within Lgr5+ stem cells within mouse colonic epithelium.

6.2 AIMS OF STUDY

To determine whether mitochondrial OXPHOS dysfunction alters the cell cycle kinetics of stem cells and stem cell progeny within mouse colonic epithelium. In order for this question to be answered, a method of determining mitochondrial OXPHOS function was required in conjunction with a method of characterising cell cycle kinetics of each cell within individual crypts. As shown in chapter 5, a method of determining the presence of mitochondrial OXPHOS complexes was available. An *in vivo* technique known as double thymidine analogue labelling was adapted for use within mouse colon in order to characterise the cell cycle kinetics of Lgr5+ stem cells and stem cell progeny within mouse colon. Cell type and cell cycle kinetic markers included:

1. Ki67 marker of cells proliferating at time of animals death
2. CldU marker of cells divided within 1 week of animals death
3. IdU marker of cells divided within ~15 hours of animals death
4. EGFP marker of Lgr5+ stem cells

Using an immunofluorescence technique to identify combinations of the markers specified, comparisons of the cell cycle kinetics of stem cells and stem cell progeny can be made between *Lgr5^(+/-)PolyA^(+/+)*, *Lgr5^(+/-)PolyA^(+/-)* and *Lgr5^(+/-)PolyA^(-/-)* mice and also crypts with and without mitochondrial dysfunction.

6.3 METHODOLOGY

6.3.1 Double thymidine analogue labelling

Lgr5-EGFP-Ires-CreERT2 (*Lgr5*+) mice were bred with heterozygote mitochondrial mutator *PolyA*^(+/-) mice within the comparative biology centre (Newcastle University) (section 2.2.2.2). *Lgr5*^(+/-)*PolyA*^(+/-) (n=4), *Lgr5*^(+/-)*PolyA*^(+/-) (n=5) and *Lgr5*^(+/-)*PolyA*^(-/-) (n=4) were aged to 11-12 months and then underwent a thymidine analogue intra-peritoneal injection schedule in order to label dividing cells (section 2.2.3). Once complete, mice were killed and mouse colons were removed for tissue processing (section 2.2.4).

6.3.2 Detection of mitochondrial dysfunction and cell cycle kinetic markers

Immunofluorescence was carried out to determine the expression levels of cytochrome *c* oxidase subunit 1 (MTCO1) of Complex IV and the NDUFB8 subunit of Complex I within mouse colon (section 2.2.5). Immunofluorescence was also carried out to detect proliferating cells (Ki67), thymidine analogue markers (CluD and IdU) and stem cell marker (EGFP-Lgr5). As all markers could not be applied to a single tissue section, to see all characteristics of individual crypts, serial sectioning was performed and matching crypts were located as described in Figure 6-1. Fluorescence microscopy and image analysis was carried out as previously described (section 2.2.7).

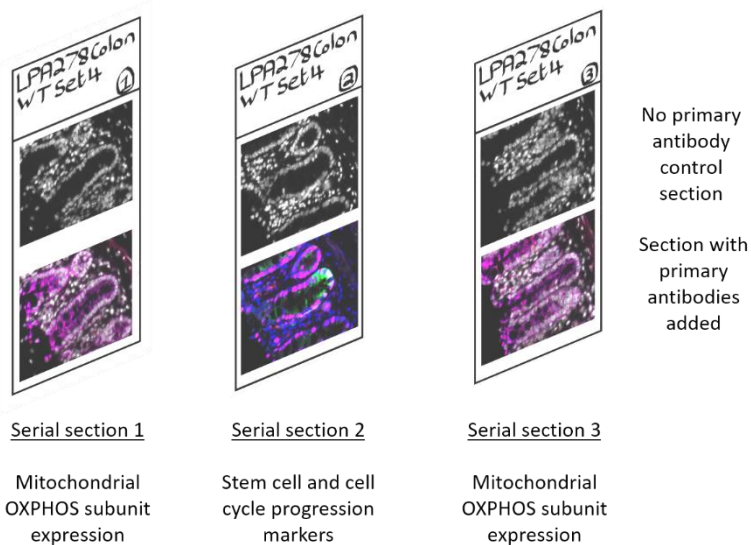


Figure 6-1 Mitochondrial dysfunction and cell cycle kinetic labelling method

Three mouse colon serial sections were cut using the microtome for the sections that would have primary antibody applied. Sections 1 and 3 underwent immunofluorescence for mitochondrial OXPHOS subunit expression. Section 2 underwent immunofluorescence for cell cycle kinetic and Lgr5 stem cell markers.

6.4 RESULTS

6.4.1 Determining cell cycle kinetics within mouse colon

Immunofluorescence and fluorescence microscopy were employed to detect the mitochondrial OXPHOS status and the cell cycle kinetics of individual crypts within mouse colon. As determined within chapter 5, it was important to include both Complex I (NDUFB8 subunit) and Complex IV (MTCO1 subunit) expression markers to ascertain the cells true mitochondrial OXPHOS status. An EGFP marker was used to detect Lgr5+ stem cells, a Ki67 cell marker was used to detect cells that were actively proliferating. CldU and IdU were used to detect cells that had entered the S phase of the cell cycle within a specific time frame. CldU was injected twice daily for 3 days and once on the fourth day. Therefore, all the cells that underwent DNA synthesis whilst CldU was in the animal's system would have incorporated the CldU thymidine analogue. IdU was injected once on the fourth day, only being present within the animal's system for approximately 15 hours before its death. Therefore, all the cells that underwent DNA synthesis during this time would have incorporated the IdU thymidine analogue. This provides information about the total number of cells proliferating at the time of the animal's death (Ki67), the total number of cells that have divided from the first CldU injection, the total number of cells that have divided from the first IdU injection, and the total number of cells that have re-entered the cell cycle in quick succession by detecting the cells that have incorporated both CldU and IdU. Figures 6-2,3,4 depict typical fluorescence images obtained from *Lgr5^(+/-)PolyA⁽⁺⁺⁾* (Figure 6-2), *Lgr5^(+/-)PolyA^(+/-)* (Figure 6-3) and *Lgr5^(+/-)PolyA^(-/-)* (Figure 6-4) mouse colon for both mitochondrial OXPHOS status and cell cycle kinetics. As can be seen, three serial sections were cut, with the first and third identifying the mitochondrial OXPHOS status of a particular crypt, and the sandwiched section identifying the cell cycle kinetics of that same crypt. This was to make sure that the mitochondrial OXPHOS status was the same from one section to the next. If that was the case, this would imply that section two had the same mitochondrial OXPHOS status. If this was not the case, those crypts were discarded. This was only the case for a small minority of crypts observed.

Only those crypts that contained EGFP+ cells were of interest as this was the means of detecting Lgr5+ cells. Figure 6-2 is from *Lgr5^(+/-)PolyA⁽⁺⁺⁾* mouse colon and shows two crypts with EGFP+ cells. Both of these crypts have normal expression levels of NDUFB8 (Complex I) and MTCO1 (Complex IV). Figure 6-3 is from *Lgr5^(+/-)PolyA^(+/-)* mouse colon

and shows one crypt with EGFP+ cells. This crypt is normal for NDUFB8 (Complex I) and MTCO1 (Complex IV). However, the crypt to the right which is EGFP- has NDUFB8 (Complex I) loss of expression. Figure 6-4 is from *Lgr5^(+/-)PolgA^(-/-)* mouse colon and shows one crypt with EGFP+ cells. This crypt is normal for MTCO1 (Complex IV) but has NDUFB8 (Complex I) loss of expression. The crypt to the farthest right is EGFP- and has both NDUFB8 (Complex I) and MTCO1 (Complex IV) loss of expression.

The majority of crypts identified from *Lgr5^(+/-)PolyA^(+/+)* mice were normal for mitochondrial OXPHOS subunit expression. There was a mosaic pattern of mitochondrial OXPHOS subunit expression for *Lgr5^(+/-)PolgA^(+/-)* mice. The majority of crypts identified from *Lgr5^(+/-)PolgA^(-/-)* had some form of mitochondrial OXPHOS subunit loss of expression. This is the same as was seen in chapter 5. As crypts were identified based on having EGFP+ cells, the mitochondrial OXPHOS status of the crypt was not explicitly selected at the time of image capture. The fractions of EGFP+ stem cells and crypts with their associated mitochondrial OXPHOS status are exemplified in Figure 6-5 and have been tabulated within Table 6.1. This affected how many crypts and Lgr5+ stem cells were included in the analysis when segregating crypts based on mitochondrial OXPHOS status group.

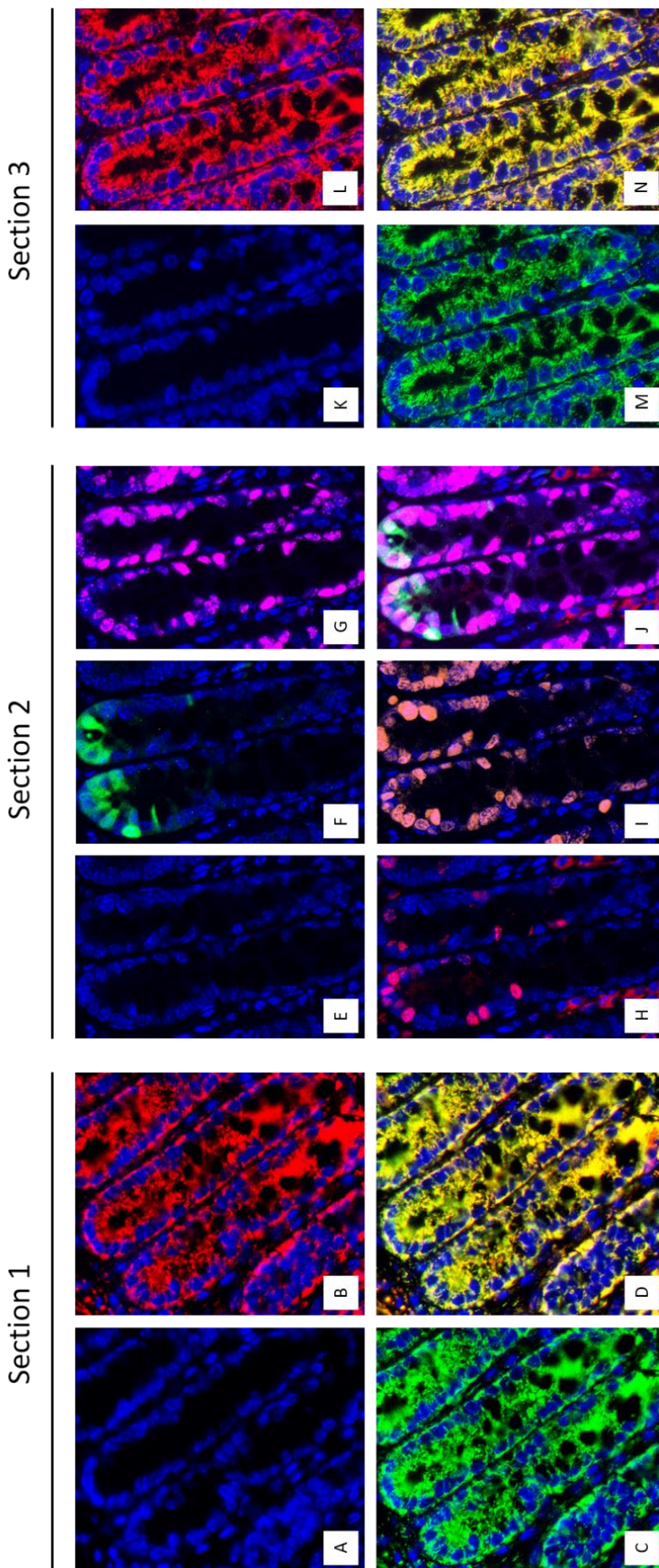


Figure 6-2 Cell cycle kinetics and mitochondrial dysfunction within *Lgr5*(^{+/−})*PolyA*(^{+/+}) mice

Immunofluorescence was carried out on 3 mouse colon serial sections from *Lgr5*(^{+/−})*PolyA*(^{+/+}) mice. Immunofluorescence for mitochondrial OXPHOS complexes I (NDUFB8) and IV (MTCO1) was carried out on sections 1 and 3. Immunofluorescence for cell cycle kinetic markers and *Lgr5*⁺ stem cells was carried out on section 2. (A E and K) DAPI nuclear counterstain. (B and L) NDUFB8 (Complex I) expression. (C and M) MTCO1 (Complex IV) expression. (D and N) NDUFB8 and MTCO1 merged image. (F) EGFP (*Lgr5*⁺ stem cell) marker. (G) CiDU marker. (H) Ki67 marker. (I) Ki67 proliferating cell marker. (J) EGFP, CiDU, IdU and Ki67 marker merged image.

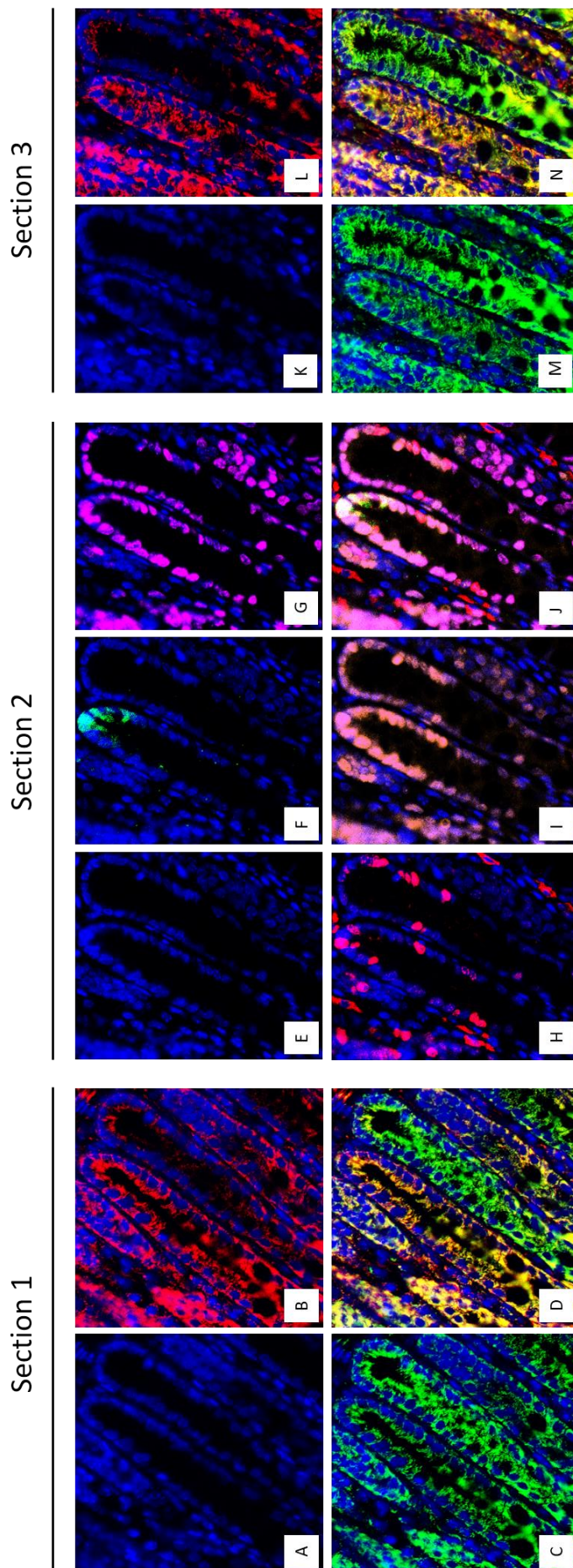


Figure 6-3 Cell cycle kinetics and mitochondrial dysfunction within *Lgr5*(^{+/+})*PolyA*(^{+/+}) mice

Immunofluorescence was carried out on 3 mouse colon serial sections from *Lgr5*(^{+/+})*PolyA*(^{+/+}) mice. Immuno fluorescence for mitochondrial OXPHOS complexes I (NDUFB8) and IV (MTCO1) was carried out on sections 1 and 3. Immuno fluorescence for cell cycle kinetic markers and *Lgr5*⁺ stem cells was carried out on section 2. (A-E and K) DAPI nuclear counterstain. (B and L) NDUFB8 (Complex I) expression. (C and M) MTCO1 (Complex IV) expression. (D and N) NDUFB8 and MTCO1 merged image. (F) EGFP (*Lgr5*⁺ stem cell) marker. (G) CldU marker. (H) Ki67 proliferating cell marker. (I) Ki67 marker. (J) EGFP, CldU, IdU and Ki67 marker merged image.

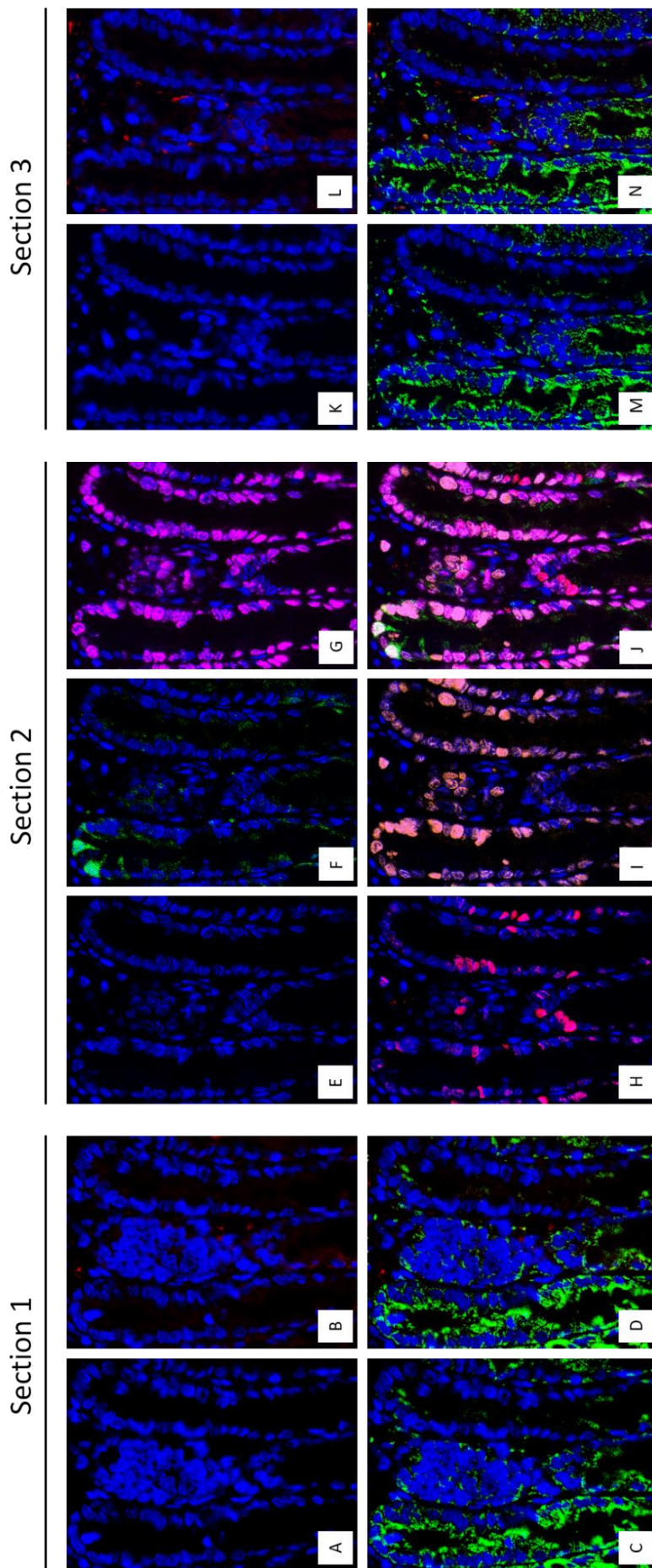


Figure 6-4 Cell cycle kinetics and mitochondrial dysfunction within *Lgr5*(^{+/−})*PolyA*(^{−/−}) mice

Immunofluorescence was carried out on 3 mouse colon serial sections from *Lgr5*(^{+/−})*PolyA*(^{−/−}) mice. Immunofluorescence for mitochondrial OXPHOS complexes I (NDUFB8) and IV (MTCO1) was carried out on sections 1 and 3. Immunofluorescence for cell cycle kinetic markers and Lgr5+ stem cells was carried out on section 2. (A E and K) DAPI nuclear counterstain. (B and L) NDUFB8 (Complex I) expression. (C and M) MTCO1 (Complex IV) expression. (D and N) NDUFB8 and MTCO1 merged image. (F) EGFP (Lgr5+ stem cell) marker. (G) CldU marker. (H) Ki67 marker. (I) IdU marker. (J) EGFP, CldU, IdU and Ki67 marker merged image.

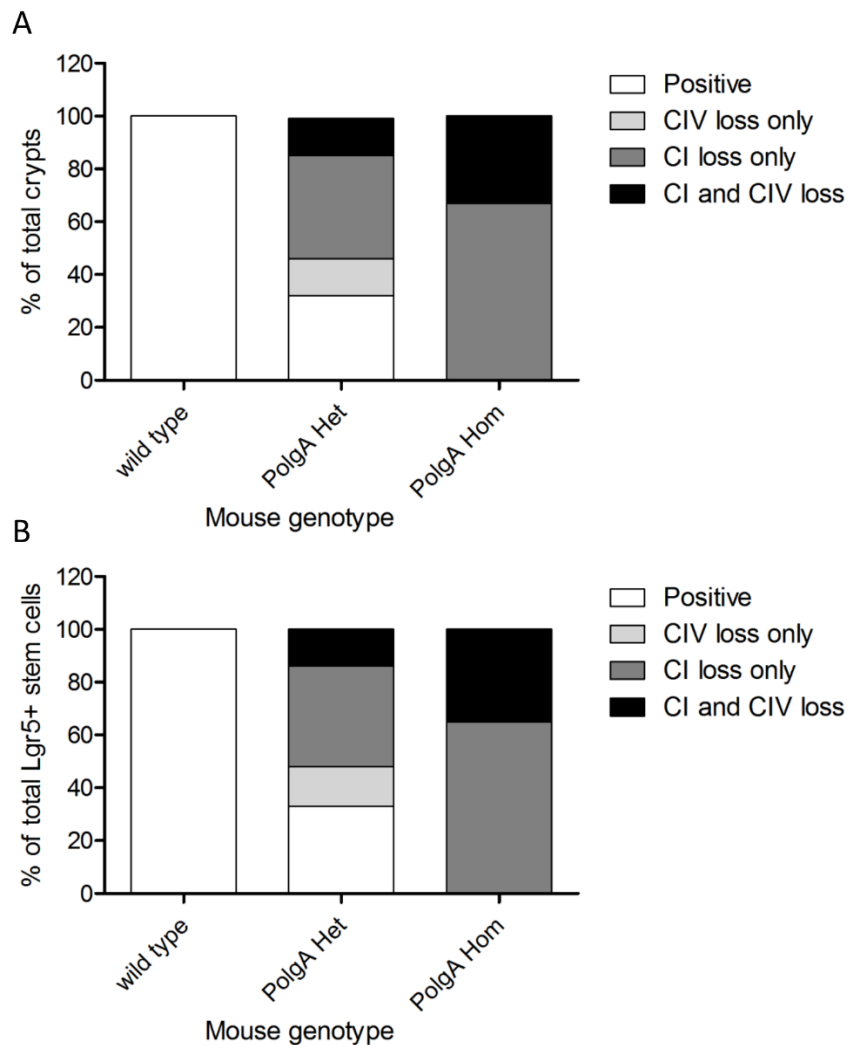


Figure 6-5 Mitochondrial OXPHOS status sampling fractions

Only EGFP+ crypts were chosen for fluorescence imaging in order to assess the cell cycle kinetics of Lgr5+ stem cells. This meant the mitochondrial OXPHOS status was not identified explicitly at the time of image capture. (A) Represents the fraction of crypts that were normal, or had CIV loss only, CI loss only, or CI and CIV loss from *Lgr5^(+/-)PolyA^(+/-)* mice (n=267), *Lgr5^(+/-)PolyA^(+/-)* mice (n=324) and *Lgr5^(+/-)PolyA^(-/-)* mice (n=137). (B) Represents the fractions of Lgr5+ stem cells that were normal, or had CIV loss only, CI loss only, or CI and CIV loss from *Lgr5^(+/-)PolyA^(+/-)* mice (n=1355), *Lgr5^(+/-)PolyA^(+/-)* mice (n=1618) and *Lgr5^(+/-)PolyA^(-/-)* mice (n=757).

Table 6-1 Number of stem cells and crypts quantified per mouse

Stem cell numbers						Crypt numbers				
Wild type	Number of stem cells	Normal	Complex I loss	Complex IV loss	Complex I and IV loss	Number of crypts	Normal	Complex I loss	Complex IV loss	Complex I and IV loss
LPA446	348	348	0	0	0	63	63	0	0	0
LPA457	407	407	0	0	0	82	82	0	0	0
LPA497	313	313	0	0	0	61	61	0	0	0
LPA499	287	287	0	0	0	61	61	0	0	0

Stem cell numbers						Crypt numbers				
PolgA Het	Number of stem cells	Normal	Complex I loss	Complex IV loss	Complex I and IV loss	Number of crypts	Normal	Complex I loss	Complex IV loss	Complex I and IV loss
LPA187	393	111	155	78	49	71	21	28	13	9
LPA245	180	38	37	54	51	47	9	8	17	13
LPA247	348	153	153	9	33	70	31	31	2	6
LPA280	358	130	165	26	37	66	24	30	5	7
LPA281	339	110	160	37	32	70	24	32	7	7

Stem cell numbers						Crypt numbers				
PolgA Hom	Number of stem cells	Normal	Complex I loss	Complex IV loss	Complex I and IV loss	Number of crypts	Normal	Complex I loss	Complex IV loss	Complex I and IV loss
LPA281	293	0	207	0	86	49	0	34	0	15
LPA242	206	0	130	0	76	42	0	26	0	16
LPA278	125	0	74	0	59	21	0	13	0	9
LPA219	133	0	98	0	35	25	0	17	0	8

6.4.2 Number of cells within crypts

The number of cells observed within longitudinal cross sections of crypts was quantified. The data was segregated based on mitochondrial OXPHOS status and mouse genotype. This is shown within Figure 6-6. It can be seen that for *Lgr5^(+/-)PolyA^(+/+)* (*wild type*) mice there is not a statistically significant difference between the number of cells that contribute to these crypts, with on average ~48 cells observed within each longitudinal crypt (Figure 6-6A). The same is true for *Lgr5^(+/-)PolyA^(+/-)* mice which have on average ~47 cells contributing towards each longitudinal crypt (Figure 6-6B). However, *Lgr5^(+/-)PolyA^(-/-)* mice have substantially larger crypts, with on average ~63 cells contributing towards each longitudinal crypt, with no statistically significant difference between each mouse (Figure 6-6C).

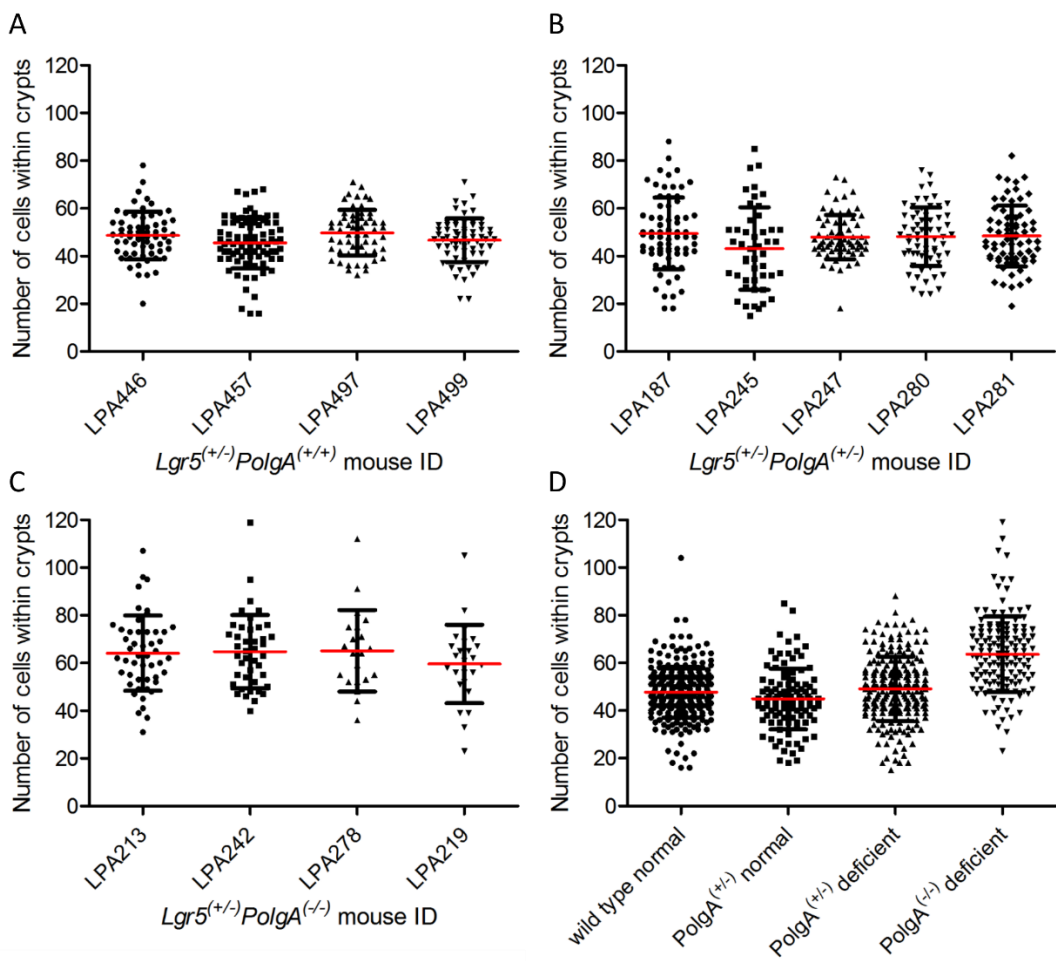


Figure 6-6 Number of cells in crypts

The number of cells within normal and respiratory deficient crypts was quantified. This was carried out on all crypts from *Lgr5*^(+/-)*PolyA*^(+/+) ($n=4$), *Lgr5*^(+/-)*PolyA*^(+/-) ($n=5$) and *Lgr5*^(+/-)*PolyA*^(-/-) ($n=4$) mouse colon that contained EGFP positive cells (i.e. Lgr5+ stem cells). (A) Number of cells within crypts, segregated for each *Lgr5*^(+/-)*PolyA*^(+/+) mouse. There was not a statistically significant difference between groups as determined by one-way ANOVA ($F(3,269) = 2.586, p = 0.054$) (B) Number of cells within crypts, segregated for each *Lgr5*^(+/-)*PolyA*^(+/-) mouse. There was not a statistically significant difference between groups as determined by one-way ANOVA ($F(4,323) = 1.759, p = 0.137$) (C) Number of cells within crypts, segregated for each *Lgr5*^(+/-)*PolyA*^(-/-) mouse. There was not a statistically significant difference between groups as determined by one-way ANOVA ($F(3,136) = 0.661, p = 0.578$) (D) Number of cells within crypts, segregated for each mouse genotype and for mitochondrial OXPHOS status of those crypts. There was a statistically significant difference between groups as determined by one-way ANOVA ($F(3,728) = 58.65, p < 0.0001$). A Dunnett's multiple comparison post-hoc test was conducted to determine which groups were significantly different compared to the *wild type* normal group. Only the *PolyA*^(-/-)deficient group showed a significant increase ($15.83 \pm 3.19, p < 0.001$).

6.4.3 Frequency of proliferating cells within mouse colon

Proliferating cells were detected using an antibody against the Ki67 protein. Ki67 is highly expressed within a cell's nucleus at all cell cycle stages, excluding G₀ (quiescence phase). This allows the proliferating cell frequency to be quantified within individual crypts. As EGFP+ cells defined Lgr5+ stem cells, those that contained EGFP were deemed stem cells and those that did not were deemed stem cell progeny. The fraction of proliferating stem cells and stem cell progeny were compared between *Lgr5*^(+/-)*PolyA*⁽⁺⁺⁾, *Lgr5*^(+/-)*PolyA*⁽⁺⁻⁾ and *Lgr5*^(+/-)*PolyA*⁽⁻⁻⁾ mice. There was not a statistically significant difference in the means between mouse groups for both stem cells (Figure 6-7A) and stem cell progeny cells (Figure 6-7B) as determined by one-way ANOVA. The mean percentage of proliferating stem cells was ~95% and the mean percentage of proliferating stem cell progeny cells was ~75% for all mouse groups. The fraction of proliferating stem cells and stem cell progeny cells was next compared between normal and respiratory deficient crypts. There was not a statistically significant difference in the means between normal and respiratory deficient crypts for both stem cells (Figure 6-7C) and stem cell progeny cells (Figure 6-7D) as determined by an unpaired t-test. This indicates that respiratory deficiency does not have an effect on the proliferative activity (i.e. the number of actively dividing cells) of stem cells and stem cell progeny cells within mouse colon.

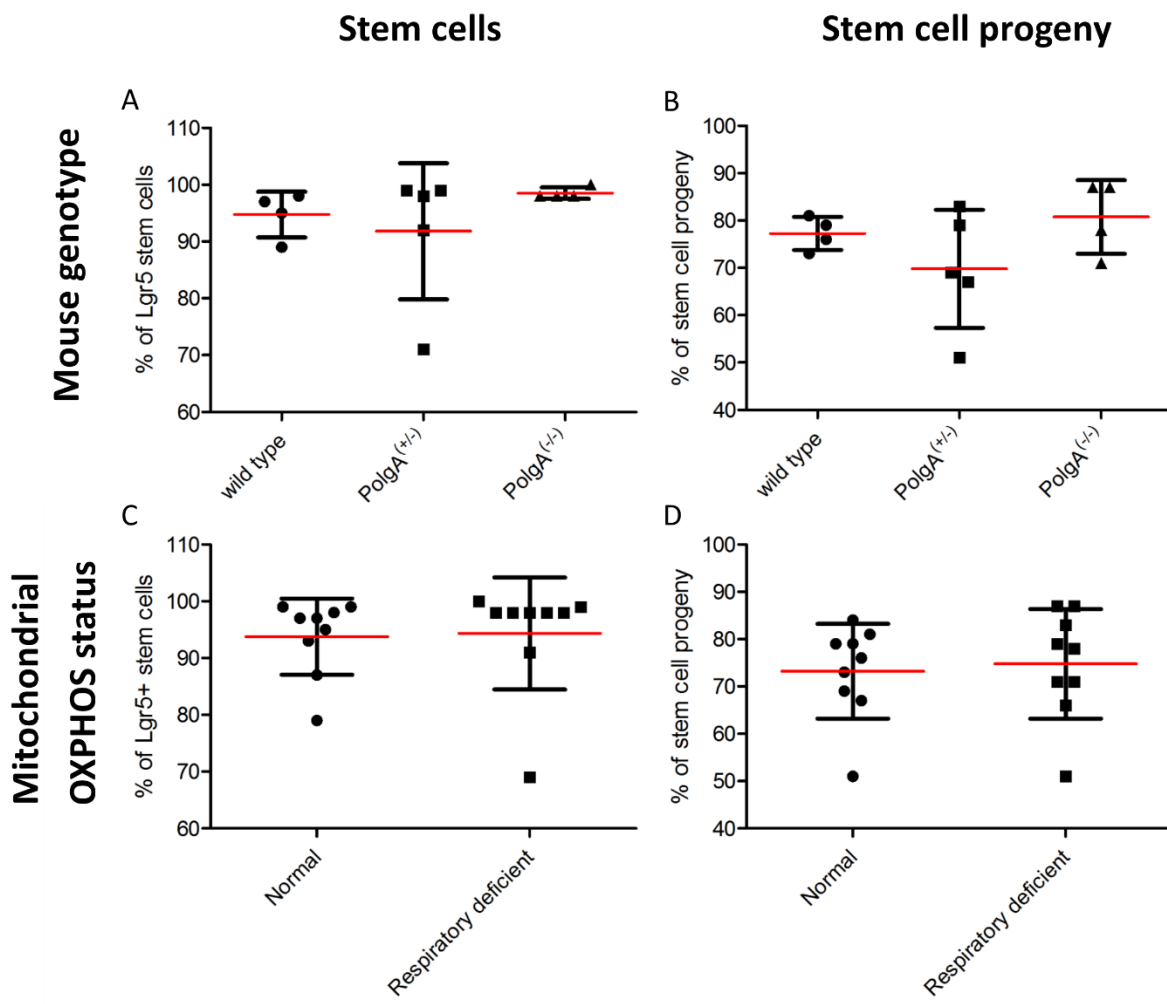


Figure 6-7 Ki67 proliferating cell marker

The frequency of actively proliferating cells at the time of the animal's death was quantified via the detection of Ki67. This was carried out on all crypts from *Lgr5*^(+/-)*PolyA*^(+/-) ($n=4$), *Lgr5*^(+/-)*PolyA*^(+/-) ($n=5$) and *Lgr5*^(+/-)*PolyA*^(-/-) ($n=4$) mouse colon that contained EGFP positive cells (i.e. Lgr5+ stem cells). (A) Percentage of Lgr5+ stem cells that are actively proliferating, segregated for mouse genotype. There was not a statistically significant difference between groups as determined by one-way ANOVA ($F(2,10) = 0.796, p = 0.48$). (B) Percentage of stem cell progeny cells that are actively proliferating, segregated for mouse genotype. There was not a statistically significant difference between groups as determined by one-way ANOVA ($F(2,10) = 1.699, p = 0.23$). (C) Percentage of Lgr5+ stem cells that are actively proliferating, segregated based on their mitochondrial OXPHOS status. There was not a statistically significant difference in the mean percentages for normal ($M=93.8, SD=6.71$) and respiratory deficient ($M=94.3, SD=9.84$) crypts as determined by an unpaired t-test; $t(16) = 0.14, p = 0.89$. (D) Percentage of stem cell progeny cells that are actively proliferating, segregated based on their mitochondrial OXPHOS status. There was not a statistically significant difference in the mean percentages for normal ($M=73.2, SD=10.01$) and respiratory deficient ($M=74.8, SD=11.54$) crypts as determined by an unpaired t-test; $t(16) = 0.31, p = 0.76$.

6.4.4 Frequency of cells that incorporated a thymidine analogue

Cells that had undergone DNA synthesis as part of their transition through the cell cycle whilst the thymidine analogues CldU and IdU were present within the animal's system would have incorporated them into their newly synthesised DNA. As antibodies are available that can specifically bind to one or the other thymidine analogue, the frequency of cells that have traversed the cell cycle could be quantified. The fraction of cells that incorporated either thymidine analogue was quantified (Figure 6-8). The fraction of stem cells and stem cell progeny that had incorporated either of the two thymidine analogues were compared between *Lgr5^(+/-)PolyA⁽⁺⁺⁾*(n=4), *Lgr5^(+/-)PolyA⁽⁺⁻⁾*(n=5) and *Lgr5^(+/-)PolyA⁽⁻⁻⁾*(n=4) mice (Figure 6-8A/B). There was no statistically significant difference in the means between mouse groups for stem cells as determined by one-way ANOVA ($F(2,10) = 0.936, p = 0.42$) (Figure 6-8A). The mean percentage of stem cells that had incorporated a thymidine analogue was 87%. However, there was a statistically significant difference in the means between mouse groups for stem cell progeny as determined by one-way ANOVA ($F(2,10) = 8.614, p = 0.007$) (Figure 6-8B). A Dunnet's multiple comparison test was conducted which showed that there was a statistically significant increase in stem cell progeny cells incorporating either thymidine analogue between *Lgr5^(+/-)PolyA⁽⁺⁺⁾*(73.5%) and *Lgr5^(+/-)PolyA⁽⁻⁻⁾*mice (84%) of ~10% of total cells ($10.5 \pm 2.54\%, p = 0.004$).

The fraction of stem cells and stem cell progeny incorporating a thymidine analogue was next compared between normal and respiratory deficient crypts. There was a statistically significant increase in the means between normal (85%) and respiratory deficient stem cells (90%) incorporating a thymidine analogue as determined by an unpaired t-test ($t(16) = 3.528, p = 0.003$) (Figure 6-8C). There was also a statistically significant increase in the means between normal (76%) and respiratory deficient stem cell progeny cells (82%) incorporating a thymidine analogue as determined by an unpaired t-test ($t(16) = 3.957, p = 0.0013$) (Figure 6-8D).

These results indicate that respiratory deficiency is having a small but significant effect on the rate of thymidine analogue incorporation over a prolonged period of time. This was true when crypts were grouped according to mouse genotype and also their mitochondrial OXPHOS status.

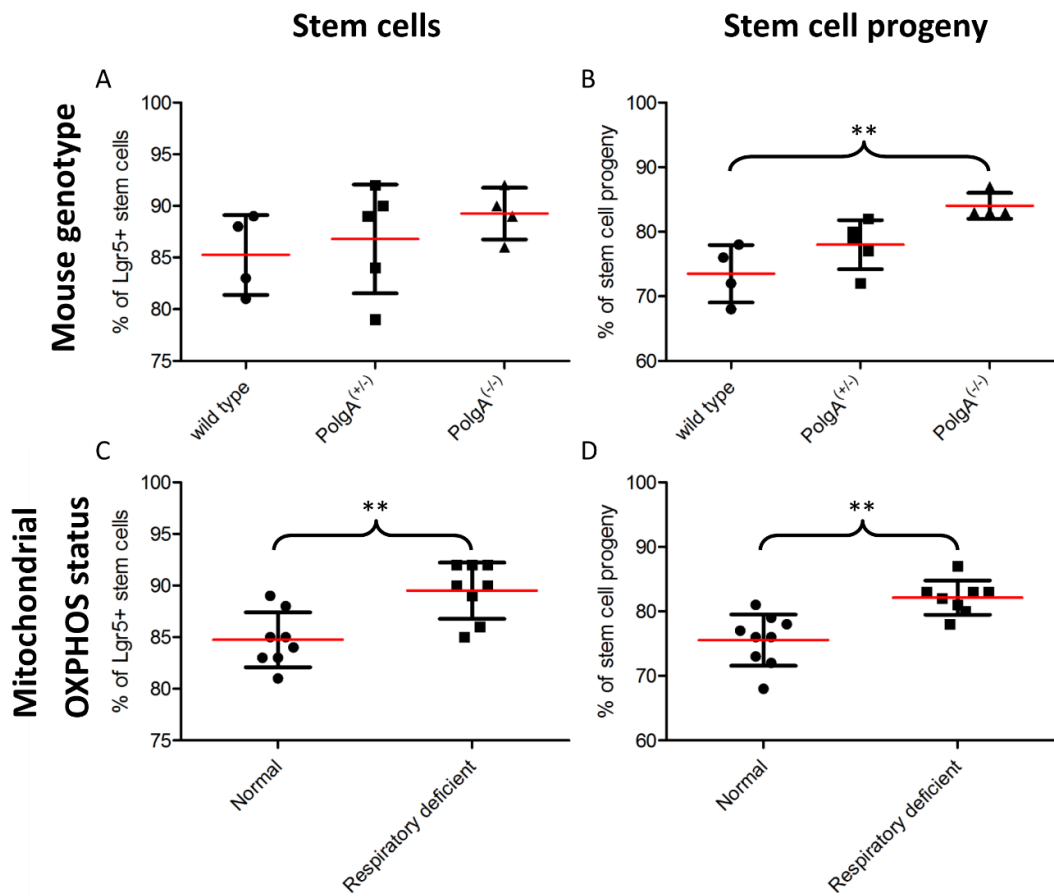


Figure 6-8 Thymidine analogue cell division marker

The frequency of cells that have incorporated a thymidine analogue upon DNA replication before the animal's death was quantified via detection of CldU and IdU. This was carried out on all crypts from *Lgr5*^(+/-)*PolyA*^(+/+)(n=4), *Lgr5*^(+/-)*PolyA*^(+/-)(n=5) and *Lgr5*^(+/-)*PolyA*^(-/-)(n=4) mouse colon that contained EGFP positive cells (i.e Lgr5+ stem cells). (A) Percentage of Lgr5+ stem cells that have incorporated a thymidine analogue, segregated for mouse genotype. There was not a statistically significant difference between groups as determined by one-way ANOVA ($F(2,10) = 0.936, p = 0.42$). (B) Percentage of stem cell progeny cells that have incorporated a thymidine analogue, segregated for mouse genotype. There was a statistically significant difference between groups as determined by one-way ANOVA ($F(2,10) = 8.614, p = 0.007$). A Dunnet multiple comparison post-hoc test was conducted to determine which groups were significantly different compared to the *Lgr5*^(+/-)*PolyA*^(+/+) mouse group. Only *Lgr5*^(+/-)*PolyA*^(-/-) mice showed a significant increase ($10.5 \pm 2.54\%, p = 0.004$). (C) Percentage of Lgr5+ stem cells that have incorporated a thymidine analogue, segregated based on their mitochondrial OXPHOS status. There was a statistically significant difference in the mean percentages for normal (M=84.8, SD=2.66) and respiratory deficient (M=89.5, SD=2.73) crypts as determined by an unpaired t-test; $t(16) = 3.528, p = 0.003$. (D) Percentage of stem cell progeny cells that have incorporated a thymidine analogue, segregated based on their mitochondrial OXPHOS status. There was a statistically significant difference in the mean percentages for normal (M=75.6, SD=3.97) and respiratory deficient (M=82.1, SD=2.64) crypts as determined by an unpaired t-test; $t(16) = 3.957, p = 0.0013$.

6.4.5 Frequency of newly divided cells

Cells that had undergone DNA synthesis as part of their transition through the cell cycle whilst the thymidine analogue IdU was present ~15 hours before the animal's death would have incorporated it into their newly synthesised DNA. The fraction of cells that had incorporated the IdU thymidine analogue was quantified (Figure 6-9). The fraction of stem cells and stem cell progeny that had incorporated the IdU thymidine analogue was compared between *Lgr5^(+/-)PolyA^(+/+)*(n=4), *Lgr5^(+/-)PolyA^(+/-)*(n=5) and *Lgr5^(+/-)PolyA^(-/-)*(n=4) mice (Figure 6-9A/B). There was not a statistically significant difference in the means between mouse groups for stem cells as determined by one-way ANOVA ($F(2,10) = 3.896, p = 0.056$) (Figure 6-9A). The mean percentage of stem cells that had incorporated the IdU thymidine analogue was 35%. However, there was a statistically significant difference in the means between mouse groups for stem cell progeny as determined by one-way ANOVA ($F(2,10) = 6.403, p = 0.016$) (Figure 6-9B). A Dunnet's multiple comparison test was conducted which showed that there was a statistically significant increase in stem cell progeny cells incorporating the IdU thymidine analogue between *Lgr5^(+/-)PolyA^(+/+)*(15%) and *Lgr5^(+/-)PolyA^(-/-)* mice (23%) of ~9% of total cells ($8.79 \pm 2.62\%, p = 0.013$).

The fraction of stem cells and stem cell progeny incorporating the IdU thymidine analogue was next compared between normal and respiratory deficient crypts. There was a statistically significant increase in the means between normal (26%) and respiratory deficient stem cells (34%) incorporating the IdU thymidine analogue as determined by an unpaired $t(16) = 2.323, p = 0.035$ (Figure 6-9C). There was also a statistically significant increase in the means between normal (15%) and respiratory deficient stem cell progeny cells (20%) incorporating the IdU thymidine analogue as determined by an unpaired t-test ($t(16) = 2.323, p = 0.016$) (Figure 6-9D).

These results indicate that respiratory deficiency is having a small but significant effect on the rate of thymidine analogue incorporation over a short ~15 hour time frame. This was true when crypts were grouped according to mouse genotype and also their mitochondrial OXPHOS status.

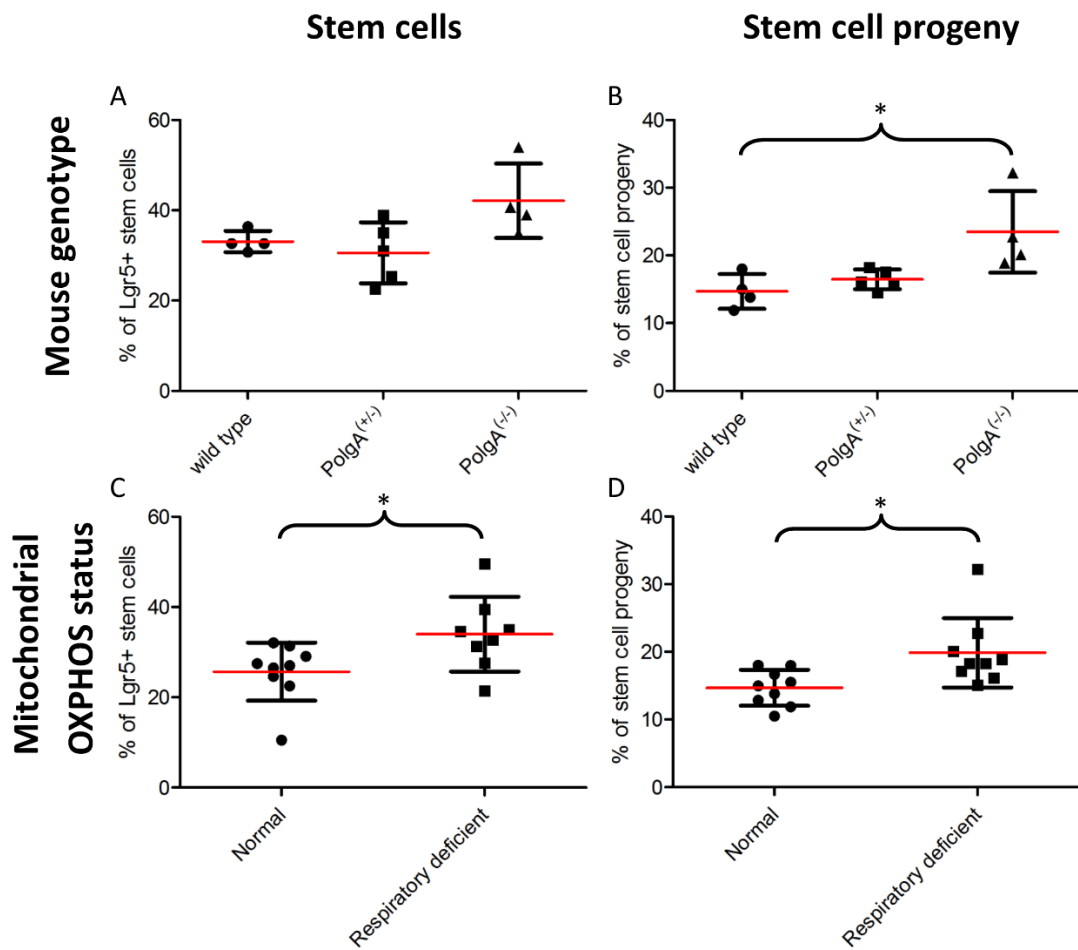


Figure 6-9 Cells undergoing division within ~15 hours of animals death

The frequency of cells that have incorporated a thymidine analogue upon DNA replication ~15 hours before the animal's death was quantified via IdU detection. This was carried out on all crypts from *Lgr5*^(+/-)*PolyA*^(+/-)(n=4), *Lgr5*^(+/-)*PolyA*^(+/-)(n=5) and *Lgr5*^(+/-)*PolyA*^(-/-)(n=4) mouse colon that contained EGFP positive cells (i.e Lgr5+ stem cells). (A) Percentage of Lgr5+ stem cells that have incorporated IdU, segregated for mouse genotype. There was not a statistically significant difference between groups as determined by one-way ANOVA ($F(2,10) = 3.896, p = 0.056$). (B) Percentage of stem cell progeny cells that have incorporated IdU, segregated for mouse genotype. There was a statistically significant difference between groups as determined by one-way ANOVA ($F(2,10) = 6.403, p = 0.016$). A Dunnett's multiple comparison post-hoc test was conducted to determine which groups were significantly different compared to the *Lgr5*^(+/-)*PolyA*^(+/-) mouse group. Only *Lgr5*^(+/-)*PolyA*^(-/-) mice showed a significant increase ($8.79 \pm 2.62\%, p = 0.013$). (C) Percentage of Lgr5+ stem cells that have incorporated IdU, segregated based on their mitochondrial OXPHOS status. There was a statistically significant difference in the mean percentages for normal (M=25.7, SD=6.43) and respiratory deficient (M=34.0, SD=8.28) crypts as determined by an unpaired t-test; $t(16) = 2.323, p = 0.0346$. (D) Percentage of stem cell progeny cells that have incorporated IdU, segregated based on their mitochondrial OXPHOS status. There was a statistically significant difference in the mean percentages for normal (M=14.7, SD=2.64) and respiratory deficient (M=19.9, SD=5.12) crypts as determined by an unpaired t-test; $t(16) = 2.323, p = 0.016$.

6.4.6 Frequency of cells re-entering the cell cycle

Cells that had undergone DNA synthesis whilst the thymidine analogue CldU was present within the animal's system, and subsequently whilst the thymidine analogue IdU was present within the animal's system would have incorporated both thymidine analogues into their newly synthesised DNA. This provides a measure of the cell cycle re-entry rate. The fraction of cells that had incorporated both CldU and IdU thymidine analogues was quantified (Figure 6-10). The fraction of stem cells and stem cell progeny that had incorporated both thymidine analogues were compared between *Lgr5^(+/-)PolyA⁽⁺⁺⁾*(n=4), *Lgr5^(+/-)PolyA⁽⁺⁻⁾*(n=5) and *Lgr5^(+/-)PolyA⁽⁻⁻⁾*(n=4) mice (Figure 6-10A/B). There was a statistically significant difference in the means between mouse groups for stem cells as determined by one-way ANOVA ($F(2,10) = 6.593, p = 0.0149$) (Figure 6-10A). A Dunnet's multiple comparison test was conducted which showed that there was a statistically significant increase in stem cells incorporating both thymidine analogues between *Lgr5^(+/-)PolyA⁽⁺⁺⁾*(22%) and *Lgr5^(+/-)PolyA⁽⁻⁻⁾* mice (32%) of ~10% of total cells ($10.00 \pm 3.42\%, p = 0.027$). There was also a statistically significant difference in the means between mouse groups for stem cell progeny cells as determined by one-way ANOVA ($F(2,10) = 10.12, p = 0.0040$) (Figure 6-10B). A Dunnet's multiple comparison test was conducted which showed that there was a statistically significant increase in stem cell progeny cells incorporating both thymidine analogues between *Lgr5^(+/-)PolyA⁽⁺⁺⁾*(10%) and *Lgr5^(+/-)PolyA⁽⁻⁻⁾* mice (18%) of ~8% of total cells ($8.25 \pm 1.97\%, p = 0.003$).

The fraction of stem cells and stem cell progeny incorporating both thymidine analogues was next compared between normal and respiratory deficient crypts. There was a statistically significant increase in the means between normal (19%) and respiratory deficient stem cells (27%) incorporating both thymidine analogues as determined by an unpaired t-test ($t(16) = 2.474, p = 0.0250$) (Figure 6-10C). There was also a statistically significant increase in the means between normal (10%) and respiratory deficient stem cell progeny cells (14%) incorporating both thymidine analogues as determined by an unpaired t-test ($t(16) = 2.622, p = 0.019$) (Figure 6-10D).

These results indicate that respiratory deficiency is having a small but significant effect on the rate of cell cycle re-entry. This was true when crypts were grouped according to mouse genotype and also their mitochondrial OXPHOS status.

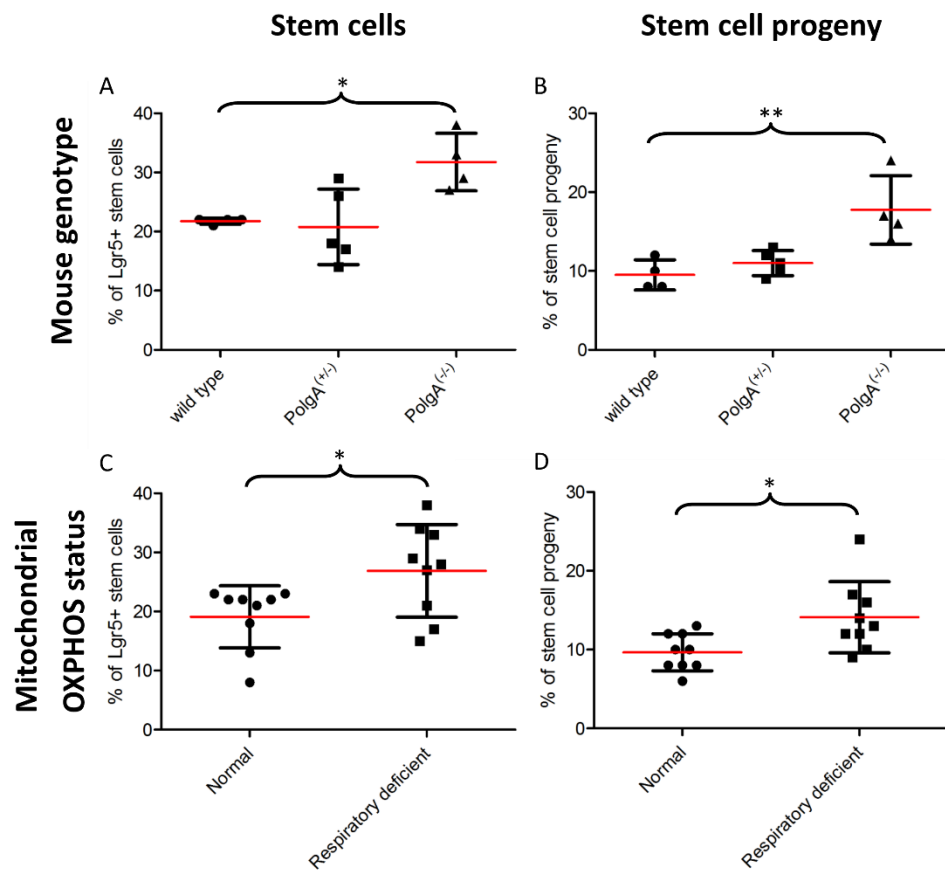


Figure 6-10 Cell cycle re-entry before animals death

The frequency of cells that have incorporated both thymidine analogues upon DNA replication before the animal's death was quantified via CldU and IdU colocalisation. This was carried out on all crypts from *Lgr5^(+/-)PolyA^(+/-)*(n=4), *Lgr5^(+/-)PolyA^(+/-)*(n=5) and *Lgr5^(+/-)PolyA^(-/-)*(n=4) mouse colon that contained EGFP positive cells (i.e Lgr5+ stem cells). (A) Percentage of Lgr5+ stem cells that have incorporated both thymidine analogues, segregated for mouse genotype. There was a statistically significant difference between groups as determined by one-way ANOVA ($F(2,10) = 6.593, p = 0.0149$). A Dunnett's multiple comparison post-hoc test was conducted to determine which groups were significantly different compared to the *Lgr5^(+/-)PolyA^(+/-)* mouse group. Only *Lgr5^(+/-)PolyA^(-/-)* mice showed a significant increase ($10.00 \pm 3.42\%, p = 0.027$). (B) Percentage of stem cell progeny cells that have incorporated both thymidine analogues, segregated for mouse genotype. There was a statistically significant difference between groups as determined by one-way ANOVA ($F(2,10) = 10.12, p = 0.0040$). A Dunnett's multiple comparison post-hoc test was conducted to determine which groups were significantly different compared to the *Lgr5^(+/-)PolyA^(+/-)* mouse group. Only *Lgr5^(+/-)PolyA^(-/-)* mice showed a significant increase ($8.25 \pm 1.97\%, p = 0.003$). (C) Percentage of Lgr5+ stem cells that have incorporated both thymidine analogues, segregated based on their mitochondrial OXPHOS status. There was a statistically significant difference in the mean percentages for normal (M=19.1, SD=5.26) and respiratory deficient (M=26.9, SD=7.83) crypts as determined by an unpaired t-test; $t(16) = 2.474, p = 0.0250$. (D) Percentage of stem cell progeny cells that have incorporated both thymidine analogues, segregated based on their mitochondrial OXPHOS status. There was a statistically significant difference in the mean percentages for normal (M=9.7, SD=2.35) and respiratory deficient (M=14.1, SD=4.51) crypts as determined by an unpaired t-test; $t(16) = 2.622, p = 0.019$.

6.4.7 Frequency of cells re-entering the cell cycle within *PolyA* heterozygote mice

Lgr5^(+/-)PolyA^(+/-) mice have a mosaic pattern of mitochondrial OXPHOS deficiency within their colonic epithelium. Therefore, normal and respiratory deficient crypts could be quantified within the same mouse genotype.

The fraction of stem cells and stem cell progeny cells incorporating both thymidine analogues was compared between normal and respiratory deficient crypts within *Lgr5^(+/-)PolyA^(+/-)* mice (Figure 6-11). There was not a statistically significant difference in the means between normal (17%) and respiratory deficient stem cells (23%) incorporating both thymidine analogues as determined by an unpaired t-test ($t(8) = 1.309$, $p = 0.23$) (Figure 6-11A).

However, there was a statistically significant mean increase between normal and respiratory deficient stem cells of the same subject of ~6% as determined by a paired t-test ($t(4) = 3.00$, $p = 0.040$). (Figure 6-11B)

There was not a statistically significant difference in the means between normal (10%) and respiratory deficient stem cell progeny cells (11%) incorporating both thymidine analogues as determined by an unpaired t-test ($t(8) = 0.948$, $p = 0.37$) (Figure 6-11C). Furthermore, there was not a statistically significant means difference between normal and respiratory deficient stem cell progeny cells of the same subject as determined by a paired t-test ($t(4) = 1.159$, $p = 0.311$) (Figure 6-11D).

These results indicate that within the *Lgr5^(+/-)PolyA^(+/-)* mouse, respiratory deficiency is only having a small but significant effect on the rate of cell cycle re-entry for the stem cells and not the stem cell progeny.

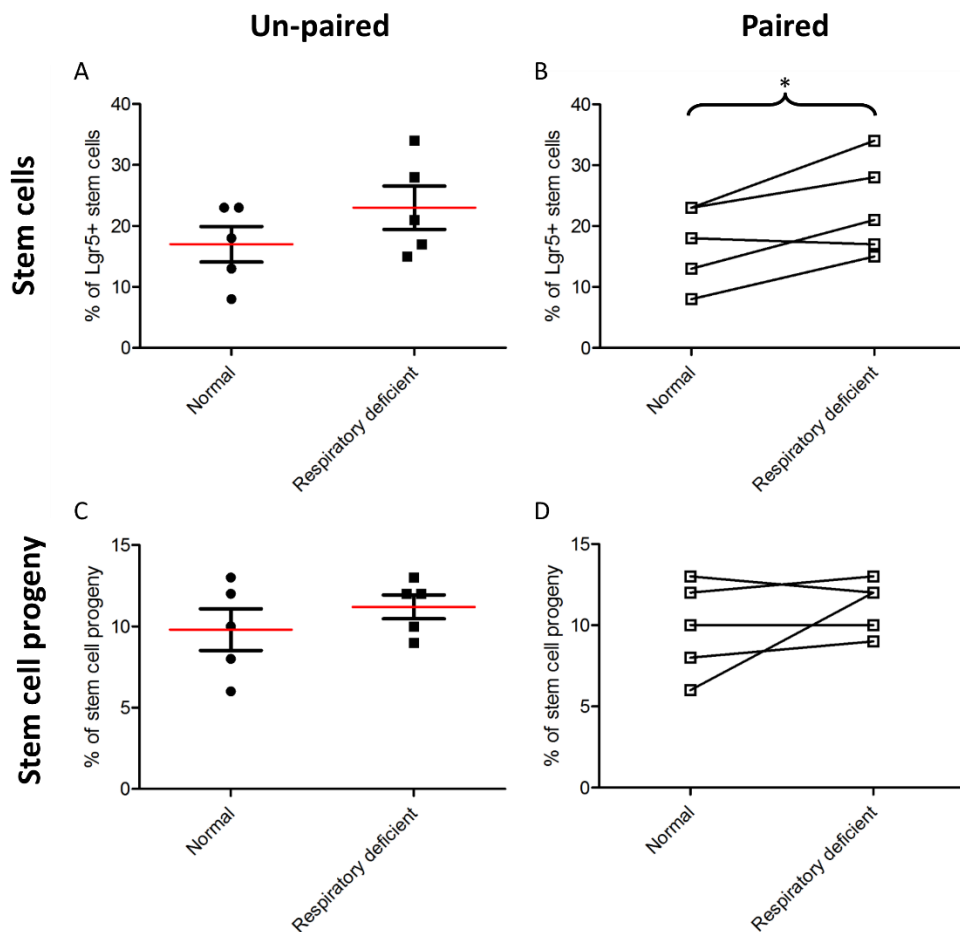


Figure 6-11 Cell cycle re-entry within *PolyA*(^{+/−}) crypts

The frequency of cells that have incorporated both thymidine analogues upon DNA replication before the animal's death was quantified via ClDU and IdU colocalisation. The difference in frequency was investigated between normal and respiratory deficient crypts within *Lgr5*(^{+/−})*PolyA*(^{+/−}) mouse colon that contained EGFP positive cells (i.e. Lgr5+ stem cells). (A) Percentage of Lgr5+ stem cells that have incorporated both thymidine analogues, segregated based on their mitochondrial OXPHOS status. There was not a statistically significant difference in the mean percentages for normal ($M=17.0$, $SD=6.52$) and respiratory deficient ($M=23.0$, $SD=7.91$) crypts as determined by an unpaired t-test; $t(8)=1.309$, $p=0.23$. (B) Percentage of Lgr5+ stem cells that have incorporated both thymidine analogues, segregated based on their mitochondrial OXPHOS status. There was a statistically significant increase in the mean percentage between normal and respiratory deficient crypts for the same subjects ($M=6.00$, $SD=4.47$) as determined by a paired t-test; $t(4)=3.00$, $p=0.040$. (C) Percentage of stem cell progeny cells that have incorporated both thymidine analogues, segregated based on their mitochondrial OXPHOS status. There was not a statistically significant difference in the mean percentages for normal ($M=9.80$, $SD=2.86$) and respiratory deficient ($M=11.2$, $SD=1.64$) crypts as determined by an unpaired t-test; $t(8)=0.948$, $p=0.37$. (D) Percentage of Lgr5+ stem cells that have incorporated both thymidine analogues, segregated based on their mitochondrial OXPHOS status. There was not a statistically significant difference in the mean percentage between normal and respiratory deficient crypts for the same subjects as determined by a paired t-test; $t(4)=1.159$, $p=0.311$.

6.4.8 Cell cycle kinetics by individual complex deficiency

As individual and multiple complex deficiency was observed and quantified within the data set, the effect of mitochondrial OXPHOS deficiency type on the cell cycle kinetics of stem cell and stem cell progeny cells was assessed (Figure 6-12). The effect of mitochondrial OXPHOS deficiency type was ascertained for the fraction of stem cells (Figure 6-12A) and stem cell progeny cells (Figure 6-12B) that are actively dividing. There was not a statistically significant difference in the means between OXPHOS expression groups for stem cells as determined by one-way ANOVA ($F(3,28) = 0.465, p = 0.709$) (Figure 6-12A). There was also not a statistically significant difference in the means between OXPHOS expression groups for stem cell progeny cells as determined by one-way ANOVA ($F(3,28) = 0.282, p = 0.838$) (Figure 6-12B).

Next, the effect of mitochondrial OXPHOS deficiency type was ascertained for the fraction of stem cells (Figure 6-12C) and stem cell progeny cells (Figure 6-12D) that had incorporated a thymidine analogue over a prolonged period of time. There was not a statistically significant difference in the means between OXPHOS expression groups for stem cells as determined by one-way ANOVA ($F(3,28) = 0.465, p = 0.709$) (Figure 6-12C). However, there was a statistically significant difference in the means between OXPHOS expression groups for stem cell progeny cells as determined by one-way ANOVA ($F(3,28) = 7.573, p = 0.001$) (Figure 6-12D). A Dunnet's multiple comparison test was conducted which showed that there was a statistically significant increase in the fraction of stem cell progeny cells incorporating a thymidine analogue between normal crypts (75.6%) and crypts with NDUFB8 (Complex I) loss (82.6%) ($7.07 \pm 1.73\%, p = 0.001$) and also between normal crypts (75.6%) and crypts with both NDUFB8 (Complex I) and MTCO1 (Complex I) loss (81.0%) ($5.94 \pm 1.73\%, p = 0.006$).

Next, the effect of mitochondrial OXPHOS deficiency type was ascertained for the fraction of stem cells (Figure 6-12E) and stem cell progeny cells (Figure 6-12F) that had incorporated the IdU thymidine analogue over a short ~15 hour time frame. There was not a statistically significant difference in the means between OXPHOS expression groups for stem cells as determined by one-way ANOVA ($F(3,28) = 0.974, p = 0.419$) (Figure 6-12E). However, there was a statistically significant difference in the means between OXPHOS expression groups for stem cell progeny cells as determined by one-way ANOVA ($F(3,28) = 4.70, p = 0.009$) (Figure 6-12F). A Dunnet's multiple comparison test was conducted which showed

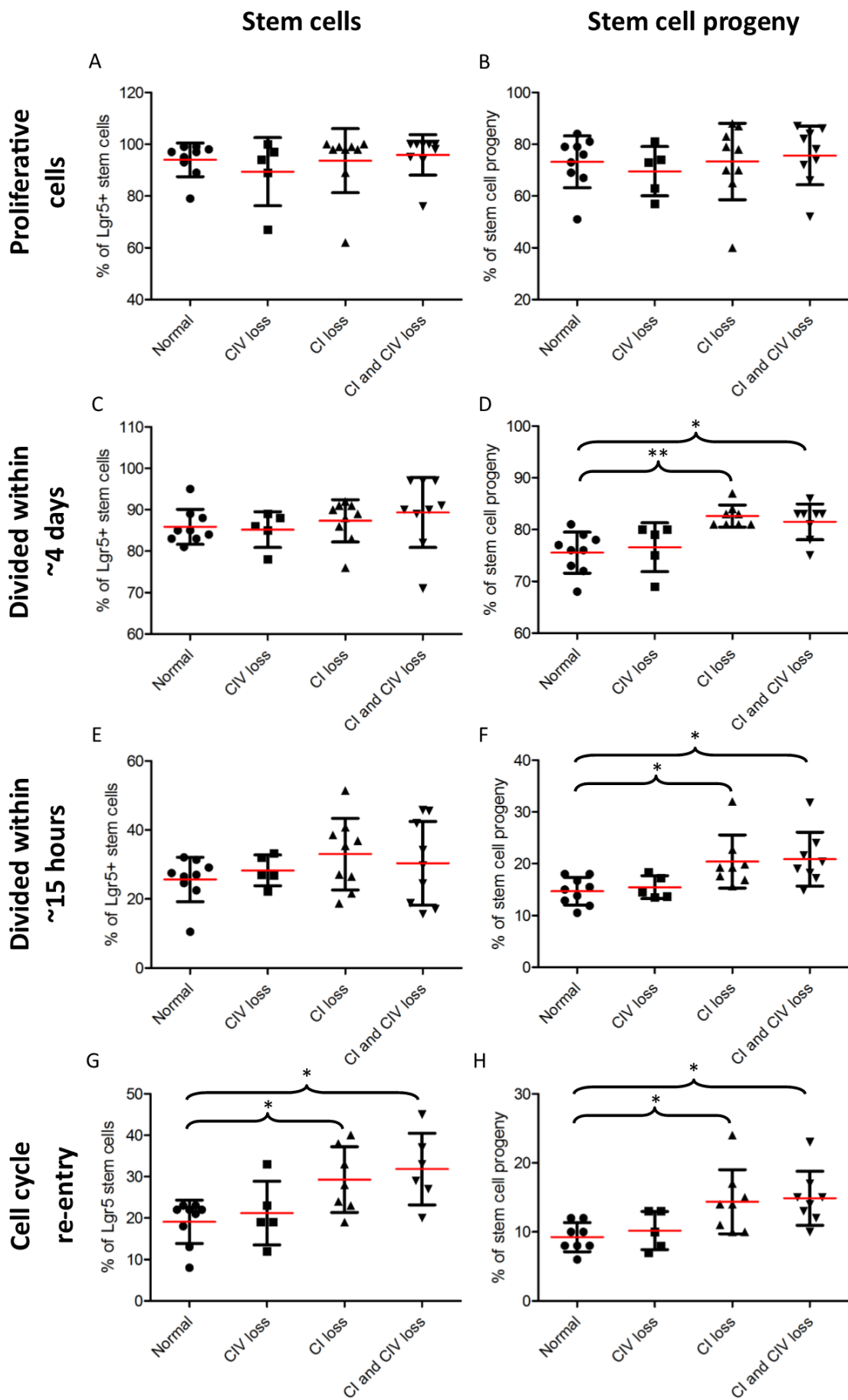
that there was a statistically significant increase in the fraction of stem cell progeny cells incorporating the IdU thymidine analogue between normal crypts (14.7%) and crypts with NDUFB8 (Complex I) loss (20.4%) ($5.72 \pm 2.02\%, p = 0.024$) and also between normal crypts (14.7%) and crypts with both NDUFB8 (Complex I) and MTCO1 (Complex I) loss (20.9%) ($6.19 \pm 2.02\%, p = 0.014$).

Finally, the effect of mitochondrial OXPHOS deficiency type was ascertained for the fraction of stem cells (Figure 6-12G) and stem cell progeny cells (Figure 6-12H) that had incorporated both IdU and CldU thymidine analogues. There was a statistically significant difference in the means between OXPHOS expression groups for stem cells as determined by one-way ANOVA ($F(3,28) = 5.025, p = 0.008$) (Figure 6-12G). A Dunnet's multiple comparison test was conducted which showed that there was a statistically significant increase in the fraction of stem cells incorporating both thymidine analogues between normal crypts (19.1%) and crypts with NDUFB8 (Complex I) loss (29.3%) ($10.17 \pm 3.66\%, p = 0.029$) and also between normal crypts (19.1%) and crypts with both NDUFB8 (Complex I) and MTCO1 (Complex I) loss (31.8%) ($12.72 \pm 3.82\%, p = 0.008$). There was also a statistically significant difference in the means between OXPHOS expression groups for stem cell progeny cells as determined by one-way ANOVA ($F(3,28) = 4.800, p = 0.009$) (Figure 6-12H). A Dunnet's multiple comparison test was conducted which showed that there was a statistically significant increase in the fraction of stem cell progeny cells incorporating both thymidine analogues between normal crypts (9.25%) and crypts with NDUFB8 (Complex I) loss (14.0%) ($5.13 \pm 1.79\%, p = 0.022$) and also between normal crypts (9.25%) and crypts with both NDUFB8 (Complex I) and MTCO1 (Complex I) loss (14.9%) ($5.63 \pm 1.79\%, p = 0.012$).

These results indicate that respiratory deficient stem cells and stem cell progeny that incorporate an element of NDUFB8 (Complex I) loss have an increased cell cycle progression and re-entry rate.

Figure 6-12 Cell cycle kinetics and multiple complex deficiency

The frequency of cells that are proliferative and have incorporated thymidine analogues upon DNA replication before the animal's death were quantified via Ki67, CldU and IdU detection. This was carried out on all crypts from *Lgr5^(+/-)PolyA⁽⁺⁺⁾*, *Lgr5^(+/-)PolyA^(+/-)* and *Lgr5^(+/-)PolyA^(-/-)* mouse colon that contained EGFP positive cells (i.e Lgr5+ stem cells). (A) Percentage of Lgr5+ stem cells that are actively proliferating, segregated based on their mitochondrial OXPHOS status. There was not a statistically significant difference between groups as determined by one-way ANOVA ($F(3,28) = 0.465, p = 0.709$). (B) Percentage of stem cell progeny cells that are actively proliferating, segregated based on their mitochondrial OXPHOS status. There was not a statistically significant difference between groups as determined by one-way ANOVA ($F(3,28) = 0.282, p = 0.838$). (C) Percentage of Lgr5+ stem cells that have incorporated a thymidine analogue, segregated based on their mitochondrial OXPHOS status. There was not a statistically significant difference between groups as determined by one-way ANOVA ($F(3,28) = 0.717, p = 0.550$). (D) Percentage of stem cell progeny cells that have incorporated a thymidine analogue, segregated based on their mitochondrial OXPHOS status. There was a statistically significant difference between groups as determined by one-way ANOVA ($F(3,28) = 7.573, p = 0.001$). A Dunnett's multiple comparison post-hoc test was conducted to determine which groups were significantly different compared to the normal group. Both the CI loss ($7.07 \pm 1.73\%, p = 0.001$) and the CI and CIV loss ($5.94 \pm 1.73\%, p = 0.006$) groups showed a significant increase. (E) Percentage of Lgr5+ stem cells that have incorporated IdU, segregated based on their mitochondrial OXPHOS status. There was not a statistically significant difference between groups as determined by one-way ANOVA ($F(3,28) = 0.974, p = 0.419$). (F) Percentage of stem cell progeny cells that have incorporated IdU, segregated based on their mitochondrial OXPHOS status. There was a statistically significant difference between groups as determined by one-way ANOVA ($F(3,28) = 4.70, p = 0.009$). A Dunnett's multiple comparison post-hoc test was conducted to determine which groups were significantly different compared to the normal group. Both the CI loss ($5.72 \pm 2.02\%, p = 0.024$) and the CI and CIV loss ($6.19 \pm 2.02\%, p = 0.014$) groups showed a significant increase. (G) Percentage of Lgr5+ stem cells that have incorporated both thymidine analogues, segregated based on their mitochondrial OXPHOS status. There was a statistically significant difference between groups as determined by one-way ANOVA ($F(3,28) = 5.025, p = 0.008$). A Dunnett's multiple comparison post-hoc test was conducted to determine which groups were significantly different compared to the normal group. Both the CI loss ($10.17 \pm 3.66\%, p = 0.029$) and the CI and CIV loss ($12.72 \pm 3.82\%, p = 0.008$) groups showed a significant increase. (H) Percentage of stem cell progeny cells that have incorporated both thymidine analogues, segregated based on their mitochondrial OXPHOS status. There was a statistically significant difference between groups as determined by one-way ANOVA ($F(3,28) = 4.800, p = 0.009$). A Dunnett's multiple comparison post-hoc test was conducted to determine which groups were significantly different compared to the normal group. Both the CI loss ($5.13 \pm 1.79\%, p = 0.022$) and the CI and CIV loss ($5.63 \pm 1.79\%, p = 0.012$) groups showed a significant increase.



6.5 DISCUSSION

Cell cycle kinetic parameters were quantified within $Lgr5^{(+-)}PolyA^{(++)}$, $Lgr5^{(+-)}PolyA^{(+-)}$ and $Lgr5^{(+-)}PolyA^{(-)}$ mouse colon, segregated into stem cell and stem cell progeny cell groups, and were further segregated according to the mitochondrial OXPHOS status. The mitochondrial OXPHOS status of stem cell and stem cell progeny cells was assumed by the status of the crypt as a whole. Lgr5+ stem cells have been shown to be the long-lived functional stem cells within mouse small intestinal and colon epithelium, having the ability to generate every cell type within crypts (Barker *et al.*, 2007; Sato *et al.*, 2009). Therefore, if the crypt as a whole had a mitochondrial OXPHOS deficiency, this would be derived solely from the Lgr5+ stem cells.

The number of cells contained within each longitudinal crypt from each mouse genotype was quantified (Figure 6-6). For each mouse within their own genotype group there was no statistically significant difference for the average number of cells observed within longitudinal crypts. The average for $Lgr5^{(+-)}PolyA^{(++)}$ mouse crypts was 48 cells, the average for $Lgr5^{(+-)}PolyA^{(+-)}$ mouse crypts was 47 cells, however the average for $Lgr5^{(+-)}PolyA^{(-)}$ mouse crypts was 63 cells. As all mouse crypts within this group averaged the same number of cells, this suggests that it is a true observation and not just variation caused by the way in which the colon tissue block was cut on the microtome. It is curious that respiratory deficient crypts from $Lgr5^{(+-)}PolyA^{(+-)}$ mice do not show a difference compared to *wild type* normal crypts whereas respiratory deficient crypts from $Lgr5^{(+-)}PolyA^{(-)}$ mice do show a substantial difference. As was shown in section 5.4.2, respiratory deficiency is acquired much earlier within $Lgr5^{(+-)}PolyA^{(-)}$ mouse crypts compared to those from $Lgr5^{(+-)}PolyA^{(+-)}$ mice. The fact that there is an observable phenotype within $Lgr5^{(+-)}PolyA^{(-)}$ respiratory deficient crypts compared to $Lgr5^{(+-)}PolyA^{(+-)}$ respiratory deficient crypts may suggest that respiratory deficiency can be tolerated for a certain amount of time before a disruption to normal crypt morphology is acquired. The effect of respiratory deficiency on crypt size within human colon has previously been investigated (Nooteboom *et al.*, 2010). This study showed that respiratory deficient crypts had a decreased crypt size compared to normal crypts (Nooteboom *et al.*, 2010). The effect of respiratory deficiency seems to have contrasting effects on human and mouse crypts and may reflect species differences.

Ki67 is a protein that is present within all stages of the cell cycle, excluding the G₀ quiescence phase. Therefore, the frequency of actively dividing cells was quantified via Ki67

labelling. It has previously been shown that there is an approximate 20% reduction in the frequency of Ki67+ stem cell progeny cells between normal and respiratory chain deficient crypts from aged human colon (Nooteboom *et al.*, 2010). The same observation was not observed within mouse colon, with no statistically significant difference between mouse groups and mitochondrial OXPHOS status for stem cell progeny cells and also the stem cells themselves (Figure 6-7 and Figure 6-12A/B). In this study, we see a greater fraction of Ki67+ stem cell progeny cells in mouse crypts (70%) compared to within the study by Nooteboom et al which saw a Ki67+ fraction of stem cell progeny of approximately 25%. This may be explained by the differences that exist between mouse and human colonic epithelium. Firstly, mouse crypts contain ~250 cells (Kellett *et al.*, 1992), whereas human crypts contain ~2000 cells (Yatabe *et al.*, 2001; Nicolas *et al.*, 2007; Nooteboom *et al.*, 2010). Furthermore, cell cycle time differences exist between human and mouse stem cells and stem cell progeny cells. Crypt stem cells divide approximately once per week within humans (Potten and Loeffler, 1990; Potten *et al.*, 1992; Kim and Shibata, 2002), whereas mouse stem cells divide once per day (Kellett *et al.*, 1992; Potten *et al.*, 1992). Therefore, mouse crypts regenerate 5 times faster than human crypts. However, as the average lifespan for humans is 80 years and 3 years for the average laboratory mouse, stem cells are expected to divide 5 times as much at the end of a human's lifespan as opposed to the end of a mouse's. These differences, along with the fact that only 11-12 month old mice were used within this study, may account for the difference we see between mouse and humans. As no difference was seen in the frequency of Ki67+ stem cell progeny cells between normal and respiratory deficient crypts in mouse, this indicates that the observed difference between normal and respiratory deficient crypts within humans may be compounded by the replicative and chronological age of the stem cells.

The *in vivo* technique of thymidine analogue labelling was used to assess the rate at which stem cells and stem cell progeny cells within mouse colon were dividing. All cells dividing and transiting through the S-phase (DNA synthesis) of the cell cycle would incorporate the thymidine analogue into the newly replicated DNA. A double thymidine analogue method of labelling dividing cells using IdU and CldU was adopted with the help of Dr Elizabeth Stoll (Newcastle University) where it had already been used to assess neurogenic decline within mouse brain subventricular zone (Stoll *et al.*, 2011). Antibodies were commercially available that could bind specifically to each thymidine analogue. This allowed cell cycle kinetic parameters to be compared between *Lgr5^(+/-)PolyA⁽⁺⁺⁾*, *Lgr5^(+/-)PolyA^(+/-)* and *Lgr5^(+/-)PolyA^(-/-)* mouse colon and also between normal and respiratory deficient crypts. The cell cycle

kinetics parameters to be compared included; number of cells that had undergone division over a 4 day time period, over a ~15 hour time period, and also those cells that had re-entered the cell cycle in quick succession.

Firstly, the frequency of stem cell and stem cell progeny cells that had undergone division over 4 days prior to the animal's death was assessed (Figure 6-8). There was an ~10% increase in the frequency of cells incorporating a thymidine analogue within stem cell progeny cells within *Lgr5^(+/-)PolyA^(-/-)* mouse colon compared to *Lgr5^(+/-)PolyA^(+/+)* mouse colon (Figure 6-8B). As *Lgr5^(+/-)PolyA^(+/+)* mouse colon purely sampled normal crypts and *Lgr5^(+/-)PolyA^(-/-)* mouse colon contained mostly respiratory deficient crypts, this can be thought of as a direct comparison between normal and respiratory deficient crypts. It has previously been shown that the number of cells actively dividing within mouse colon is the same between different mouse groups (Figure 6-7), the fact that there is a greater thymidine analogue incorporation within respiratory deficient crypts indicates that these crypts are regenerating at a faster rate. This result is replicated by the frequency of stem cell progeny cells that have incorporated only the IdU thymidine analogue (Figure 6-9). There was no statistically significant difference for Lgr5+ stem cells between mouse groups (Figure 6-8 and Figure 6-9). As the effects of respiratory deficiency on cell cycle kinetics may be small, wider variation in the data sets may make it difficult to resolve those differences via statistical significance testing.

As the data within this study shows that there was increased cell division for respiratory deficient crypts compared with normal crypts, the frequency of stem cells and stem cell progeny that incorporated both CldU and IdU thymidine analogues, hence cell cycle re-entry, was quantified (Figure 6-10). This would determine whether the increased cell division observed could be explained by a more rapid progression through the cell cycle. This time there were observable differences for stem cells and stem cell progeny cells between mouse groups (Figure 6-10A/B) and between normal and respiratory deficient crypts (Figure 6-10C/D). This was also done within the *PolyA^(+/-)* mouse group that contained both normal and respiratory deficient crypts (Figure 6-11). There was a small 6% increase in the frequency of cell cycle re-entry for respiratory deficient stem cells, but not stem cell progeny cells. Again, reducing the number of cells and crypts analysed, which looking at one mouse group will do, adds to the variability in the data set, suggesting a possible reason why a difference could not be seen for stem cell progeny cells within the *PolyA^(+/-)* mouse group. These data provide evidence that there is increased cell division for respiratory deficient crypts and that this is

due to an increased rate of cell cycle progression for respiratory deficient cells. Furthermore, when the cell cycle kinetics data was segregated based on each mitochondrial OXPHOS deficiency type (Figure 6-12), Complex I deficient crypts showed a more substantial increase in cell division rate and cell cycle re-entry. This suggests that Complex I loss triggers more pronounced cell cycle kinetic perturbations.

Perturbations to cell cycle kinetics within stem cells and stem cell progeny cells were more apparent within *Lgr5^(+/-)PolyA^(-/-)* mouse crypts. As has been stated previously, respiratory deficiency is acquired much earlier within *Lgr5^(+/-)PolyA^(-/-)* mouse crypts, suggesting that perturbations to cell cycle kinetics and crypt morphology occur long after the acquisition of respiratory deficiency, meaning that the stem cells are able to tolerate the respiratory deficiency for a certain amount of time before it starts to perturb the stem cells cellular function.

6.6 CONCLUSION

Even though mouse and human crypts have similar structural architecture and provide the same function, they are still unique, adding to the complexity for comparing mouse crypts to human crypts. This can be emphasised within this study when proliferation and cell cycle progression are so different between the two species, but plays an integral part within this study. As the frequency of actively dividing cells remains constant between normal and respiratory deficient crypts within mouse colon, the fact that we see increased cell division and cell cycle re-entry within respiratory deficient crypts provides evidence that respiratory deficient cells progress through the cell cycle at a much faster rate. This is true for both stem cells and stem cell progeny. This is the first study that has shown respiratory deficiency does alter the cell cycle kinetics of stem cells of the colon.

Future work includes investigating what the mechanism is behind respiratory deficiency altering cell cycle kinetics within colonic epithelium, and also discovering how stem cells are able to tolerate respiratory deficiency before alterations to cellular function arise.

Chapter 7

Final Discussion and Future

Work

Chapter 7 Final discussion and future work

The accumulation of mitochondrial dysfunction within colonic epithelium and its impact on the stem cells and stem cell progeny have been investigated in depth within this thesis using both experimental and computational methodologies. Understanding the accumulation of mitochondrial dysfunction and its impact on ageing tissues is extremely important as it has the ability to compromise a tissues function, leading to tissue failure (Taylor and Turnbull, 2005). Mitochondrial dysfunction has been linked to a variety of age-related diseases such as macular degeneration (Blasiak *et al.*, 2013), diabetes mellitus (Sivitz and Yorek, 2010) and certain neurodegenerative diseases such as Alzheimer's and Parkinson's disease (Reeve *et al.*, 2008). Mitochondrial dysfunction has also been linked to cancer development within ageing tissues due to favourable metabolic perturbations that exist within those cells with mitochondrial dysfunction (Warburg, 1956; Toyokuni *et al.*, 1995; Carew and Huang, 2002; Park *et al.*, 2009). Colorectal cancer is the third most commonly diagnosed cancer worldwide, and the fourth most common cause of death from cancer (Ferlay *et al.*, 2010), with age being the biggest risk factor (CDC, 2015). Therefore, understanding the functional consequences of mitochondrial dysfunction within the colon is of high importance.

7.1 ACCUMULATION OF MITOCHONDRIAL DYSFUNCTION

Investigating the accumulation of mitochondrial dysfunction within human colonic epithelium has revealed important characteristics about the biology of the colon as a whole. The biological data, as well as model optimisations, were able to determine that there are an average of 5 stem cells contained within human colonic crypts. This is similar to previously published numbers of stem cells within mouse (7 stem cells) and human (4-6 stem cells) colonic crypts (Kozar *et al.*, 2013; Baker *et al.*, 2014). The number of functional stem cells that are contained at the base of crypts is an important factor as this will influence the rate at which niche succession occurs, hence the rate at which mitochondrial dysfunction, or mutations to the nuclear DNA, are able to accumulate. Furthermore, the ratio between partially and fully COX deficient crypts meant that simulations could only be matched when the majority of stem cell divisions were asymmetric. This was true for all numbers of stem cells simulated, with a model of 5 stem cells requiring asymmetric stem cell divisions to occur 99% of the time. This is in contrast to reports that suggest symmetric division occurs all the time (Snippert *et al.*, 2010; Baker *et al.*, 2014). This discrepancy may be due to the explicit way in which the stem cell dynamics are simulated within the model presented,

resulting in a more biologically accurate model. The Cairns Hypothesis postulates that upon stem cell division, newly replicated DNA is segregated out of the stem cell pool and passed onto the non-stem cell daughter cells, minimising the number of mutations that accumulate within the stem cells (Cairns, 1975). This would mean stem cells are in fact dividing asymmetrically at the point of division. This is in agreement with findings from this study. As colonic stem cells have a high turnover rate in order to regenerate the crypt on weekly basis (Potten and Loeffler, 1990), it makes sense that asymmetric division occurs the majority of the time as a measure of minimising nuclear mutations over the human lifespan.

It was soon realised that a model of neutral drift stem cell dynamics was unable to match the biological data, due to the increase in partially COX deficient crypts with age. This meant that the rate at which COX deficient stem cells were being generated and were accumulating within the colon was increasing over time. An increasing mtDNA mutation rate has the potential to increase the rate at which COX deficient stem cells are acquired. However, a previous study looking at mtDNA mutation rate within ageing human colon has shown that there is no statistically significant increase in mtDNA mutation rate with age (Greaves *et al.*, 2014). On the other hand, as it has previously been discussed (section 4.5), the RMC assay used to infer mtDNA mutation rate includes high intrinsic variability; therefore a subtle increase in mutation rate cannot be completely ruled out and should be incorporated into the model (Greaves *et al.*, 2014).

The ability of COX deficient stem cells to expand was assessed. This was done by increasing the probability of symmetric stem cell division (2 stem cells) for COX deficient stem cells. This resulted in an increasing frequency of partially COX deficient crypts with age, reminiscent of what was observed within the biological data, suggesting that mitochondrial dysfunction is having an advantageous impact on a COX deficient stem cells ability to expand.

Using two sets of biological data, it was shown that mutated mtDNA clonal expansion within the colon was unlikely to occur via relaxed replication and random segregation. It has previously been shown that mammary epithelial cells segregate their young and old mitochondria asymmetrically upon division (Katajisto *et al.*, 2015). Therefore, it was rationalised that newly replicated mtDNA (mtDNA acquiring mutation) may be segregated out of the stem cell pool upon asymmetric stem cell division. This hypothesis allowed the model to match both COX deficiency frequency and the number of mutations within

individual cells with an extremely marginal segregation bias being set. This suggests that stem cells may have a mechanism for the prevention of mutated mtDNA accumulation, via biasing the segregation of newly replicated mtDNA out of the stem cell pool.

7.2 IMPACT OF MITOCHONDRIAL DYSFUNCTION

In order to investigate the impact of mitochondrial dysfunction within colonic stem cells, mouse models were employed. Lgr5 is a well-accepted stem cell marker within mouse colon, with *Lgr5-EGFP-Ires-CreERT2* (*Lgr5^(+/-)*) mice expressing a detectable EGFP molecule within Lgr5+ stem cells (Barker *et al.*, 2007). Wild type *C57Bl/6J* mice do not accumulate significant levels of mitochondrial dysfunction within their colons (Greaves *et al.*, 2011). However, mitochondrial mutator (*PolyA^(+/-)* and *PolyA^(-/-)*) mice do accumulate substantial mitochondrial dysfunction within their colons (Baines *et al.*, 2014). Therefore, in order to visualise a substantial number of stem cells and stem cell progeny cells harbouring mitochondrial dysfunction within mouse colon, *Lgr5^(+/-)* mice were crossed with *PolyA^(+/-)* mice. The use of the *Lgr5^(+/-)PolyA^(+/-)* and *Lgr5^(+/-)PolyA^(-/-)* was validated due to their accumulation of substantial levels of mitochondrial dysfunction at 11-12 months.

Mitochondrial dysfunction was assessed via OXPHOS subunit expression levels for NDUFB8 (Complex I) and MTCO1 (Complex IV). It was observed that NDUFB8 expression was more likely to be lost than MTCO1, indicating its greater susceptibility to random mtDNA mutations overtime. Furthermore, it shows that a mosaic pattern of respiratory deficiency can result due to mtDNA mutations within ageing tissues. This has also been shown within human aged colonic epithelium (Greaves *et al.*, 2010). Therefore, it is important to recognise all respiratory complexes when assessing the mitochondrial OXPHOS status of individual cells and crypts.

The double thymidine analogue labelling methodology was able to compare the stem cell and stem cell progeny cell turnover times between mouse genotypes and between normal and respiratory deficient crypts. The fraction of proliferative cells stayed the same between all mouse genotypes and the same is true between normal and respiratory deficient crypts. However, there was on average an increased stem cell and stem cell progeny cell turnover rate between normal and respiratory deficient crypts due to the increased fraction of respiratory deficient stem cells and stem cell progeny incorporating a thymidine analogue within a defined time frame. This suggests that mitochondrial dysfunction is increasing the rate at which cells are transitioning through the cell cycle. This was more apparent within the

Lgr5^(+/-)PolyA^(-/-) mouse, indicating that stem cells that have endured respiratory deficiency for longer are more likely to develop perturbed stem cell dynamics and cell cycle kinetics over time. This may mean that respiratory deficient stem cells not only have an advantage to expand within the colon, but they may also have an increased rate of cell cycle progression. With this, stem cells with mitochondrial dysfunction are more likely to out-compete normal stem cells over time. This has implications for cancer development as well. For instance, stem cells with mitochondrial dysfunction may have fewer cellular barriers to overcome before malignant transformation results, making malignant transformation more likely. Furthermore, if malignant transformation does occur within stem cells with mitochondrial dysfunction, tumour growth is faster.

7.3 MODELLING COMBINED EFFECTS

Results from chapter 6 show that there is a 6-12% increase in the frequency of OXPHOS deficient stem cells re-entering the cell cycle compared to OXPHOS normal cells. Within the model, this would equate to 5 COX deficient stem cell divisions for every 4 normal stem divisions. Model code was developed that allowed this parameter to be entered into the model. Results for this are shown in Figure 7-1.

A combination of small changes in parameter values were simulated within the model. Small changes in parameter values included: 2-fold mutation rate increase from 0-80 years, a 3-fold COX deficient stem cell division advantage, and a 1.25-fold cell cycle rate increase for COX deficient stem cells. The best fit to the biological data was achieved when all three perturbations were incorporated into the simulation (Figure 7-1D).

A better fit to the biological data via this method suggests that ageing is a multi-factorial process that cannot be described by one parameter, indicating that a combination of small perturbations in cellular homeostasis may be enough to drive the accumulation of mitochondrial dysfunction within tissues, contributing to the ageing process.

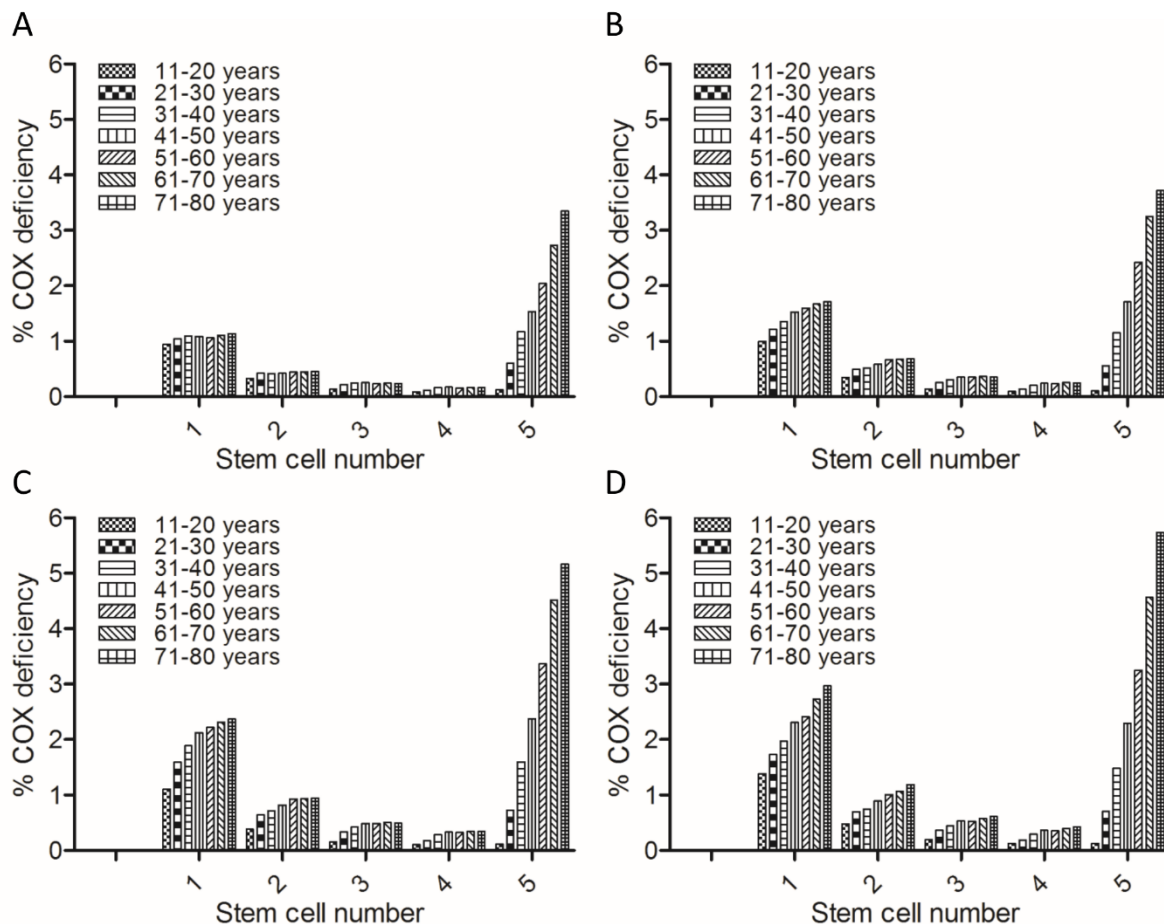


Figure 7-1 Modelling combined effects within niche succession model

A parameter scan was conducted with small alterations to the COX deficient stem cell advantages and mutation rate increase to simulate the effects of small perturbations to COX deficient stem cells. 5000 crypts were simulated, 75% mutated mtDNA conferred COX deficiency to a stem cell. 5 stem cells were simulated, each with 100 mtDNA molecules present. Asymmetric division probability was set to 0.99. A constant *de novo* mutation rate was set at 2×10^{-4} mutated mtDNA(mtDNA) replication unless otherwise stated. A division segregation factor was set at 1.03. (A) No advantage to COX deficient stem cells. (B) 1.25x increase in COX deficient stem cell divisions compared to normal. (C) 1.25x increase in COX deficient stem cell divisions compared to normal, plus a 3x increase in COX deficient stem cell divisions occurring symmetrically (2 stem cells). (D) The best fit simulation is acquired with a 1.25x increase in COX deficient stem cell divisions compared to normal, plus a 3x increase in COX deficient stem cell divisions occurring symmetrically (2 stem cells), plus a 2x increase in mutation rate from 0 to 80 years of age.

7.4 FUTURE WORK

As the model of human COX deficiency accumulation suggests there is an advantage for stem cells to divide symmetrically (2 stem cells) more often, this should be verified within an *in vivo* animal model. One method of determining division type involves visualising the orientation of the mitotic spindle within the stem cell compartment (Quyn *et al.*, 2010).

Asymmetrically dividing stem cells orient their mitotic spindle perpendicular to the apical surface, whilst symmetrically dividing stem cells orient their mitotic spindle parallel to the apical surface (Quyn *et al.*, 2010). High resolution multiphoton microscopy was required to determine the orientation of the mitotic spindle within dividing colonic stem cells (Quyn *et al.*, 2010). Quyn et al showed that precancerous and cancerous tissue from APC^{Min/-} mice lost their perpendicular alignment of the mitotic spindle, indicating that symmetric divisions were more prevalent (Quyn *et al.*, 2010). Determining whether this is true for colonic stem cells with mitochondrial dysfunction would strengthen the link between mitochondrial dysfunction and increased probability of malignant transformation, whilst also validating model findings.

As the work presented as part of this thesis suggests there is an advantage for stem cells with mitochondrial dysfunction to out-compete normal stem cells via a cell expansion advantage and a reduced cell cycle time, the mechanism by which this is brought about requires further investigation. One potential method of identifying this mechanism is by conducting RNA sequencing (RNA-seq) on normal and respiratory deficient stem cells (Tang *et al.*, 2009; Islam *et al.*, 2011; Hashimshony *et al.*, 2012). RNA-seq uses next generation sequencing technology to identify gene expression changes between two samples. In order to do this, single Lgr5+ stem cells from *Lgr5*^(+/-) mouse colons would need to be sorted via their innate fluorescence using a fluorescently activated cell sorting (FACS) method (Munoz *et al.*, 2012). Currently, it is not possible to determine the mitochondrial OXPHOS status of a cell before it has been FACS sorted, which would have to be done if one wants to compare normal versus respiratory deficient stem cells. However, as the majority of colonic stem cells from *Lgr5*^(+/-)*PolyA*^(-/-) mice are respiratory deficient (i.e. at least Complex I deficient) (section 5.4.4) stem cells sorted from *Lgr5*^(+/-)*PolyA*^(-/-) mouse colons can be classed as respiratory deficient and stem cells sorted from *Lgr5*^(+/-)*PolyA*^(+/+) mouse colons can be classed as normal. Therefore, the differentially expressed genes between normal and respiratory deficient cells can be investigated to determine candidate genes that influence cell cycle and division characteristics. If mitochondrial dysfunction is conveying an advantage to colonic stem cells, understanding the mechanism driving this is extremely important in order to target

the cellular pathways responsible. Slowing down the accumulation of mitochondrial dysfunction with age could slow down the rate at which tissues acquire dysfunction, which may be a key factor for allowing people to live healthier for longer.

Furthermore, as a dynamic relationship exists between the stem cell niches external environment and the stem cells themselves (section 1.8.3), it would also be advantageous to determine how ageing and mitochondrial dysfunction within the niche perturbs the actual function of normal stem cells, as this may be a contributory factor for cancer initiation and disease progression before an observable stem cell phenotype can be observed.

7.5 FINAL CONCLUSION

This thesis has provided evidence for mitochondrial dysfunction influencing the stem cell dynamics and cell cycle kinetics of mouse and human colonic stem cells. It has also provided evidence that there are 5 stem cells within normal human colonic crypts which divide asymmetrically the majority of the time under tissue homeostasis.

Due to the advantage stem cells with mitochondrial dysfunction possess, this significantly impacts on the rate at which mitochondrial dysfunction is accumulated within the colonic epithelium as a whole. Furthermore, due to this advantage, this may make it more likely for malignant transformation to take hold, and allow those stem cells to form tumours at a faster rate. This could be via ROS causing nuclear DNA damage, or increased number of cell divisions increasing the chance of nuclear DNA mutations. It has previously been suggested that tissues with higher number of cell divisions were more likely to develop cancer due to increased incorporation of DNA errors (Tomasetti and Vogelstein, 2015).

Understanding the mechanism by which this advantage acts is of great importance for it to be possible to target those cellular pathways responsible.

Chapter 8

Bibliography

Chapter 8 Bibliography

- Abramov, A.Y. and Duchen, M.R. (2010) 'Impaired mitochondrial bioenergetics determines glutamate-induced delayed calcium deregulation in neurons', *Biochim Biophys Acta*, 1800(3), pp. 297-304.
- Acin-Perez, R., Fernandez-Silva, P., Peleato, M.L., Perez-Martos, A. and Enriquez, J.A. (2008) 'Respiratory active mitochondrial supercomplexes', *Mol Cell*, 32(4), pp. 529-39.
- Agarwal, S. and Sohal, R.S. (1996) 'Relationship between susceptibility to protein oxidation, aging, and maximum life span potential of different species', *Exp Gerontol*, 31(3), pp. 365-72.
- Al Rawi, S., Louvet-Vallee, S., Djeddi, A., Sachse, M., Culetto, E., Hajjar, C., Boyd, L., Legouis, R. and Galy, V. (2011) 'Postfertilization autophagy of sperm organelles prevents paternal mitochondrial DNA transmission', *Science*, 334(6059), pp. 1144-7.
- Alberts, B. (2002) *Molecular biology of the cell*. 4th edn. New York: Garland Science.
- Alston, C.L., Lowe, J., Turnbull, D.M., Maddison, P. and Taylor, R.W. (2010) 'A novel mitochondrial tRNAGlu (MTTE) gene mutation causing chronic progressive external ophthalmoplegia at low levels of heteroplasmy in muscle', *J Neurol Sci*, 298(1-2), pp. 140-4.
- Anderson, S., Bankier, A.T., Barrell, B.G., de Bruijn, M.H., Coulson, A.R., Drouin, J., Eperon, I.C., Nierlich, D.P., Roe, B.A., Sanger, F., Schreier, P.H., Smith, A.J., Staden, R. and Young, I.G. (1981) 'Sequence and organization of the human mitochondrial genome', *Nature*, 290(5806), pp. 457-65.
- Ardail, D., Privat, J.P., Egret-Charlier, M., Levrat, C., Lerme, F. and Louisot, P. (1990) 'Mitochondrial contact sites. Lipid composition and dynamics', *J Biol Chem*, 265(31), pp. 18797-802.
- Ashley, M.V., Laipis, P.J. and Hauswirth, W.W. (1989) 'Rapid segregation of heteroplasmic bovine mitochondria', *Nucleic Acids Res*, 17(18), pp. 7325-31.
- Baines, H.L., Stewart, J.B., Stamp, C., Zupanic, A., Kirkwood, T.B., Larsson, N.G., Turnbull, D.M. and Greaves, L.C. (2014) 'Similar patterns of clonally expanded somatic mtDNA mutations in the colon of heterozygous mtDNA mutator mice and ageing humans', *Mech Ageing Dev*, 139, pp. 22-30.
- Baker, A.M., Cereser, B., Melton, S., Fletcher, A.G., Rodriguez-Justo, M., Tadrous, P.J., Humphries, A., Elia, G., McDonald, S.A., Wright, N.A., Simons, B.D., Jansen, M. and Graham, T.A. (2014) 'Quantification of crypt and stem cell evolution in the normal and neoplastic human colon', *Cell Rep*, 8(4), pp. 940-7.
- Balaban, R.S., Nemoto, S. and Finkel, T. (2005) 'Mitochondria, oxidants, and aging', *Cell*, 120(4), pp. 483-95.
- Baradaran, R., Berrisford, J.M., Minhas, G.S. and Sazanov, L.A. (2013) 'Crystal structure of the entire respiratory complex I', *Nature*, 494(7438), pp. 443-8.
- Barker, N., Ridgway, R.A., van Es, J.H., van de Wetering, M., Begthel, H., van den Born, M., Danenberg, E., Clarke, A.R., Sansom, O.J. and Clevers, H. (2009) 'Crypt stem cells as the cells-of-origin of intestinal cancer', *Nature*, 457(7229), pp. 608-11.
- Barker, N., van Es, J.H., Kuipers, J., Kujala, P., van den Born, M., Coijnsen, M., Haegebarth, A., Korving, J., Begthel, H., Peters, P.J. and Clevers, H. (2007) 'Identification of stem cells in small intestine and colon by marker gene Lgr5', *Nature*, 449(7165), pp. 1003-7.
- Baron, S. (1996) 'Medical Microbiology 4th Edition'.
- Barrell, B.G., Anderson, S., Bankier, A.T., de Bruijn, M.H., Chen, E., Coulson, A.R., Drouin, J., Eperon, I.C., Nierlich, D.P., Roe, B.A., Sanger, F., Schreier, P.H., Smith, A.J., Staden, R. and Young, I.G. (1980)

- 'Different pattern of codon recognition by mammalian mitochondrial tRNAs', *Proc Natl Acad Sci U S A*, 77(6), pp. 3164-6.
- Bender, A., Krishnan, K.J., Morris, C.M., Taylor, G.A., Reeve, A.K., Perry, R.H., Jaros, E., Hersheson, J.S., Betts, J., Klopstock, T., Taylor, R.W. and Turnbull, D.M. (2006) 'High levels of mitochondrial DNA deletions in substantia nigra neurons in aging and Parkinson disease', *Nat Genet*, 38(5), pp. 515-7.
- Beregi, E., Regius, O., Hutt, T. and Gobl, Z. (1988) 'Age-related changes in the skeletal muscle cells', *Z Gerontol*, 21(2), pp. 83-6.
- Bereiter-Hahn, J. (1978) 'Intracellular motility of mitochondria: role of the inner compartment in migration and shape changes of mitochondria in XTH-cells', *J Cell Sci*, 30, pp. 99-115.
- Berg, J.M., Tymoczko, J.L. and Stryer, L. (2011) *Biochemistry*. 7th edn. New York: W.H. Freeman.
- Berg, R.D. (1996) 'The indigenous gastrointestinal microflora', *Trends Microbiol*, 4(11), pp. 430-5.
- Bibb, M.J., Van Etten, R.A., Wright, C.T., Walberg, M.W. and Clayton, D.A. (1981) 'Sequence and gene organization of mouse mitochondrial DNA', *Cell*, 26(2 Pt 2), pp. 167-80.
- Bjorksten, J. and Tenhu, H. (1990) 'The crosslinking theory of aging--added evidence', *Exp Gerontol*, 25(2), pp. 91-5.
- Blackwood, J.K., Williamson, S.C., Greaves, L.C., Wilson, L., Rigas, A.C., Sandher, R., Pickard, R.S., Robson, C.N., Turnbull, D.M., Taylor, R.W. and Heer, R. (2011) 'In situ lineage tracking of human prostatic epithelial stem cell fate reveals a common clonal origin for basal and luminal cells', *J Pathol*, 225(2), pp. 181-8.
- Blasiak, J., Glowacki, S., Kauppinen, A. and Kaarniranta, K. (2013) 'Mitochondrial and nuclear DNA damage and repair in age-related macular degeneration', *Int J Mol Sci*, 14(2), pp. 2996-3010.
- Bleazard, W., McCaffery, J.M., King, E.J., Bale, S., Mozdy, A., Tieu, Q., Nunnari, J. and Shaw, J.M. (1999) 'The dynamin-related GTPase Dnm1 regulates mitochondrial fission in yeast', *Nat Cell Biol*, 1(5), pp. 298-304.
- Boulet, L., Karpati, G. and Shoubridge, E.A. (1992) 'Distribution and threshold expression of the tRNA(Lys) mutation in skeletal muscle of patients with myoclonic epilepsy and ragged-red fibers (MERRF)', *Am J Hum Genet*, 51(6), pp. 1187-200.
- Brand, M.D. (2010) 'The sites and topology of mitochondrial superoxide production', *Exp Gerontol*, 45(7-8), pp. 466-72.
- Brierley, E.J., Johnson, M.A., Lightowers, R.N., James, O.F. and Turnbull, D.M. (1998) 'Role of mitochondrial DNA mutations in human aging: implications for the central nervous system and muscle', *Ann Neurol*, 43(2), pp. 217-23.
- Brown, T.A., Tkachuk, A.N., Shtengel, G., Kopek, B.G., Bogenhagen, D.F., Hess, H.F. and Clayton, D.A. (2011) 'Superresolution fluorescence imaging of mitochondrial nucleoids reveals their spatial range, limits, and membrane interaction', *Mol Cell Biol*, 31(24), pp. 4994-5010.
- Cadenas, E. and Davies, K.J. (2000) 'Mitochondrial free radical generation, oxidative stress, and aging', *Free Radic Biol Med*, 29(3-4), pp. 222-30.
- Cairns, J. (1975) 'Mutation selection and the natural history of cancer', *Nature*, 255(5505), pp. 197-200.
- Carew, J.S. and Huang, P. (2002) 'Mitochondrial defects in cancer', *Mol Cancer*, 1, p. 9.
- Cavalli, L.R. and Liang, B.C. (1998) 'Mutagenesis, tumorigenicity, and apoptosis: are the mitochondria involved?', *Mutat Res*, 398(1-2), pp. 19-26.
- CDC (2015) 'United States Cancer Statistics: 1999–2012 Incidence and Mortality Web-based Report'.

- Cerritelli, S.M., Frolova, E.G., Feng, C., Grinberg, A., Love, P.E. and Crouch, R.J. (2003) 'Failure to produce mitochondrial DNA results in embryonic lethality in Rnaseh1 null mice', *Mol Cell*, 11(3), pp. 807-15.
- Chang, D.D. and Clayton, D.A. (1984) 'Precise identification of individual promoters for transcription of each strand of human mitochondrial DNA', *Cell*, 36(3), pp. 635-43.
- Chen, L.B. (1988) 'Mitochondrial membrane potential in living cells', *Annu Rev Cell Biol*, 4, pp. 155-81.
- Chomyn, A., Martinuzzi, A., Yoneda, M., Daga, A., Hurko, O., Johns, D., Lai, S.T., Nonaka, I., Angelini, C. and Attardi, G. (1992) 'MELAS mutation in mtDNA binding site for transcription termination factor causes defects in protein synthesis and in respiration but no change in levels of upstream and downstream mature transcripts', *Proc Natl Acad Sci U S A*, 89(10), pp. 4221-5.
- Cipolat, S., Martins de Brito, O., Dal Zilio, B. and Scorrano, L. (2004) 'OPA1 requires mitofusin 1 to promote mitochondrial fusion', *Proc Natl Acad Sci U S A*, 101(45), pp. 15927-32.
- Clayton, D.A. (1982) 'Replication of animal mitochondrial DNA', *Cell*, 28(4), pp. 693-705.
- Coller, H.A., Khrapko, K., Bodyak, N.D., Nekhaeva, E., Herrero-Jimenez, P. and Thilly, W.G. (2001) 'High frequency of homoplasmic mitochondrial DNA mutations in human tumors can be explained without selection', *Nat Genet*, 28(2), pp. 147-50.
- Cottrell, D.A., Blakely, E.L., Johnson, M.A., Ince, P.G. and Turnbull, D.M. (2001) 'Mitochondrial enzyme-deficient hippocampal neurons and choroidal cells in AD', *Neurology*, 57(2), pp. 260-4.
- Cuervo, A.M. and Dice, J.F. (2000) 'Age-related decline in chaperone-mediated autophagy', *J Biol Chem*, 275(40), pp. 31505-13.
- Cummings, J.G. (1975) 'The colon: Absorptive, seccretory and metabolic functions', *Digestion*, 13(4), pp. 232-40.
- Cummins, J.M., Wakayama, T. and Yanagimachi, R. (1997) 'Fate of microinjected sperm components in the mouse oocyte and embryo', *Zygote*, 5(4), pp. 301-8.
- Dubrovsky, E.B., Dubrovskaya, V.A., Levinger, L., Schiffer, S. and Marchfelder, A. (2004) 'Drosophila RNase Z processes mitochondrial and nuclear pre-tRNA 3' ends in vivo', *Nucleic Acids Res*, 32(1), pp. 255-62.
- Duchen, M.R. (2000) 'Mitochondria and calcium: from cell signalling to cell death', *J Physiol*, 529 Pt 1, pp. 57-68.
- Efremov, R.G., Baradaran, R. and Sazanov, L.A. (2010) 'The architecture of respiratory complex I', *Nature*, 465(7297), pp. 441-5.
- Ekstrand, M.I., Terzioglu, M., Galter, D., Zhu, S., Hofstetter, C., Lindqvist, E., Thams, S., Bergstrand, A., Hansson, F.S., Trifunovic, A., Hoffer, B., Cullheim, S., Mohammed, A.H., Olson, L. and Larsson, N.G. (2007) 'Progressive parkinsonism in mice with respiratory-chain-deficient dopamine neurons', *Proc Natl Acad Sci U S A*, 104(4), pp. 1325-30.
- Elson, J.L., Samuels, D.C., Turnbull, D.M. and Chinnery, P.F. (2001) 'Random intracellular drift explains the clonal expansion of mitochondrial DNA mutations with age', *Am J Hum Genet*, 68(3), pp. 802-6.
- Falkenberg, M., Gaspari, M., Rantanen, A., Trifunovic, A., Larsson, N.G. and Gustafsson, C.M. (2002) 'Mitochondrial transcription factors B1 and B2 activate transcription of human mtDNA', *Nat Genet*, 31(3), pp. 289-94.
- Falkenberg, M., Larsson, N.G. and Gustafsson, C.M. (2007) 'DNA replication and transcription in mammalian mitochondria', *Annu Rev Biochem*, 76, pp. 679-99.

- Fan, W., Waymire, K.G., Narula, N., Li, P., Rocher, C., Coskun, P.E., Vannan, M.A., Narula, J., Macgregor, G.R. and Wallace, D.C. (2008) 'A mouse model of mitochondrial disease reveals germline selection against severe mtDNA mutations', *Science*, 319(5865), pp. 958-62.
- Faxen, K., Gilderson, G., Adelroth, P. and Brzezinski, P. (2005) 'A mechanistic principle for proton pumping by cytochrome c oxidase', *Nature*, 437(7056), pp. 286-9.
- Fellous, T.G., Islam, S., Tadrous, P.J., Elia, G., Kocher, H.M., Bhattacharya, S., Mears, L., Turnbull, D.M., Taylor, R.W., Greaves, L.C., Chinnery, P.F., Taylor, G., McDonald, S.A., Wright, N.A. and Alison, M.R. (2009) 'Locating the stem cell niche and tracing hepatocyte lineages in human liver', *Hepatology*, 49(5), pp. 1655-63.
- FERLAY, J., SHIN, H.R., BRAY, F., FORMAN, D., MATHERS, C. and PARKIN, D.M. (2010) 'Estimates of worldwide burden of cancer in 2008: GLOBOCAN 2008', *Int J Cancer*, 127(12), pp. 2893-917.
- Finch, C.E. and Tanzi, R.E. (1997) 'Genetics of aging', *Science*, 278(5337), pp. 407-11.
- Fisher, R.P., Lisowsky, T., Parisi, M.A. and Clayton, D.A. (1992) 'DNA wrapping and bending by a mitochondrial high mobility group-like transcriptional activator protein', *J Biol Chem*, 267(5), pp. 3358-67.
- Fleming, J.E., Miquel, J., Cottrell, S.F., Yengoyan, L.S. and Economos, A.C. (1982) 'Is cell aging caused by respiration-dependent injury to the mitochondrial genome?', *Gerontology*, 28(1), pp. 44-53.
- Fletcher, A.G., Breward, C.J. and Jonathan Chapman, S. (2012) 'Mathematical modeling of monoclonal conversion in the colonic crypt', *J Theor Biol*, 300C, pp. 118-133.
- Frey, T.G. and Mannella, C.A. (2000) 'The internal structure of mitochondria', *Trends Biochem Sci*, 25(7), pp. 319-24.
- Garcia, S.B., Park, H.S., Novelli, M. and Wright, N.A. (1999) 'Field cancerization, clonality, and epithelial stem cells: the spread of mutated clones in epithelial sheets', *J Pathol*, 187(1), pp. 61-81.
- Garrido, N., Griparic, L., Jokitalo, E., Wartiovaara, J., van der Bliek, A.M. and Spelbrink, J.N. (2003) 'Composition and dynamics of human mitochondrial nucleoids', *Mol Biol Cell*, 14(4), pp. 1583-96.
- Gavaghan, D.J., Simpson, A.C., Lloyd, S., Mac Randal, D.F. and Boyd, D.R.S. (2005) 'Towards a Grid infrastructure to support integrative approaches to biological research', *Philosophical Transactions of the Royal Society a-Mathematical Physical and Engineering Sciences*, 363(1833), pp. 1829-1841.
- Giles, R.E., Blanc, H., Cann, H.M. and Wallace, D.C. (1980) 'Maternal inheritance of human mitochondrial DNA', *Proc Natl Acad Sci U S A*, 77(11), pp. 6715-9.
- Graham, T.A., Humphries, A., Sanders, T., Rodriguez-Justo, M., Tadrous, P.J., Preston, S.L., Novelli, M.R., Leedham, S.J., McDonald, S.A. and Wright, N.A. (2011) 'Use of methylation patterns to determine expansion of stem cell clones in human colon tissue', *Gastroenterology*, 140(4), pp. 1241-1250 e1-9.
- Gray, H. and Wong, T.W. (1992) 'Purification and identification of subunit structure of the human mitochondrial DNA polymerase', *J Biol Chem*, 267(9), pp. 5835-41.
- Greaves, L.C., Barron, M.J., Campbell-Shiel, G., Kirkwood, T.B. and Turnbull, D.M. (2011) 'Differences in the accumulation of mitochondrial defects with age in mice and humans', *Mech Ageing Dev*, 132(11-12), pp. 588-91.
- Greaves, L.C., Barron, M.J., Plusa, S., Kirkwood, T.B., Mathers, J.C., Taylor, R.W. and Turnbull, D.M. (2010) 'Defects in multiple complexes of the respiratory chain are present in ageing human colonic crypts', *Exp Gerontol*, 45(7-8), pp. 573-9.
- Greaves, L.C., Beadle, N.E., Taylor, G.A., Commane, D., Mathers, J.C., Khrapko, K. and Turnbull, D.M. (2009) 'Quantification of mitochondrial DNA mutation load', *Aging Cell*, 8(5), pp. 566-72.

- Greaves, L.C., Nooteboom, M., Elson, J.L., Tuppen, H.A., Taylor, G.A., Commane, D.M., Arasaradnam, R.P., Khrapko, K., Taylor, R.W., Kirkwood, T.B., Mathers, J.C. and Turnbull, D.M. (2014) 'Clonal expansion of early to mid-life mitochondrial DNA point mutations drives mitochondrial dysfunction during human ageing', *PLoS Genet*, 10(9), p. e1004620.
- Greaves, L.C., Preston, S.L., Tadrous, P.J., Taylor, R.W., Barron, M.J., Oukrif, D., Leedham, S.J., Deheragoda, M., Sasienski, P., Novelli, M.R., Jankowski, J.A., Turnbull, D.M., Wright, N.A. and McDonald, S.A. (2006) 'Mitochondrial DNA mutations are established in human colonic stem cells, and mutated clones expand by crypt fission', *Proc Natl Acad Sci U S A*, 103(3), pp. 714-9.
- Griffiths, D.F.R., Williams, G.T., Davies, S., Williams, D. and Williams, E.D. (1988) 'Visualization of Somatic Mutation Provides an Inducible Clonal Marker System That Shows That Colonic Crypts Are Maintained by a Single Stem-Cell', *Gut*, 29(5), pp. A722-A722.
- Hagerhall, C. (1997) 'Succinate: quinone oxidoreductases. Variations on a conserved theme', *Biochim Biophys Acta*, 1320(2), pp. 107-41.
- Haraguchi, N., Ohkuma, M., Sakashita, H., Matsuzaki, S., Tanaka, F., Mimori, K., Kamohara, Y., Inoue, H. and Mori, M. (2008) 'CD133+CD44+ population efficiently enriches colon cancer initiating cells', *Ann Surg Oncol*, 15(10), pp. 2927-33.
- Haramis, A.P., Begthel, H., van den Born, M., van Es, J., Jonkheer, S., Offerhaus, G.J. and Clevers, H. (2004) 'De novo crypt formation and juvenile polyposis on BMP inhibition in mouse intestine', *Science*, 303(5664), pp. 1684-6.
- Harley, C.B., Vaziri, H., Counter, C.M. and Allsopp, R.C. (1992) 'The telomere hypothesis of cellular aging', *Exp Gerontol*, 27(4), pp. 375-82.
- Harman, D. (1956) 'Aging: a theory based on free radical and radiation chemistry', *J Gerontol*, 11(3), pp. 298-300.
- Harman, D. (1972) 'The biological clock: the mitochondria?', *J Am Geriatr Soc*, 20(4), pp. 145-7.
- Hart, R.W. and Setlow, R.B. (1974) 'Correlation between deoxyribonucleic acid excision-repair and life-span in a number of mammalian species', *Proc Natl Acad Sci U S A*, 71(6), pp. 2169-73.
- Hashimshony, T., Wagner, F., Sher, N. and Yanai, I. (2012) 'CEL-Seq: single-cell RNA-Seq by multiplexed linear amplification', *Cell Rep*, 2(3), pp. 666-73.
- Hatifi, Y. (1985) 'The mitochondrial electron transport and oxidative phosphorylation system', *Annu Rev Biochem*, 54, pp. 1015-69.
- Hauswirth, W.W. and Laipis, P.J. (1982) 'Mitochondrial DNA polymorphism in a maternal lineage of Holstein cows', *Proc Natl Acad Sci U S A*, 79(15), pp. 4686-90.
- Hawlicsek, G., Schneider, H., Schmidt, B., Tropschug, M., Hartl, F.U. and Neupert, W. (1988) 'Mitochondrial protein import: identification of processing peptidase and of PEP, a processing enhancing protein', *Cell*, 53(5), pp. 795-806.
- He, X.C., Zhang, J., Tong, W.G., Tawfik, O., Ross, J., Scoville, D.H., Tian, Q., Zeng, X., He, X., Wiedemann, L.M., Mishina, Y. and Li, L. (2004) 'BMP signaling inhibits intestinal stem cell self-renewal through suppression of Wnt-beta-catenin signaling', *Nat Genet*, 36(10), pp. 1117-21.
- Herzig, S., Long, F., Jhala, U.S., Hedrick, S., Quinn, R., Bauer, A., Rudolph, D., Schutz, G., Yoon, C., Puigserver, P., Spiegelman, B. and Montminy, M. (2001) 'CREB regulates hepatic gluconeogenesis through the coactivator PGC-1', *Nature*, 413(6852), pp. 179-83.
- Hinttala, R., Smeets, R., Moilanen, J.S., Ugalde, C., Uusimaa, J., Smeitink, J.A. and Majamaa, K. (2006) 'Analysis of mitochondrial DNA sequences in patients with isolated or combined oxidative phosphorylation system deficiency', *J Med Genet*, 43(11), pp. 881-6.

- Hirst, J., Carroll, J., Fearnley, I.M., Shannon, R.J. and Walker, J.E. (2003) 'The nuclear encoded subunits of complex I from bovine heart mitochondria', *Biochim Biophys Acta*, 1604(3), pp. 135-50.
- Holt, I.J., Lorimer, H.E. and Jacobs, H.T. (2000) 'Coupled leading-and lagging-strand synthesis of mammalian mitochondrial DNA', *Cell*, 100(5), pp. 515-24.
- Holzmann, J., Frank, P., Loffler, E., Bennett, K.L., Gerner, C. and Rossmanith, W. (2008) 'RNase P without RNA: identification and functional reconstitution of the human mitochondrial tRNA processing enzyme', *Cell*, 135(3), pp. 462-74.
- Hoppins, S., Lackner, L. and Nunnari, J. (2007) 'The machines that divide and fuse mitochondria', *Annu Rev Biochem*, 76, pp. 751-80.
- Inomata, H., Haraguchi, T. and Sasai, Y. (2008) 'Robust stability of the embryonic axial pattern requires a secreted scaffold for chordin degradation', *Cell*, 134(5), pp. 854-65.
- Islam, S., Kjallquist, U., Moliner, A., Zajac, P., Fan, J.B., Lonnerberg, P. and Linnarsson, S. (2011) 'Characterization of the single-cell transcriptional landscape by highly multiplex RNA-seq', *Genome Res*, 21(7), pp. 1160-7.
- Ivanova, R., Lepage, V., Loste, M.N., Schachter, F., Wijnen, E., Busson, M., Cayuela, J.M., Sigaux, F. and Charron, D. (1998) 'Mitochondrial DNA sequence variation in human leukemic cells', *Int J Cancer*, 76(4), pp. 495-8.
- Jacobson, J. and Duchen, M.R. (2004) 'Interplay between mitochondria and cellular calcium signalling', *Mol Cell Biochem*, 256-257(1-2), pp. 209-18.
- Jeronimo, C., Nomoto, S., Caballero, O.L., Usadel, H., Henrique, R., Varzim, G., Oliveira, J., Lopes, C., Fliss, M.S. and Sidransky, D. (2001) 'Mitochondrial mutations in early stage prostate cancer and bodily fluids', *Oncogene*, 20(37), pp. 5195-8.
- Johansson, M.E., Phillipson, M., Petersson, J., Velcich, A., Holm, L. and Hansson, G.C. (2008) 'The inner of the two Muc2 mucin-dependent mucus layers in colon is devoid of bacteria', *Proc Natl Acad Sci U S A*, 105(39), pp. 15064-9.
- Jouaville, L.S., Pinton, P., Bastianutto, C., Rutter, G.A. and Rizzuto, R. (1999) 'Regulation of mitochondrial ATP synthesis by calcium: evidence for a long-term metabolic priming', *Proc Natl Acad Sci U S A*, 96(24), pp. 13807-12.
- Kaguni, L.S. (2004) 'DNA polymerase gamma, the mitochondrial replicase', *Annu Rev Biochem*, 73, pp. 293-320.
- Katajisto, P., Dohla, J., Chaffer, C.L., Penttikätko, N., Marjanovic, N., Iqbal, S., Zoncu, R., Chen, W., Weinberg, R.A. and Sabatini, D.M. (2015) 'Asymmetric apportioning of aged mitochondria between daughter cells is required for stemness', *Science*, 348(6232), pp. 340-343.
- Kellett, M., Potten, C.S. and Rew, D.A. (1992) 'A comparison of in vivo cell proliferation measurements in the intestine of mouse and man', *Epithelial Cell Biol*, 1(4), pp. 147-55.
- Kim, K.M. and Shibata, D. (2002) 'Methylation reveals a niche: stem cell succession in human colon crypts', *Oncogene*, 21(35), pp. 5441-9.
- Kirichok, Y., Krapivinsky, G. and Clapham, D.E. (2004) 'The mitochondrial calcium uniporter is a highly selective ion channel', *Nature*, 427(6972), pp. 360-4.
- Kirkwood, T.B. (1977) 'Evolution of ageing', *Nature*, 270(5635), pp. 301-4.
- Kirkwood, T.B. (1995) 'What can evolution theory tell us about the mechanism of ageing?', *Molecular Aspects of Ageing*.
- Kirkwood, T.B. (2005) 'Understanding the odd science of aging', *Cell*, 120(4), pp. 437-47.

- Kirkwood, T.B. (2008) 'Understanding ageing from an evolutionary perspective', *J Intern Med*, 263(2), pp. 117-27.
- Kolesar, J.E., Safdar, A., Abadi, A., MacNeil, L.G., Crane, J.D., Tarnopolsky, M.A. and Kaufman, B.A. (2014) 'Defects in mitochondrial DNA replication and oxidative damage in muscle of mtDNA mutator mice', *Free Radic Biol Med*, 75, pp. 241-51.
- Kopsidas, G., Kovalenko, S.A., Kelso, J.M. and Linnane, A.W. (1998) 'An age-associated correlation between cellular bioenergy decline and mtDNA rearrangements in human skeletal muscle', *Mutat Res*, 421(1), pp. 27-36.
- Korhonen, J.A., Gaspari, M. and Falkenberg, M. (2003) 'TWINKLE Has 5' -> 3' DNA helicase activity and is specifically stimulated by mitochondrial single-stranded DNA-binding protein', *J Biol Chem*, 278(49), pp. 48627-32.
- Koshiba, T., Detmer, S.A., Kaiser, J.T., Chen, H., McCaffery, J.M. and Chan, D.C. (2004) 'Structural basis of mitochondrial tethering by mitofusin complexes', *Science*, 305(5685), pp. 858-62.
- Kozar, S., Morrissey, E., Nicholson, A.M., van der Heijden, M., Zecchini, H.I., Kemp, R., Tavare, S., Vermeulen, L. and Winton, D.J. (2013) 'Continuous clonal labeling reveals small numbers of functional stem cells in intestinal crypts and adenomas', *Cell Stem Cell*, 13(5), pp. 626-33.
- Kraytsberg, Y., Bodyak, N., Myerow, S., Nicholas, A., Ebralidze, K. and Khrapko, K. (2009) 'Quantitative analysis of somatic mitochondrial DNA mutations by single-cell single-molecule PCR', *Methods Mol Biol*, 554, pp. 329-69.
- Kraytsberg, Y., Kudryavtseva, E., McKee, A.C., Geula, C., Kowall, N.W. and Khrapko, K. (2006) 'Mitochondrial DNA deletions are abundant and cause functional impairment in aged human substantia nigra neurons', *Nat Genet*, 38(5), pp. 518-20.
- Kreso, A., van Galen, P., Pedley, N.M., Lima-Fernandes, E., Frelin, C., Davis, T., Cao, L., Baiazitov, R., Du, W., Sydorenko, N., Moon, Y.C., Gibson, L., Wang, Y., Leung, C., Iscove, N.N., Arrowsmith, C.H., Szentgyorgyi, E., Gallinger, S., Dick, J.E. and O'Brien, C.A. (2014) 'Self-renewal as a therapeutic target in human colorectal cancer', *Nat Med*, 20(1), pp. 29-36.
- Kujoth, G.C., Hiona, A., Pugh, T.D., Someya, S., Panzer, K., Wohlgemuth, S.E., Hofer, T., Seo, A.Y., Sullivan, R., Jobling, W.A., Morrow, J.D., Van Remmen, H., Sedivy, J.M., Yamasoba, T., Tanokura, M., Weindruch, R., Leeuwenburgh, C. and Prolla, T.A. (2005) 'Mitochondrial DNA mutations, oxidative stress, and apoptosis in mammalian aging', *Science*, 309(5733), pp. 481-4.
- Kushnareva, Y., Murphy, A.N. and Andreyev, A. (2002) 'Complex I-mediated reactive oxygen species generation: modulation by cytochrome c and NAD(P)+ oxidation-reduction state', *Biochem J*, 368(Pt 2), pp. 545-53.
- Lee, H.C., Yin, P.H., Lin, J.C., Wu, C.C., Chen, C.Y., Wu, C.W., Chi, C.W., Tam, T.N. and Wei, Y.H. (2005) 'Mitochondrial genome instability and mtDNA depletion in human cancers', *Ann NY Acad Sci*, 1042, pp. 109-22.
- Lerin, C., Rodgers, J.T., Kalume, D.E., Kim, S.H., Pandey, A. and Puigserver, P. (2006) 'GCN5 acetyltransferase complex controls glucose metabolism through transcriptional repression of PGC-1alpha', *Cell Metab*, 3(6), pp. 429-38.
- Li, L. and Neaves, W.B. (2006) 'Normal stem cells and cancer stem cells: the niche matters', *Cancer Res*, 66(9), pp. 4553-7.
- Lievre, A., Chapusot, C., Bouvier, A.M., Zinzindohoue, F., Piard, F., Roignot, P., Arnould, L., Beaune, P., Faivre, J. and Laurent-Puig, P. (2005) 'Clinical value of mitochondrial mutations in colorectal cancer', *J Clin Oncol*, 23(15), pp. 3517-25.

- Lightowlers, R.N., Chinnery, P.F., Turnbull, D.M. and Howell, N. (1997) 'Mammalian mitochondrial genetics: heredity, heteroplasmy and disease', *Trends Genet*, 13(11), pp. 450-5.
- Linnane, A.W., Marzuki, S., Ozawa, T. and Tanaka, M. (1989) 'Mitochondrial DNA mutations as an important contributor to ageing and degenerative diseases', *Lancet*, 1(8639), pp. 642-5.
- Litonin, D., Sologub, M., Shi, Y., Savkina, M., Anikin, M., Falkenberg, M., Gustafsson, C.M. and Temiakov, D. (2010) 'Human mitochondrial transcription revisited: only TFAM and TFB2M are required for transcription of the mitochondrial genes in vitro', *J Biol Chem*, 285(24), pp. 18129-33.
- Liu, L. and Rando, T.A. (2011) 'Manifestations and mechanisms of stem cell aging', *J Cell Biol*, 193(2), pp. 257-66.
- Loeffler, M., Birke, A., Winton, D. and Potten, C. (1993) 'Somatic mutation, monoclonality and stochastic models of stem cell organization in the intestinal crypt', *J Theor Biol*, 160(4), pp. 471-91.
- Loeffler, M., Bratke, T., Paulus, U., Li, Y.Q. and Potten, C.S. (1997) 'Clonality and life cycles of intestinal crypts explained by a state dependent stochastic model of epithelial stem cell organization', *J Theor Biol*, 186(1), pp. 41-54.
- Logan, A., Shabalina, I.G., Prime, T.A., Rogatti, S., Kalinovich, A.V., Hartley, R.C., Budd, R.C., Cannon, B. and Murphy, M.P. (2014) 'In vivo levels of mitochondrial hydrogen peroxide increase with age in mtDNA mutator mice', *Aging Cell*, 13(4), pp. 765-8.
- Lopez-Garcia, C., Klein, A.M., Simons, B.D. and Winton, D.J. (2010) 'Intestinal stem cell replacement follows a pattern of neutral drift', *Science*, 330(6005), pp. 822-5.
- Loschen, G., Gunzler, W.A. and Flohe, L. (1972) '[Kinetic mechanism of glutathione:H₂O₂ - oxidoreductase]', *Hoppe Seylers Z Physiol Chem*, 353(5), p. 733.
- Margulis, L. (1971) 'Symbiosis and evolution', *Sci Am*, 225(2), pp. 48-57.
- Martin, W. and Muller, M. (1998) 'The hydrogen hypothesis for the first eukaryote', *Nature*, 392(6671), pp. 37-41.
- Maslov, A.Y., Barone, T.A., Plunkett, R.J. and Pruitt, S.C. (2004) 'Neural stem cell detection, characterization, and age-related changes in the subventricular zone of mice', *J Neurosci*, 24(7), pp. 1726-33.
- McCord, J.M. and Fridovich, I. (1969) 'Superoxide dismutase. An enzymic function for erythrocuprein (hemocuprein)', *J Biol Chem*, 244(22), pp. 6049-55.
- McCormack, J.G., Halestrap, A.P. and Denton, R.M. (1990) 'Role of calcium ions in regulation of mammalian intramitochondrial metabolism', *Physiol Rev*, 70(2), pp. 391-425.
- McDonald, S.A., Greaves, L.C., Gutierrez-Gonzalez, L., Rodriguez-Justo, M., Deheragoda, M., Leedham, S.J., Taylor, R.W., Lee, C.Y., Preston, S.L., Lovell, M., Hunt, T., Elia, G., Oukrif, D., Harrison, R., Novelli, M.R., Mitchell, I., Stoker, D.L., Turnbull, D.M., Jankowski, J.A. and Wright, N.A. (2008) 'Mechanisms of field cancerization in the human stomach: the expansion and spread of mutated gastric stem cells', *Gastroenterology*, 134(2), pp. 500-10.
- McKay, D.M. (2005) 'Good bug, bad bug: in the case of enteric inflammatory disease does the epithelium decide?', *Mem Inst Oswaldo Cruz*, 100 Suppl 1, pp. 205-10.
- Medawar, P.B. (1952) *An unsolved problem of biology*. London,: Published for the college by H. K. Lewis.
- Meineke, F.A., Potten, C.S. and Loeffler, M. (2001) 'Cell migration and organization in the intestinal crypt using a lattice-free model', *Cell Proliferation*, 34(4), pp. 253-266.

- Miquel, J., Economos, A.C., Fleming, J. and Johnson, J.E., Jr. (1980) 'Mitochondrial role in cell aging', *Exp Gerontol*, 15(6), pp. 575-91.
- Mitchell, P. (1961) 'Coupling of phosphorylation to electron and hydrogen transfer by a chemi-osmotic type of mechanism', *Nature*, 191, pp. 144-8.
- Mitchell, P. (1976) 'Possible molecular mechanisms of the protonmotive function of cytochrome systems', *J Theor Biol*, 62(2), pp. 327-67.
- Montoya, J., Christianson, T., Levens, D., Rabinowitz, M. and Attardi, G. (1982) 'Identification of initiation sites for heavy-strand and light-strand transcription in human mitochondrial DNA', *Proc Natl Acad Sci U S A*, 79(23), pp. 7195-9.
- Moran, P.A.P. (1962) *The statistical processes of evolutionary theory*. Oxford,: Clarendon Press.
- Moreno-Lastres, D., Fontanesi, F., Garcia-Consuegra, I., Martin, M.A., Arenas, J., Barrientos, A. and Ugalde, C. (2012) 'Mitochondrial complex I plays an essential role in human respirasome assembly', *Cell Metab*, 15(3), pp. 324-35.
- Moreno, R.D., Ramalho-Santos, J., Chan, E.K., Wessel, G.M. and Schatten, G. (2000) 'The Golgi apparatus segregates from the lysosomal/acrosomal vesicle during rhesus spermiogenesis: structural alterations', *Dev Biol*, 219(2), pp. 334-49.
- Morrison, S.J. and Spradling, A.C. (2008) 'Stem cells and niches: mechanisms that promote stem cell maintenance throughout life', *Cell*, 132(4), pp. 598-611.
- Mozdy, A.D., McCaffery, J.M. and Shaw, J.M. (2000) 'Dnm1p GTPase-mediated mitochondrial fission is a multi-step process requiring the novel integral membrane component Fis1p', *J Cell Biol*, 151(2), pp. 367-80.
- Muller-Hocker, J. (1990) 'Cytochrome c oxidase deficient fibres in the limb muscle and diaphragm of man without muscular disease: an age-related alteration', *J Neurol Sci*, 100(1-2), pp. 14-21.
- Munoz, J., Stange, D.E., Schepers, A.G., van de Wetering, M., Koo, B.K., Itzkovitz, S., Volckmann, R., Kung, K.S., Koster, J., Radulescu, S., Myant, K., Versteeg, R., Sansom, O.J., van Es, J.H., Barker, N., van Oudenaarden, A., Mohammed, S., Heck, A.J. and Clevers, H. (2012) 'The Lgr5 intestinal stem cell signature: robust expression of proposed quiescent '+4' cell markers', *EMBOJ*, 31(14), pp. 3079-91.
- Nakamura, M., Okano, H., Blendy, J.A. and Montell, C. (1994) 'Musashi, a neural RNA-binding protein required for Drosophila adult external sensory organ development', *Neuron*, 13(1), pp. 67-81.
- Newmeyer, D.D. and Ferguson-Miller, S. (2003) 'Mitochondria: releasing power for life and unleashing the machineries of death', *Cell*, 112(4), pp. 481-90.
- Nicolas, P., Kim, K.M., Shibata, D. and Tavare, S. (2007) 'The stem cell population of the human colon crypt: analysis via methylation patterns', *PLoS Comput Biol*, 3(3), p. e28.
- Nijtmans, L., Ugalde C, van den Heuvel LP, Smeitink JAM. (2004) 'Function and dysfunction of the oxidative phosphorylation system', *Mitochondrial Function and Biogenesis*, 8, pp. 149-176.
- Nishikawa, M., Oshitani, N., Matsumoto, T., Nishigami, T., Arakawa, T. and Inoue, M. (2005) 'Accumulation of mitochondrial DNA mutation with colorectal carcinogenesis in ulcerative colitis', *Br J Cancer*, 93(3), pp. 331-7.
- Nishimura, S., Wakabayashi, N., Toyoda, K., Kashima, K. and Mitsufuji, S. (2003) 'Expression of Musashi-1 in human normal colon crypt cells: a possible stem cell marker of human colon epithelium', *Dig Dis Sci*, 48(8), pp. 1523-9.
- Noji, H., Yasuda, R., Yoshida, M. and Kinoshita, K., Jr. (1997) 'Direct observation of the rotation of F1-ATPase', *Nature*, 386(6622), pp. 299-302.

- Nomoto, S., Yamashita, K., Koshikawa, K., Nakao, A. and Sidransky, D. (2002) 'Mitochondrial D-loop mutations as clonal markers in multicentric hepatocellular carcinoma and plasma', *Clin Cancer Res*, 8(2), pp. 481-7.
- Nooteboom, M., Johnson, R., Taylor, R.W., Wright, N.A., Lightowers, R.N., Kirkwood, T.B., Mathers, J.C., Turnbull, D.M. and Greaves, L.C. (2010) 'Age-associated mitochondrial DNA mutations lead to small but significant changes in cell proliferation and apoptosis in human colonic crypts', *Aging Cell*, 9(1), pp. 96-9.
- Novelli, M.R., Williamson, J.A., Tomlinson, I.P., Elia, G., Hodgson, S.V., Talbot, I.C., Bodmer, W.F. and Wright, N.A. (1996) 'Polyclonal origin of colonic adenomas in an XO/XY patient with FAP', *Science*, 272(5265), pp. 1187-90.
- Nunnari, J., Marshall, W.F., Straight, A., Murray, A., Sedat, J.W. and Walter, P. (1997) 'Mitochondrial transmission during mating in *Saccharomyces cerevisiae* is determined by mitochondrial fusion and fission and the intramitochondrial segregation of mitochondrial DNA', *Mol Biol Cell*, 8(7), pp. 1233-42.
- O'Brien, C.A., Pollett, A., Gallinger, S. and Dick, J.E. (2007) 'A human colon cancer cell capable of initiating tumour growth in immunodeficient mice', *Nature*, 445(7123), pp. 106-10.
- Ojala, D., Montoya, J. and Attardi, G. (1981) 'tRNA punctuation model of RNA processing in human mitochondria', *Nature*, 290(5806), pp. 470-4.
- Otera, H., Wang, C., Cleland, M.M., Setoguchi, K., Yokota, S., Youle, R.J. and Mihara, K. (2010) 'Mff is an essential factor for mitochondrial recruitment of Drp1 during mitochondrial fission in mammalian cells', *J Cell Biol*, 191(6), pp. 1141-58.
- Ozawa, T. (1997) 'Genetic and functional changes in mitochondria associated with aging', *Physiol Rev*, 77(2), pp. 425-64.
- Palade, G.E. (1952) 'The fine structure of mitochondria', *Anat Rec*, 114(3), pp. 427-51.
- Paradkar, P.N., Zumbrennen, K.B., Paw, B.H., Ward, D.M. and Kaplan, J. (2009) 'Regulation of mitochondrial iron import through differential turnover of mitoferrin 1 and mitoferrin 2', *Mol Cell Biol*, 29(4), pp. 1007-16.
- Park, H.S., Goodlad, R.A. and Wright, N.A. (1995) 'Crypt fission in the small intestine and colon. A mechanism for the emergence of G6PD locus-mutated crypts after treatment with mutagens', *Am J Pathol*, 147(5), pp. 1416-27.
- Park, J.S., Sharma, L.K., Li, H.Z., Xiang, R.H., Holstein, D., Wu, J., Lechleiter, J., Naylor, S.L., Deng, J.J., Lu, J.X. and Bai, Y.D. (2009) 'A heteroplasmic, not homoplasmic, mitochondrial DNA mutation promotes tumorigenesis via alteration in reactive oxygen species generation and apoptosis', *Human Molecular Genetics*, 18(9), pp. 1578-1589.
- Peterson, L.W. and Artis, D. (2014) 'Intestinal epithelial cells: regulators of barrier function and immune homeostasis', *Nat Rev Immunol*, 14(3), pp. 141-53.
- Pfaff, E. and Klingenberg, M. (1968) 'Adenine nucleotide translocation of mitochondria. 1. Specificity and control', *Eur J Biochem*, 6(1), pp. 66-79.
- Pfanner, N., Hartl, F.U. and Neupert, W. (1988) 'Import of proteins into mitochondria: a multi-step process', *Eur J Biochem*, 175(2), pp. 205-12.
- Pinto, D., Gregorieff, A., Begthel, H. and Clevers, H. (2003) 'Canonical Wnt signals are essential for homeostasis of the intestinal epithelium', *Genes Dev*, 17(14), pp. 1709-13.
- Pinz, K.G. and Bogenhagen, D.F. (1998) 'Efficient repair of abasic sites in DNA by mitochondrial enzymes', *Mol Cell Biol*, 18(3), pp. 1257-65.

- Pitt-Francis, J., Bernabeu, M.O., Cooper, J., Garny, A., Momtahan, L., Osborne, J., Pathmanathan, P., Rodriguez, B., Whiteley, J.P. and Gavaghan, D.J. (2008) 'Chaste: using agile programming techniques to develop computational biology software', *Philosophical Transactions of the Royal Society a-Mathematical Physical and Engineering Sciences*, 366(1878), pp. 3111-3136.
- Polyak, K., Li, Y., Zhu, H., Lengauer, C., Willson, J.K., Markowitz, S.D., Trush, M.A., Kinzler, K.W. and Vogelstein, B. (1998) 'Somatic mutations of the mitochondrial genome in human colorectal tumours', *Nat Genet*, 20(3), pp. 291-3.
- Potten, C.S. (1998) 'Stem cells in gastrointestinal epithelium: numbers, characteristics and death', *Philos Trans R Soc Lond B Biol Sci*, 353(1370), pp. 821-30.
- Potten, C.S., Kellett, M., Roberts, S.A., Rew, D.A. and Wilson, G.D. (1992) 'Measurement of in vivo proliferation in human colorectal mucosa using bromodeoxyuridine', *Gut*, 33(1), pp. 71-8.
- Potten, C.S., Kovacs, L. and Hamilton, E. (1974) 'Continuous labelling studies on mouse skin and intestine', *Cell Tissue Kinet*, 7(3), pp. 271-83.
- Potten, C.S. and Loeffler, M. (1990) 'Stem cells: attributes, cycles, spirals, pitfalls and uncertainties. Lessons for and from the crypt', *Development*, 110(4), pp. 1001-20.
- Potten, C.S., Owen, G. and Booth, D. (2002) 'Intestinal stem cells protect their genome by selective segregation of template DNA strands', *J Cell Sci*, 115(Pt 11), pp. 2381-8.
- Pozzan, T., Magalhaes, P. and Rizzuto, R. (2000) 'The comeback of mitochondria to calcium signalling', *Cell Calcium*, 28(5-6), pp. 279-83.
- Puigserver, P. and Spiegelman, B.M. (2003) 'Peroxisome proliferator-activated receptor-gamma coactivator 1 alpha (PGC-1alpha): transcriptional coactivator and metabolic regulator', *Endocr Rev*, 24(1), pp. 78-90.
- Puigserver, P., Wu, Z., Park, C.W., Graves, R., Wright, M. and Spiegelman, B.M. (1998) 'A cold-inducible coactivator of nuclear receptors linked to adaptive thermogenesis', *Cell*, 92(6), pp. 829-39.
- Quyn, A.J., Appleton, P.L., Carey, F.A., Steele, R.J., Barker, N., Clevers, H., Ridgway, R.A., Sansom, O.J. and Nathke, I.S. (2010) 'Spindle orientation bias in gut epithelial stem cell compartments is lost in precancerous tissue', *Cell Stem Cell*, 6(2), pp. 175-81.
- Radermacher, M., Ruiz, T., Clason, T., Benjamin, S., Brandt, U. and Zickermann, V. (2006) 'The three-dimensional structure of complex I from *Yarrowia lipolytica*: a highly dynamic enzyme', *J Struct Biol*, 154(3), pp. 269-79.
- Rebelo, A.P., Dillon, L.M. and Moraes, C.T. (2011) 'Mitochondrial DNA transcription regulation and nucleoid organization', *J Inherit Metab Dis*, 34(4), pp. 941-51.
- Reeve, A.K., Krishnan, K.J. and Turnbull, D. (2008) 'Mitochondrial DNA mutations in disease, aging, and neurodegeneration', *Ann NY Acad Sci*, 1147, pp. 21-9.
- Reya, T., Morrison, S.J., Clarke, M.F. and Weissman, I.L. (2001) 'Stem cells, cancer, and cancer stem cells', *Nature*, 414(6859), pp. 105-11.
- Reyes, A., Mezzina, M. and Gadaleta, G. (2002) 'Human mitochondrial transcription factor A (mtTFA): gene structure and characterization of related pseudogenes', *Gene*, 291(1-2), pp. 223-32.
- Ritsma, L., Ellenbroek, S.I., Zomer, A., Snippert, H.J., de Sauvage, F.J., Simons, B.D., Clevers, H. and van Rheenen, J. (2014) 'Intestinal crypt homeostasis revealed at single-stem-cell level by in vivo live imaging', *Nature*, 507(7492), pp. 362-5.
- Rossi, D.J., Bryder, D., Zahn, J.M., Ahlenius, H., Sonu, R., Wagers, A.J. and Weissman, I.L. (2005) 'Cell intrinsic alterations underlie hematopoietic stem cell aging', *Proc Natl Acad Sci U S A*, 102(26), pp. 9194-9.

- Rossignol, R., Malgat, M., Mazat, J.P. and Letellier, T. (1999) 'Threshold effect and tissue specificity. Implication for mitochondrial cytopathies', *J Biol Chem*, 274(47), pp. 33426-32.
- Rouault, T.A. and Tong, W.H. (2005) 'Iron-sulphur cluster biogenesis and mitochondrial iron homeostasis', *Nat Rev Mol Cell Biol*, 6(4), pp. 345-51.
- Ryu, J.M., Lee, H.J., Jung, Y.H., Lee, K.H., Kim, D.I., Kim, J.Y., Ko, S.H., Choi, G.E., Chai, II, Song, E.J., Oh, J.Y., Lee, S.J. and Han, H.J. (2015) 'Regulation of Stem Cell Fate by ROS-mediated Alteration of Metabolism', *Int J Stem Cells*, 8(1), pp. 24-35.
- Sangiorgi, E. and Capecchi, M.R. (2008) 'Bmi1 is expressed in vivo in intestinal stem cells', *Nat Genet*, 40(7), pp. 915-20.
- Sato, T. and Clevers, H. (2013) 'Growing self-organizing mini-guts from a single intestinal stem cell: mechanism and applications', *Science*, 340(6137), pp. 1190-4.
- Sato, T., van Es, J.H., Snippert, H.J., Stange, D.E., Vries, R.G., van den Born, M., Barker, N., Shroyer, N.F., van de Wetering, M. and Clevers, H. (2011) 'Paneth cells constitute the niche for Lgr5 stem cells in intestinal crypts', *Nature*, 469(7330), pp. 415-8.
- Sato, T., Vries, R.G., Snippert, H.J., van de Wetering, M., Barker, N., Stange, D.E., van Es, J.H., Abo, A., Kujala, P., Peters, P.J. and Clevers, H. (2009) 'Single Lgr5 stem cells build crypt-villus structures in vitro without a mesenchymal niche', *Nature*, 459(7244), pp. 262-U147.
- Sazanov, L.A. (2007) 'Respiratory complex I: mechanistic and structural insights provided by the crystal structure of the hydrophilic domain', *Biochemistry*, 46(9), pp. 2275-88.
- Schagger, H. and Pfeiffer, K. (2000) 'Supercomplexes in the respiratory chains of yeast and mammalian mitochondria', *EMBO J*, 19(8), pp. 1777-83.
- Schepers, A.G., Snippert, H.J., Stange, D.E., van den Born, M., van Es, J.H., van de Wetering, M. and Clevers, H. (2012) 'Lineage tracing reveals Lgr5+ stem cell activity in mouse intestinal adenomas', *Science*, 337(6095), pp. 730-5.
- Schmidt, G.H., Winton, D.J. and Ponder, B.A. (1988) 'Development of the pattern of cell renewal in the crypt-villus unit of chimaeric mouse small intestine', *Development*, 103(4), pp. 785-90.
- Schuijers, J., van der Flier, L.G., van Es, J. and Clevers, H. (2014) 'Robust cre-mediated recombination in small intestinal stem cells utilizing the olfm4 locus', *Stem Cell Reports*, 3(2), pp. 234-41.
- Schultz, B.E. and Chan, S.I. (2001) 'Structures and proton-pumping strategies of mitochondrial respiratory enzymes', *Annu Rev Biophys Biomol Struct*, 30, pp. 23-65.
- Sciacco, M., Bonilla, E., Schon, E.A., DiMauro, S. and Moraes, C.T. (1994) 'Distribution of wild-type and common deletion forms of mtDNA in normal and respiration-deficient muscle fibers from patients with mitochondrial myopathy', *Hum Mol Genet*, 3(1), pp. 13-9.
- Scoville, D.H., Sato, T., He, X.C. and Li, L. (2008) 'Current view: intestinal stem cells and signaling', *Gastroenterology*, 134(3), pp. 849-64.
- Shadel, G.S. and Clayton, D.A. (1997) 'Mitochondrial DNA maintenance in vertebrates', *Annu Rev Biochem*, 66, pp. 409-35.
- Sharpless, N.E. and DePinho, R.A. (2007) 'How stem cells age and why this makes us grow old', *Nat Rev Mol Cell Biol*, 8(9), pp. 703-13.
- Shin, H.W., Shinotsuka, C., Torii, S., Murakami, K. and Nakayama, K. (1997) 'Identification and subcellular localization of a novel mammalian dynamin-related protein homologous to yeast Vps1p and Dnm1p', *J Biochem*, 122(3), pp. 525-30.

- Shmelkov, S.V., Butler, J.M., Hooper, A.T., Hormigo, A., Kushner, J., Milde, T., St Clair, R., Baljevic, M., White, I., Jin, D.K., Chadburn, A., Murphy, A.J., Valenzuela, D.M., Gale, N.W., Thurston, G., Yancopoulos, G.D., D'Angelica, M., Kemeny, N., Lyden, D. and Rafii, S. (2008) 'CD133 expression is not restricted to stem cells, and both CD133+ and CD133- metastatic colon cancer cells initiate tumors', *J Clin Invest*, 118(6), pp. 2111-20.
- Shoubridge, E.A. and Wai, T. (2007) 'Mitochondrial DNA and the mammalian oocyte', *Curr Top Dev Biol*, 77, pp. 87-111.
- Silva, J.P. and Larsson, N.G. (2002) 'Manipulation of mitochondrial DNA gene expression in the mouse', *Biochim Biophys Acta*, 1555(1-3), pp. 106-10.
- Sivitz, W.I. and Yorek, M.A. (2010) 'Mitochondrial dysfunction in diabetes: from molecular mechanisms to functional significance and therapeutic opportunities', *Antioxid Redox Signal*, 12(4), pp. 537-77.
- Skulachev, V.P. (2001) 'Mitochondrial filaments and clusters as intracellular power-transmitting cables', *Trends Biochem Sci*, 26(1), pp. 23-9.
- Smits, P., Smeitink, J. and van den Heuvel, L. (2010) 'Mitochondrial translation and beyond: processes implicated in combined oxidative phosphorylation deficiencies', *J Biomed Biotechnol*, 2010, p. 737385.
- Snippert, H.J., van der Flier, L.G., Sato, T., van Es, J.H., van den Born, M., Kroon-Veenboer, C., Barker, N., Klein, A.M., van Rheenen, J., Simons, B.D. and Clevers, H. (2010) 'Intestinal crypt homeostasis results from neutral competition between symmetrically dividing Lgr5 stem cells', *Cell*, 143(1), pp. 134-44.
- Sohal, R.S., Svensson, I., Sohal, B.H. and Brunk, U.T. (1989) 'Superoxide anion radical production in different animal species', *Mech Ageing Dev*, 49(2), pp. 129-35.
- Starkov, A.A. (2008) 'The role of mitochondria in reactive oxygen species metabolism and signaling', *Ann NY Acad Sci*, 1147, pp. 37-52.
- Stewart, J.B., Freyer, C., Elson, J.L., Wredenberg, A., Cansu, Z., Trifunovic, A. and Larsson, N.G. (2008) 'Strong purifying selection in transmission of mammalian mitochondrial DNA', *PLoS Biol*, 6(1), p. e10.
- Stoll, E.A., Habibi, B.A., Mikheev, A.M., Lasiene, J., Massey, S.C., Swanson, K.R., Rostomily, R.C. and Horner, P.J. (2011) 'Increased re-entry into cell cycle mitigates age-related neurogenic decline in the murine subventricular zone', *Stem Cells*, 29(12), pp. 2005-17.
- Sugioka, K., Nakano, M., Totsune-Nakano, H., Minakami, H., Tero-Kubota, S. and Ikegami, Y. (1988) 'Mechanism of O₂- generation in reduction and oxidation cycle of ubiquinones in a model of mitochondrial electron transport systems', *Biochim Biophys Acta*, 936(3), pp. 377-85.
- Sui, G., Zhou, S., Wang, J., Canto, M., Lee, E.E., Eshleman, J.R., Montgomery, E.A., Sidransky, D., Califano, J.A. and Maitra, A. (2006) 'Mitochondrial DNA mutations in preneoplastic lesions of the gastrointestinal tract: a biomarker for the early detection of cancer', *Mol Cancer*, 5, p. 73.
- Szilard, L. (1959) 'On the Nature of the Aging Process', *Proc Natl Acad Sci U S A*, 45(1), pp. 30-45.
- Taanman, J.W. (1999) 'The mitochondrial genome: structure, transcription, translation and replication', *Biochim Biophys Acta*, 1410(2), pp. 103-23.
- Takeda, N., Jain, R., LeBoeuf, M.R., Wang, Q., Lu, M.M. and Epstein, J.A. (2011) 'Interconversion between intestinal stem cell populations in distinct niches', *Science*, 334(6061), pp. 1420-4.
- Tan, D.J., Bai, R.K. and Wong, L.J. (2002) 'Comprehensive scanning of somatic mitochondrial DNA mutations in breast cancer', *Cancer Res*, 62(4), pp. 972-6.

- Tang, F., Barbacioru, C., Wang, Y., Nordman, E., Lee, C., Xu, N., Wang, X., Bodeau, J., Tuch, B.B., Siddiqui, A., Lao, K. and Surani, M.A. (2009) 'mRNA-Seq whole-transcriptome analysis of a single cell', *Nat Methods*, 6(5), pp. 377-82.
- Taylor, R.W., Barron, M.J., Borthwick, G.M., Gospel, A., Chinnery, P.F., Samuels, D.C., Taylor, G.A., Plusa, S.M., Needham, S.J., Greaves, L.C., Kirkwood, T.B. and Turnbull, D.M. (2003) 'Mitochondrial DNA mutations in human colonic crypt stem cells', *J Clin Invest*, 112(9), pp. 1351-60.
- Taylor, R.W. and Turnbull, D.M. (2005) 'Mitochondrial DNA mutations in human disease', *Nat Rev Genet*, 6(5), pp. 389-402.
- Temperley, R., Richter, R., Dennerlein, S., Lightowers, R.N. and Chrzanowska-Lightowers, Z.M. (2010) 'Hungry codons promote frameshifting in human mitochondrial ribosomes', *Science*, 327(5963), p. 301.
- Tian, H., Biehs, B., Warming, S., Leong, K.G., Rangell, L., Klein, O.D. and de Sauvage, F.J. (2011) 'A reserve stem cell population in small intestine renders Lgr5-positive cells dispensable', *Nature*, 478(7368), pp. 255-9.
- Tomasetti, C. and Vogelstein, B. (2015) 'Cancer etiology. Variation in cancer risk among tissues can be explained by the number of stem cell divisions', *Science*, 347(6217), pp. 78-81.
- Tong, W.H. and Rouault, T. (2000) 'Distinct iron-sulfur cluster assembly complexes exist in the cytosol and mitochondria of human cells', *EMBO J*, 19(21), pp. 5692-700.
- Toyokuni, S., Okamoto, K., Yodoi, J. and Hiai, H. (1995) 'Persistent oxidative stress in cancer', *FEBS Lett*, 358(1), pp. 1-3.
- Trifunovic, A., Wredenberg, A., Falkenberg, M., Spelbrink, J.N., Rovio, A.T., Bruder, C.E., Bohlooly, Y.M., Gidlof, S., Oldfors, A., Wibom, R., Tornell, J., Jacobs, H.T. and Larsson, N.G. (2004) 'Premature ageing in mice expressing defective mitochondrial DNA polymerase', *Nature*, 429(6990), pp. 417-23.
- Tsukihara, T., Aoyama, H., Yamashita, E., Tomizaki, T., Yamaguchi, H., Shinzawa-Itoh, K., Nakashima, R., Yaono, R. and Yoshikawa, S. (1996) 'The whole structure of the 13-subunit oxidized cytochrome c oxidase at 2.8 Å', *Science*, 272(5265), pp. 1136-44.
- Turrens, J.F. and Boveris, A. (1980) 'Generation of superoxide anion by the NADH dehydrogenase of bovine heart mitochondria', *Biochem J*, 191(2), pp. 421-7.
- Valko, M., Leibfritz, D., Moncol, J., Cronin, M.T., Mazur, M. and Telser, J. (2007) 'Free radicals and antioxidants in normal physiological functions and human disease', *Int J Biochem Cell Biol*, 39(1), pp. 44-84.
- van der Flier, L.G., van Gijn, M.E., Hatzis, P., Kujala, P., Haegebarth, A., Stange, D.E., Begthel, H., van den Born, M., Guryev, V., Oving, I., van Es, J.H., Barker, N., Peters, P.J., van de Wetering, M. and Clevers, H. (2009) 'Transcription factor achaete scute-like 2 controls intestinal stem cell fate', *Cell*, 136(5), pp. 903-12.
- van Leeuwen, I.M., Mirams, G.R., Walter, A., Fletcher, A., Murray, P., Osborne, J., Varma, S., Young, S.J., Cooper, J., Doyle, B., Pitt-Francis, J., Momtahan, L., Pathmanathan, P., Whiteley, J.P., Chapman, S.J., Gavaghan, D.J., Jensen, O.E., King, J.R., Maini, P.K., Waters, S.L. and Byrne, H.M. (2009) 'An integrative computational model for intestinal tissue renewal', *Cell Prolif*, 42(5), pp. 617-36.
- van Leeuwen, I.M.M., Edwards, C.M., Ilyas, M. and Byrne, H.M. (2007) 'Towards a multiscale model of colorectal cancer', *World Journal of Gastroenterology*, 13(9), pp. 1399-1407.
- Vermeulen, L., Todaro, M., de Sousa Mello, F., Sprick, M.R., Kemper, K., Perez Alea, M., Richel, D.J., Stassi, G. and Medema, J.P. (2008) 'Single-cell cloning of colon cancer stem cells reveals a multi-lineage differentiation capacity', *Proc Natl Acad Sci U S A*, 105(36), pp. 13427-32.

- Vernochet, C., Mourier, A., Bezy, O., Macotela, Y., Boucher, J., Rardin, M.J., An, D., Lee, K.Y., Ilkayeva, O.R., Zingaretti, C.M., Emanuelli, B., Smyth, G., Cinti, S., Newgard, C.B., Gibson, B.W., Larsson, N.G. and Kahn, C.R. (2012) 'Adipose-specific deletion of TFAM increases mitochondrial oxidation and protects mice against obesity and insulin resistance', *Cell Metab*, 16(6), pp. 765-76.
- Walker, J.E. (1992) 'The NADH:ubiquinone oxidoreductase (complex I) of respiratory chains', *Q Rev Biophys*, 25(3), pp. 253-324.
- Wallace, D.C. (1992) 'Mitochondrial genetics: a paradigm for aging and degenerative diseases?', *Science*, 256(5057), pp. 628-32.
- Walther, V. and Graham, T.A. (2014) 'Location, location, location! The reality of life for an intestinal stem cell in the crypt', *J Pathol*, 234(1), pp. 1-4.
- Wang, C. and Youle, R.J. (2009) 'The role of mitochondria in apoptosis*', *Annu Rev Genet*, 43, pp. 95-118.
- Wang, J. and Pantopoulos, K. (2011) 'Regulation of cellular iron metabolism', *Biochem J*, 434(3), pp. 365-81.
- Wang, Y. and Bogenhagen, D.F. (2006) 'Human mitochondrial DNA nucleoids are linked to protein folding machinery and metabolic enzymes at the mitochondrial inner membrane', *J Biol Chem*, 281(35), pp. 25791-802.
- Wang, Y.E., Marinov, G.K., Wold, B.J. and Chan, D.C. (2013) 'Genome-wide analysis reveals coating of the mitochondrial genome by TFAM', *PLoS One*, 8(8), p. e74513.
- Warburg, O. (1956) 'On the origin of cancer cells', *Science*, 123(3191), pp. 309-14.
- Watt, I.N., Montgomery, M.G., Runswick, M.J., Leslie, A.G. and Walker, J.E. (2010) 'Bioenergetic cost of making an adenosine triphosphate molecule in animal mitochondria', *Proc Natl Acad Sci U S A*, 107(39), pp. 16823-7.
- Wei, M.C., Zong, W.X., Cheng, E.H., Lindsten, T., Panoutsakopoulou, V., Ross, A.J., Roth, K.A., MacGregor, G.R., Thompson, C.B. and Korsmeyer, S.J. (2001) 'Proapoptotic BAX and BAK: a requisite gateway to mitochondrial dysfunction and death', *Science*, 292(5517), pp. 727-30.
- Williams, G.C. (1957) 'Pleiotropy, natural selection and the evolution of senescence', *Evolution*, 11(4), pp. 398-411.
- Willis, S.N., Fletcher, J.I., Kaufmann, T., van Delft, M.F., Chen, L., Czabotar, P.E., Ierino, H., Lee, E.F., Fairlie, W.D., Bouillet, P., Strasser, A., Kluck, R.M., Adams, J.M. and Huang, D.C. (2007) 'Apoptosis initiated when BH3 ligands engage multiple Bcl-2 homologs, not Bax or Bak', *Science*, 315(5813), pp. 856-9.
- Winge, D.R. (2012) 'Sealing the mitochondrial respirasome', *Mol Cell Biol*, 32(14), pp. 2647-52.
- Winton, D.J., Blount, M.A. and Ponder, B.A. (1988) 'A clonal marker induced by mutation in mouse intestinal epithelium', *Nature*, 333(6172), pp. 463-6.
- Winton, D.J. and Ponder, B.A. (1990) 'Stem-cell organization in mouse small intestine', *Proc Biol Sci*, 241(1300), pp. 13-8.
- Wittig, I. and Schagger, H. (2008) 'Structural organization of mitochondrial ATP synthase', *Biochim Biophys Acta*, 1777(7-8), pp. 592-8.
- Wittig, I., Velours, J., Stuart, R. and Schagger, H. (2008) 'Characterization of domain interfaces in monomeric and dimeric ATP synthase', *Mol Cell Proteomics*, 7(5), pp. 995-1004.

- Wredenberg, A., Freyer, C., Sandstrom, M.E., Katz, A., Wibom, R., Westerblad, H. and Larsson, N.G. (2006) 'Respiratory chain dysfunction in skeletal muscle does not cause insulin resistance', *Biochem Biophys Res Commun*, 350(1), pp. 202-7.
- Wright, N.A. and Alison, M. (1984) *The biology of epithelial cell populations*. (2 vols). Oxford Oxfordshire
New York: Clarendon Press ;
Oxford University Press.
- Xia, D., Yu, C.A., Kim, H., Xia, J.Z., Kachurin, A.M., Zhang, L., Yu, L. and Deisenhofer, J. (1997) 'Crystal structure of the cytochrome bc1 complex from bovine heart mitochondria', *Science*, 277(5322), pp. 60-6.
- Xu, B. and Clayton, D.A. (1992) 'Assignment of a yeast protein necessary for mitochondrial transcription initiation', *Nucleic Acids Res*, 20(5), pp. 1053-9.
- Yakubovskaya, E., Chen, Z., Carrodeguas, J.A., Kisker, C. and Bogenhagen, D.F. (2006) 'Functional human mitochondrial DNA polymerase gamma forms a heterotrimer', *J Biol Chem*, 281(1), pp. 374-82.
- Yakubovskaya, E., Mejia, E., Byrnes, J., Hambardjieva, E. and Garcia-Diaz, M. (2010) 'Helix unwinding and base flipping enable human MTERF1 to terminate mitochondrial transcription', *Cell*, 141(6), pp. 982-93.
- Yan, K.S., Chia, L.A., Li, X., Ootani, A., Su, J., Lee, J.Y., Su, N., Luo, Y., Heilshorn, S.C., Amieva, M.R., Sangiorgi, E., Capecchi, M.R. and Kuo, C.J. (2012) 'The intestinal stem cell markers Bmi1 and Lgr5 identify two functionally distinct populations', *Proc Natl Acad Sci U S A*, 109(2), pp. 466-71.
- Yasukawa, T., Reyes, A., Cluett, T.J., Yang, M.Y., Bowmaker, M., Jacobs, H.T. and Holt, I.J. (2006) 'Replication of vertebrate mitochondrial DNA entails transient ribonucleotide incorporation throughout the lagging strand', *EMBO J*, 25(22), pp. 5358-71.
- Yatabe, Y., Tavare, S. and Shibata, D. (2001) 'Investigating stem cells in human colon by using methylation patterns', *Proc Natl Acad Sci U S A*, 98(19), pp. 10839-44.
- Yoneda, M., Chomyn, A., Martinuzzi, A., Hurko, O. and Attardi, G. (1992) 'Marked replicative advantage of human mtDNA carrying a point mutation that causes the MELAS encephalomyopathy', *Proc Natl Acad Sci U S A*, 89(23), pp. 11164-8.
- Yoshida, M., Muneyuki, E. and Hisabori, T. (2001) 'ATP synthase--a marvellous rotary engine of the cell', *Nat Rev Mol Cell Biol*, 2(9), pp. 669-77.
- Zhang, H., Barcelo, J.M., Lee, B., Kohlhagen, G., Zimonjic, D.B., Popescu, N.C. and Pommier, Y. (2001) 'Human mitochondrial topoisomerase I', *Proc Natl Acad Sci U S A*, 98(19), pp. 10608-13.
- Zollo, O., Tiranti, V. and Sondheimer, N. (2012) 'Transcriptional requirements of the distal heavy-strand promoter of mtDNA', *Proc Natl Acad Sci U S A*, 109(17), pp. 6508-12.